

# **Energy and Charge Control in Mass Spectrometry of Synthetic Polymers**

Cover Design: Andreas Nasioudis



The work described in this thesis was performed at  
**AkzoNobel Research, Development & Innovation**  
P.O. Box 10, 7400 AA Deventer, The Netherlands  
and

**FOM Institute AMOLF**  
Science Park 104, 1098 XG Amsterdam, The Netherlands

ISBN/EAN: 978-90-77209-48-6

Energy and Charge Control in Mass Spectrometry of Synthetic Polymers  
2011, Andreas Nasioudis (andreasnasioudis@hotmail.com)

# **Energy and Charge Control in Mass Spectrometry of Synthetic Polymers**

**Controle van energie en ladingstoestand in  
massaspectrometrie van synthetisch polymeren**  
(met een samenvatting in het Nederlands)

Proefschrift

ter verkrijging van de graad van doctor aan de Universiteit Utrecht op gezag van de rector magnificus, prof.dr. G.J. van der Zwaan, ingevolge het besluit van het college voor promoties in het openbaar te verdedigen op donderdag 23 juni 2011 des middags te 2.30 uur

door

**Andreas Nasioudis**

geboren op 27 January 1978  
te Thessaloniki, Griekenland

Promotor: Prof.dr. R. M. A. Heeren

Co-promotor: Dr. O. F. Van den Brink

This thesis was partly accomplished with financial support from the European Commission in the framework of the Marie Curie Early Stage Training Program “POLY-MS” on multistage mass spectrometry of synthetic polymers and synthetically modified biopolymers (MEST-CT-2005-021029). This work was also supported by AkzoNobel Research, Development & Innovation (financially and in kind) and by the FOM Institute for Atomic and Molecular Physics (in kind).

Ω ΦΙΛΕ ΠΑΝ ΤΕ ΚΑΙ ΑΛΛΟΙ ΟΣΟΙ ΤΗΔΕ ΘΕΟΙ ΔΟΙΗΤΕ ΜΟΙ ΚΑΛΩ  
ΓΕΝΕΣΘΑΙ ΤΑΝΔΟΘΕΝ ΕΙΣΩΘΕΝ ΔΕ ΟΣΑ ΕΧΩ ΤΟΙΣ ΕΝΤΟΣ ΕΙΝΑΙ ΜΟΙ  
ΦΙΛΙΑ ΠΛΟΥΣΙΟΝ ΔΕ ΝΟΜΙΖΟΙΜΙ ΤΟΝ ΣΟΦΟΝ ΤΟ ΔΕ ΧΡΥΣΟΥ  
ΠΛΗΘΟΣ ΕΙΗ ΜΟΙ ΟΣΟΝ ΜΗΤΕ ΦΕΡΕΙΝ ΜΗΤΕ ΔΓΕΙΝ ΔΥΝΑΙΤΟ ΑΛΛΟΣ  
Η Ο ΣΩΦΡΟΝΩΝ.

**Socrate's Prayer to Pan from Plato's "Phaedrus".**

*"Oh dear Pan and all the other gods of this place, grant that I may be beautiful inside. Let all my external possessions be in friendly harmony with what is within. May I consider the wise man rich. As for gold, let me have as much as a moderate man could bear and carry with him".*

*Στην οικογένειά μου  
(to my family)*

# Table of Contents

<b>INTRODUCTION .....</b>	<b>9</b>
1.1 Introduction .....	10
1.2 Mass spectrometry of synthetic polymers .....	11
1.3 Scope of this thesis .....	12
<b>POLYMER ANALYSIS BY MASS SPECTROMETRY: FUNDAMENTALS, INSTRUMENTATION, APPLICATIONS .....</b>	<b>15</b>
2.1 Introduction .....	16
2.2 Polymer characteristics .....	16
2.2.1 Molar mass distribution .....	17
2.2.2 Functionality type distribution (end-groups and monomers) .....	20
2.2.3 Sequence and structural distribution: MS analysis of copolymers and large networks .....	21
2.3 Mass spectrometry .....	23
2.3.1 Ionization Techniques .....	25
2.3.2 MS Instrumentation .....	29
2.4 Polymer characterization by MS: Applications .....	39
2.4.1 Introduction .....	39
2.4.2 LC-MS and MS <sup>n</sup> analysis of homopolymers .....	40
2.4.3 LC-MS <sup>n</sup> analysis of copolymers .....	44
2.4.4 Outlook .....	47
<b>DETERMINATION OF THE POLYMERIZATION PRODUCTS OF ETHOXYLATION OF CASTOR OIL BY LIQUID CHROMATOGRAPHY MULTISTAGE MASS SPECTROMETRY .....</b>	<b>49</b>
3.1 Introduction .....	51
3.2 Experimental section .....	52
3.2.1 Chemicals .....	52
3.2.2 Instrumentation .....	52
3.3 Results and discussion .....	53
3.3.1 LC-MS(+) analysis of CASEO .....	53
3.3.2 LC-MS(-) analysis of CASEO .....	55
3.3.3 LC-MS analysis of CASEO with different ionization techniques .....	57
3.3.4 LC-MS <sup>n</sup> analysis of CASEO .....	59
3.3.5 LC-MS <sup>n</sup> analysis of castor oil ethoxylate isobars/isomers .....	66
3.4 Conclusions .....	71
<b>CHALLENGES IN ENERGY-DEPENDENT TANDEM MASS SPECTROMETRY IN AN ION TRAP .....</b>	<b>73</b>
4.1 Introduction .....	75
4.2 Experimental setup .....	76
4.2.1 Chemicals and sample preparation .....	76

4.2.2 Methods .....	77
4.2.3 Instrumentation.....	78
4.3 Optimization of MS/MS instrumental parameters .....	79
4.3.1 Mass analysis.....	79
4.3.2 Isolation frequency and width.....	80
4.3.3 Cooling time.....	81
4.3.4 Resonance excitation width and frequency.....	82
4.3.5 Excitation time.....	84
4.4 Size dependence study of synthetic polymers.....	86
4.5 Conclusions .....	89
<b>POLYMER ANALYSIS BY USING THEIR CHARACTERISTIC COLLISION ENERGY IN TANDEM MASS SPECTROMETRY .....</b>	<b>91</b>
5.1 Introduction .....	93
5.2 Experimental section .....	94
5.2.1 Chemicals .....	94
5.2.2 Sample preparation and instrumentation .....	94
5.3 Results and discussion .....	97
5.3.1 Energy-dependent analysis of homopolymers.....	97
5.3.2 Energy-dependent analysis of block copolymers .....	107
5.4 Conclusions .....	113
<b>FORMATION OF LOW CHARGE STATE IONS OF SYNTHETIC POLYMERS USING QUATERNARY AMMONIUM COMPOUNDS.....</b>	<b>115</b>
6.1 Introduction .....	117
6.2 Experimental section .....	118
6.2.1 Chemicals .....	118
6.2.2 Sample preparation.....	119
6.2.3 Instrumentation.....	120
6.3 Results and discussion .....	120
6.3.1 DI-MS and SEC-MS analysis of PEGS with the use of Quats .....	120
6.3.2 Effect of Quat concentration on the production of low charge state adduct ions .....	125
6.3.3 Effect of Quat structure on the production of low charge state adduct ions.....	128
6.3.4 DI-MS and SEC-MS analysis of other synthetic polymers with addition of Quats .....	133
6.4 Conclusions .....	136
<b>ELECTROSPRAY IONIZATION MASS SPECTROMETRY OF THE NON-COVALENT COMPLEXES OF AMMONIUM IONS WITH HIGH MOLAR MASS POLYETHERS.....</b>	<b>139</b>
7.1 Introduction .....	141
7.2 Experimental section .....	142
7.2.1 Chemicals .....	142
7.2.2 Sample preparation and methods .....	143

7.2.3 Instrumentation.....	143
7.3 Results and discussion .....	144
7.3.1 MS analysis of PEG with addition of Quats and amines.....	144
7.3.2 MS analysis of block copolymers with addition of Quats and amines .....	149
7.4 Conclusions .....	151
<b>ELECTROSPRAY IONIZATION TANDEM MASS SPECTROMETRY OF AMMONIUM CATIONIZED POLYETHERS.....</b>	<b>153</b>
8.1 Introduction .....	155
8.2 Experimental section .....	156
8.2.1 Chemicals and sample preparation.....	156
8.2.2 Instrumentation and methods.....	157
8.3 Results and discussion .....	158
8.3.1 <i>q</i> -TOF MS/MS of singly and doubly charged non-covalent complex ions.....	158
8.3.2 LIT and QIT MS/MS of singly and doubly charged non-covalent complex ions .....	164
8.3.3 Energy-dependent analysis of singly charged non-covalent complex ions.....	172
8.4 Conclusions .....	174
<b>REFERENCES .....</b>	<b>175</b>
<b>GLOSSARY OF SYMBOLS AND ABBREVIATIONS .....</b>	<b>185</b>
<b>SUMMARY .....</b>	<b>189</b>
<b>SAMENVATTING .....</b>	<b>195</b>
<b>ACKNOWLEDGEMENTS .....</b>	<b>201</b>
<b>CURRICULUM VITAE .....</b>	<b>205</b>
<b>LIST OF PUBLICATIONS .....</b>	<b>207</b>
Publications .....	208
Oral and Poster Presentations at Conferences & Meetings.....	208

# 1

## Introduction

## 1.1 Introduction

“Never judge a book by its cover” is one of the most common advices given by teachers to their students. A teacher of science, however, will be more specific and advise: “Never judge a scientific book by its cover, but pay attention to its title”. This is true since the title of a scientific book, dissertation, article, abstract and presentation should introduce the reader into the content and catch his attention. In this respect, two terms in the title of this dissertation stand out: “Polymers” and “Mass Spectrometry”. The study of the title continues as a study of terms.

The term polymer was introduced into the scientific lexicon by Jons Jacob Berzelius in 1833. The term is the Greek word “*Πολυμερές*” which is the combination of two other words: *Πολυμερές* = *Πολύ* + *μέρος*, meaning multiple parts. Although the word is quite generic and gives an idea about the composition of a substance it fails to give additional vital information about the nature of the substance itself. Throughout the 19<sup>th</sup> century and the early years of the 20<sup>th</sup> century, scientists believed that polymers are just small molecules in a colloidal state and that does not exist such a thing as a molecule of very high molecular weight. It was not until 1920, when Herman Staudinger introduced the theory that polymers are actually long chains held together by covalent bonds and with molecular weights reaching thousands to hundreds of thousands,<sup>1</sup> that this notion about polymers was modified. The term “macromolecules” was born and it has been used ever since (almost) as a synonym for “polymer”. The term mass spectrometry is more recent, hence more complex but also more informative. It consists of two Greek words, “*μάζα*” and “*μέτρο*”, and one Latin, “*spectrum*”. Literally, it translates to visual measurement of the mass. From this linguistic analysis it is evident that the technique of mass spectrometry could easily have provided a confirmation to Staudinger’s theory, but unfortunately another 70 years were necessary to achieve this with the application of ionization techniques such as fast-atom bombardment and field desorption. The pionnering work of J.B. Fenn,<sup>2-5</sup> K. Tanaka,<sup>6</sup> M. Karas and F. Hillenkamp<sup>7,8</sup> on soft ionization techniques created an even stronger link between polymers and mass spectrometry, than fast-atom bombardment and field desorption. Finally, two elements that were destined to become a good match were finally united.

## 1.2 Mass spectrometry of synthetic polymers

Synthetic polymers can be considered as human's answer to one of nature's wonders: gigantic molecular chain architectures. As nature uses natural polymers for a variety of different functions, from building material (*e.g.*, cellulose) to energy storage (*e.g.*, glycogen and starch) and genetical information carrier (DNA), humans developed a variety of tailor-made macromolecules to satisfy their needs.

The biggest challenge for the scientists, and especially polymer chemists, is to create an understanding of how the chemical structure of the polymer and its macrostructure influence a polymer's physicochemical and mechanical properties. In the last years, an additional challenge has been added to this, *viz.* environmental concerns; how to synthesize a biodegradable polymer which maintains the properties of a conventional synthetic polymer.

In this endeavor of understanding what the result of a synthetic polymerization process is various analytical techniques have been applied. Each of these techniques can only provide part of the information on the size and micro/macrostructure of the synthetic polymer. Nuclear magnetic resonance (NMR), size-exclusion chromatography (SEC), light scattering, Fourier-transform infrared spectroscopy, and Raman spectroscopy can provide information about the molecular weight distribution, dispersity, monomer unit, and, sometimes, end-group composition. Capillary electrophoresis and liquid chromatography (LC) in its various modes (*i.e.*, isocratic, gradient elution, gradient polymer elution, and at critical conditions) can separate the individual chains of relatively low molar mass polymers (for LC <3,000-5,000 Da) based on their size, morphology and chemical composition. Thus, qualitative and quantitative information can be obtained. Other techniques such as differential scanning calorimetry, scanning/transmission electron microscopy and thermal gravimetric/mechanical analysis provide information about physical/mechanical properties such as crystallinity and morphology. Although all these techniques can provide complementary information, most of them exhibit the same limitation: The information obtained is an average of the whole distribution.

On the other hand, mass spectrometry (MS) is a technique that provides information about individual molecules. MS can provide detailed information about the elemental

composition, monomer unit and end-group structure. Its sensitivity allows the detection of very low concentrations of substances used or produced during the synthetic process (*e.g.*, additives, byproducts, etc), and can be used for the analysis of impurities. This last characteristic is very important for polymers used in the health sector. However, MS also has its limitations. The analysis of high molar mass polymers can be partially achieved by soft ionization techniques such as matrix-assisted laser desorption/ionization (MALDI),<sup>6-12</sup> but it is limited to monodisperse synthetic polymers. Electrospray ionization (ESI)<sup>2-5,13,14</sup> is another soft ionization technique that exhibits less achievements in the analysis of high molar mass synthetic polymers (effective range is till 10,000 Da) than MALDI. Disperse synthetic polymers are also a challenge for ESI, since the multiply charged distributions can convolute with the size distribution. On the other hand, ESI is perfectly coupled to chromatographic techniques thus increasing the capabilities of MS in the analysis of structurally complicated polymers.

In addition, the use of tandem mass spectrometry (MS/MS) allows the selective study of a specific polymer molecule and, through the fragmentation process, provides additional information about the micro/macrostructure and the monomer sequence. This last element is of great importance for structurally complicated polymers such as branched polymers and copolymers. Nevertheless, it is still an area that has not yet been fully explored. The knowledge of fragmentation mechanisms of polymers is rather limited. This lack of knowledge in combination with the fact, that the sequence in complex polymers follows a statistical distribution and it is not specific, like with proteins, limits the use of MS/MS to simple systems.

### **1.3 Scope of this thesis**

In this thesis, the challenge of the analysis of high molar mass and structurally complicated synthetic polymers is addressed. The main focus is around three major challenges: (1) How to extend the mass limits in the analysis of high molar mass synthetic polymers taking in consideration that in the future more and more structurally complicated polymeric systems will be synthesized, (2) to explore MS/MS as a selective tool in the

analysis of synthetic polymers, and (3) to investigate the capabilities of combined LC and MS/MS methods for the characterization of structurally complicated synthetic polymers.

**Chapter 2** presents the fundamentals of synthetic polymers and mass spectrometry. Special attention is given to the theoretical background of ion formation by ESI and mass analysis. A general description of the MS instrumentation used in this thesis will be presented. In addition, some recent applications of MS and LC-MS in the analysis of synthetic polymers will demonstrate the current practical state of the art.

**Chapter 3** provides an example of the current performance of LC coupled to multistage mass spectrometry ( $MS^n$ ) in the analysis of more structurally complicated polymeric systems. These are polymer products following the ethoxylation of vegetable oils. It will be shown that optimization of the LC conditions results in a high separation selectivity of closely related polymer structures (33 different polymer distributions, with some being nominally isobaric and/or isomeric structures). MS and  $MS^n$  provide additional dimensions in the more detailed analysis of these structurally complicated polymeric systems.

**Chapter 4** presents the methodology needed to achieve an accurate and reproducible control of the applied excitation energy in a quadrupole ion trap. The major instrumental parameters that influence MS/MS analysis are investigated and optimized. A control of the optimization method is performed by studying the dependence of size of poly(ethylene glycols) to the required excitation energy for fragmentation.

In **Chapter 5**, the use of the energy-dependent MS/MS analysis to discriminate between different polymer classes is demonstrated. This is achieved by using the method presented in Chapter 4. It will be shown that discrimination is achieved by determining a “characteristic” parameter (*i.e.*, the characteristic collision voltage), related to the polymer’s structure. This value expresses the stability of a polymer ion upon fragmentation. The application of this method in the analysis of structurally complicated copolymer systems that cannot be analyzed by conventional MS and  $MS^n$  methods is presented.

The challenge of extending the mass limits in ESI-MS analysis of high molar mass synthetic polymers is discussed in Chapters 6 to 8. **Chapter 6** investigates in a structural way the parameters that influence the formation of low charge state adducts ions by addition of ammonium ions as cationization agents, whereas **Chapter 7** presents the

practical aspects of this methodology, its performance and limitations. **Chapter 8** attempts to connect the knowledge of Chapter 6-7 with Chapter 4 and 5. An investigation of the fragmentation behavior and stability of these low charge state adduct ions is performed.

In summary, this thesis presents solutions or improvements of current methods for the analysis of disperse, structurally complicated and/or high molar mass synthetic polymers. The investigation and comparison of various LC-MS<sup>n</sup> methods (*e.g.*, different ionization modes and techniques, use of various cationization agents) provides a toolbox to the polymer chemists that can be applied to their industrial applications. The use of ion/molecule interactions allows a control over the charge of the adduct ions. By controlling the charge, high molar mass (up to 40 kDa) and disperse synthetic polymers are analyzed with ESI-MS. The generated information about the molar mass distribution is in agreement with other techniques such as SEC and MALDI-MS. This paradigm opens an alternative route in the analysis of synthetic polymers with MS. Finally, control over the excitation energy and determination of the characteristic collision voltage permits the classification of polymers into groups. In addition, controlling the excitation energy a selective deconvolution of structurally complicated polymeric systems is achieved by targeted fragmentation of “weaker” molecules over “stronger” molecules. This method introduces a new qualitative approach in the analysis of synthetic polymers with MS

**2**

**Polymer Analysis by Mass Spectrometry: Fundamentals, Instrumentation, Applications**

## 2.1 Introduction

Synthetic polymers have become very important materials in everyday life, replacing other traditional materials such as metal, glass and natural materials. This success derives from the great variety of monomer units that can be used and linked in various ways, forming polymers with versatile properties. This plethora of structures and characteristics renders the development of characterization techniques essential. These techniques can support polymer chemists in their endeavour of linking the chemical structure to physical/mechanical properties and synthesizing new polymers. Among the techniques available, mass spectrometry (MS) is gaining popularity and ground.

In this chapter, an introduction to some of the polymer characteristics that can be determined by MS is given. A detailed theoretical explanation of polymers, polymer synthesis, polymerization mechanisms, polymer properties and chromatographic techniques is omitted since no prior knowledge of these aspects is compulsory. To the contrary, a more detailed presentation of MS fundamentals and instrumentation is provided. In addition, some examples of the practical state of the art in the MS analysis of structurally complicated polymeric systems are presented.

## 2.2 Polymer characteristics

To understand the magnitude of the challenge that MS faces, it is useful to create a classification of the synthetic polymers. This classification should not be based on the traditional ways of grouping polymers, such as based on their origin (*i.e.*, natural, semi-synthetic, synthetic) or their polymerization mechanism (*e.g.*, step, chain, etc), but on their structural characteristics relevant for their physical behavior. Chart 2.1 presents this polymer classification

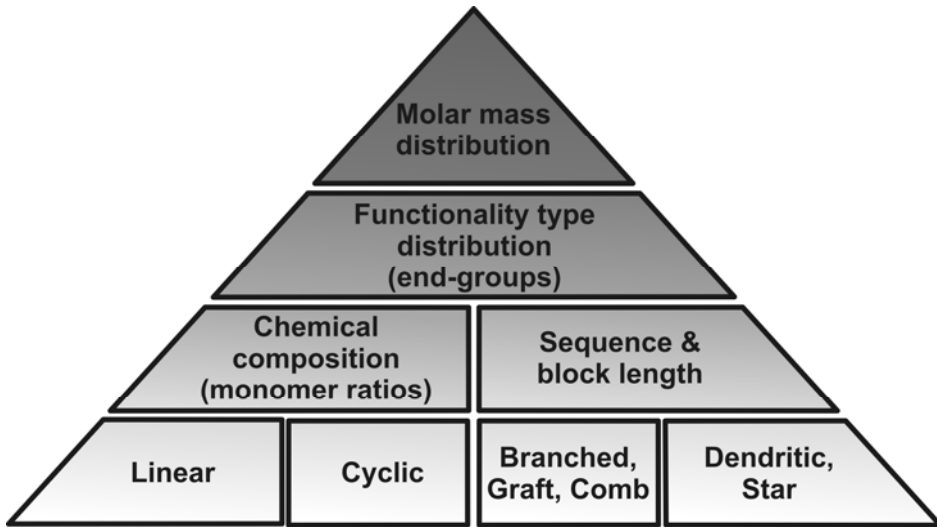


**Chart 2.1.** Levels of polymer classification based on structural properties.

### 2.2.1 Molar mass distribution

In contrast to proteins, synthetic polymers are mixtures of molecules of different sizes. This polydispersity is a result of the polymerization process, where the propagation of the polymerization is governed by random events. One of the most important characteristics of a synthetic polymer is its molar mass distribution (MMD). MMD provides information about the weight and the number of chains that comprise the synthetic polymer.

There are three main parameters that are used to define the MMD of a synthetic polymer.<sup>15</sup> These are: the number average molecular weight ( $\bar{M}_n$ ), the weight average molecular weight ( $\bar{M}_w$ ) and the polydispersity ( $D$ ). Their equations are given below.

$$\bar{M}_n = \frac{\sum_i n_i m_i}{\sum_i n_i} \quad \text{Equation 2.1}$$

$$\bar{M}_w = \frac{\sum_i n_i m_i^2}{\sum_i n_i m_i} \quad \text{Equation 2.2}$$

$$D = \frac{\bar{M}_w}{\bar{M}_n} \quad \text{Equation 2.3}$$

where  $n_i$  and  $m_i$  are the number of polymer molecules  $i$  and the molecular weight, respectively. In addition there are two other parameters that are less frequently used; the z-average molecular weight ( $\bar{M}_z$ ) and the viscosity average molecular weight ( $\bar{M}_v$ ).<sup>15</sup> Figure 2.1 illustrates a typical MMD curve and the position of the various MMD parameters.

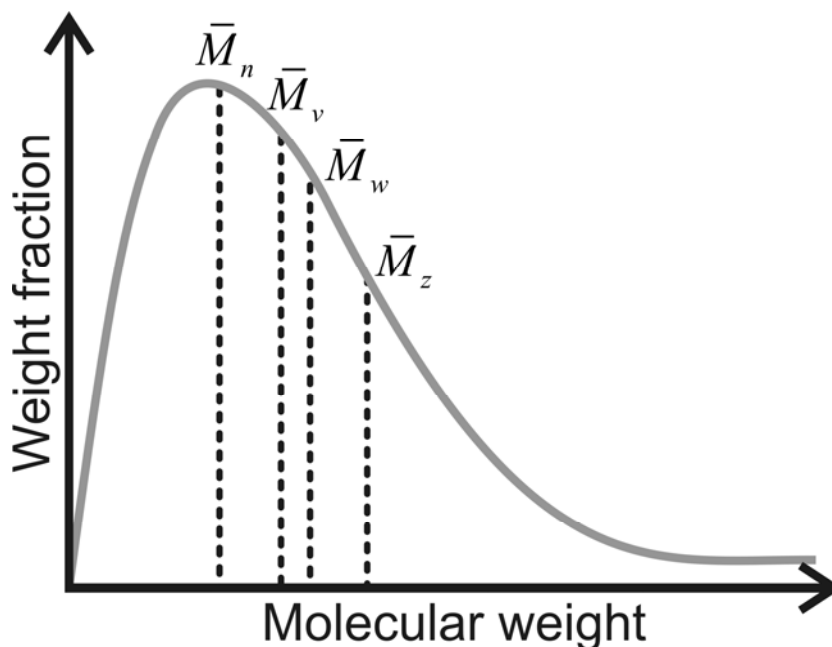


**Figure 2.1.** MMD curve of a polymer.

The polydispersity  $D$  as shown in equation 2.3 is a parameter that indicates the width of the MMD. Figure 2.2 shows three distinct types. A polymer can have a unimodal distribution which varies from low  $D$  to high  $D$  values. There is an additional type of MMD which is characterized as bimodal, because of the presence of two maxima.

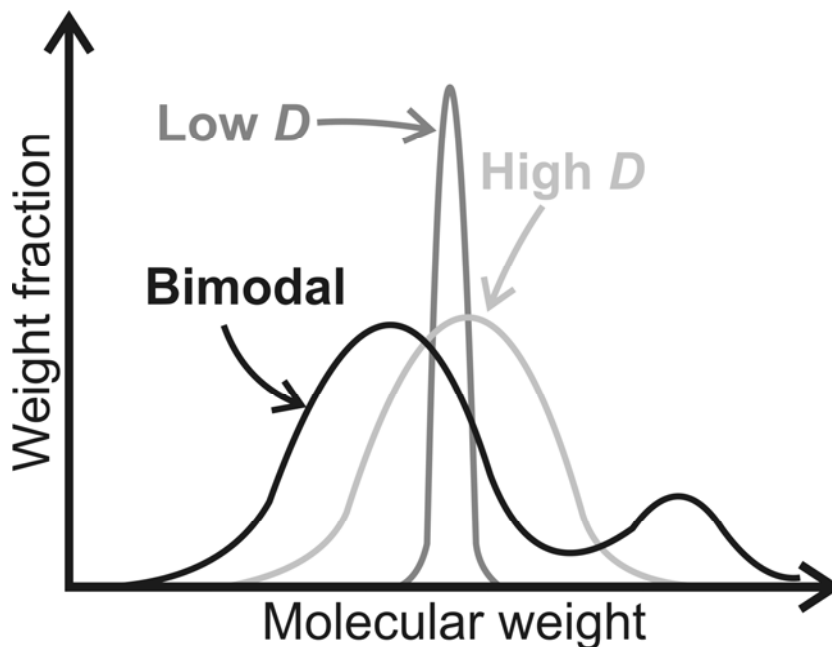


**Figure 2.2.** Types of MMDs.

The determination of the parameters used to define the MMD of polymers can be separated in two categories: the “indirect” methods, such as intrinsic viscosity and size-exclusion chromatography (SEC), which require calibration prior to analysis, and the “direct” methods, such as light scattering, osmometry and ultracentrifuge, which do not need any calibration. All these techniques (except of SEC) provide an average value of the MMD, whereas MS can be considered as a “direct” method that provides specific molecular mass information of the individual polymer molecules.

Although mass spectrometry would seem to be an ideal tool for MMD determination, there are a few shortcomings that are related to quantitation which make MMD determination by MS a challenging task. The relation between polymer abundance and signal in the mass spectrometer is greatly influenced by the ionization efficiency of the polymer (which is influenced by many factors such as setting of the ion source and chemical environment of the sample during the ionization process) and by the detection efficiency in relation to the mass of the detected ion. Matrix-assisted laser desorption/ionization (MALDI) MS can provide accurate MMD information when the  $D$  is

below 1.1.<sup>9-10</sup> MMD information on polymers with higher  $D$  values when analyzed with MALDI-MS deviates dramatically from the MMD information obtained by the conventional methods.<sup>10-12</sup> Mass discrimination effects are observed in MALDI MS, when polymers with broad distributions are analyzed. Electrospray ionization (ESI) MS can also be used for the determination of the MMD. However, it is limited when high molar mass polymers are analyzed and multiply charged ions distributions are observed (for more information, see Section 2.3). These distributions will be convoluted with the size distribution (the singly charged ion distribution) and with each other. This makes the MMD determination complicated, especially when low resolution MS instruments are used. More accurate information about the MMD can be obtained when MALDI and ESI-MS are coupled to SEC.<sup>11,16-21</sup>

### ***2.2.2 Functionality type distribution (end-groups and monomers)***

A polymer's properties are largely determined by its chemical structure. Determination of the end-groups contributes to the understanding of the relation between the polymer's chemical structure and its properties. In addition, it provides valuable information about the polymerization mechanisms that play a role in its production.

Determining the amount and type of end-groups in a polymer can be performed with various techniques. Wet chemical methods can be used for end-group quantitation but have specific disadvantages. They are time consuming, specific for one type of end-group per method and mostly applied to low molar mass polymers. Nuclear magnetic resonance (NMR) is another technique which is often used for end-group determination. NMR determination of end-groups is limited to low molar mass, because the intensity of the distinct signal of the end-group decreases to eventually disappear in the background noise on increase of polymer size.

The combination of high resolution MS (HR-MS) and (multistage) MS ( $MS^{(n)}$ ) often provide information about the elemental composition and location of the end-group in the polymer chain. The former parameter, the elemental composition, can be determined by using HRMS and the linear regression method.<sup>22,23</sup> The latter can be identified by MS/MS.<sup>24-26</sup>

The linear regression method is based on plotting the accurate measured mass  $m_{meas}$  as a function of the degree of polymerization  $n$ .

$$m_{meas} = n \cdot m_{mon} + m_{end} + m_{cat/an} \quad \text{Equation 2.4}$$

where  $m_{mon}$ ,  $m_{end}$ , and  $m_{cat/an}$  are the theoretical masses of the monomer unit, end-group and cation or anion, respectively. The combined mass of the end-groups and the cation/anion can be determined from the intercept of the regression line, whereas the monomer mass is derived from the slope. An additional correction needs to be applied. The mass of the electron  $m_e$  needs to be subtracted from the mass of the atom that carries the charge (this is valid when the charge is positive. When negative ions are measured then the  $m_e$  needs to be added).

Examples of the use of MS/MS for end-group determination will be shown later in this Chapter and in Chapter 3.

### ***2.2.3 Sequence and structural distribution: MS analysis of copolymers and large networks***

As mentioned earlier, synthetic polymers exhibit an additional type of distribution, which is closely related to the intramolecular arrangement of the monomers inside the polymer chain. This type of distribution is apparent when various types of copolymers are analyzed, such as random, block, statistical, alternating, branched and grafted copolymers. An overview of these types of copolymers is presented in Chart 2.2.

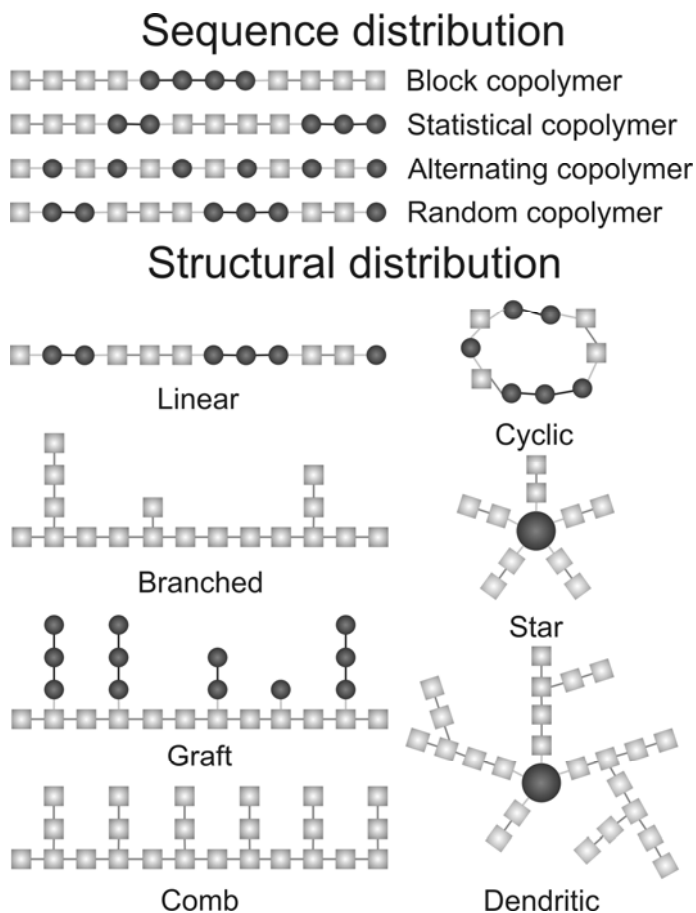


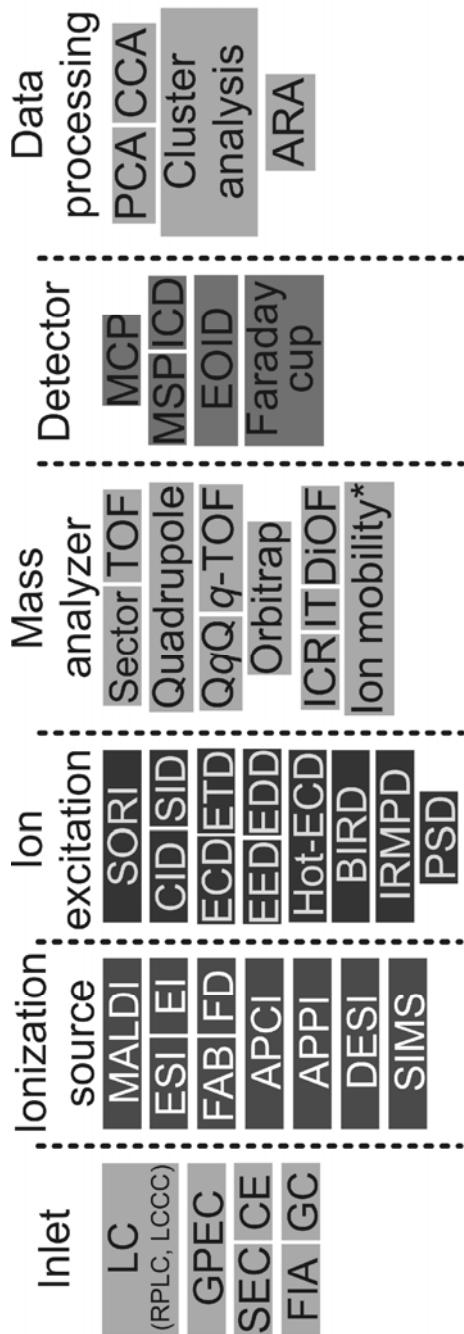
**Chart 2.2.** Variety of sequence and structural distribution of synthetic polymers. Note: Spheres and squares denote different type of monomers. Some steric distributions may both be homopolymeric and copolymeric.

There are various methods to analyze these structurally complicated polymeric systems by MS. Determination of copolymer composition and sequence can be performed by MS or  $MS^n$  methods, but the success always depends on the complexity of the structure in relation to the type of information that can be obtained from MS. The analysis of copolymers with an organized distribution such as block, alternating and graft copolymers is considered more straightforward than the analysis of random-like structures such as branched, star and dendritic polymers. Some MS methods use a combination of mass spectral intensities and the chain statistics approach.<sup>27,28</sup>  $MS^n$  methods can provide detailed sequence information

as long as the excitation methods do not result in consecutive fragmentation of product ions. MS<sup>n</sup> can distinguish between some type of synthetic polymer isomers (*e.g.*, an alternating and a block copolymer). However, the discrimination between closely related isomeric structures (*e.g.*, random and statistical copolymers) is more challenging. Nevertheless, the potentially large number isolation-fragmentation cycles in MS<sup>n</sup> may prove to be useful for sequence elucidation. Degradation methodologies can facilitate the determination of the sequence to some extent, especially when selective degradation methods (*e.g.*, enzymatic) are used. A final approach that can facilitate the analysis of structurally complicated polymers is the coupling of liquid chromatographic techniques to MS and MS<sup>n</sup>. In this way, the complexity of the mixture is reduced prior to MS analysis and ion suppression effects are greatly reduced. The separation of the polymer in one, or even two dimensions (2D-LC<sup>29</sup>), with the addition of the MS dimension, allows a “three-dimensional” discrimination. If MS<sup>n</sup> is applied in place of MS, the number of dimensions is further increased by the number of isolation-fragmentation cycles. Examples of such methods will be presented later in this article and in Chapter 3.

## 2.3 Mass spectrometry

MS is a great analytical tool in the hands of polymer chemists as it can provide detailed information about the polymer’s structure. The great variety of MS techniques developed throughout the last few decades creates a portfolio of instrumentation that can address diverse needs: from screening and fingerprinting to quantitative analysis and from basic structural information to high resolution analysis of complicated systems. The chart below (Chart 2.3) summarizes the different techniques that are available. Their classification follows the basic setup of a mass spectrometer: (1) inlet, (2) ionization, (3) ion excitation, (4) mass analyzer, (5) detector, and (6) data handling. A detailed explanation of all available techniques is outside the scope of this thesis (detailed explanation of all techniques can be found in the literature<sup>30-32</sup>). However, the techniques used in this thesis are presented later in this chapter.



Explanation of the abbreviations used above which are not used in this thesis: Gradient polymer elution chromatography (GPEC), flow injection analysis (FIA), desorption electrospray ionization (DESI), secondary ion mass spectrometry (SIMS), sustained off-resonance irradiation (SORI), surface induced dissociation (SID), electron capture dissociation (ECD), electron transfer dissociation (ETD), electronic-excitation dissociation (EED), electronic detachment dissociation (EDD), blackbody infrared radiative dissociation (BIRD), infrared multiphoton dissociation (IRMPD), post-source decay (PSD), distance of flight (DIOF), microchannel plate (MCP), microsphere plate (MSP), image charge detector (ICD), electro-optical ion detector (EOID), principal component analysis (PCA), canonical correspondence analysis (CCA), and automated regression analysis (ARA).

**Chart 2.3.** Different setup possibilities of mass spectrometers. \*: Ion mobility is not a mass analyzer strictly speaking. It separates ions according to their  $m/z$  and their cross-sections.

### **2.3.1 Ionization Techniques**

#### **2.3.1.1 Matrix-assisted laser desorption/ionization**

Matrix-assisted laser desorption/ionization (MALDI) was developed by Karas and Hillenkamp<sup>7,8</sup> in the late 1980s. It is one of the two basic ionization techniques used for the analysis of synthetic polymers. Its success is based on the fact that MALDI is a “soft” (*i.e.*, minimum fragmentation) ionization technique that produces simple mass spectra, mostly intact and singly charged adduct ions. Since most of the synthetic polymers produced have a high molar mass, MALDI combined with a time-of-flight mass analyzer is the ideal tool for polymer analysis.<sup>33</sup>

The MALDI process is illustrated in Figure 2.3. The analyte is mixed with an excess of another substance used as a matrix (see left panel of Figure 2.3) and left to dry on a metal plate. This substance needs to absorb in the laser’s wavelength, so that once the laser beam hits the surface, the matrix will absorb the photon energy, desorb and ionize. This desorption/ionization process takes place in vacuum and can be described as an explosion, since a gas-phase plume is created<sup>34,35</sup> (see right panel, Figure 2.3). This plume contains analyte and matrix (neutral) molecules and ions. The ionization of the analyte molecules happens via gas-phase proton transfer reactions with the matrix ions. Adduct formation is also readily observed when salts are mixed with the matrix.

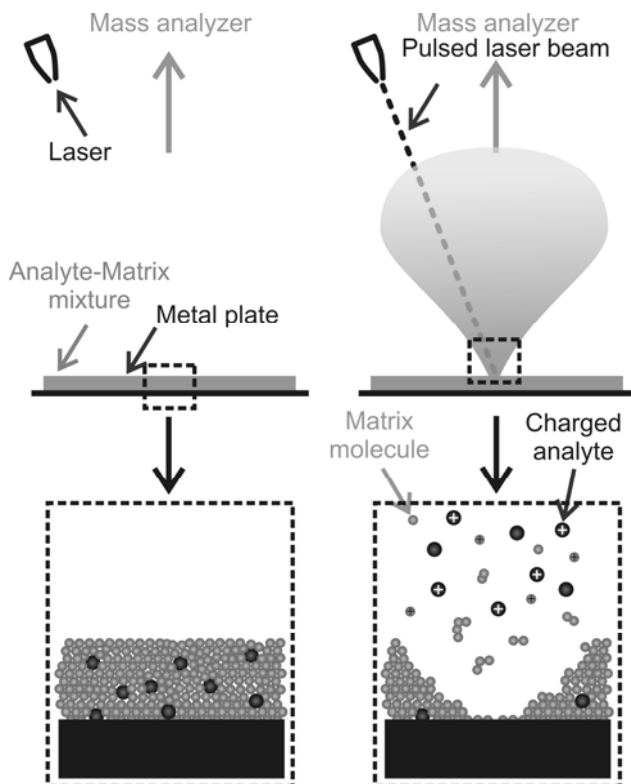


**Figure 2.3.** MALDI process. *Note:* Left panel illustrates the state before the laser is fired and the right panel the actual MALDI process.

### 2.3.1.2 Electrospray ionization

Electrospray ionization (ESI) is also a “soft” ionization technique. It can successfully transfer intact molecules to the gas phase and allows the formation of intact adduct ions. Although its first description was made as early as 1917,<sup>36</sup> it wasn’t until the late 1960s that Dole *et al.*,<sup>37,38</sup> studied ESI as an ionization technique for large polymers. Dole’s work paved the way for J.B. Fenn and M. Yamashita who demonstrated for the first time the application of ESI for ionization in MS. They showed that ESI can produce positive and negative ions in the gas phase.<sup>2-4</sup> Subsequent work by Fenn indicated that ESI could be used very effectively for the analysis high molar mass biopolymers with conventional MS instrumentation with standard scan mass ranges.<sup>5</sup> This was achieved as a result of the multiple charging of the polymers.

The function principle of ESI is the following: A continuous stream of liquid passes through a capillary, which under the influence of an electric field and in atmospheric pressure produces a fine spray of charged droplets. Figure 2.4 illustrates this process. A voltage difference is applied between the capillary tip and a counter electrode which creates the required electric field that will transfer the ions into the mass analyzer. The presence of this field leads to an enrichment at the tip of the capillary of positive or negative ions depending on the direction of the electric field. This causes a destabilization of the meniscus and formation of a cone (called “Taylor cone”<sup>39</sup>). If the electric field strength is high enough, a jet of fine droplets will emerge from the Taylor cone. These droplets start to shrink due to solvent evaporation.

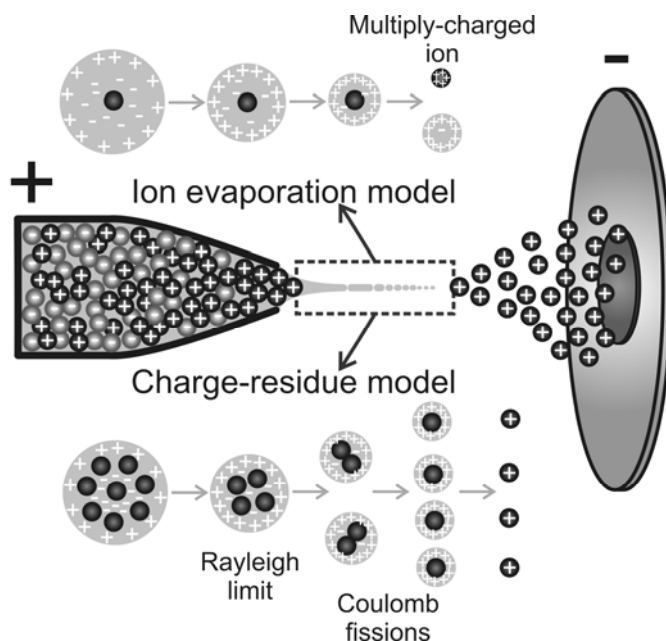


**Figure 2.4.** Schematic of the ESI process in positive ion mode and representation of the CRM (bottom) and IEM (top) models.

The mechanism by which gas-phase ions are generated from these charged droplets is not fully understood. Figure 2.4 presents the two dominating models: The Charge Residue Model (CRM) developed by Dole<sup>37</sup> and the Ion Evaporation Model (IEM) developed by Iribarne and Thomson.<sup>40,41</sup> According to CRM, as the droplets shrink, the coulombic

repulsion of the surface charges increases and when it becomes equal to the surface tension (Rayleigh stability limit<sup>42</sup>), forces the droplets to split. This process continues until the gas phases ions are formed. The IEM implies that ions are released directly into the gas phase from the droplet surface. The CRM describes better the ion formation from large molecules, whereas the IEM is more representative of the formation of ions from small molecules.

During ion formation with ESI, liquid-phase chemical and electrochemical processes are taking place. These processes will determine the abundance and nature of the formed ions. Acid-base reactions will result in the formation of protonated or deprotonated ions. Adduct formation is obtained by the interaction of neutrals and ions (*e.g.*, alkali metal ions). The formation of ions in the gas phase is also possible. Recent work of McLuckey<sup>43-46</sup> provides an overview of the ion/ion and ion/molecule interactions that can occur in the gas phase by ESI. By choosing the proper system one can optimize the MS response, charge reduction in multiply charged ions<sup>43-55</sup> and supercharging of low charge states ions.<sup>56-57</sup> Recent reviews<sup>58,59</sup> summarize the current knowledge on ESI.

### 2.3.1.3 Other API techniques

There is a plethora of API techniques<sup>59</sup> available to the mass spectrometrists but only some of them have been applied for the analysis of synthetic polymers. From these, atmospheric-pressure chemical ionization (APCI)<sup>60</sup> and atmospheric-pressure photoionization (APPI)<sup>61,62</sup> were utilized in this thesis.

APCI was commercially developed many years before ESI. It involves a gas-phase ionization process rather than the liquid-phase ionization process of ESI, as mentioned previously. The main difference from the ESI source is the presence of a corona discharge electrode that induces ionization. The technique favors the ionization of compounds which have sufficient gas phase basicity or acidity to extract or donate a proton from the solvent. Although adduct formation is possible with APCI, the main ions formed are protonated or deprotonated ions.

APPI was developed to facilitate the ionization of molecules that were not easily ionized by APCI and ESI. The principle is to use photons as a means to ionize gas-phase molecules. The setup of the APPI source is similar to APCI. The only difference is that

instead of a corona discharge that ionizes the solvent molecules (which in turn interact with the analyte molecules), in APPI, the photons ionize the analytes directly. It is a selective procedure that results in reduced background noise, since the solvent molecules are not readily ionized. However, APPI has a low efficiency because the photon sources deliver a limited amount of photons per second. From this limited amount, most photons are absorbed by the solvent molecules. This leaves only a limited number of “effective” photons that can ionize the analytes. A solution to this drawback is to use a dopant, such as toluene or acetone, in excess (the technique is called dopant-assisted APPI). APPI produces two main types of ions: the protonated molecule and the radical cation. In Chapter 3, APPI was used to investigate the presence of apolar compounds in a structurally complicated polymeric mixture.

### 2.3.2 MS Instrumentation

#### 2.3.2.1 Orthogonal accelerated time-of-flight and quadrupole time-of-flight MS

The concept of a time-of-flight (TOF) analyzer was first introduced in 1946 by Stephens.<sup>63</sup> Its operation principle is quite simple: ions of fixed energy travel along a field free flight tube. The “time-of-flight” of the ions can be linked to their  $m/z$ . This principle derives from the following rationale: An ion with mass  $m$  and total charge  $q$  ( $q=ze$ , where  $z$  the integer number of electron charges  $e$ ) is accelerated by a potential  $V$ . The potential energy  $E_{el}$  ( $E_{el}=zeV$ ) of this ion is then converted into kinetic energy  $E_{kin}$ . Based on this conversion:

$$E_{el} = ezV = \frac{1}{2}mv^2 = E_{kin} \Leftrightarrow v = \sqrt{\frac{2ezV}{m}} \quad \text{Equation 2.5}$$

Equation 2.5 shows that the velocity  $v$  of the ion is inversely proportional to the square root of its  $m/z$ . In addition, the “time-of-flight”  $t_f$  is related to the distance  $s$  that the ion needs to cover and its velocity  $v$ . Therefore,

$$t_f = \frac{s}{v} = \frac{s}{\sqrt{\frac{2ezV}{m}}} \Leftrightarrow \frac{m}{z} = \frac{2eVt_f^2}{s^2} \quad \text{Equation 2.6}$$

Equation 2.6 is the basis of the mass measurement: the  $m/z$  determination is done by measuring the time  $t_f$ . The other parameters (*i.e.*,  $V$  and  $s$ ) are defined and known.

TOF mass spectrometers are connected to the ion source in two different geometries: linear and orthogonal. Linear TOF is easily coupled with MALDI due to the pulsed nature of the source. When non-pulsed ionization methods (*e.g.*, ESI, APCI, APPI) need to be applied, an orthogonal accelerated TOF (oa-TOF) mass spectrometer is more suitable since the ions do not need to be packed prior to entrance in the flight tube. Since in this thesis, only non-pulsed ionization methods were employed, the configuration of an orthogonal accelerated quadrupole TOF (oaq-TOF) mass spectrometer is presented.

Figure 2.5 presents the main elements of a oaq-TOF mass spectrometer. Between the source and the flight tube a series of quadrupoles and hexapoles are used to focus the ion beam and performing isolation and subsequent collisional excitation of specific ions. Once the ions enter into the flight tube, a pusher gives a sharp pulse (5-10 kV) that accelerates a part of the ion beam orthogonally. Based on the TOF principle the ions of different  $m/z$  cover the distance in different times. Lighter ions (dark spheres in Figure 2.5) arrive earlier on the detector than heavier ions (grey spheres). In Figure 2.5 another important element is presented, which increased the performance and capabilities of the TOF mass spectrometers: the reflectron.<sup>64</sup> The reflectron consists of a series of grids at increasing potential that form a retarding electric field. Although the ion beam can be focussed with the use of various focus lenses and quadrupoles, the ions do not have the same direction and/or position when they enter into the flight tube. This means that during the orthogonal acceleration, ions with the same  $m/z$  have slightly different positions and velocities. The reflectron functions like a guidance system and compensates small differences in  $E_{kin}$  of the ions. These corrections substantially improve the resolving power of the TOF mass spectrometers.<sup>65</sup>

During the last years attempts to increase the resolving power of TOF mass spectrometers resulted in the construction of flight tubes with extra long flight paths<sup>66</sup>, with double reflectrons<sup>67</sup> (W shaped in place of the V shaped configuration presented in Figure 2.5) or even with “spiral” and “square” shapes.

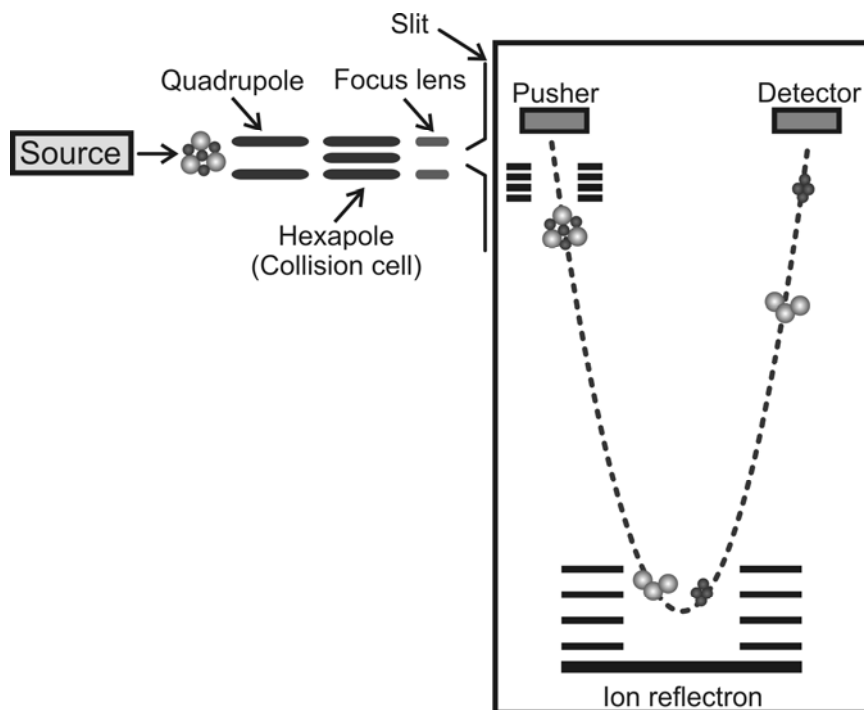


**Figure 2.5.** Illustration of a oaq-TOF mass spectrometer equipped with an ion reflectron. The principle of TOF is also demonstrated.

### 2.3.2.2 Ion trap analyzers

Ion trap analyzers are devices that are able to “trap” ions. Various ion trap analyzers were developed with differences in the geometry of the design, the way ions are confined, and of course the person who invented them. Thus, there are Paul/quadrupole (three dimensions), linear (two dimensions), cylindrical, toroidal, halo, Penning (*i.e.*, ICR), and Kingdon ion trap analyzers. In this thesis, quadrupole, linear, Penning and electrostatic (QIT, LIT, ICR and Orbitrap, respectively) ion trap analyzers were used. Therefore, only these designs will be described in more detail.

#### 2.3.2.2.1 Quadrupole ion trap

The quadrupole ion trap (QIT)<sup>68</sup> was invented by W. Paul and H. Steinwedel in 1953.<sup>69,70</sup> It is also referred to as a Paul trap. It consists of three electrodes as schematically depicted in Figure 2.6. Two of the three electrodes have the same hyperboloidal geometry

and are called end-cap electrodes. In the centre of these electrodes there are holes that allow the ions to enter the trap and be ejected towards the detector. The third electrode is a ring electrode.

The confinement of ions in these traps is achieved by two complementary actions: (1) a radiofrequency (RF) potential is applied on the ring electrode (end-cap electrodes are grounded) that oscillates sinusoidally. This creates a pseudo-potential well that confines ions in the center of the trap. (2) The ion trap is kept at relatively high pressures by the presence of helium gas. Since ions are concentrated in the center of the trap, repulsion forces expand the ion trajectories. They collide with the helium molecules, which removes the ions' excess kinetic energy by collisions (collisional cooling). Subsequently, the ions return to the center of the trap.<sup>68</sup>

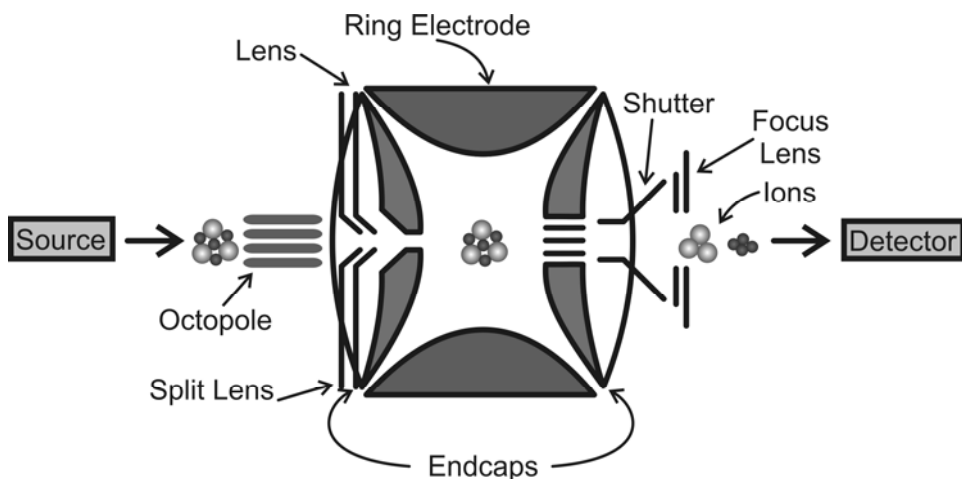


**Figure 2.6.** Illustration of a QIT mass spectrometer.

The working principle of the QIT (isolation, excitation and mass analysis) is based on creating stable trajectories for specific ions and removing unwanted ions by ejecting them outside the trap or by colliding them to the electrodes. The latter is achieved by destabilizing their trajectories. The conditions under which an ion can switch from a stable to an unstable trajectory can be described mathematically by the solutions of the Mathieu equation. These are (for positive ions):

$$\text{(DC) } a_z = \frac{-16zeU}{m(r_0^2 + 2z_0^2)\omega^2} \quad \text{and} \quad q_z = \frac{8zeV}{m(r_0^2 + 2z_0^2)\omega^2} \quad \text{(RF)}$$

These solutions (*i.e.*, values for the direct current (DC) and RF potentials) can be expressed as regions of stability and instability. Figure 2.7 depicts a diagram that shows the overlapped stability regions, based on the solutions of Mathieu's equation, for both radial  $r$  and axial  $z$  directions. This diagram is called the "stability diagram". All ions with an  $a_z$  and  $q_z$  values that bring them inside the matrix region defined by the iso- $\beta$  lines will have stable trajectories and can be confined inside the traps. All ions that fall outside this region will have unstable trajectories. In Figure 2.7 a specific point is marked. It is the point that defines the ion of the lowest  $m/z$  that can be trapped. This point is called the low mass cut-off.

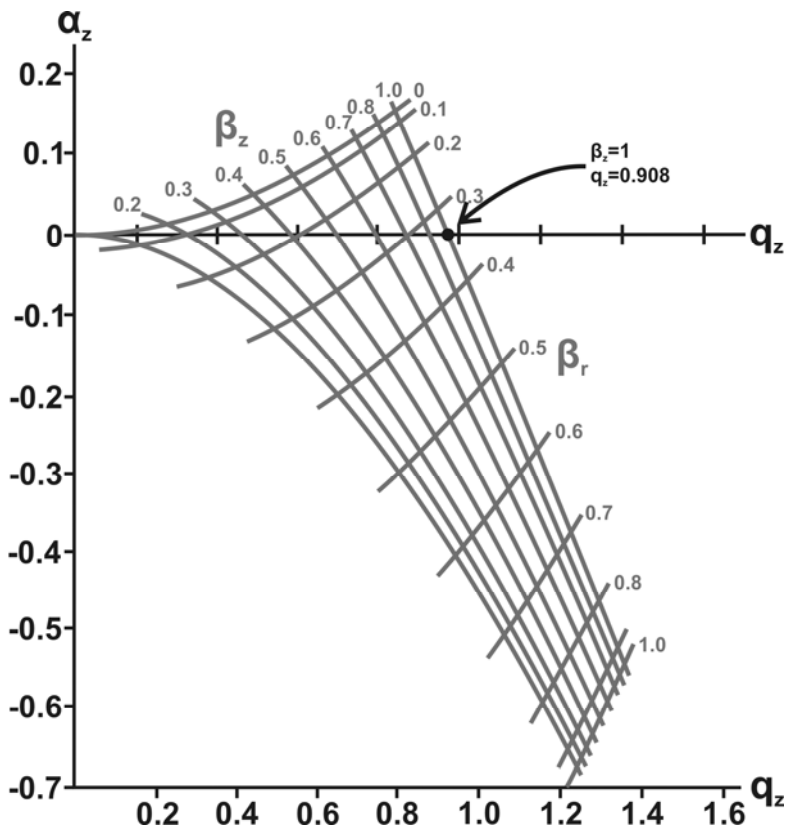
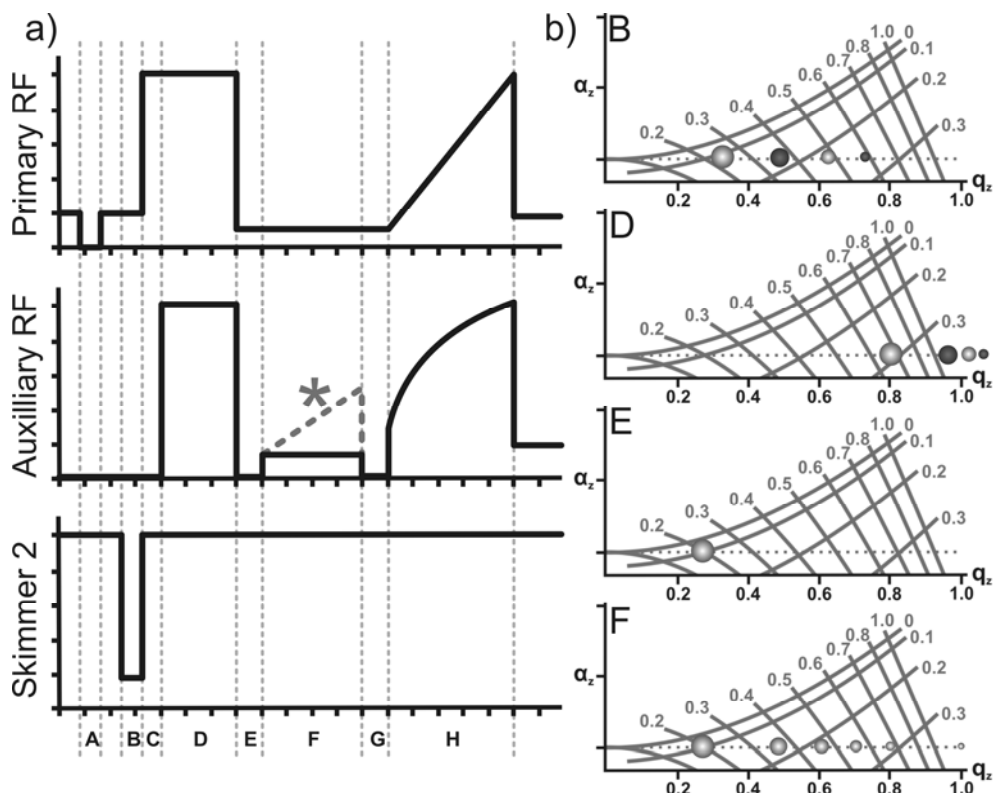


Figure 2.7. Stability diagram for the QIT.

Based on the stability diagram, the MS/MS scan sequence in a QIT as presented in Figure 2.8 can be described in detail as follows:

- Step A: Quench of the trap.
- Step B: Ion accumulation by dropping the repelling voltage on vacuum partition (Skimmer 2) to allow the ions to enter the trap. The ions are then confined and follow specific trajectories based on their  $m/z$  (see Figure 2.8, Upper right panel).
- Step C: Thermalization delay.
- Step D: Precursor ion isolation by destabilizing the trajectories of all ions that are unwanted (ions fall outside the stability diagram as shown in Figure 2.8, second from the top right panel).
- Step E: Delay period before fragmentation, where the precursor ion can return to the center of the trap by collisional cooling and the quadrupolar field.
- Step F: Fragmentation by increasing the energy of the ion by resonance excitation with the dipole field. This can be performed in two ways: stable or ramped (see grey section indicated with an asterisk in Figure 2.8) excitation.
- Step G: Delay period before mass analysis.
- Step H: Mass analysis by destabilizing the ions by starting from low to high  $m/z$ .



**Figure 2.8.** MS/MS scan sequence in a QIT: a) Steps of the sequence along with the function of the instrument, and b) MS/MS major events in the stability diagram. Note: Explanation of the stages is made in the text. Asterisk “\*” indicates an alternative excitation step, where the collision energy is ramped between two values.

### 2.3.2.2.2 Linear ion trap

A LIT consists of four parallel hyperbolic shaped rods that create a quadrupolar field and lenses at both ends of the electrodes that redirect approaching ions along the centered axis of the trap. The ions are trapped in the radial dimension by the quadrupole field and in the axial dimension by the electric field created by the lenses. A simple schematic of a LIT is shown in Figure 2.9. LIT has two major advantages over a QIT: ion trapping capacity and sensitivity. The number of ions that can be trapped is ten times higher than in the QIT, because of the greater volume of the trap and the fact that the ions are not focused at a central point but in a line along the electrodes. These two characteristics result in a larger pilling capacity before space charge effects occur. In addition, LIT has a trapping efficiency

of 50% whereas a QIT only 5%.<sup>31</sup> The other advantage is that the ejection of ions occurs in the radial directions. Two ion exit slots placed opposite each other feed two detectors. In this way sensitivity is maximized.

The way a LIT is working is in general terms the same as a QIT. Therefore detailed explanation of the MS/MS sequence will not be explained. A recent review by Douglas *et al.*<sup>71</sup> provides detailed information.

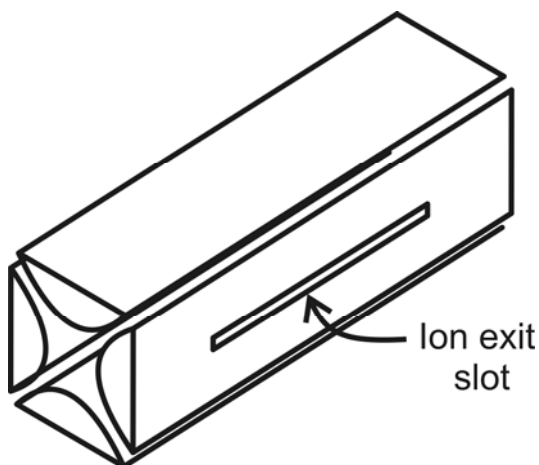


**Figure 2.9.** Illustration of a LIT.

#### 2.3.2.2.3 Hybrid MS instruments

Different types of mass analyzer can be combined together to form hybrid MS instruments. It is obvious that the reason behind the construction of a hybrid mass spectrometer is to combine the advantageous characteristics of each of the individual mass analyzer. The first hybrid mass spectrometers were sector instruments such as a  $BqQ$ ,<sup>72</sup>  $EBqQ$ ,<sup>73</sup> or  $BeqQ$ .<sup>74</sup> The last decade numerous other hybrids have been constructed such as  $q$ -TOF,  $q$ -ICR, QIT-TOF,<sup>75</sup> LIT-ICR, and LIT-Orbitrap. In this thesis, three hybrid MS instruments were used. The first, an  $oaq$ -TOF mass spectrometer was described in Paragraph 2.3.2.1. The other two were based on the combination of an LIT (to perform  $MS^n$  experiments) with an Orbitrap, or a Fourier-transform ion cyclotron resonance (FT-ICR) mass analyzer. These were used to perform accurate mass MS and  $MS^n$  experiments and

high resolution MS analysis. Their description will focus only on the parts of the instruments not mentioned before (*i.e.*, Orbitrap, and FT-ICR).

The Orbitrap is an electrostatic ion trap that was developed recently by A. Makarov.<sup>76</sup> It is a modification of the ion trap developed by Kingdon in the 1920's.<sup>77</sup> It consists of a barrel shape electrode cut in two parts and a central spindle shape electrode (Figure 2.10). The ions enter off-axis into the trap through a small hole in the external electrode. An electrostatic voltage is applied to the inner electrode while the outer electrodes are at ground potential. The electrostatic field created forces the ions to oscillate in intricate spirals around the inner electrode (see Figure 2.10a). The frequency at which ions oscillate is related to their  $m/z$ . This is illustrated in Figure 2.10b, where the trajectories of ions with different  $m/z$  are presented. This convoluted oscillation induces an image charge which is measured and converted by a FT to the individual frequencies and intensities, producing a mass spectrum. The power of the Orbitrap is based on the gradual insertion of ions of different  $m/z$ . In this way, an efficient grouping of the ions is achieved, reducing any space charge effects. The movement of the ions with the same  $m/z$  will be very coherent which results in high mass accuracy and, to a certain extent, also resolution. More detailed information can be found elsewhere.<sup>78</sup>

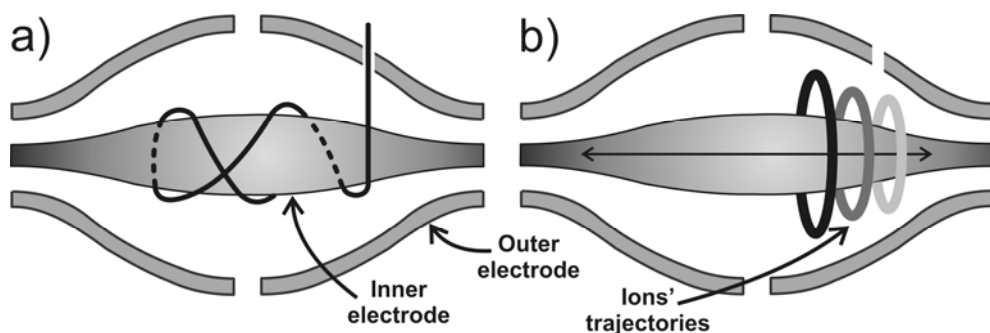


**Figure 2.10.** Function principle of an Orbitrap mass analyzer. Left panel illustrates the trajectory of the ions around the inner electrode. Right panel shows the principle of mass analysis, where ions with different  $m/z$  have a different trajectory and oscillation frequency.

The physical principle behind the modern ICR mass spectrometers was introduced in the 1930s by E.O. Lawrence,<sup>79</sup> but it was only after the second world war that H. Sommer presented the first application of ICR to MS.<sup>80</sup> The function principle of the cyclotron is

that ion trajectories are curved in a magnetic field. Low ion radial velocity combined with intense field can force the ion in a circular trajectory inside the magnetic field.

Some decades later M.B Comisarow and A.G. Marshal initiated the major breakthrough by introducing FT algorithms for deconvolution of the measured superposition of the image currents of ions with different masses.<sup>81-83</sup> The function principle is based on simultaneous excitation of all ions in the ICR cell in a very short period of time. The applied excitation forces all ions to start in phase and to move in a circular trajectory close to the cell walls. Ions of each mass have their own characteristic cyclotron frequency and every time they pass close to the detection plates they induce an image current, which is recorded as a time domain signal. The present state-of-the-art FT-ICR mass analyzers have great capabilities. MS/MS experiments can be performed, sensitivity is so high that even ten ions of multiple charges can be detected in the cell, and the resolution (above 1,000,000) and accuracy (ppb level) are the highest achieved compared to other MS instruments.<sup>84-85</sup>

Figure 2.11 presents the FT-ICR function principle. Figure 2.11a depicts the ICR cell which is the heart of the FT-ICR-MS. Various ICR designs have been developed; the one presented is a closed cylindrical cell. The ICR cell is placed in the center of a superconducting magnet (magnetic fields can range from 1 to 15 T, although magnets with 21 and 25 T fields are also used<sup>86</sup>). The cell consists of six plates: two trapping plates, two detection plates and two excitation plates. As mentioned before, ions that enter into the cell follow a circular motion under the influence of the magnetic field. The trapping plates make sure that ions are confined inside the cell while the other four plates perform the ion excitation and detection.

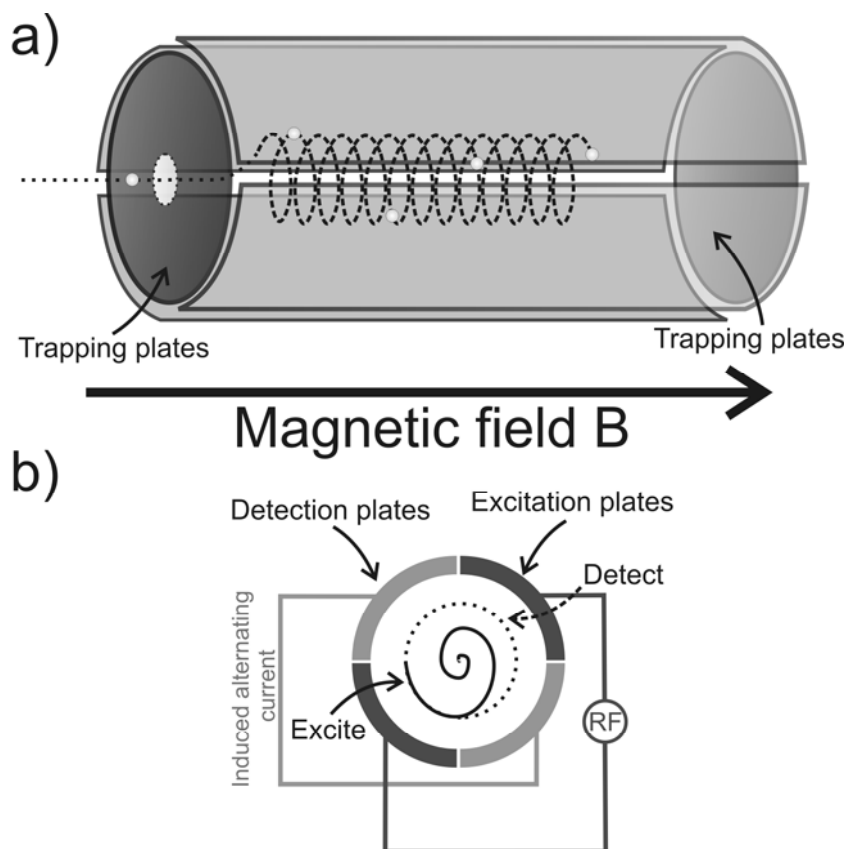


**Figure 2.11.** Illustration of a closed cylindrical cell in an FT-ICR mass spectrometer: a) The trajectory of the ion inside the ICR cell, b) Configuration of the excitation and detection plates.

## 2.4 Polymer characterization by MS: Applications

### 2.4.1 Introduction

As presented in Chart 2.1, information about the polymer is distributed in various levels of detail: From polymer size to detailed structural characterization. MS is a tool that can provide information for most of the levels to some extent, especially for homopolymers, because their structural complexity is minimal. End-group differences can be easily differentiated from the mass spectra, as long as their elemental composition is not the same or equal to the one of the monomer units. HR-MS can still discriminate between end-group with the same nominal mass.<sup>23</sup> In addition MS/MS can provide end-group information even

for isomeric polymers (if the two end-groups have different elemental composition).<sup>88,89</sup> On the other hand, structurally complicated polymeric systems require the additional support of other techniques such as LC.<sup>90-92</sup>

LC-MS/MS<sup>n</sup> is a helpful tool in the analysis of structurally complicated mixtures when there are isomeric structures present and/or the polymer sample is a mixture of numerous components. In the first case, separation of isomers can be achieved according to their functionality and confirmed by MS.<sup>93</sup> For the case of structurally complicated mixtures, LC-MS/MS<sup>n</sup> does not suffer from the problem of ion suppression (common in MS) and diverse ionization efficiencies of the components. In a direct-infusion (DI) experiments, the ionization process of the polymers is related to their concentration, affinity to the cation and stability. It is very common that even when a polymer with high ionization efficiency, such as poly(ethyleneglycols) (PEGs) is present in traces, it can suppress the signal created by molecules with low ionization efficiency. By allowing a gradual elution of the separated components into the source, the competition between the individual components is greatly reduced. This results to a more comprehensive analysis of all components found in a polymer sample.

#### ***2.4.2 LC-MS and MS<sup>n</sup> analysis of homopolymers***

An example of the added value of using hyphenated techniques instead of MS (only) is demonstrated below in the case of a mixture of polymers after the ethoxylation of a fatty acid mixture.<sup>93</sup> Figure 2.12 depicts a comparison of the mass spectra obtained after DI-MS and after LC-MS using a QIT.

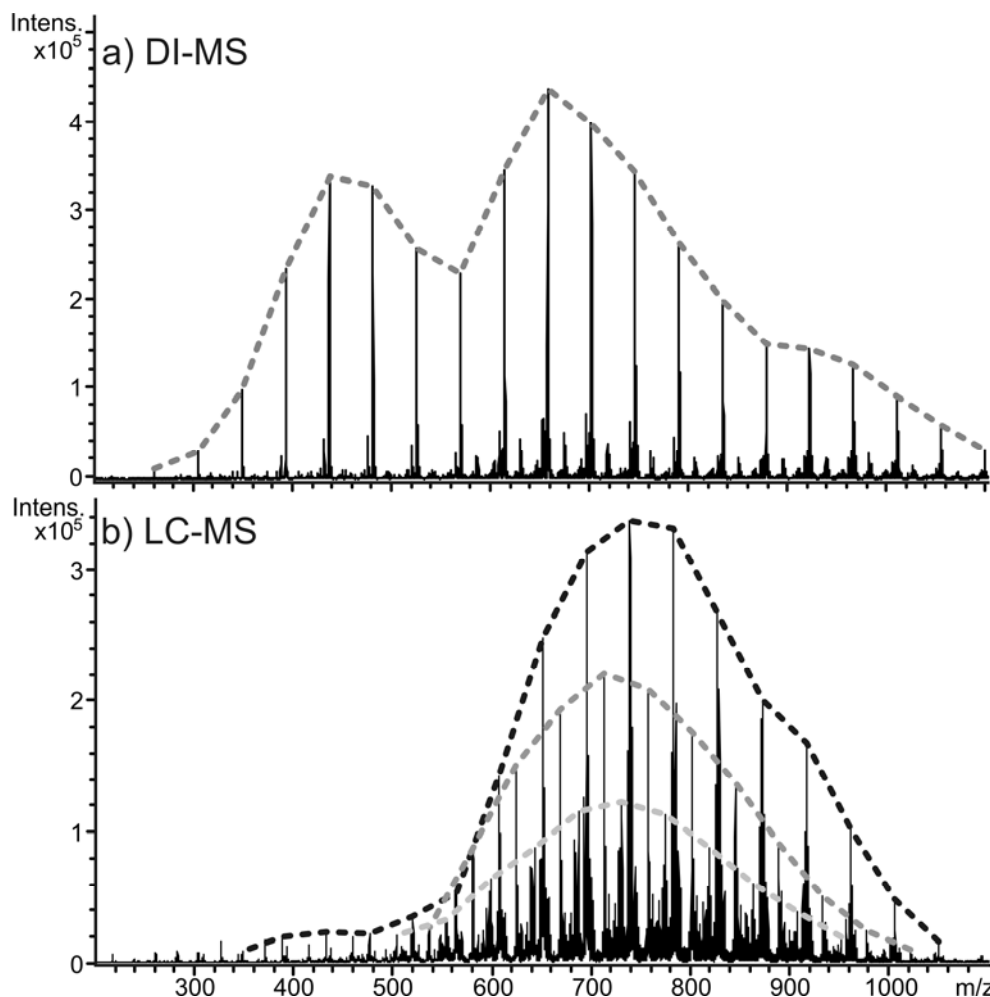


**Figure 2.12.** Mass spectra of a fatty acid ethoxylate (FAE) with: a) DI-MS, and b) after LC-MS in a QIT (summation of the whole chromatogram). Note: Both figures are after summation of the same number of mass spectra.

As expected, DI-MS (Figure 2.12a) results in a simple mass spectrum where one intense (seemingly) bimodal distribution is observed. This bimodal appearance of the distribution indicates that there could be two different distributions that overlap. The nominal mass of the peaks of the distribution suggests that the ions detected are sodium cationized PEGs. Based on the initial information that this is a FAE, one can suggest that the distribution could be also a PEG ester of oleic acid (Ole)  $[\text{Ole-PEG}_n+\text{Na}]^+$ . Oleic acid has the same

nominal mass as PEG<sub>6</sub> (*i.e.*, 282 Da) but a different exact mass. A [Ole-PEG<sub>3</sub>+Na]<sup>+</sup> has an exact mass of 437.3243u, whereas a [PEG<sub>9</sub>+Na]<sup>+</sup> 437.2363u. This mass difference cannot be resolved in a QIT due to its low resolving power (R=500). A resolving power of approximately 5,000 is needed at *m/z* 437. This is a typical resolving power of a standard TOF mass spectrometer. The mass spectrum of the same compound after summation of the whole LC-MS chromatogram trace (Figure 2.12b) has a totally different profile. Multiple distributions have been identified (in Figure 2.12b only the three major distributions are highlighted) which were not detected in DI-MSn. In addition, the intensity of the peaks in the low-mass region (*viz.* 200-500 Da) is lower than in the mass spectrum obtained by DI-MS. This clearly demonstrates that ion suppression plays a key role in the resulting mass spectrum. PEG oligomers ionize readily and suppress the signal of the larger and more structurally complicated ethoxylated components. Figure 2.13 depicts the base peak chromatogram (BPC) of FAE after LC-MS. The extracted ion chromatograms (EICs) of the oligomers with the same degree of polymerization but different end-groups are also shown.

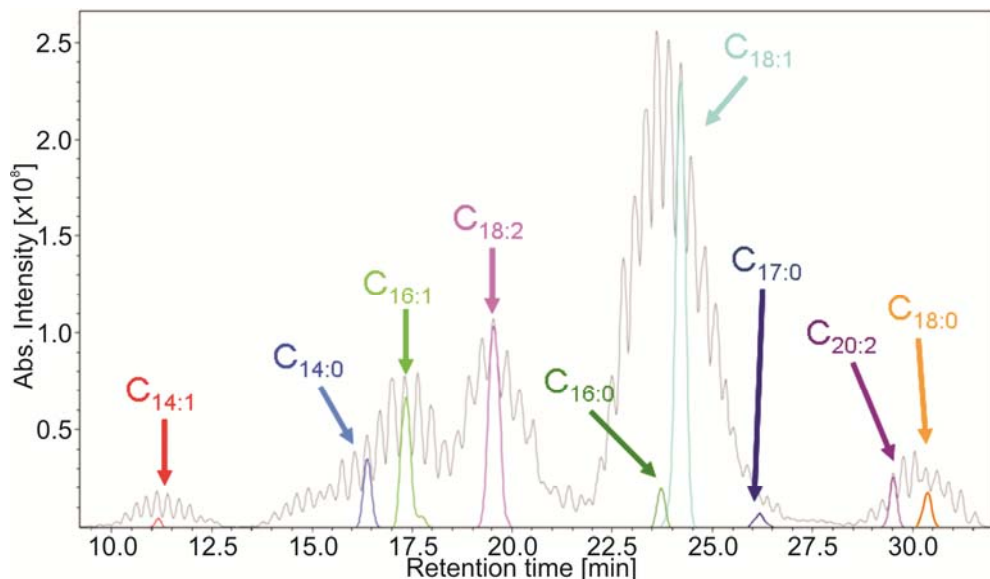


**Figure 2.13.** BPC of FAE after LC-MS. The highlighted peaks are EICs of selected FAE components. Note: The notation indicates the type of end-group (First number is the number of carbon atoms and the second the number of double bonds in the fatty acid chain).

The separation of the FAE oligomers is influenced by two different parameters: the fatty acid chain length and the degree of unsaturation. Short fatty acid chains elute faster since there are less hydrophobic than the larger chains. In addition, fatty acid chains with higher degree of unsaturation elute also faster than chains with fewer double bonds. A variety of common (*e.g.*, oleic, linoleic and stearic) fatty acid end-groups is observed as well as some rare ones such as margaric ( $C_{17:0}$ ) and eicosadienoic acid ( $C_{20:2}$ ). PEG-margarate has such a low intensity that it would have been difficult to detect it in a DI-MS experiment. Also, PEG-margarate oligomers have the same nominal mass as oligomers with a  $C_{14:1}$  chain. Figure 2.14 presents the discrimination of these two nominally isobaric peaks by LC-MS/MS.

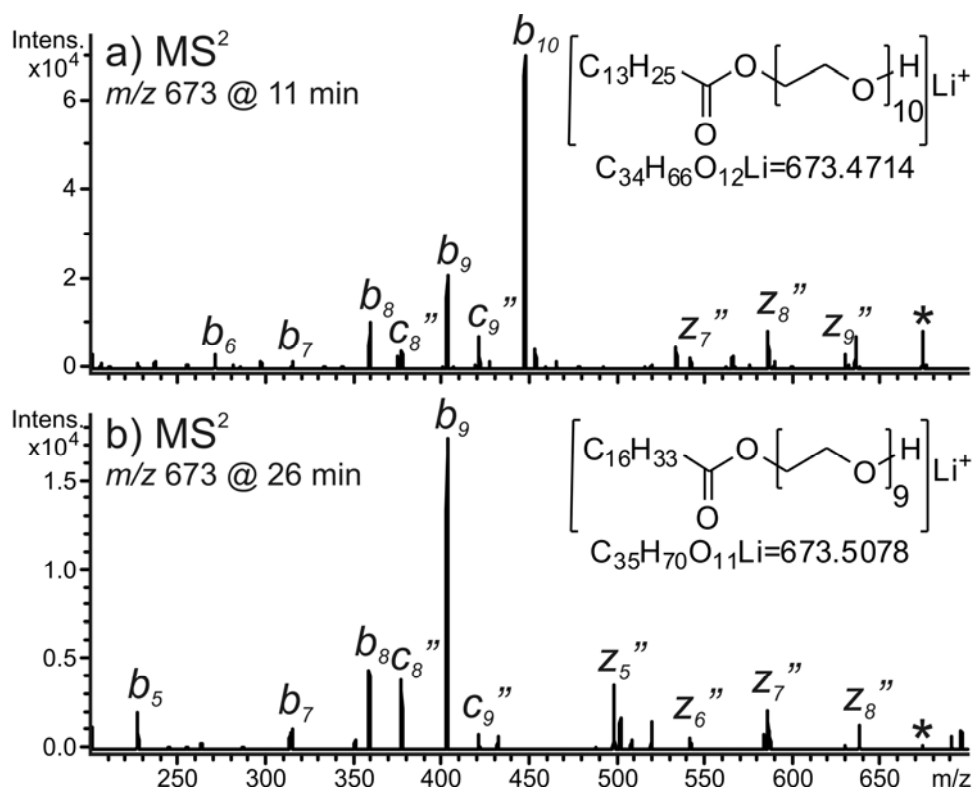


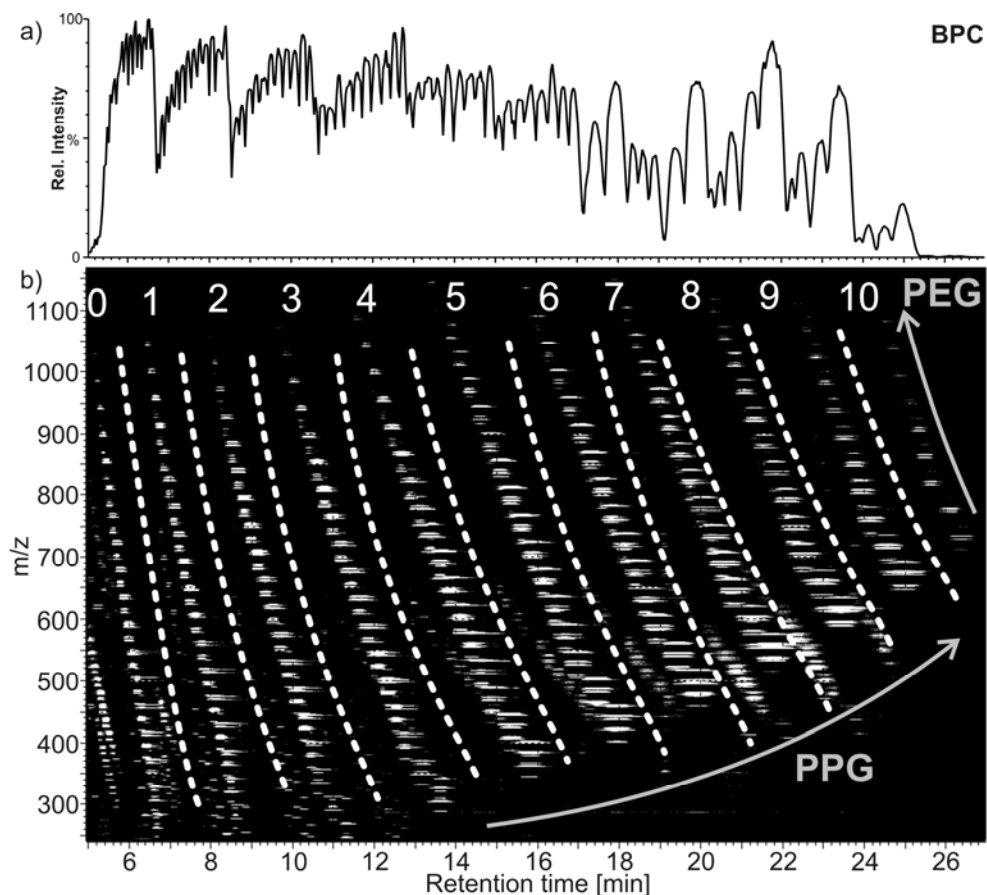
**Figure 2.14.** Product ion mass spectra of two FAE nominally isobaric components with  $m/z$  at 673: the product ion mass spectrum of the peak eluting at a) 11 min, and b) 26 min. Note: Asterisk “\*” indicates the precursor ion. Fragmentation nomenclature is explained in chapter 8.

### 2.4.3 LC-MS<sup>n</sup> analysis of copolymers

When structurally complicated copolymers need to be analyzed by MS, the major challenge is the discrimination of the copolymer isomers. The main question is: What kind of a copolymer is it? A random or a block copolymer?

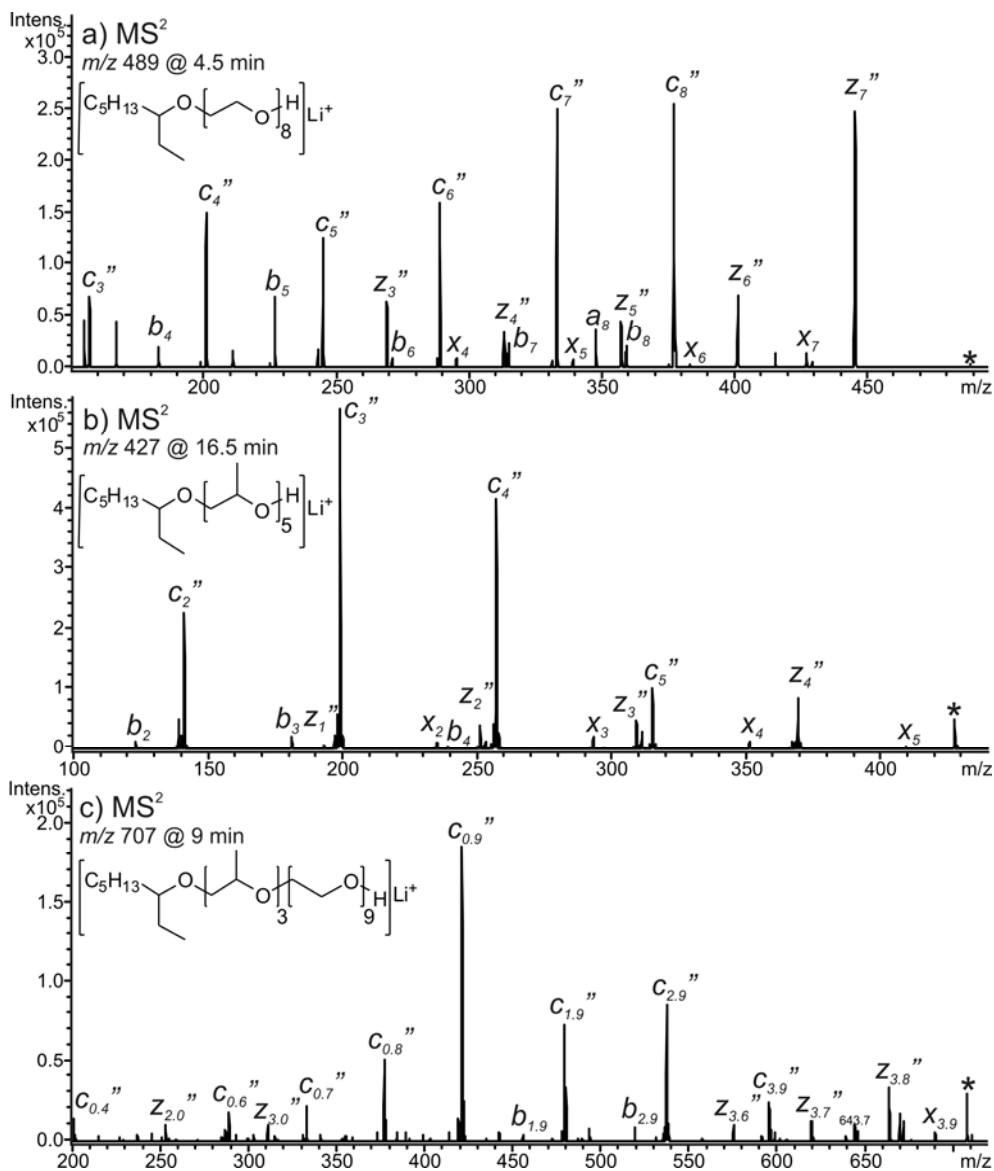
It is certain that MS alone, even of the highest resolving power, will not be able to distinguish between a block and a random copolymer solely based on the exact mass measurement. Although MS<sup>n</sup> experiments could confirm the blocky nature of a block copolymer, they can not easily discriminate between a block and random copolymer. LC can provide separation in one dimension and simplify in some extent the complicated task.

Figure 2.15 depicts the LC-MS separation of a PEG-poly(propylene glycol) (PPG) copolymer of unknown sequence distribution.<sup>93</sup> The BPC (Figure 2.15a) demonstrates the complexity of the copolymer sample, but it does not provide any detailed information about its composition. The contour plot (Figure 2.15b), however, does provide a detailed (three-dimensional) presentation of the copolymer's composition in a two-dimensional figure: a) retention time (horizontal axis), b)  $m/z$  (vertical axis), and c) intensity (grey color intensity of the points). In addition, it shows that the chromatographic behavior of the copolymer is strongly influenced by the number of hydrophobic PPG monomer units. The influence of PEG monomer units, which are also present in the copolymer, on the separation is significantly weaker. Based on this chromatographic separation, the various components are adequately resolved. Performing MS/MS experiments, confirmation of the various structures can be achieved.



**Figure 2.15.** LC-TOF-MS analysis of a PEG/PPG copolymer: a) the BPC and b) the contour plot. The horizontal axis represents the retention time and the vertical the  $m/z$ . White dotted lines separate the various distributions based on the number of PPG units (number indicated at the top of each distribution) in the copolymer.

Figure 2.16 depicts the product ion mass spectra of three different components present in the sample: a PEG and PPG homopolymer and their copolymer. Figure 2.16a shows that the PEG homopolymer has 2-ethyl-hexanol as an end-group. The same applies also for the PPG homopolymer at Figure 2.16b. The MS/MS experiment of the copolymer (Figure 2.16c) confirms the blocky structure. The product ions follow a blocky sequence: (1) neutral loss of the end-group ( $c_{3,9}''$ ), (2) followed by neutral losses of PPG monomer units (product ions  $c_{2,9}''$ ,  $c_{1,9}''$ , and  $c_{0,9}''$ ), and (3) followed by neutral losses of PEG monomer units (product ions  $c_{0,8}''$ ,  $c_{0,7}''$ ,  $c_{0,6}''$ , and  $c_{0,4}''$ ).



**Figure 2.16.** Product ion mass spectra of three components of the PEG-*block*-PPG copolymer: product ion mass spectrum of the peak eluting at a) 4.5 min (PEG homopolymer), b) 16.5 min (PPG homopolymer), and c) 9 min (PEG-*block*-PPG copolymer). **Note:** Asterisk “\*” indicates the precursor ion. Fragmentation nomenclature is explained in Chapter 8. The two subscripted numbers indicate the number of PPG and PEG monomer units, respectively.

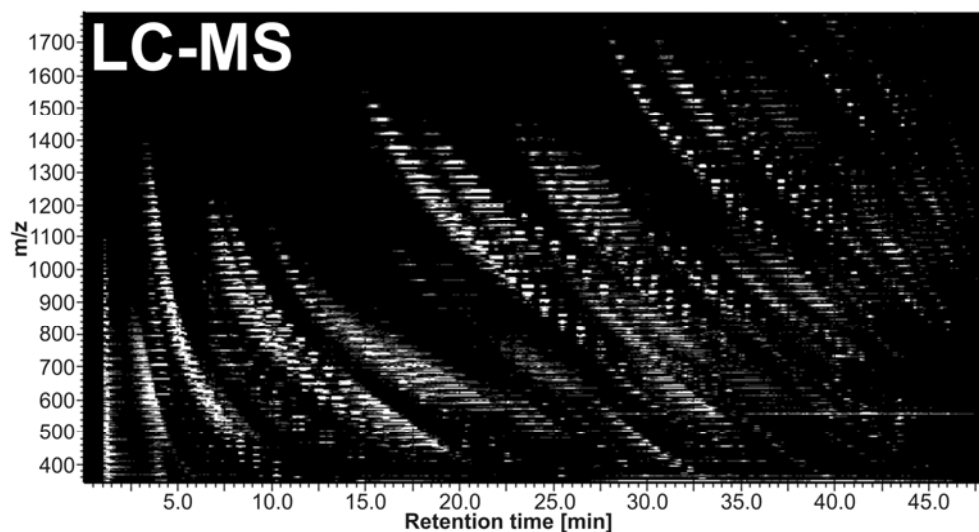
#### **2.4.4 Outlook**

The analysis of structurally complicated mixtures of polymers and copolymers is greatly facilitated with the use of hyphenated techniques. The chromatographic separation allows the distinction between the different mixture components based on their end-group or copolymer composition. In addition, ion suppression effects are greatly reduced and a more accurate representation of the sample is obtained in a single LC-MS run. This simplification and lack of ion suppression permits their analysis with conventional MS instruments of low resolving power (*e.g.*, QIT). Information about the end-group (*e.g.*, starting material), the polymerization process (*e.g.*, type of monomers used, block or random copolymerization, etc) and the MMD is generated. LC-MS/MS experiments provide a more detailed structural characterization and a confirmation of the various structures. Nevertheless, there are still a lot of areas that can be studied and approaches to be tested. LC-MS<sup>n</sup> has been extensively used in the analysis of biopolymers (*e.g.*, proteins and peptides), since it can provide detailed proteome sequence information in a single run. In addition, performing the same analysis in different ion modes and ionization techniques allows the increase in the amount of information that can be obtained. Chapter 3 investigates some of these methodologies for the analysis of structurally complicated synthetic polymeric systems.



# 3

## Determination of the Polymerization Products of Ethoxylation of Castor Oil by Liquid Chromatography Multistage Mass Spectrometry



The polymerization products of ethoxylation of castor oil were studied by liquid chromatography (LC) quadrupole ion trap multistage mass spectrometry ( $MS^n$ ) and LC time-of-flight MS. The developed LC method allowed the separation of the polymerization products, and especially, the baseline separation of nominal isobars and isomers.  $MS^n$  was used for the structure elucidation of various structures. Different ionization modes, ionization techniques and adduct ions were also tested for optimization of the MS detection and  $MS^n$  fragmentation. A unique fragmentation pathway of ricinoleic acid is proposed, which can be used as a marker of the polymerization process and the group selectivity of ethoxylation of castor oil. In addition, characteristic neutral losses of ricinoleic acid reveal its (terminal or internal) position in the molecule.

**Nasioudis, A.; van Velde, J. W.; Heeren, R. M. A.; van den Brink, O. F. submitted**

### 3.1 Introduction

Non-ionic surfactants are widely used in the polymer industry, because they exhibit a versatility that allows the custom synthesis of polymers with specific physicochemical properties. Among the non-ionic surfactants commercially available, castor oil ethoxylate (CASEO) has found an extensive use in the pharmaceutical industry as a component of drug delivery systems. It is produced by the ethoxylation of castor oil, a natural oil rich in ricinoleic acid. As any other natural oil, castor oil is a mixture of different mono-, di-, and triacylglycerols and fatty acids which can all be polymerized. Thus, the end product is a mixture of different polymeric structures. The use of these materials in the pharmaceutical sector requires a complete determination of its polymeric components. Besides the regulatory issues, a comprehensive analysis will also facilitate a further understanding of the polymerization processes that facilitates the design of custom made products.

Among the analytical techniques available for the analysis of non-ionic surfactants, mass spectrometry (MS) has had a prominent position as a preferred tool in the last two decades. MS can provide detailed information about the end-group,<sup>22,23,89,94</sup> the average molar mass (to some extent)<sup>95</sup> and the copolymer distribution.<sup>87,96,97</sup> Lattimer *et al.*<sup>98-99</sup> paved the way for the analysis of non-ionic surfactants by studying simple polyether systems by fast atom bombardment. Studies with electrospray ionization (ESI) and matrix-assisted laser desorption/ionization (MALDI) combined with collision-induced dissociation (CID) followed, showing that detailed structure information of the polyethers can be obtained.<sup>88,97,100-105</sup> Since most of the non-ionic surfactants are mixtures, the coupling of high-performance liquid chromatography (HPLC) with its various modes (*e.g.*, reverse-phase, normal-phase, critical conditions) to MS was the next logical step.<sup>92,93,106</sup> By careful selection of the chromatographic conditions the separation of the non-ionic surfactant components was made according to the end-group<sup>92,93</sup> or the copolymer distribution.<sup>93</sup> Examples of these analyses were presented in the previous chapter (Chapter 2).

Although the MS analysis of the majority of the commercially available non-ionic surfactants has been demonstrated extensively, there are only limited reports in the analysis of CASEO. To the best of our knowledge, Meyer *et al.*<sup>107-109</sup> was the only group that used MS for the analysis of CASEO. They developed two different techniques for the analysis of

CASEO: (1) separation of the mixture to a hydrophilic and hydrophobic fraction and consecutive MS analysis by using statistical approaches,<sup>107</sup> and (2) a cyclodextrin-modified micellar electrokinetic capillary chromatography method (developed in an earlier stage<sup>110</sup>) combined with delayed-extraction MALDI time-of flight (TOF) MS using a fractionating robot.<sup>108,109</sup> These techniques allowed a more detailed analysis of the CASEO mixture, after the initial identification approach of Müller back in 1966.<sup>111</sup> Although successful, the developed methods require complicated instrumentation, robotic systems and statistical processing and are not ideal for routine analysis.

The aim of this chapter is to show: (1) the development of a simple and straightforward method for the analysis of CASEO that requires only standard MS instrumentation, and (2) the identification of the polymerization products after the ethoxylation of castor oil. Since CASEO samples have a heterogeneous composition, MS will be combined with HPLC. The use of multistage mass spectrometry (MS<sup>n</sup>) is also investigated as a tool for detailed structural analysis of the various components.

## **3.2 Experimental section**

### **3.2.1 Chemicals**

Commercially available CASEOs with different degrees of polymerization were kindly donated by Joke Speelman (AkzoNobel Surface Chemistry, The Netherlands). Sodium iodide (NaI) and ammonium chloride (NH<sub>4</sub>Cl) were from J.T. Baker (Deventer, Netherlands). Lithium chloride (LiCl) and formic acid (FA) were purchased from Fluka (Buchs, Switzerland). Tetrahydrofuran (THF) was of HPLC-grade (Sigma-Aldrich, Germany). Ultra-pure water with a resistivity of 18.2 MΩ·cm (at 25 °C) was obtained from a Millipore Direct-Q 3 (Molsheim, France) water purification system. All reagents and solvents were used without further purification.

### **3.2.2 Instrumentation**

HPLC was carried out using an Agilent 1100 series HPLC system (Palo Alto, CA) equipped with a binary pump and controlled by the Agilent Chemstation software for LC systems. Chromatographic separation was performed on an Alltech Kromasil C<sub>18</sub> column (5

$\mu\text{m}$  particle size, 4.6x150 mm). A gradient solvent system, specified in Table 3.1, was used at a flow rate of 1 mL/min. The appropriate salt solution ( $\sim 400 \mu\text{g/mL}$ ) was mixed with the LC effluent post-column with a Cole-Palmer syringe pump (Vernon Hills, IL) at a flow rate of 10  $\mu\text{L/min}$ .

**Table 3.1. Composition of the HPLC Gradient Elution System**

Time [min]	H <sub>2</sub> O + 0.1 % FA <sup>a</sup> [%]	THF + 0.1 % FA <sup>a</sup> [%]
0	60	40
2	55	45
14	50	50
38	30	70
44	20	80
50	0	100
52	0	100
54	60	40
56	60	40

<sup>a</sup>The use of FA was shown to improve the chromatographic separation

The mixed effluent was introduced to a Bruker Esquire 3000<sup>plus</sup> quadrupole ion trap (QIT) mass spectrometer (Bruker Daltonics, Bremen, Germany) or a Waters LCT TOF mass spectrometer (Micromass, Manchester, UK), both equipped with an ESI source. MS<sup>n</sup> experiments were performed in the QIT. The ESI-MS, the isolation and collision-induced dissociation conditions were optimized for each precursor ion studied aiming for a high abundance of precursor ion and effective formation of product ions. Accurate mass measurements and accurate mass MS/MS experiments were performed with an LTQ Orbitrap XL (Thermo Scientific, San Jose, CA).

### 3.3 Results and discussion

#### 3.3.1 LC-MS(+) analysis of CASEO

Figure 3.1 shows a contour plot of the mass-to-charge ratio ( $m/z$ ) versus the retention time of a CASEO sample obtained by LC-ESI-TOF-MS. The long analysis time (48 min) allowed the baseline separation of a great variety of components. For reasons of clarity and easy processing, the contour plot has been separated in sectors (labeled A to W). The identified distributions of each sector are presented in Table 3.2.

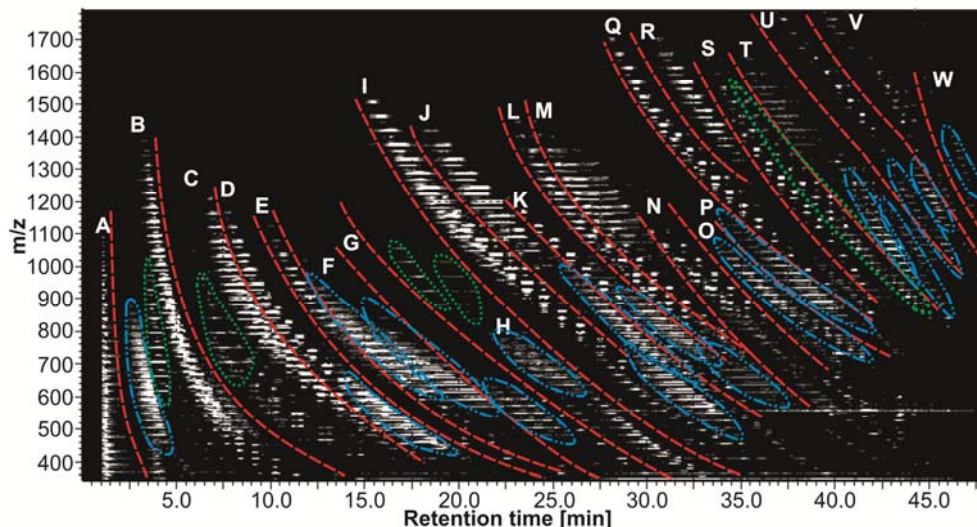
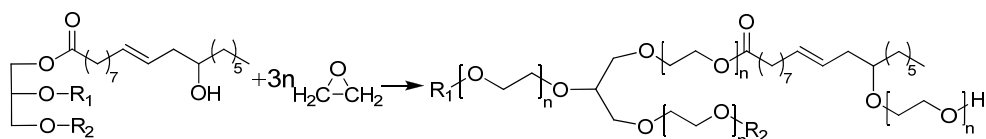


**Figure 3.1.** Contour plot of the LC-ESI-TOF-MS analysis of a CASEO. Note: Red dotted lines separate the sector areas indicated by capital letters. Blue dotted areas are doubly charged ions and green dotted areas fragment ions of specific distributions.

**Table 3.2. List of Components of the LC-ESI-TOF-MS Analysis (per sector)**

Sector	Component Type
A	PEG, Glycerol PEG
B	Glycerol PEG monoricinoleate, PEG monoricinoleate
C	Glycerol PEG monolinoleate, PEG monolinoleate
D	Glycerol PEG monooleate, PEG monooleate
E	Glycerol PEG monostearate, PEG monostearate
F	Doubly charged distributions of sector I and J
G	Doubly charged distributions
H	Doubly charged distributions
I	Glycerol PEG diricinoleate, Glycerol PEG dioleate or PEG diricinoleate-monolinoleate
J	Isomer of Glycerol PEG diricinoleate
K	Glycerol PEG dioleate or Isomer of PEG diricinoleate-monolinoleate
L	Isomer of Glycerol PEG monoricinoleate-monolinoleate , PEG monoricinoleate-monooleate
M	Glycerol PEG monoricinoleate-monooleate (+ its isomer), PEG monoricinoleate-monolinoleate, PEG monoricinoleate-monostearate
N	Isomer of PEG monoricinoleate-monolinoleate , Isomer of PEG monoricinoleate-monooleate , Isomer of PEG monoricinoleate-monostearate
O	Doubly charged distributions
P	Doubly charged distributions
Q	Glycerol PEG triricinoleate, PEG triricinoleate
R	Isomer of Glycerol PEG triricinoleate
S	Isomer of PEG triricinoleate
T	Doubly charged distributions of sector U
U	Glycerol PEG triricinoleate, PEG tetrarinoleate, Doubly charged distributions
V	Isomer of Glycerol PEG triricinoleate, Isomer of PEG tetrarinoleate , Doubly charged distributions
W	Doubly charged distribution

In short, the main polymerization products detected are in agreement with previous studies<sup>108-110</sup> and Scheme 3.1. These are: (1) poly(ethylene glycol) (PEG), (2) glycerol PEG (G-PEG), (3) various fatty acid (*e.g.*, ricinoleic, linoleic, oleic, and stearic acid) ester ethoxylates (Ric/Lin/Ole/Ste-PEG, where Ric/Lin/Ole/Ste are abbreviations of the above mentioned fatty acids, respectively), (4) G-PEG mono-, di- and tri-Ric/Lin/Ole/Ste (G-PEG-Ric<sub>W</sub>/Lin<sub>X</sub>/Ole<sub>Y</sub>/Ste<sub>Z</sub>, where W, X, Y, Z = 0, 1, 2 or 3 and W+X+Y+Z = 3).



**Scheme 3.1.** Ethoxylation of castor oil. Note: For the sake of clarity, the ethoxylation process of a triglyceride with at least one ricinoleic acid is shown. R<sub>1</sub> and R<sub>2</sub> can be either ricinoleic, linoleic, oleic, stearic, and/or didehydrostearic acid.

The PEG ester of didehydrostearic acid (DHSTE-PEG) (9,11-octadecadienoic acid), observed by Meyer *et al.*,<sup>110</sup> cannot be distinguished from its isomer Lin-PEG by MS. Therefore the distinction of Lin-PEG from DHSTE-PEG cannot be confirmed by LC-MS. MS/MS could potentially discriminate between these two structures, but this was not achieved in this work. Besides the main products, multiple unknown distributions have also been detected. Some have the same *m/z* or nominal mass with some of the main products or with each other. The presence of isomers is expected because the position of the fatty acids in the acylglycerols varies between the three possible positions. In addition the presence of nominal isobars is expected because some pairs of structures have the same nominal mass (*e.g.*, oleic acid and PEG hexamer [*i.e.*, 282 Da] and G-PEG<sub>n</sub>-Lin and PEG<sub>n+2</sub>-Ste [*i.e.*, 372+n44 Da]).

### 3.3.2 LC-MS(-) analysis of CASEO

To characterize some of these distributions the LC-MS analysis was repeated in the negative ion mode. Figure 3.2 depicts the LC-MS base peak chromatograms (BPC) in positive and negative ion mode obtained in a QIT mass spectrometer. The chromatographic profile in negative ion mode has similarities with the one in positive ion mode. The signal intensity, however, is reduced. This is expected since polyethers do not ionize efficiently in

negative mode. The BPC in negative ion mode shows intense peaks which are not present in positive ion mode.

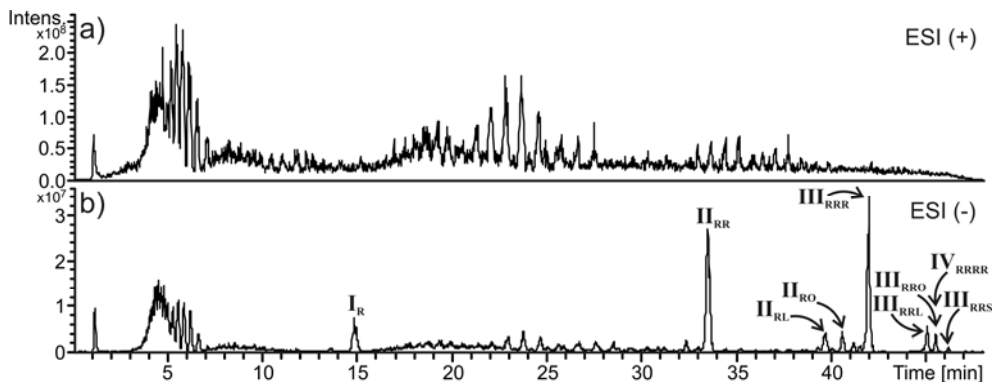


**Figure 3.2.** BPCs of the LC-ESI-QIT-MS analysis of a CASEO in a) positive ion mode and b) negative ion mode. Note: Peaks **I**, **II**, **III**, **IV** are assigned to anions of fatty acid mono-, di-, tri- and tetramers, respectively. Subscript letters indicate the constituting fatty acids (*i.e.*, R: Ricinoleic acid, L: Linoleic acid, O: Oleic acid, and S: Stearic acid).

The summed mass spectra of each chromatographic peak showed the presence of anions of: (1) ricinoleic acid **I<sub>R</sub>**, (2) di-ricinoleate **II<sub>RR</sub>**, Ricinoleate-Linoleate **II<sub>RL</sub>**, Ricinoleate-Oleate **II<sub>RO</sub>**, (3) tri-ricinoleate **III<sub>RRR</sub>**, di-ricinoleate-linoleate **III<sub>RRL</sub>**, di-ricinoleate-oleate **III<sub>RRO</sub>**, di-ricinoleate-stearate **III<sub>RRS</sub>**, and (4) tetra-ricinoleate **IV<sub>RRRR</sub>**. The structures of the ricinoleate derivative anions are presented in Chart 3.1.

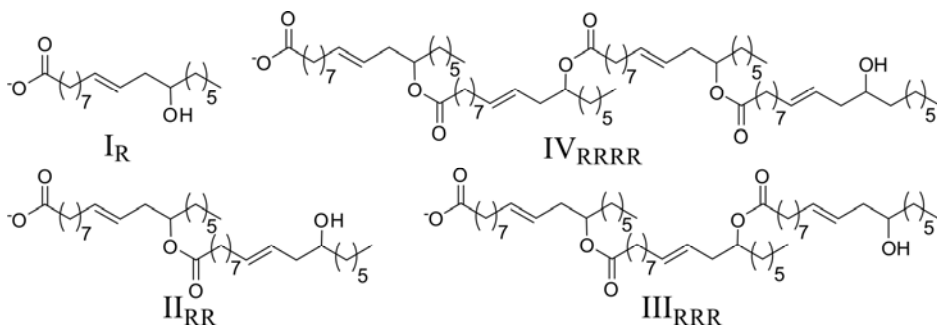


**Chart 3.1.** Structures of the four anions of polymerized ricinoleic acid detected in the LC-ESI-QIT-MS analysis of CASEO in negative ion mode (see also Figure 3.2b). Note: Structure annotation is the same as for the BPC peaks in Figure 3.2b. The structures of **II<sub>RL</sub>**, **II<sub>RO</sub>**, **III<sub>RRL</sub>**, **III<sub>RRO</sub>**, and **III<sub>RRS</sub>** anions can be derived from the above structures by changing one ricinoleic acid with the respective fatty acid.

Their structures were confirmed by MS/MS experiments (Figure 3.3). The presence of “polymerized” ricinoleic acid in negative ion mode hints at the presence of the respective ethoxylated compound in positive ion mode. Indeed some of the unknown distributions could be assigned to these structures. Confirmation of this suggestion will be shown further in this chapter.

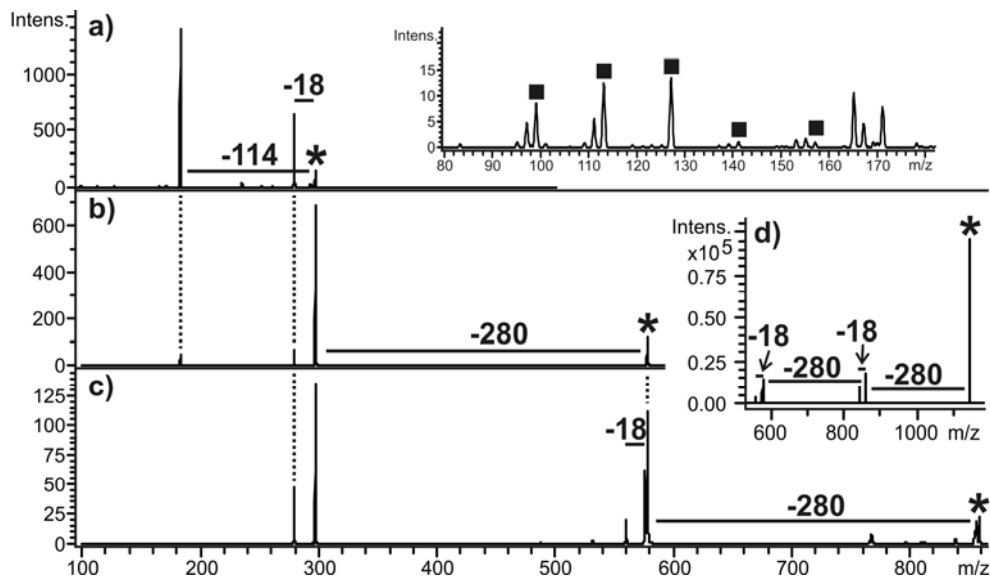


**Figure 3.3.** Product ion mass spectra (negative ion mode) of: a)  $I_R$ , b)  $II_{RR}$ , c)  $III_{RRR}$ , and (d)  $IV_{RRRR}$ . Note: Structures of the four anions are presented in Chart 3.1. Asterisks (\*) indicate the respective precursor ions and squares (■) product ions associated with backbone cleavages of the fatty alkyl chain (*i.e.*,  $\alpha_{C_n}$  type of ions, see also Chart 3.2).

### 3.3.3 LC-MS analysis of CASEO with different ionization techniques

ESI is known to efficiently ionize polar compounds. To investigate if the CASEO sample contains less polar or non-polar compounds, atmospheric-pressure chemical ionization (APCI) and atmospheric-pressure photoionization (APPI) were used. These ionization techniques are known to ionize molecules of low polarity more efficiently than ESI. Figure 3.4 depicts the overlaid BPC in the different ionization modes used. In both cases the MS response was lower than with ESI and no new distributions and compounds were detected.

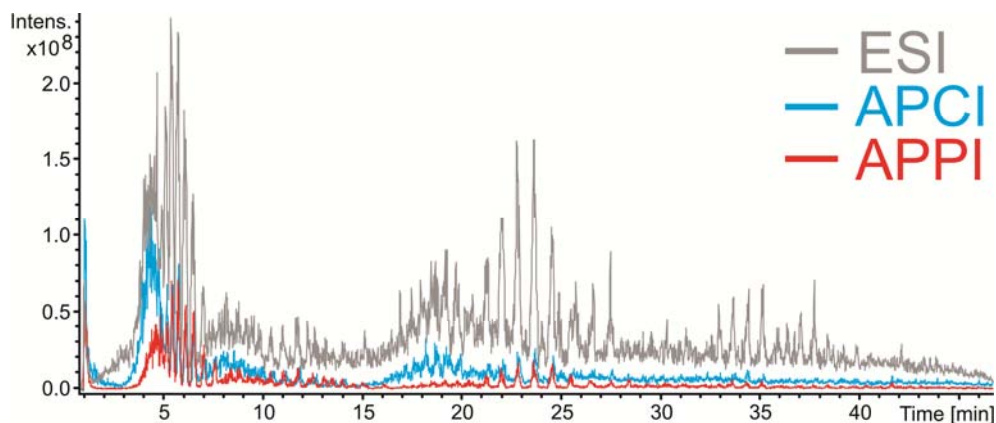


**Figure 3.4.** BPCs of the LC-MS analysis of a CASEO. Note: ESI (grey), APCI (blue) and APPI (red), all in positive ion mode.

Figure 3.5 depicts the summed mass spectra of the same LC peak by ESI, APCI and APPI. The summed mass spectra obtained by using ESI show the presence of ions cationized with various cations such as sodium, potassium, ammonium and protons. This is expected since potassium and sodium are known to be present into all solvents stored in glass bottles. The presence of ammonium ions is attributed to contamination of the column in previous work and protons because of the acidic environment of the eluent created by the addition of formic acid. With APCI, the mass spectra contain only protonated ions. This behavior is in agreement with the theory behind ion formation in APCI. In addition, a lot of lower mass ions are detected. These are the result of up-front fragmentation of the precursor ion. The specific geometry of the QIT used is not known to favorize up-front fragmentation. Therefore, it is suggested that the protonated ions of the ethoxylates are quite labile ions and prone to fragmentation. With APPI, the type of ions in the mass spectra is a combination of ESI and APCI.

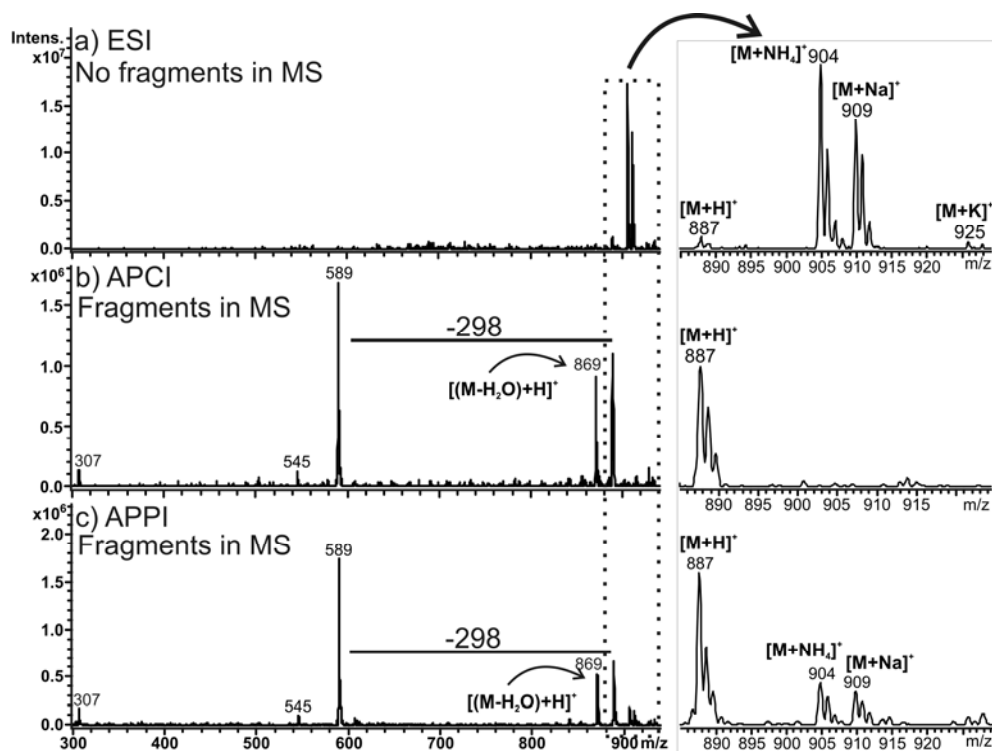


**Figure 3.5.** Summed mass spectra of the LC-MS peak with retention time 25.8 min by: a) ESI, b) APCI, and c) APPI.

### 3.3.4 LC-MS<sup>n</sup> analysis of CASEO

To confirm the structures of the detected polymeric series and elucidate the structures of the unknown distributions, CID was performed for specific ions of each distribution. In addition, different cationization agents (*i.e.*, sodium, lithium, ammonium and potassium) were investigated and the type of information was evaluated. Figure 3.6 depicts the CID of Ric-PEG<sub>7</sub> cationized with these four agents.

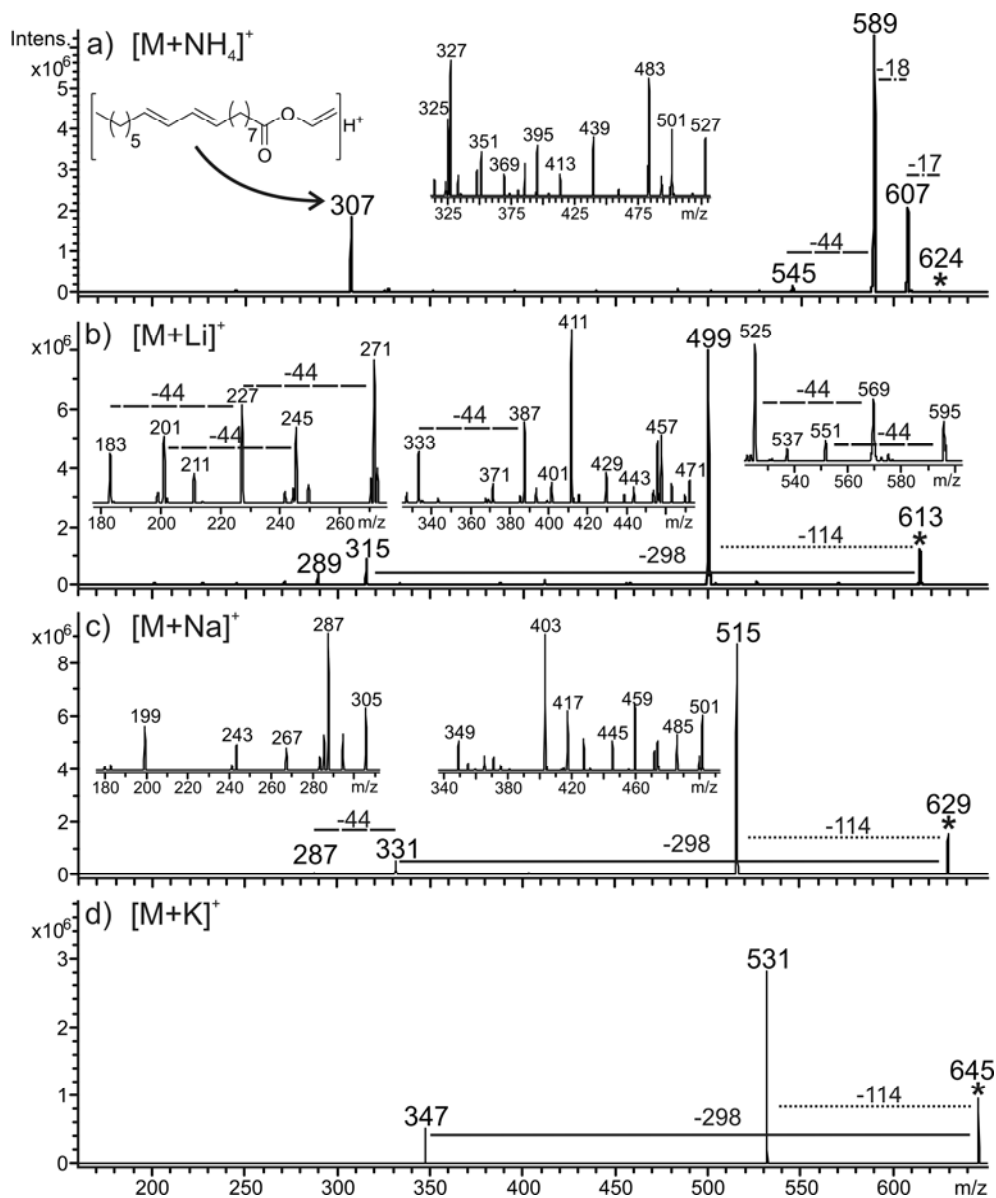


**Figure 3.6.** Product ion mass spectra of Ric-PEG<sub>7</sub> with different cation adducts: a) ammonium, b) lithium, c) sodium, and d) potassium. **Note:** Asterisk (\*) indicates the precursor ion. The numbers above the peak are the nominal masses and the numbers above the horizontal lines indicate the neutral losses (in Da). Inset figures are magnified areas from the respective panels.

Figure 3.6a shows the product ion mass spectrum of an ammonium cationized Ric-PEG<sub>7</sub>. The precursor ion loses ammonia to form the protonated Ric-PEG<sub>7</sub>. The ion at  $m/z$  589 is formed after loss of water from the protonated ion. Two ions deriving from loss of a greater number of PEG monomer units are also detected completing the series of product ions. Another series of product ions starting at  $m/z$  571 and ending at  $m/z$  307 is observed. Although the fragmentation mechanism behind the ion at  $m/z$  571 is not known, the losses of homologous series of PEG monomer units fit the degree of polymerization of Ric-PEG<sub>7</sub>. The ion at  $m/z$  307 is also present during MS and is characteristic of ricinoleic acid. Similar characteristic ions were observed with the other fatty acid ester ethoxylates (*e.g.*, Lin-PEG gives a peak at  $m/z$  289). This suggests that the analysis of ammonium cationized ions can provide initial information about the nature of the fatty acid present in the polymer even on MS mode when CID is not available. This can be very useful for fast screening analysis.

Figure 3.6b depicts the product ion mass spectrum of the lithium cationized Ric-PEG<sub>7</sub>. The spectrum has two major product ions. The base peak is a product ion after neutral loss of 114 Da (The fragmentation mechanism behind this neutral loss will be discussed later in this article). The peak at  $m/z$  315 derives from neutral loss of 298 and can be used for end-group confirmation. Besides these, there are multiple low abundance product ions. Based on the polymer fragmentation nomenclature proposed by Wesdemiotis *et al.*<sup>112</sup> (see also Chart 3.2), the ions at  $m/z$  595 and 551 are  $b_n$  type of ions. Ions at  $m/z$  569, 525 and 471 are  $c_n$  type. Product ions such as  $x_n$  and  $z_n$  type were also identified; (*viz.* the peaks at  $m/z$  183, 227, 271, 315 [ $x_n$ ], and 201, 245, 289, 333 [ $z_n$ ]). Low abundance ions after cleavage of the acyl chain were also observed (*viz.* the peaks at  $m/z$  371, 387, 401, 429, 443, and 457).

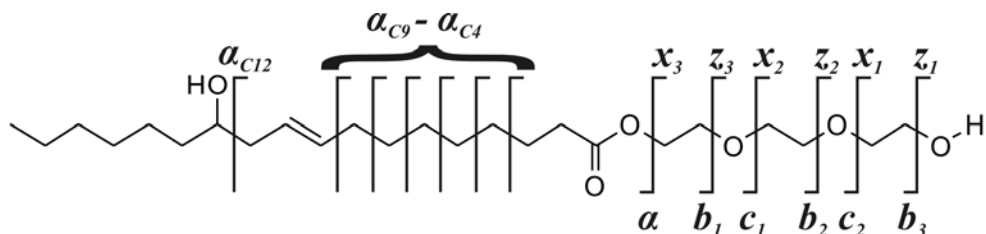


**Chart 3.2.** Fragmentation nomenclature of Ric-PEG. The annotation is based on Wesdemiotis *et al.*<sup>112</sup> with a few new notations proposals for the fragments of the acyl chain. Note:  $c_n$  and  $z_n$  type of ions are not shown, since they are  $c_n$  and  $z_n$  type of ions with a saturated end (*i.e.*, additional two hydrogen atoms, hence the double prime).

This kind of fragmentation pattern (acyl chain cleavage) was previously observed by Cheng *et al.*<sup>113</sup> and explained as charge remote fragmentations. Since these fragments can indicate the position of the double bonds in the acyl chain, they might be used to discriminate Lin-PEG from DHSTE-PEG. However the low abundance of these fragment ions in our experiments did not allow this discrimination.

The product ion mass spectra of sodium and potassium cationized Ric-PEG<sub>7</sub> (Figure 3.6c and 3.6d) follow the fragmentation pattern of the lithium cationized Ric-PEG<sub>7</sub>. However, the number and abundance of the product ions detected was lower. Nevertheless, the two main product ions after neutral loss of 114 and 298 Da, which are unique for the ricinoleic acid moiety, are still observed. The absence of high intensity product ion peaks is a phenomenon in agreement with the general notion that lithium is the cation of preference for the CID of polyethers. The cation is small enough to create strong non-covalent interactions with the ether oxygens and thereby promotes the dissociation of the polymer over cation detachment. On the other hand, sodium and potassium are larger and they do not bind as strongly.

The investigation of the nature of the ion after neutral loss of 114 Da required accurate mass MS/MS. This was performed in a LTQ Orbitrap XL mass spectrometer. Figure 3.7 shows the product ion mass spectrum of a lithium cationized Ric-PEG<sub>7</sub>. Although the profile of the product ion mass spectrum differs from the one obtained in the QIT, the type of product ions is the same.

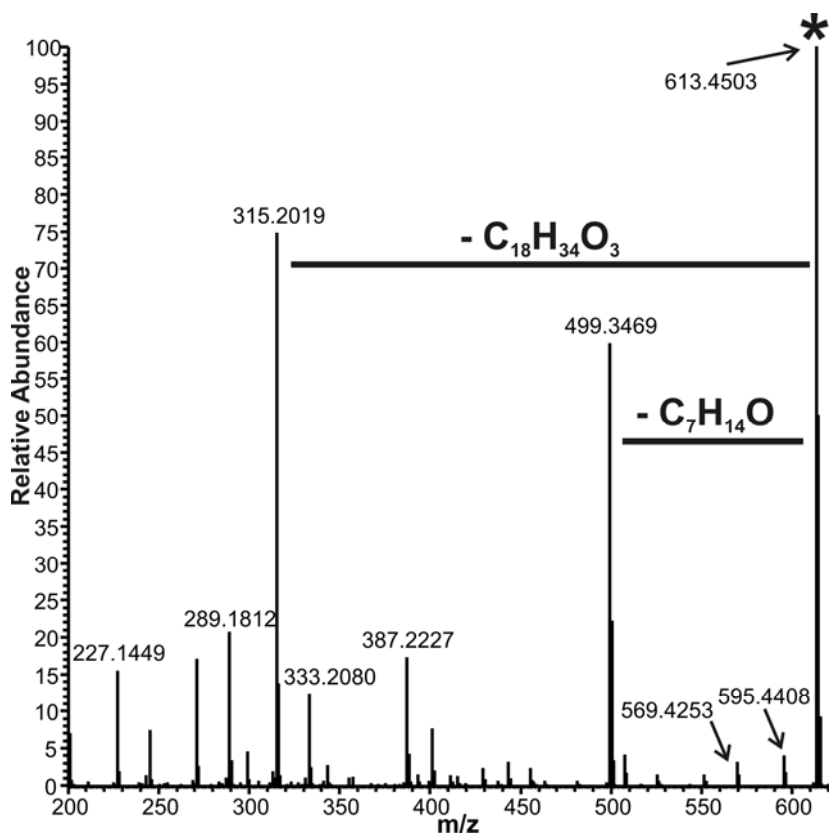


**Figure 3.7.** Accurate mass product ion mass spectrum of lithium cationized Ric-PEG<sub>7</sub>.

Table 3.3 shows the accurate mass data of all the product ions detected, together with their attribution, the corresponding elemental composition, theoretical mass and difference between experimental and theoretical mass. The neutral loss of 298.2484 Da ( $\Delta=8$  ppm) has an elemental composition (C<sub>18</sub>H<sub>34</sub>O<sub>3</sub>;  $m_{Th}=298.2508$ ) that confirms the presence of a ricinoleic acid residue in the structure. The elemental composition of the neutral loss of 114.1034 Da is C<sub>7</sub>H<sub>14</sub>O ( $\Delta=9.6$  ppm;  $m_{Th}=114.1045$ ). This loss cannot be related to the PEG chain or to the carboxylic moiety of the fatty acid. The proposed fragmentation is shown in Scheme 3.2.

**Table 3.3. Accurate Mass Measurement<sup>a</sup> of Peaks in Figure 3.7**

Peak No	Measured mass [Da]	Theoretical mass [Da]	Error [ppm]	Elemental composition	Assigned ion
1	613.4503	613.4503	-	C <sub>32</sub> H <sub>62</sub> O <sub>10</sub> Li	[M+Li] <sup>+</sup>
2	595.4408	595.4397	1.75	C <sub>32</sub> H <sub>60</sub> O <sub>9</sub> Li	<i>b</i> <sub>7</sub> <sup>''</sup>
3	569.4253	569.4241	2.20	C <sub>30</sub> H <sub>58</sub> O <sub>9</sub> Li	<i>c</i> <sub>6</sub>
4	551.4141	551.4135	0.95	C <sub>30</sub> H <sub>56</sub> O <sub>8</sub> Li	<i>b</i> <sub>6</sub> <sup>''</sup>
5	525.3991	525.3979	2.31	C <sub>28</sub> H <sub>54</sub> O <sub>8</sub> Li	<i>c</i> <sub>5</sub>
6	507.3877	507.3873	0.85	C <sub>28</sub> H <sub>52</sub> O <sub>7</sub> Li	<i>b</i> <sub>5</sub>
7	499.3469	499.3458	2.08	C <sub>25</sub> H <sub>48</sub> O <sub>9</sub> Li	<i>α</i> <sub>C12</sub> <sup>''</sup>
8	481.3732	481.3717	3.24	C <sub>26</sub> H <sub>50</sub> O <sub>7</sub> Li	<i>c</i> <sub>4</sub>
9	463.3617	463.3611	1.65	C <sub>26</sub> H <sub>48</sub> O <sub>6</sub> Li	<i>b</i> <sub>4</sub>
10	457.3015	457.2989	5.71	C <sub>22</sub> H <sub>42</sub> O <sub>9</sub> Li	<i>α</i> <sub>C9</sub>
11	443.2851	443.2832	3.70	C <sub>21</sub> H <sub>40</sub> O <sub>9</sub> Li	<i>α</i> <sub>C8</sub> <sup>''</sup>
12	437.3471	437.3454	3.7	C <sub>24</sub> H <sub>46</sub> O <sub>6</sub> Li	<i>c</i> <sub>3</sub>
13	429.2693	429.2676	2.86	C <sub>20</sub> H <sub>38</sub> O <sub>9</sub> Li	<i>α</i> <sub>C7</sub>
14	415.2540	415.2519	4.99	C <sub>19</sub> H <sub>36</sub> O <sub>9</sub> Li	<i>α</i> <sub>C6</sub>
15	401.2383	401.2329	5.01	C <sub>18</sub> H <sub>34</sub> O <sub>9</sub> Li	<i>α</i> <sub>C5</sub>
16	387.2227	387.2206	5.25	C <sub>17</sub> H <sub>32</sub> O <sub>9</sub> Li	<i>α</i> <sub>C4</sub> <sup>''</sup>
17	333.2080	333.2101	6.22	C <sub>14</sub> H <sub>30</sub> O <sub>8</sub> Li	<i>z</i> <sub>8</sub>
18	331.1924	331.1944	6.11	C <sub>14</sub> H <sub>28</sub> O <sub>8</sub> Li	<i>z</i> <sub>8</sub>
19	315.2019	315.1966	7.46	C <sub>14</sub> H <sub>28</sub> O <sub>7</sub> Li	<i>x</i> <sub>7</sub>
20	305.2694	305.2646	8.49	C <sub>18</sub> H <sub>34</sub> O <sub>3</sub> Li	<i>α</i>
21	289.1812	289.1839	9.19	C <sub>12</sub> H <sub>26</sub> O <sub>7</sub> Li	<i>z</i> <sub>7</sub> <sup>''</sup>
22	287.1667	287.1682	5.25	C <sub>12</sub> H <sub>24</sub> O <sub>7</sub> Li	<i>z</i> <sub>7</sub>
23	271.1759	271.1733	9.57	C <sub>12</sub> H <sub>24</sub> O <sub>6</sub> Li	<i>x</i> <sub>6</sub> <sup>''</sup>
24	245.1560	245.1576	6.71	C <sub>10</sub> H <sub>22</sub> O <sub>6</sub> Li	<i>z</i> <sub>6</sub> <sup>''</sup>
25	243.1404	243.1420	6.56	C <sub>10</sub> H <sub>20</sub> O <sub>6</sub> Li	<i>z</i> <sub>6</sub>
26	227.1499	227.1449	12.55	C <sub>10</sub> H <sub>20</sub> O <sub>5</sub> Li	<i>x</i> <sub>5</sub> <sup>''</sup>
27	201.1343	201.1314	14.47	C <sub>8</sub> H <sub>18</sub> O <sub>5</sub> Li	<i>z</i> <sub>5</sub> <sup>''</sup>

<sup>a</sup>Performed in LTQ Orbitrap XL mass spectrometer with internal calibration (Precursor ion mass). The notation of the assigned ions is presented in Chart 3.2

Scheme 3.2 shows a mechanism in which the neighboring double bond facilitates the hydrogen rearrangement and the transfer of the hydroxyl proton to the acyl chain. This fragmentation can be observed when the hydroxyl group is free (not polymerized with PEG). To check whether this fragmentation pattern is only present in Ric-PEG, the CID behavior of a comparable structure, G-PEG-Ric<sub>1</sub> was investigated. An additional interesting point is that Ric-PEG has ultimately only two ethoxylation sites, whereas G-PEG-Ric<sub>1</sub> has four (two from the glycerol hydroxyl groups, one from the hydroxyl group of the ricinoleate, and one from the carboxylic/third glycerol hydroxyl group) as demonstrated in Scheme 3.1.



assume that the ester bond between the glycerol and ricinoleic acid will be a favorable site to obtain most of the ethoxylation.

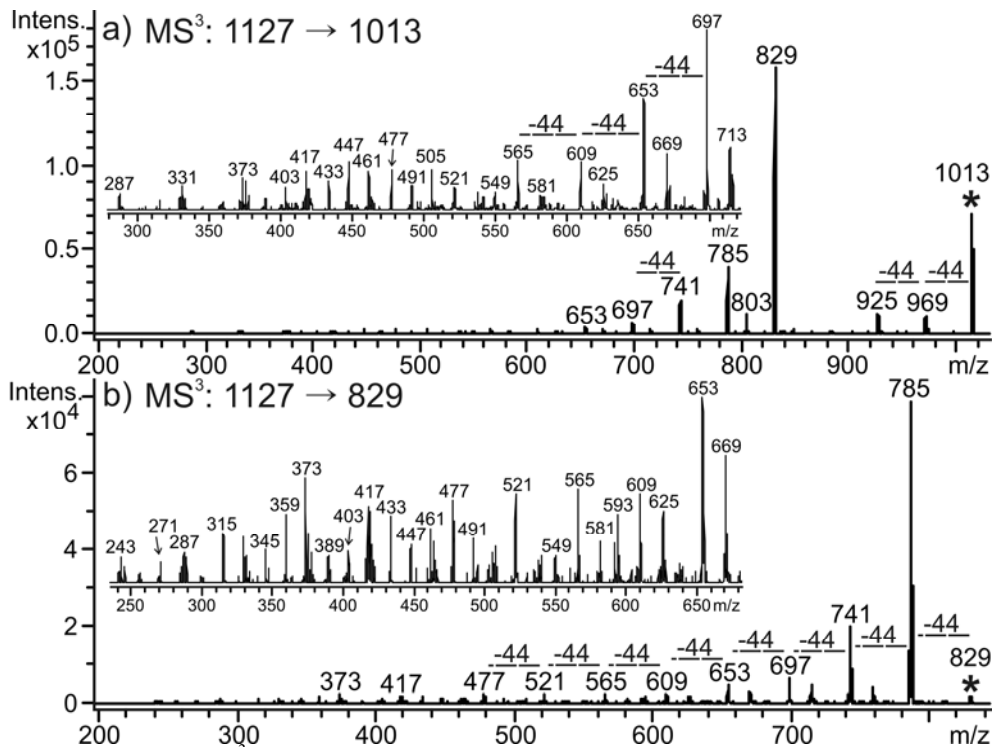
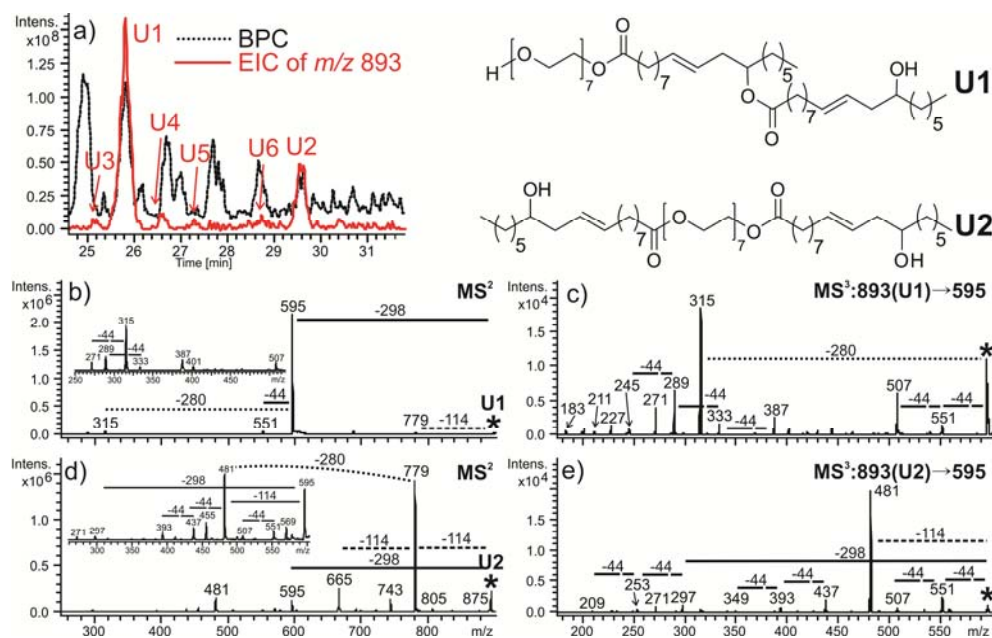


**Figure 3.9.** LC-MS<sup>3</sup> product ion mass spectra of lithium cationized Glycerol PEG Ricinoleate (G-PEG<sub>17</sub>-Ric) after neutral loss of a) 114 Da, and b) 298 Da. Note: Asterisks (\*) indicate the precursor ions. The numbers above the peak are the nominal masses and the numbers above the horizontal lines indicate the neutral losses (in Da). Inset figures are magnified areas from the respective panels.

### 3.3.5 LC-MS<sup>n</sup> analysis of castor oil ethoxylate isobars/isomers

As mentioned above, during the LC-ESI-MS analysis multiple unknown distributions were identified that had either the same nominal mass (nominal isobars) or even the same elemental composition (isomers). Figure 3.10a shows the BPC and the extracted ion chromatogram (EIC) of the peak at *m/z* 893. The EIC shows that there are at least six major peaks (labeled U1 to U6). Possible structures are: Ric<sub>2</sub>-PEG<sub>7</sub>, Ric-PEG<sub>7</sub>-Ric, Ric<sub>2</sub>Ole-PEG<sub>2</sub>, RicOle-PEG<sub>2</sub>-Ric, Ric<sub>2</sub>-PEG<sub>2</sub>-Ole and G-PEG<sub>12</sub>-Ste (as well as all other possible

positional isomers). The analysis by QIT-MS does not provide enough resolving power to discriminate between nominal isobars. Furthermore the use of QIT-MS in single stage mode does not allow the discrimination between isomers. Therefore, MS<sup>n</sup> was used to elucidate the structures of these peaks.



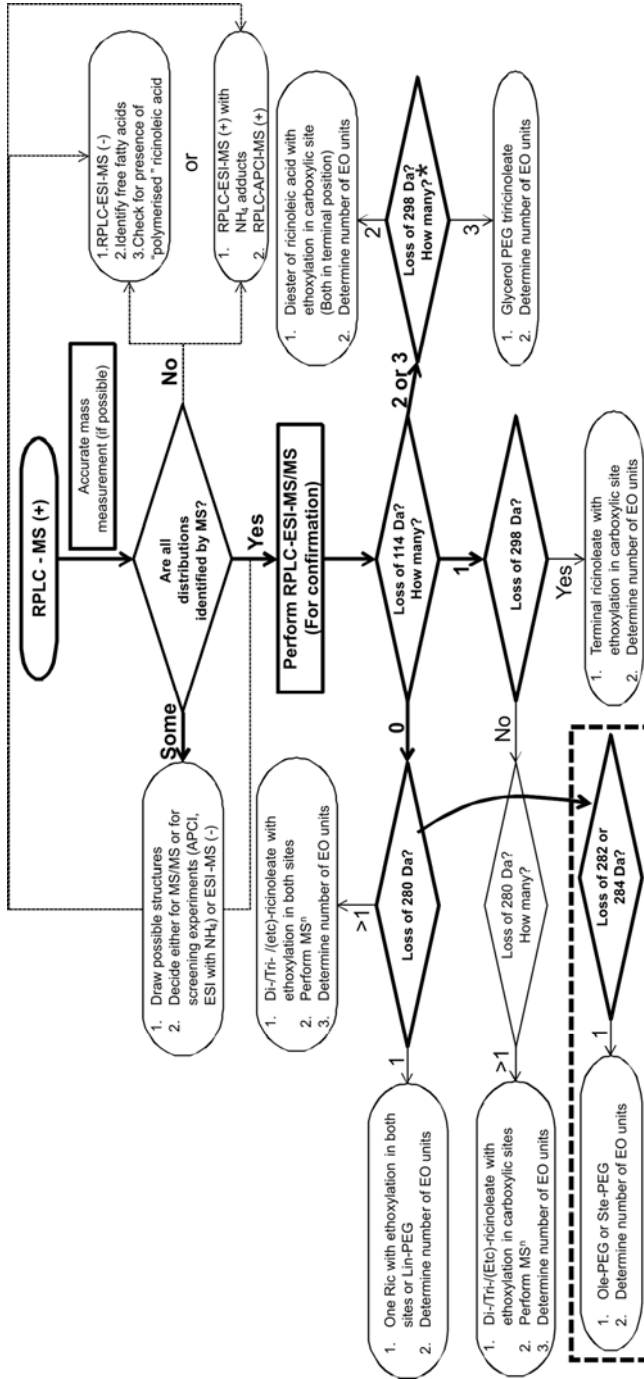
**Figure 3.10.** LC-MS<sup>n</sup> of lithium cationized isomeric peaks. a) BPC and EIC of  $m/z$  893 (6 peaks were detected in the elution window from 24.5 to 32 minutes), b) MS<sup>2</sup> mass spectrum of peak U1, c) MS<sup>3</sup> mass spectrum of peak U1 (Product ion after neutral loss of ricinoleic acid (*i.e.*,  $m/z$  595), d) MS<sup>2</sup> mass spectrum of peak U2, and e) MS<sup>3</sup> mass spectrum of peak U2 (Product ion after neutral loss of ricinoleic acid (*i.e.*,  $m/z$  595). Upper right the elucidated structures of U1 and U2 are presented.

Figure 3.10(b-d) depicts the LC-MS<sup>n</sup> analysis of the two major peaks, U1 and U2. The results of the peaks U3 to U6 are shown in Figure 3.11. Figure 3.10b and 3.10d present the product ion mass spectra of Peak U1 and U2, respectively. Their fragmentation pattern has distinct differences: (1) U1 shows major 298 and 578 (298+280) Da neutral losses, whereas U2 shows 298 and 596 (two times 298) Da neutral losses, and (2) U2 shows 114 and 228 (two times 114) Da neutral losses, whereas U1 shows a very low intensity 114 Da neutral loss. The double loss of 298 Da indicates that the two ricinoleic acids are in terminal

positions. This suggestion is also supported by the simultaneous presence of at least two 114 Da neutral losses (if only one 114 Da neutral loss was observed then the hydroxyl group of one ricinoleic acid would be ethoxylated or connected with another molecule).

In this case, it would not have been possible to confirm the hypothesis that both ricinoleic acids are in terminal positions. On the other hand, the losses of 298 and 280 Da indicate that the one ricinoleic acid group is terminal and the other internal. These observations are in agreement with the MS/MS experiments of the “polymerized” ricinoleic acid anions (Figure 3.3). The LC-MS<sup>3</sup> mass spectra of peaks U1 and U2 are presented in Figures 3.10c and 3.10e, respectively. These (MS<sup>3</sup>) mass spectra show also differences, which complement the interpretations of the MS<sup>2</sup> mass spectra shown in Figure 3.10b and 3.10d. In Figure 3.10c the product ion mass spectrum contains a neutral loss of 280 Da, whereas in Figure 3.10d neutral losses of 114 and 298 Da are observed. The absence of a neutral loss of 284 Da (stearic acid) and the presence of more than two PEG monomer units, allowed the exclusion of specific possible structures proposed earlier (*viz.* those with building block compositions (r)-Ric<sub>2</sub>-PEG<sub>2</sub>-Ole and (r)-G-PEG<sub>12</sub>-Ste). Using these LC-MS<sup>n</sup> comparisons, the structures were elucidated. The two proposed structures are also shown in Figure 3.10. U1 is a Ric<sub>2</sub>-PEG (Diricinoleate PEG ester) and U2 is a Ric-PEG-Ric (Ricinoleate PEG diester).

Scheme 3.3 presents a flow chart that summarizes all the rules derived and applied so far for structure elucidation of castor oil ethoxylate components.



**Scheme 3.3.** Flow chart showing the methodology for the structural elucidation of castor oil ethoxylates components by LC-MS. Note: In the decision cell indicated with an asterisk “\*” the number of 298 Da neutral losses can never exceed the number of 114 Da neutral losses.

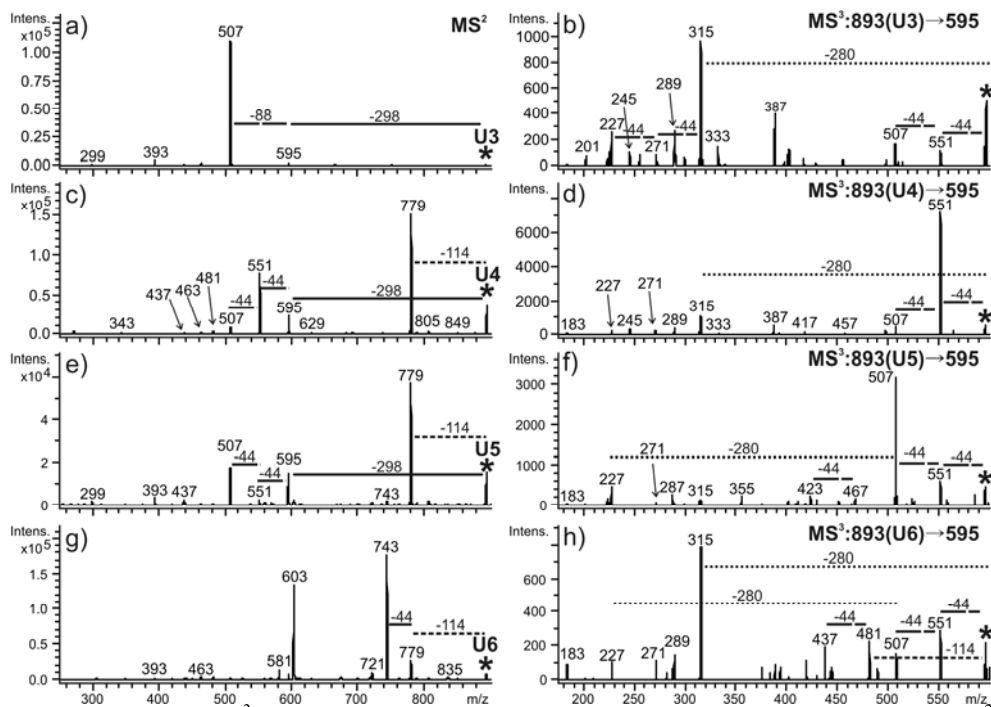
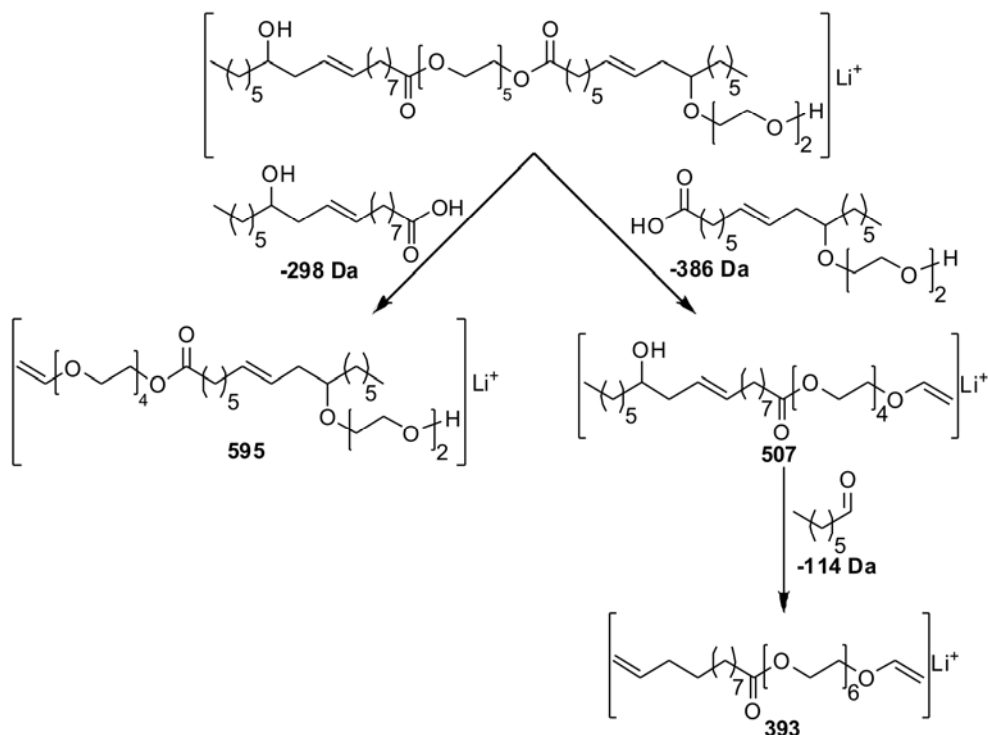


**Figure 3.11.** LC- $MS^3$  of lithium cationized nominally isobaric peaks. a), c), e), g)  $MS^2$  mass spectra of peak U3, U4, U5, U6, respectively ( $m/z$  893), b), d), f), h)  $MS^3$  mass spectra of the respective peaks after neutral loss of ricinoleic acid ( $m/z$  595).

The product ion mass spectra of peaks U3 to U6 also have distinct differences in both the  $MS^2$  and  $MS^3$  stages (Figure 3.11). Complete structural elucidation of these peaks using the flow chart in Scheme 3.3, however, was not achieved due to the lack of unique fragmentation patterns and low intensity product ion peaks. Nevertheless, U3 (Figure 3.11a) might well be a structure with an ethoxylated hydroxyl group of the ricinoleic acid (a tentative interpretation and assignment of U3 is given in Scheme 3.4), whereas U4, U5, and U6 may be structures with at least one non-ethoxylated hydroxyl group. To assign specific structures in these peaks, the  $MS^3$  analysis of other product ions must be performed. Fractionation of the chromatographic peaks will increase the amount of specific material available for  $MS^n$  and thus allow more elaborate  $MS^n$  analysis.



**Scheme 3.4.** Proposed structural elucidation of peak U3.

### 3.4 Conclusions

The LC-MS<sup>n</sup> analysis of CASEO allowed the successful determination and identification of more components than assigned in previous studies. The analysis in negative mode proves to be complementary to the positive mode information, especially providing information about the type of fatty acids present in the mixture. The presence of di-, tri-, tetra- ricinoleate, as well as other di- and tri-esters is shown for the first time.

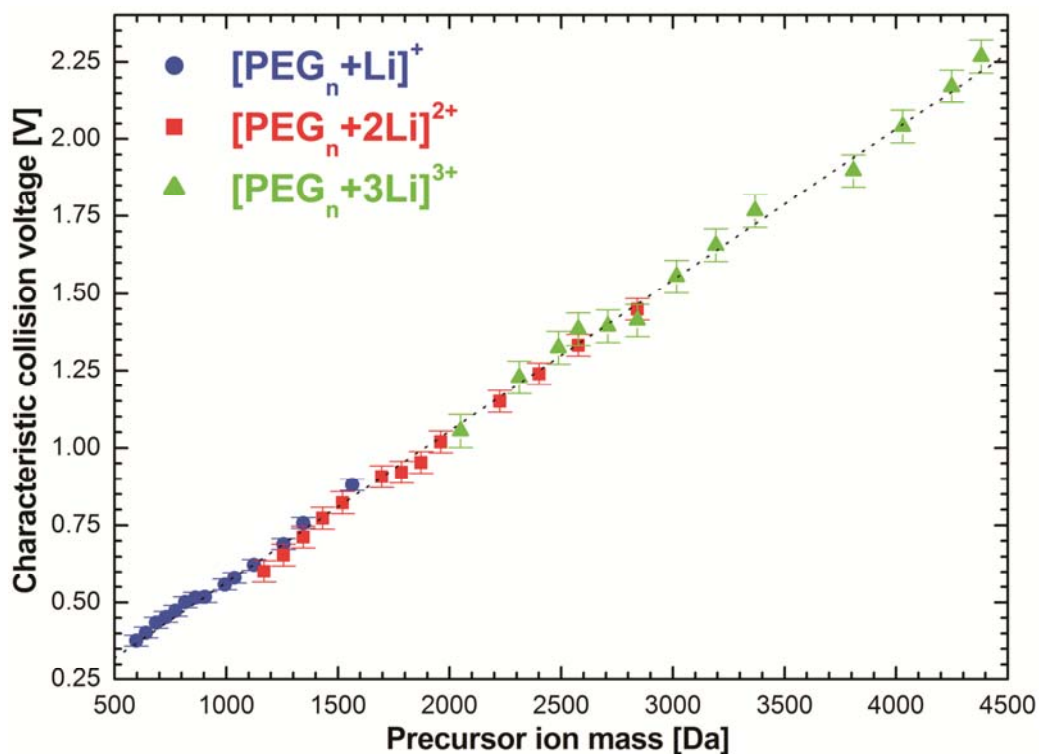
The investigation with different ionization techniques (*e.g.*, ESI, APCI, APPI) revealed that ESI gives the best MS response. However, APCI gives complementary structural information already in MS, due to up-front fragmentation of the protonated ions. This means that if no MS instrument capable to perform MS/MS experiments is available, APCI-MS can provide part of the information normally produced by ESI-MS/MS.

The comparison of the product ion mass spectra obtained with different cation adducts (*i.e.*, sodium, lithium, ammonium and potassium) showed that lithium and ammonium

cationized ions provide the most detailed structural information. In addition, the ammonium cationized ions, via the formation of the protonated ions after the neutral loss of ammonia, give fragments in MS mode, like in the case with APCI. This phenomenon can be of great help for fast screening protocols. The fragmentation patterns of oligomers containing ricinoleic acid have a unique characteristic, the neutral loss of 114 Da which is confirmed as a cleavage of the carbon-carbon bond in the C<sub>11</sub>-C<sub>12</sub> position of the ricinoleic acid chain. This unique fragmentation is present when the hydroxyl group of the ricinoleic acid is not ethoxylated. In addition, characteristic neutral losses of 298 and 280 Da indicate the terminal or internal position of the ricinoleic acid in the molecule, respectively.

# 4

## Challenges in Energy-dependent Tandem Mass Spectrometry in an Ion Trap



**Nasioudis, A.; Memboeuf, A.; Heeren R. M. A.; Smith, D. F.; Vékey, K.; Drahos, L.; van den Brink, O. F. *Anal. Chem.* 2010, 82, 9350-9356.**

**Memboeuf, A.; Nasioudis, A.; Indelicato, S.; Pollreisz, F.; Kuki, A.; Kéki, S.; van den Brink, O. F.; Vékey, K.; Drahos, L. *Anal. Chem.* 2010, 82, 2294-2302.**

## 4.1 Introduction

Multi-stage mass spectrometry ( $MS^n$ ) has been proven to be a powerful tool for the structural characterization of macromolecules. This success derives from its ability to provide qualitative information about the polymers studied, and particularly impacted the research of biopolymers such as peptides and proteins. In the field of synthetic polymers, issues such as high molar mass, complexity and dispersity are constant challenges. The major obstacle of high molar mass was overcome with the development of soft-ionization techniques, such as electrospray ionization (ESI)<sup>115</sup> and matrix-assisted laser desorption/ionization,<sup>116</sup> whereas the challenge of analyzing structurally complex polymeric systems has been dealt with so far by introducing auxiliary analytical tools, such as separation techniques<sup>16,17,117</sup> and statistical processing.<sup>87</sup>  $MS^n$  is an additional tool that helps to deal with the challenge of complexity. The number of applications based on the hyphenation of liquid chromatography and  $MS^n$  are numerous. This is possible because the fragmentation behavior of simple polymers (*e.g.*, some homopolymers) is well explained.<sup>112,118-123</sup> On the other hand, for the  $MS^n$  study of complex polymeric systems (*e.g.*, copolymers, multi-branched polymers, etc) can be puzzling, even when combined with separation techniques.

An approach to deal with sample complexity is to develop standardized excitation methods that allow the selective extraction of structural information from the fragmentation patterns. A prerequisite to meet this challenge is to have a good understanding of the fragmentation behavior of molecules in different excitation conditions and as a function of their composition and size. Accurate control of the experimental parameters is mandatory for this type of research.

So far, the major studies on collision regimes in multistage mass spectrometry were focused on the following issues: a) the determination of the internal energy content of fragmenting ions,<sup>124-129</sup> b) instrumental parameters and conditions (*e.g.*, cooling time, excitation time, energy deposition, etc),<sup>129-132</sup> and c) analyte characteristics (*e.g.*, precursor ion mass, charge state and polymer type).<sup>133</sup> Although these studies produced great insights in the field of small molecules analysis, their applicability to large polymeric systems is not straightforward due to the degrees of freedom (DoF) effect. The DoF effect is the trend that

the kinetic shift, which is the difference between the activation energy and the amount of energy necessary to drive the reaction fast enough to observe fragments, increases with the size of the molecule. The importance of this effect is generally recognized and has more often been discussed in qualitative rather than quantitative<sup>134-135</sup> terms. Recently, we investigated this issue in a quantitative way for the case of peptides and polyethers.<sup>131</sup> We demonstrated that there is a good linear correlation between the collision energy necessary to observe fragments and the molecular ion mass of polymers as measured with various instruments, such as a triple quadrupole (QqQ) mass spectrometer, a quadrupole time-of-flight (*q*-TOF) mass spectrometer, and (especially) a quadrupole ion trap (QIT).<sup>133</sup>

QqQ and *q*-TOF mass spectrometers perform tandem-in-space experiments which are more simple and straightforward from theoretical point of view than tandem-in-time experiments, which are usually performed in trapped ion instruments. QIT has a different collision regime than QqQ and *q*-TOF. The collision energy is smaller, the number of collisions is very high (hundreds to thousands), and the residence time is in the range of milliseconds to seconds (the residence time in the other instruments mentioned is in the microseconds range). These characteristics render QIT as a challenging instrument for energetic studies.

In this chapter, we present the optimization procedure to obtain reliable and repeatable energy-dependent product ion mass spectra in a QIT. This optimization procedure aimed to define the influence of the most important instrumental parameters of the QIT and accomplish standardization to facilitate comparative work. Applying this procedure, accurately controlled excitation methods can be developed for the study of synthetic polymers.

## **4.2 Experimental setup**

### ***4.2.1 Chemicals and sample preparation***

Poly(ethylene glycols) (PEGs) from 600 to 4,000 Da, methanol (MeOH) (HPLC grade), and lithium hydroxide (LiOH) were purchased from Sigma-Aldrich (St. Louis, MO). Cation exchange resin AG MP-50 was purchased from Bio-Rad Laboratories (Hercules, CA).

Ultra-pure water with a resistivity of 18.2 M $\Omega$ ·cm (at 25 °C) was obtained from a Millipore Direct-Q 3 (Molsheim, France) water purification system.

The samples were dissolved in a 50/50 (v/v) water/methanol at a concentration of 5–50  $\mu$ M. The solvents were purified with the cation exchange resin prior to dissolution and LiOH was added at a concentration of 0.1–0.2 mM. Sample solutions were introduced via a Cole-Palmer syringe pump (Vernon Hills, IL) at a flow rate of 5  $\mu$ L/min.

#### 4.2.2 Methods

As mentioned in the introduction of this chapter, optimization and accurate control of the instrumental parameters are important for anyone who wants to perform energetic studies in a QIT. The survival yield (SY) is a good quantitative expression of the efficiency of fragmentation since it is related to the internal energy of the ion, which is, in turn, related to the collision energy.<sup>136,137</sup> Therefore, it can be used for investigating the DoF effect.<sup>133</sup> SY is calculated from the following equation:

$$SY = \frac{I_M}{I_M + \sum I_F} \quad \text{Equation 4.1}$$

where  $I_M$  is the intensity of the precursor ion, and  $\sum I_F$  the sum of all product ions intensities. Using this equation, the energy-dependent analysis of a PEG oligomer results in the following graph (Figure 4.1). It should be noted that the horizontal axis of Figure 4.1 depicts the value of the applied fragmentation voltage as set in the instrument, which is related to the collision energy. The exact relation between the fragmentation voltage and the collision energy was not determined.

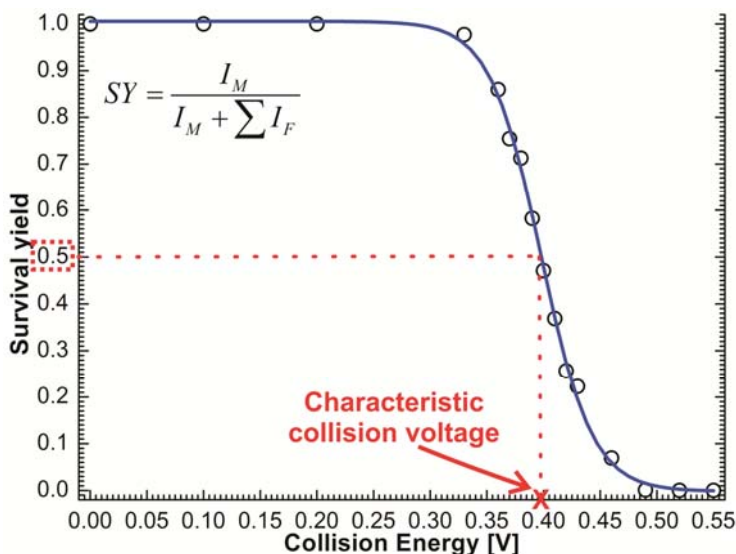


**Figure 4.1.** Survival Yield vs Collision Energy (expressed as collision voltage, instrument setting) plot for  $[\text{PEG}_{10}+\text{Li}]^+$  precursor ion.

It is observed that the shape of the SY curve follows a sigmoidal function. Sigmoidal functions are described by four different parameters: the points in the sigmoidal curve where their respective ordinate value starts to differ from unity and where it reaches zero; the width and height of the curve between these two points. Among these parameters the equivalent point is a characteristic point positioned at half-height (50% SY). At this point the first derivative has its greatest (negative) value. This means that even subtle changes in the collision energy will result in a relatively big shift in the SY. Therefore, the collision energy where the SY becomes 50 % is used as a “characteristic value” of the polymer ion studied. It should be noted that the value is highly dependent on the instrumental conditions and type of instrument used. Therefore, any inter-laboratory comparisons require standardization.

### 4.2.3 Instrumentation

Experiments were performed in a Bruker Esquire 3000<sup>plus</sup> QIT mass spectrometer (Bruker Daltonics, Bremen, Germany) equipped with an ESI source. The settings of the instrument were the following: capillary voltage 3 kV; nebulizer pressure 11 psi; dry gas

flow 4 L/min; dry gas temperature 250 °C; the collision gas was He; the average pressure in the ion trap was  $8.82 \times 10^{-6}$  mbar (uncorrected gauge reading, although the real pressure in the trap is known to be 2-3 orders of magnitude higher<sup>138</sup>).

The instrumental parameters investigated were the following: scanning mass range, scan speed, number of trapped ion, isolation frequency, isolation width, cooling time, excitation frequency, excitation width, and excitation time. Two other very important parameters, the temperature inside the trap and the trap pressure, were not studied due to instrumental limitations in controlling and monitoring these parameters. These two parameters were considered to remain stable throughout the whole experimental work.

## 4.3 Optimization of MS/MS instrumental parameters

### 4.3.1 Mass analysis

As a first step, the instrumental parameters related to the mass analysis need to be optimized and standardized. Variations in the mass detect range will result in small deviations in the contribution of the scan time in the duty cycle of the experiment. Therefore, the scan range was kept constant between  $m/z$  100 and 3,000. Although the QIT used has a lower mass limit of 20 Da, it was observed that the signal intensity drops significantly when the lower mass range is 90 Da. Therefore, the lower mass limit was set to 100 Da. On the other hand, the upper mass limit was set to 3,000 Da, which is the instrument maximum. The scan speed was set to “normal scan”, which translates to 13,000  $m/z$  per second.

The most important instrumental parameter in an MS/MS experiment is the one that controls the filling of the trap. By using a feature of the instrument called the “ion charge control” (ICC), the number of trapped ions is kept constant throughout all MS/MS experiments. The principle behind this feature is the following: The instrument calculates in a fast MS scan the necessary accumulation time to fill the trap with a pre-selected number of ions. Then, it uses this accumulation time to perform the MS/MS experiment. After one cycle the procedure is repeated. The ICC was set to 5,000. One can understand that if the abundance of the selected trapped ions is too low, then the accumulation time will be too long (*i.e.*, 10 to 500 ms). This will result to overload of the trap and consequently intense

space charge effects. Therefore, the accumulation time limit was set to 5 ms. This limitation was necessary to avoid space charge effects prior to the isolation step and did not influence the results, since the number of ions (in the range of 1,000 to 10,000) in the trap prior to excitation does not influence the fragmentation behavior.

#### **4.3.2 Isolation frequency and width**

Precursor ion isolation is one of the most important stages in any MS/MS experiment. The efficiency (*i.e.*, amount of trapped ions of the selected  $m/z$  in relation to the number of ions of that  $m/z$  in the trap before isolation) and quality (*i.e.*, monoisotopic isolation) of isolation are greatly influenced by the isolation frequency ( $m/z_{isol}$ ) and the isolation width. These two parameters thus have a direct impact on the quality and accuracy of the product ion mass spectrum generated. The importance of these two parameters is especially relevant when unknowns and/or structures with complicated fragmentation patterns are studied. A “clean” isolation reduces the uncertainty in the product ion assignment. In addition, an “efficient” isolation allows the confinement of a great amount of precursor ions, which increases the number of fragmentation cycles that can be performed.

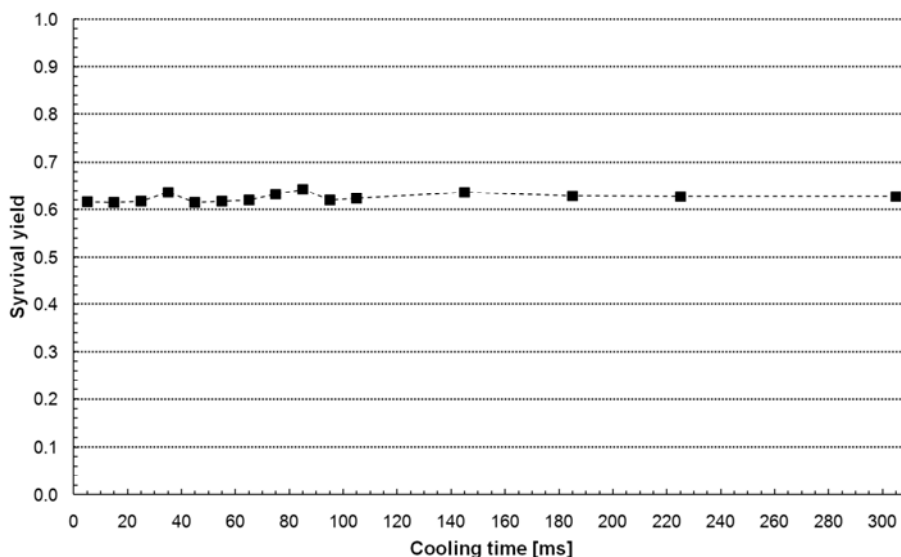
Optimization of the isolation frequency is quite an easy task, since it is achieved by changing the isolation mass in the instrument software and simultaneously monitoring the intensity of the precursor ion. On the other hand, the isolation width, although it is easy to control and modify, has two contradictory effects. Lowering the isolation width to 1 Th will result in “cleaner” product ion mass spectra since monoisotopic isolation of the precursor ion is achieved. On the other hand, the isolation width has an effect on the internal energy of the isolated ion.<sup>127</sup> Too narrow isolation widths cause excitation of the ions isolated. This can lead to unwanted “premature” fragmentations, uncontrolled initial energy deposition to the precursor ion and reduction of the isolated ion population.

It is therefore important for the mass spectrometist to balance these advantages and disadvantages. In our case, PEGs are known for their efficient ionization. Therefore, the challenge of efficient isolation is not so important. On the other hand, monoisotopic isolation is a prerequisite since it is known that specific PEG product ions differ only by two Da. The presence of the first isotopic peaks will complicate the product ion mass

spectra and make data processing more challenging. In addition, initial energy deposition is expected in this narrow isolation width. To overcome this challenge, we used another experimental parameter to neutralize this effect. This was the cooling time between isolation and fragmentation.

### 4.3.3 Cooling time

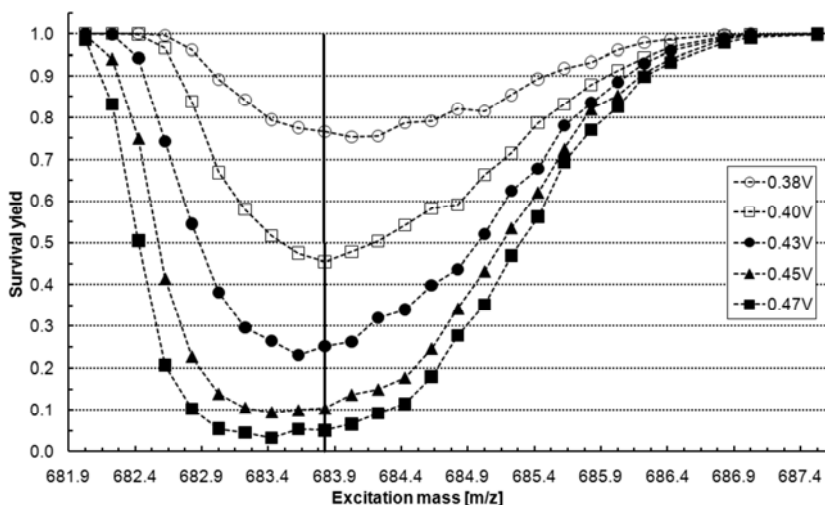
In order to cancel out the effect of the precursor ion activation due to isolation, we investigated the influence of the cooling time in the SY of a PEG oligomer. If the precursor takes up initial energy in the isolation step, this will influence its SY at a given collision energy. Figure 4.2 depicts this influence. It should be noted, that the instrument applies a default cooling time of 5 ms. The figure shows that variation of the cooling time between 5 ms (default cooling time of the instrument) and 305 ms prior to excitation did not result in any change of the SY at a given collision energy for  $[\text{PEG}_{15}+\text{Li}]^+$ . These data indicate that the 5 ms default cooling time is sufficient. Nevertheless, to increase the certainty that the precursor ion is fully thermalized an additional cooling time (*e.g.*, 50 ms) is advised.



**Figure 4.2.** Influence of the cooling time before excitation on the SY of  $[\text{PEG}_{15}+\text{Li}]^+$  precursor ion. Note: Fragmentation amplitude (instrumental parameter that refers to collision energy) was 0.39 V.

#### 4.3.4 Resonance excitation width and frequency

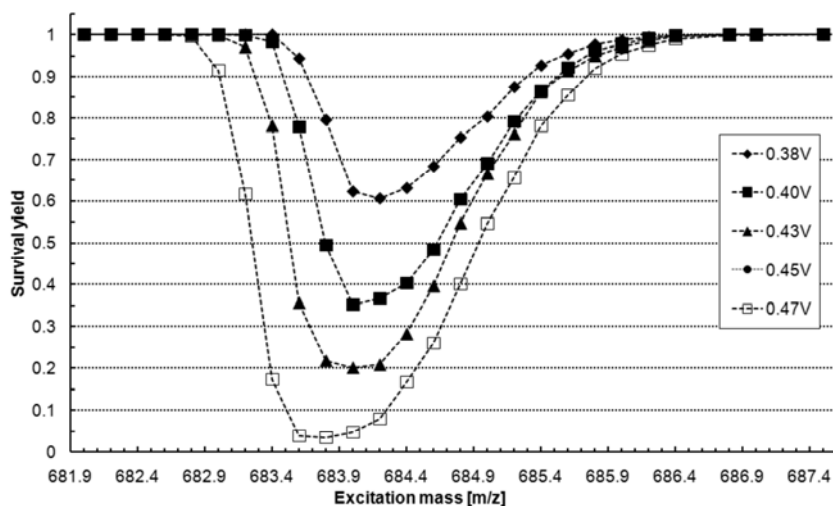
An examination of the instrumental parameters related to the excitation step was performed. First of all, in order to ensure that the same amount of excitation energy is applied throughout the entire excitation step, features such as “Smart Frag” (a ramping function of the collision energy) must be deselected. The effect of variation of the resonance excitation frequency, determining the mass-to-charge ratio for excitation ( $m/z_{exc}$ ) was studied using a procedure similar to the one used by Goeringer *et al.*<sup>127</sup> This was done by performing the isolation and excitation of the precursor ion in two independent stages: a) isolation without fragmentation, followed by b) excitation of the ion population previously isolated without additional isolation. In this way, variation of the  $m/z_{exc}$  was possible without changing the optimized  $m/z_{isol}$  value.



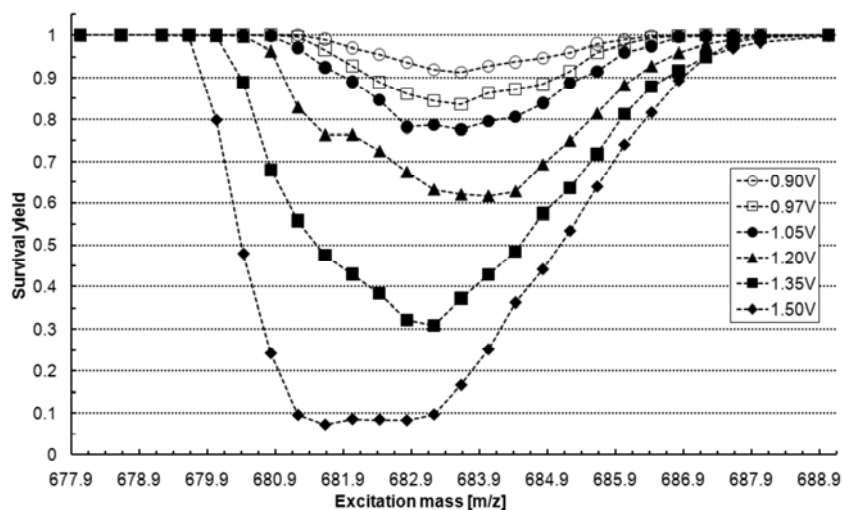
**Figure 4.3.** Influence of the  $m/z_{exc}$  (Presented as corresponding “Excitation mass”) on the SY of  $[\text{PEG}_{15}+\text{Li}]^+$  precursor ion. Excitation width applied is 6 Th. **Note:** The vertical solid line indicates the selected  $m/z_{exc}$  (at  $m/z$  683.8) for the energy-dependent analysis of the  $[\text{PEG}_{15}+\text{Li}]^+$  precursor ion. This value is different from the actual  $m/z$  of the  $[\text{PEG}_{15}+\text{Li}]^+$  precursor ion (at  $m/z$  685.3).

Figure 4.3 shows the influence of the  $m/z_{exc}$  (“excitation mass” in the diagram) on the SY of  $[\text{PEG}_{15}+\text{Li}]^+$  for a variety of fragmentation amplitudes (as mentioned previously, fragmentation amplitude is the instrumental parameter of the QIT that refers to collision

energy). The resonance excitation width during this experiment was 6 Th. Similar tests were performed with 4 Th and 8 Th (see below, Figures 4.4 and 4.5, respectively) resonance excitation widths.



**Figure 4.4.** Influence of the selected mass-to-charge ratio for excitation ( $m/z_{exc}$ ) on the SY of  $[\text{PEG}_{15}+\text{Li}]^+$  precursor ion. Note: Excitation width applied is 4 Th.



**Figure 4.5.** Influence of the selected  $m/z_{exc}$  on the SY of  $[\text{PEG}_{15}+\text{Li}]^+$  precursor ion. Note: Excitation width applied is 8 Th.

A first observation from this plot is that the collision energy is not equally distributed along the entire range of excitation. Secondly, the selected  $m/z_{exc}$  that produces the most efficient fragmentation (curve minimum) is different from the expected  $m/z$  of the precursor ion. This behavior is in agreement with the behavior observed by Goeringer *et al.*<sup>127</sup> This difference, between the  $m/z$  of the precursor ion and the  $m/z_{exc}$  for optimum fragmentation, implies that care must be taken when narrow excitation ranges (Figure 4.4) are applied in studies of the effect of collision energy on the SY.

Furthermore, it requires that calibration of the instrumental parameters must be made when collision energies are to be compared. A third observation (previously reported by Cooks *et al.*<sup>139</sup>) is that in the case of QIT instruments the fragmentation amplitude influences the  $m/z_{exc}$  for optimum fragmentation (curve minimum). This means, that during the energy-dependence study and by keeping the  $m/z_{exc}$  stable, the precursor ion will be excited with an amount of collision energy not only influenced by the collision energy profile but also by the fragmentation amplitude. This is reflected in the plots in Figures 4.3, 4.4 and 4.5, where the lowest point of the curves shifts to higher frequencies when the fragmentation amplitude is increased.

Although the fragmentation amplitude is considered to be a controlled parameter, the change in the collision energy profile with the fragmentation amplitude cannot be accurately controlled and measured. This complication can be dealt with by applying a large excitation window (Figure 4.3 and 4.5) so that the minimum of the curve is sufficiently flat and its shift with the fragmentation amplitude does not affect the collision energy.

#### **4.3.5 Excitation time**

The excitation time has a great influence on the fragmentation pattern. Increasing the excitation time leads to an increase in the number of collisions that an ion experiences. This results in an increase in the energy deposited in the precursor ion. When too short excitation times are applied only partial activation of the precursor ion population will occur. In addition, larger increments of excitation energy need to be considered so that a considerable change in the SY will be observed. A third reason can derive from the observations made in

section 4.3.4. It was shown that the fragmentation amplitude has an influence on the optimum excitation frequency  $m/z_{exc}$  by shifting its value. Larger increments in the fragmentation amplitude result in greater shifts. On the other hand, long excitation times can result in full dissociation of the precursor ion even at low values of fragmentation amplitude. This effect will not allow the measurement of an adequate number of data points that will allow the accurate calculation of the CCV value. Therefore, the excitation time needs to be optimized.

To investigate the influence of this parameter, the value of the fragmentation amplitude effecting 50% SY was plotted versus the excitation time. The choice of this point will be explained in the next section. Figure 4.6 depicts the resulting plot. It is observed that on increasing the excitation time from 10 to 30 ms the required fragmentation amplitude gets significantly lower. With every additional increase in the excitation time, the fragmentation amplitude continues to decrease but at a lower rate to reach an asymptotic minimum. An excitation period of around 60 ms can be considered as a good compromise between not long duty cycles and “effective” activation of the whole ion population.

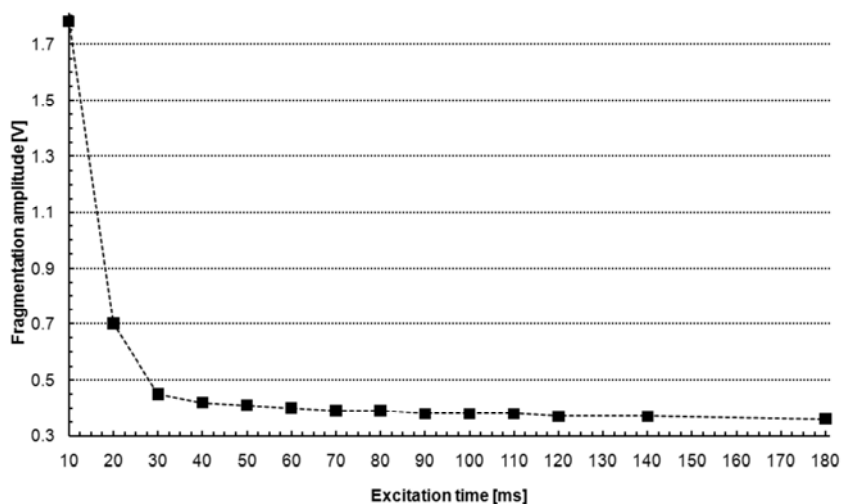


**Figure 4.6.** Fragmentation amplitude, necessary to achieve 50% SY of  $[\text{PEG}_{15}+\text{Li}]^+$  precursor ion, as a function of excitation time. The plot shows that the values of fragmentation amplitude and excitation time to attain a 50% SY for  $[\text{PEG}_{15}+\text{Li}]^+$  are inversely related. The data points reach asymptotically a minimum value, indicating that the influence of the excitation time is reduced after a specific value.

#### 4.4 Size dependence study of synthetic polymers

Investigation of the DoF effect was made by determining the characteristic collision voltage (CCV) of oligomers of various sizes. The CCV value expresses the collision energy value to obtain a precursor ion SY of 50%. Figure 4.7 presents an example of the process.

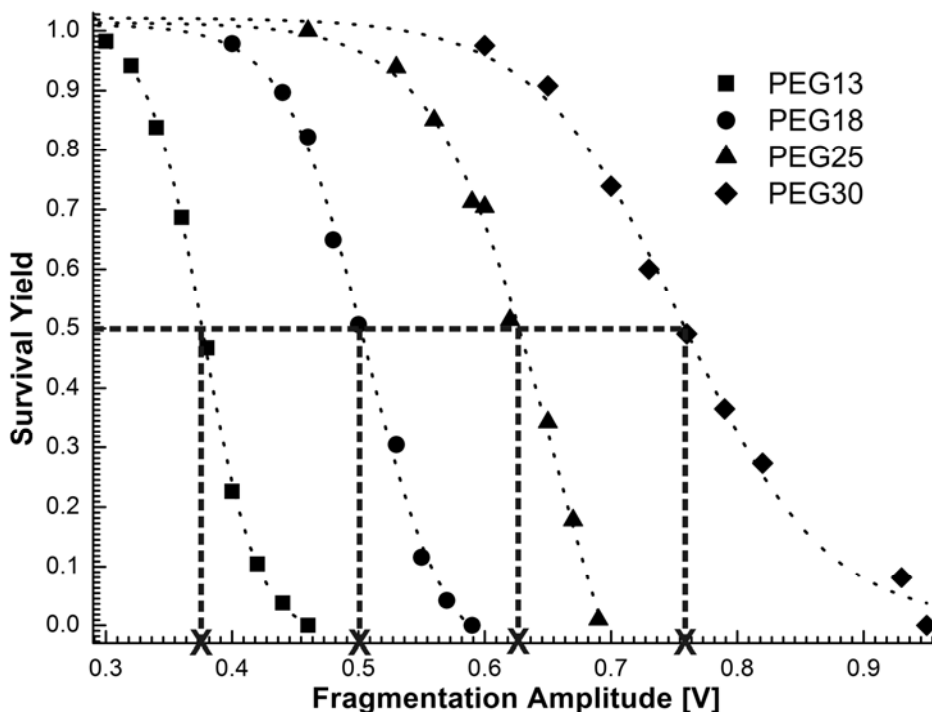


**Figure 4.7.** SY curves for different sizes of singly lithium cationized PEG oligomers (Label number next to PEG indicates the number of monomers). The experimental data points are presented along with the corresponding sigmoidal fits. The determination of the CCV value was defined as the abscissa of the characteristic point at 50% SY of the sigmoidal fit (indicated with a cross on the x-axis).

Based on this procedure, the CCV values of a series of PEG oligomers of various sizes and charge states were measured. Figure 4.8 presents the change of the CCV with the  $m/z$  for singly, doubly and triply lithium cationized PEG oligomers. The data points were linearly fitted. The coefficients of determination were the following:  $R^2_{(1+)}=0.993$ ;  $R^2_{(2+)}=0.996$ ;  $R^2_{(3+)}=0.964$ . The coefficients of determination suggest that, in the mass range studied, there is a linear correlation between the CCV and the  $m/z$ , independent of the

charge state. In addition, it is observed that the fitted line and the data points of the singly charged species are higher than the other two series. This indicates that although the charge state does not influence the linearity, it still has an influence on the CCV values. This “energetic shift” may have different causes. The cross-sections of the oligomers change with the charge state. It was previously observed that the multiply charged PEG oligomers have a more extended structure than the singly charged ones<sup>140</sup>. A large cross-section will result in an increase in the number of collisions that the precursor ion experiences, which in turn, leads to more effective fragmentation at a given collision energy. This means that the CCV value will be lower than the one observed in singly charged ions with the same  $m/z$ . In addition the presence of a second or more charges may open additional fragmentation pathways with lower activation energies and/or may increase the probability of charge catalyzed fragmentations.

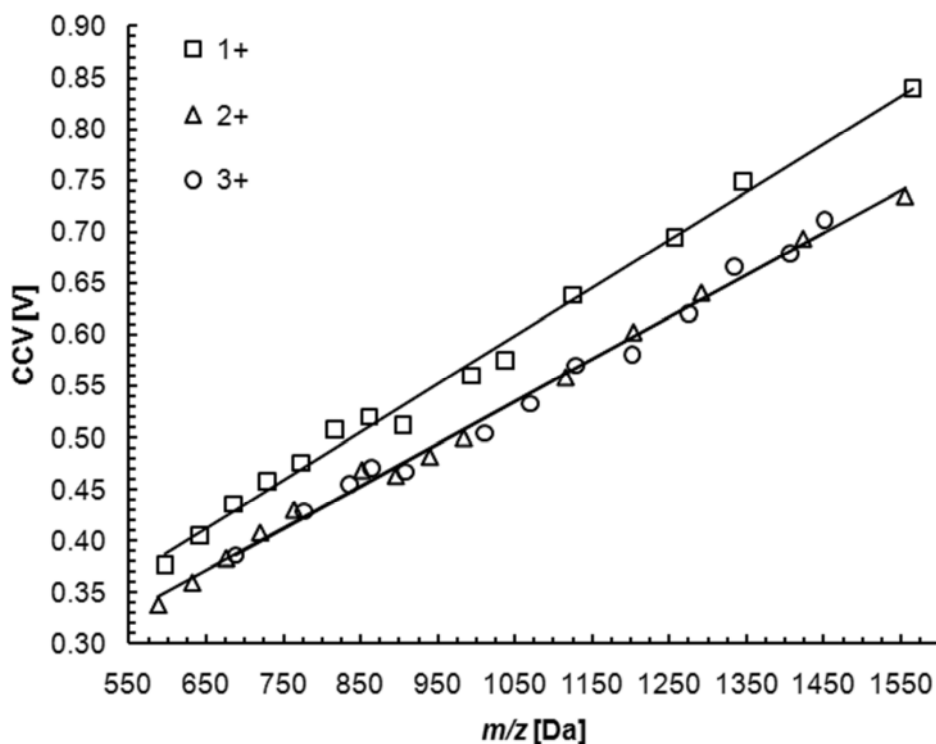


**Figure 4.8.** CCV vs the  $m/z$  of singly (1+), doubly (2+) and triply (3+) lithium cationized polymers. Note: The data points per charge state were linear fitted.

To investigate if this shift is significant, the results were plotted in a different way. Instead of using the  $m/z$ , the CCV values were plotted against the precursor ion mass (Figure 4.9).

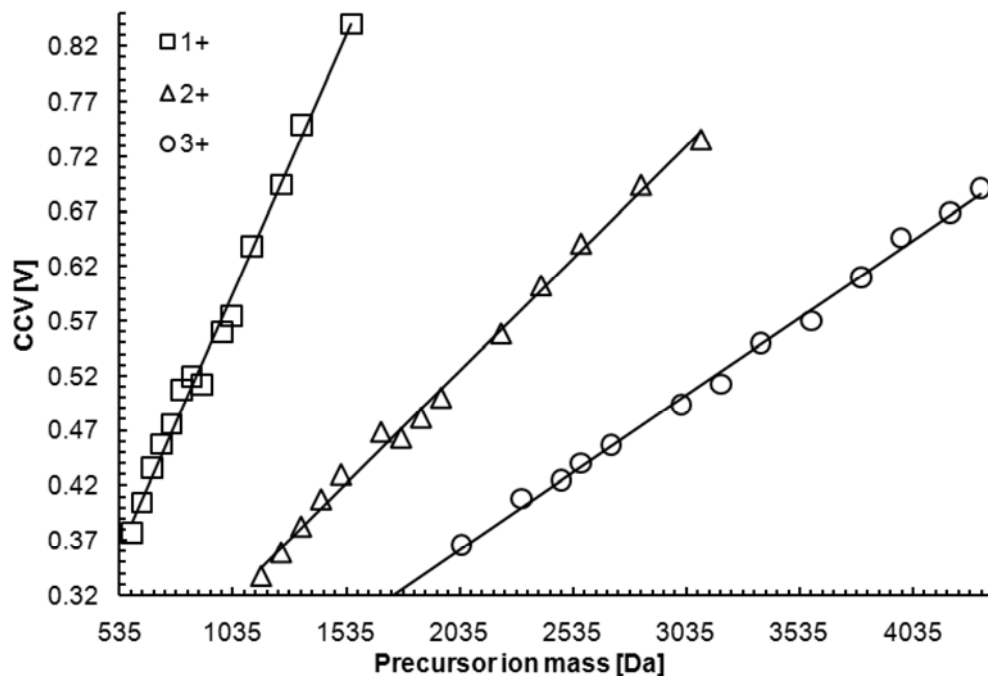


**Figure 4.9.** CCV vs the precursor ion masses of singly (1+), doubly (2+) and triply (3+) lithium cationized PEGs.

In this way the CCV values are directly linked to the mass of the oligomers and subsequently the DoF. A further step is to correct also the CCV value with the charge state (Figure 4.10). The corrected CCV value is calculated by multiplying the CCV value with the charge state. In both cases the linear correlation remains. In addition, after correcting the CCV value by taking consideration the charge state, all data points (from all three charge states) surprisingly follow almost the same linear trend. The data points of the singly and doubly charged precursor ions overlap, whereas the data points of the triply charged precursor ions are shifted to higher values. This shift suggests that correction of the CCV by multiplying it with the charge state is not fully accurate (as mentioned earlier, the cross-sections of ions with the same  $m/z$  vary with the charge state).

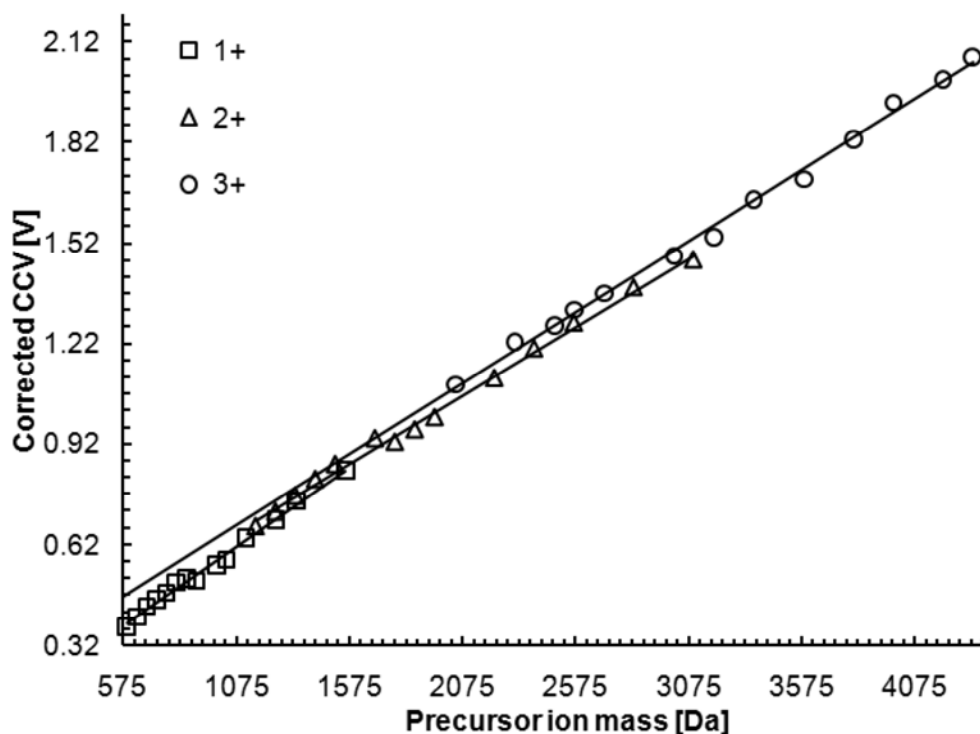


**Figure 4.10.** Corrected CCV vs the precursor ion masses of singly (1+), doubly (2+) and triply (3+) lithium cationized PEGs.

The linear correlation between the CCV value and the  $m/z$  or precursor ion mass as is in agreement with the one observed in other MS instruments, such as a QqQ and a  $q$ -TOF.<sup>133</sup> This is a further confirmation of the fact that the collision energy can be accurately controlled in a QIT instrument, if the necessary optimizations of the instrumental parameters is performed.

## 4.5 Conclusions

The SY is used as an expression of the degree of fragmentation of a polymer ion. The collision energy value, where the SY equals 50% (*i.e.*, CCV), is used as a characteristic value that reflects the fragmentation energy requirements for that specific ion.

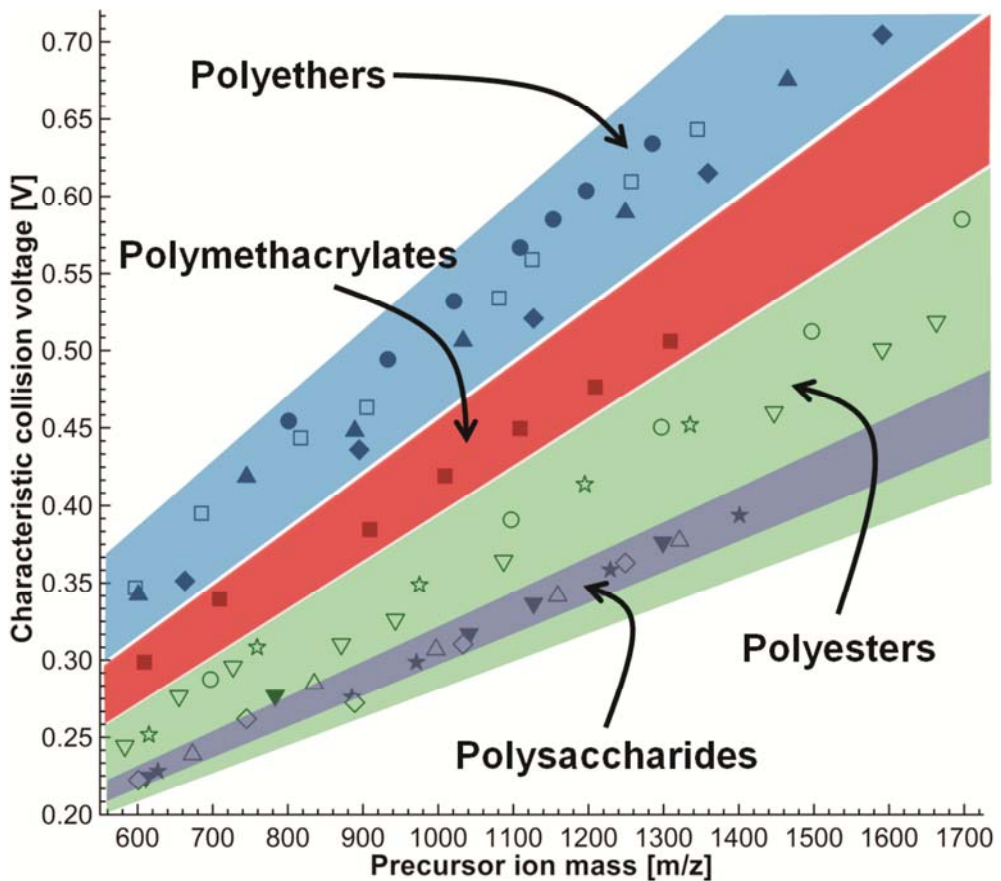
Investigation and optimization of various instrumental parameters allow the standardization of the excitation method in a QIT instrument. In this way the applied

collision energy is accurate and reproducible. Parameters related with the pre-isolation and isolation steps contribute to the quality of the product ion mass spectra by excluding any space charge effects. The cooling time between the isolation and excitation step ensures that the precursor ions are fully thermalized. During the excitation step parameters such as fragmentation frequency, fragmentation width, and excitation time have an impact on the SY curves, and consequently the determination of the CCV.

The method was tested by investigating the DoF effect. This was achieved by determining the CCV values of polymer ions of different sizes. The CCV values of PEG oligomers of different sizes and different charge states show a good linear correlation with the  $m/z$  (and the precursor ion mass). This linear correlation is in agreement with those observed in other MS instruments.<sup>133</sup>

# 5

## Polymer Analysis by Using Their Characteristic Collision Energy in Tandem Mass Spectrometry



The characteristic collision energy to obtain 50% fragmentation, expressed as the characteristic collision voltage (CCV), was used as a tool to discriminate different classes of polymers. The CCV value of different polymers was determined in a quadrupole ion trap mass spectrometer. Good linear correlation ( $0.980 < R^2 < 0.999$ ) between the CCV values and precursor ion mass was found for all polymers studied. The position of the various linear trend lines varied among the various polymers, which allowed their grouping based on the respective CCV values. The collision energy necessary to drive fragmentation was decreasing in the order of: polyethers > polymethacrylates > polyesters > polysaccharides. This suggests that polysaccharides fragment most easily (low CCVs), while polyethers require the highest collision energy among the polymers studied. The effect of endgroup on the CCV was also studied, showing a minor influence in most cases. In addition the applicability of CCV as discriminator was studied for a mixture of (1) polylactic acid (PLA), (2) poly(tetramethylene glycol) (PTMEG) and (3) PLA-*block*-PTMEG-*block*-PLA block copolymer. Differences between the CCV values of four nominally isobaric polymers (of which two copolymers, and two homopolymers) were observed. These results demonstrate that the insertion of a “weak” link into a polymer chain significantly affects the energy required for fragmentation.

**Nasioudis, A.; Memboeuf, A.; Heeren R. M. A.; Smith, D. F.; Vékey, K.; Drahos, L.; van den Brink, O. F *Anal Chem.* 2010, 82, 9350-9356.**

**Memboeuf, A.; Nasioudis, A.; Indelicato, S.; Pollreis, F.; Kuki, A.; Kéki, S.; van den Brink, O. F.; Vékey, K.; Drahos, L. *Anal Chem.* 2010, 82, 2294-2302.**

## 5.1 Introduction

One of the biggest challenges in polymer analysis by mass spectrometry (MS) is how to use multistage mass spectrometry ( $MS^n$ ) as a selective tool for the extraction of structural information from the fragmentation patterns of structurally complicated polymeric systems. A prerequisite to meet this challenge is to have a good understanding of the fragmentation behavior of molecules in different excitation conditions and as a function of their composition. As shown previously, accurate and reproducible control of the applied collision energy can be achieved even for a quadrupole ion trap (QIT), if proper optimization of the instrumental parameters is made. The degrees of freedom (DoF) effect complicates the size dependence analysis of polymer by tandem MS ( $MS/MS$ ).

We have demonstrated that the DoF effect is valid for polyethyleneglycols (PEGs) (see also Chapter 4) and polytetramethyleneglycols (PTMEGs).<sup>133</sup> A follow-up study, focused in more detail on PTMEGs, confirms their linear correlation.<sup>141</sup> Recent work by Kertesz *et al.*<sup>142</sup> showed that the determination of the characteristic collision energy for a 50% survival yield (SY) of the precursor ion can be used as a method for small molecule identification and discrimination. This latest insight, when applied to larger molecules, can aid the structural analysis of structurally complicated polymeric systems. To demonstrate the use of the collision energy as a source of structural information, the validity of the linear correlation between the characteristic collision energy and ion mass has to be proven for a variety of classes of polymer compounds.

In this chapter, we investigate the relation between collision energy and size for some polymers of different types (ether, ester and carbon-carbon bonds) as well as the possible influence of end-groups. We have previously demonstrated the agreement between various MS instrumentation (*i.e.*, triple quadrupole (QqQ), quadrupole time of flight (*q*-TOF) and QIT mass spectrometers), which cover the most common energy ranges and timescales.<sup>133</sup> This study will use a QIT, because it is a versatile (from the point of view of  $MS^n$ ), challenging (from the point of view of instrument and energetic control), relatively cheap and readily available instrument.

## 5.2 Experimental section

### 5.2.1 Chemicals

PEG 600, 1,000 and 1,450 Da, PEG dimethyl ether (MePEGMe) 1,000 Da, polybutylene adipate diol end capped (PBAd) 1,000 Da, terathane polyether glycol (PTMEG) 650, 1,000 and 2,000 Da, acetonitrile (ACN) and methanol (MeOH) solvents (both of HPLC grade), and lithium hydroxide (LiOH) were purchased from Sigma-Aldrich (St. Louis, MO). Poly(methyl methacrylate) (PMMA) 850 and 1,450 Da were from Polymer Standards Services (Mainz, Germany). Poly(propylene glycol) (PPG) 790 and 1,500 Da were from Waters Associates (Framingham, MA). Linear polylactic acid (PLA), linear polylactic acid methyl ester (MePLA), cyclic polylactic (CPLA), poly(3-hydroxybutyric acid) (PHB), PHB with crotonate end-group (CrotPHB) and PLA-*block*-PTMEG-*block*-PLA triblock copolymer were synthesized<sup>143</sup> and characterized in the Centre of Polymer and Carbon Materials of the Polish Academy of Sciences (Zabrze, Poland). The analysis of maltodextrin oligomers was performed on STAR-DRI 42R Maltodextrin (Tate & Lyle PLC, London, UK). The structures of the polymers are provided in Chart 5.1. Cation exchange resin AG MP-50 was purchased from Bio-Rad Laboratories (Hercules, CA). Ultra-pure water with a resistivity of 18.2 M $\Omega$ ·cm (at 25 °C) was obtained from a Millipore Direct-Q 3 (Molsheim, France) water purification system.

### 5.2.2 Sample preparation and instrumentation

The samples were dissolved in a 50/50 (v/v) water/methanol or acetonitrile/water solution (depending on the polymer's solubility) at a concentration of 5–50  $\mu$ M. The solvents were purified with the cation exchange resin prior to dissolution and LiOH was added at a concentration of 0.1–0.2 mM.

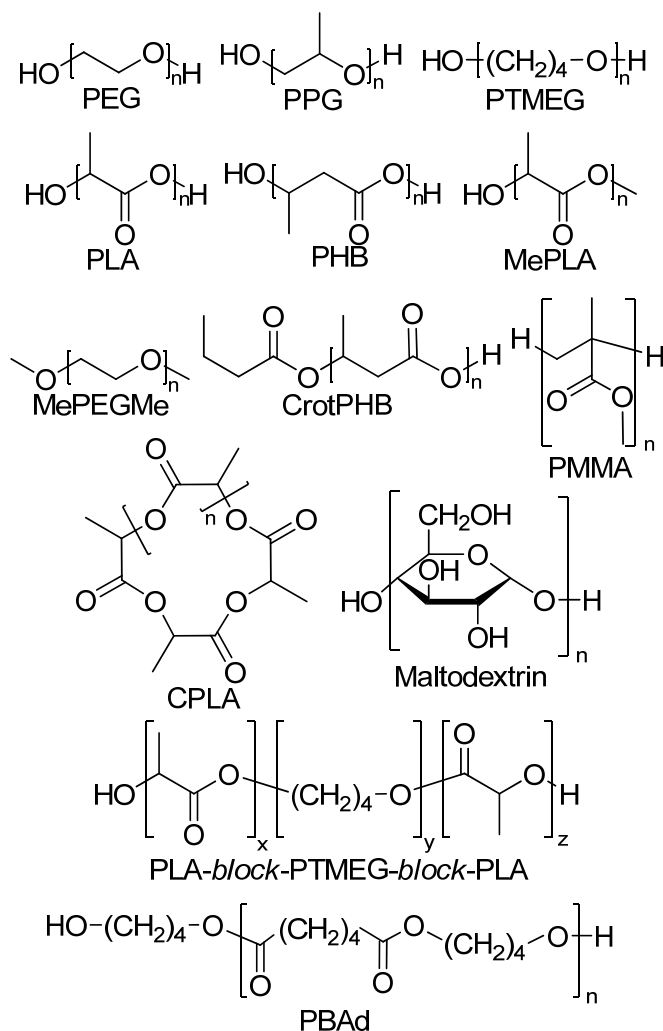


**Chart 5.1.** Structures of polymers studied.

Experiments were performed in a Bruker Esquire 3000<sup>plus</sup> QIT mass spectrometer (Bruker Daltonics, Bremen, Germany) equipped with an electrospray ionization (ESI) source. To perform accurate energy-dependent experiments on this instrument, the same excitation regime needs to be applied to all ions, so that only changes of the fragmentation amplitude may influence the effective energy deposition. This was achieved by following the optimization procedure presented in Chapter 4. The other settings of the instrument were the same as presented in Chapter 4.

For the analysis of the PLA-*block*-PTMEG-*block*-PLA triblock copolymer an LTQ-Fourier-transform ion cyclotron resonance (FTICR) hybrid mass spectrometer (Thermo Scientific, San Jose, CA) equipped with a 7 T magnet and a Thermo IonMax ESI source was used. The isolation and excitation steps were performed in the linear ion trap whereas the mass analysis of the ion population was done in the ICR cell. The LTQ-FTICR hybrid mass spectrometer software does not allow the control and optimization of all the parameters mentioned before (in the case of the QIT). Consequently, a size dependence study similar to the one performed on the QIT was not performed for this instrument. In the experiments performed on the PLA-*block*-PTMEG-*block*-PLA triblock copolymer the collision energy was varied by setting the percentage of ‘normalized collision energy’ (NCE) in the LTQ-FTICR’s acquisition software. The other settings of the instrument were the following: Automatic gain control feature on; wide band excitation feature off; capillary voltage 3.5 kV; heated metal capillary temperature 275 °C; isolation width 0.6 Th; excitation time 15 ms;  $q_z$  value 0.25; resolving power 100,000. The sample was infused with the onboard syringe pump at a flow rate of 3  $\mu\text{L}/\text{min}$ .

In order to allow semi-quantitative comparison among the different polymers, the robustness of the method needed to be assessed. To evaluate the experimental accuracy, curves of the SY of lithium cationized  $[\text{PEG}_{15}+\text{Li}]^+$  and  $[\text{PEG}_{10}+\text{Li}]^+$  as a function of collision energy (expressed in the QIT as fragmentation amplitude in Volts) were measured several times in succession. Experimental conditions were maintained constant as much as possible throughout the complete set of measurements. As a measure of quality control, SY curves of  $[\text{PEG}_{15}+\text{Li}]^+$  were generated regularly during our study to ensure instrument stability and to obtain repeatable results. The standard deviation (SD) and the relative standard deviation (RSD) for the CCV of  $[\text{PEG}_{15}+\text{Li}]^+$  were  $1.3 \cdot 10^{-3}$  V and 0.33%, respectively. Measurement of SY curves for this compound at different concentrations was not performed because previously reported work<sup>133</sup> showed that the abundance of the precursor ion does not influence the results. To avoid systematic errors during the measurement of the SY curves of the various polymers, the order in which the oligomers were analyzed was randomized.

## 5.3 Results and discussion

### 5.3.1 Energy-dependent analysis of homopolymers

The SY curves of various sizes of the studied polymers were measured and the voltage values (fragmentation amplitude), connected with the characteristic point of 50% precursor ion SY, hereafter referred to as CCVs, were determined using the same method presented in Chapter 4. Figure 5.1 presents an example of this process for the case of PMMA oligomers.

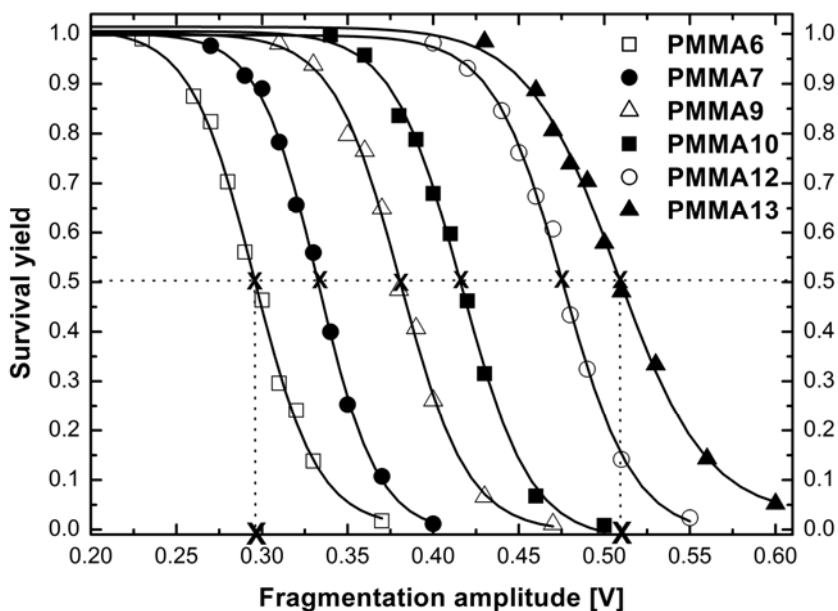


**Figure 5.1.** SY curves for different sizes of singly lithium cationized PMMA oligomers (Label number next to PMMA indicates the number of monomers). The experimental data points are presented along with the corresponding sigmoidal fits.

Figure 5.2 depicts the CCV values of different oligomers as a function of the precursor ion mass. For each series of polymer types the CCV values were linearly fitted. The parameters of the linear fits are presented in Table 5.1. A graph of the CCV values as a function of the DoF was also made (Figure 5.3) and the data points were linearly fitted (Table 5.2). We focused, however, on the study of the CCV vs precursor ion mass because the use of the mass-to-charge ratio ( $m/z$ ) as a reference requires no prior knowledge of the polymer structure.

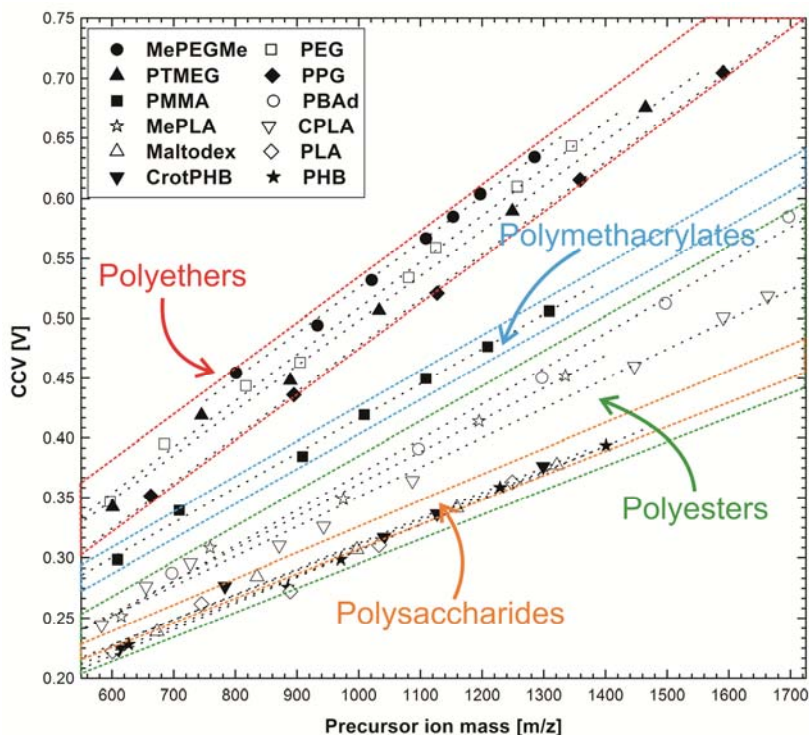


**Figure 5.2.** CCV vs the precursor ion masses of the studied singly lithium cationized polymers. The data points per polymer were linear fitted (parameters shown in Table 5.1) and grouped in four groups: polyethers (red), polymethacrylates (blue), polyesters (green), and polysaccharides (orange).

**Table 5.1. Parameters of the Fitted Linear Trend Lines<sup>a</sup> Obtained for Various Polymers**

Group	Polymer	Slope		Intercept		Linearity R <sup>2</sup>
		Value	Error	Value	Error	
Polyethers	PEG	$3.834 \times 10^{-4}$	$\pm 0.120 \times 10^{-4}$	0.127	$\pm 0.012$	0.993
	PPG	$3.817 \times 10^{-4}$	$\pm 0.047 \times 10^{-4}$	0.095	$\pm 0.006$	0.999
	MePEGMe	$3.813 \times 10^{-4}$	$\pm 0.091 \times 10^{-4}$	0.144	$\pm 0.010$	0.997
	PTMEG	$3.749 \times 10^{-4}$	$\pm 0.140 \times 10^{-4}$	0.123	$\pm 0.015$	0.994
Polymethacrylates	PMMA	$2.901 \times 10^{-4}$	$\pm 0.074 \times 10^{-4}$	0.126	$\pm 0.007$	0.997
Polyesters	PBAd	$2.952 \times 10^{-4}$	$\pm 0.121 \times 10^{-4}$	0.074	$\pm 0.016$	0.995
	MePLA	$2.686 \times 10^{-4}$	$\pm 0.141 \times 10^{-4}$	0.093	$\pm 0.014$	0.992
	CPLA	$2.468 \times 10^{-4}$	$\pm 0.078 \times 10^{-4}$	0.104	$\pm 0.009$	0.993
	PHB	$2.182 \times 10^{-4}$	$\pm 0.064 \times 10^{-4}$	0.088	$\pm 0.007$	0.997
	CrotPHB	$2.108 \times 10^{-4}$	$\pm 0.136 \times 10^{-4}$	0.101	$\pm 0.014$	0.988
	PLA	$2.098 \times 10^{-4}$	$\pm 0.173 \times 10^{-4}$	0.096	$\pm 0.016$	0.980
Polysaccharides	Maltodextrin	$2.055 \times 10^{-4}$	$\pm 0.108 \times 10^{-4}$	0.105	$\pm 0.011$	0.992

<sup>a</sup>The reported error values reflect the 95% confidence level

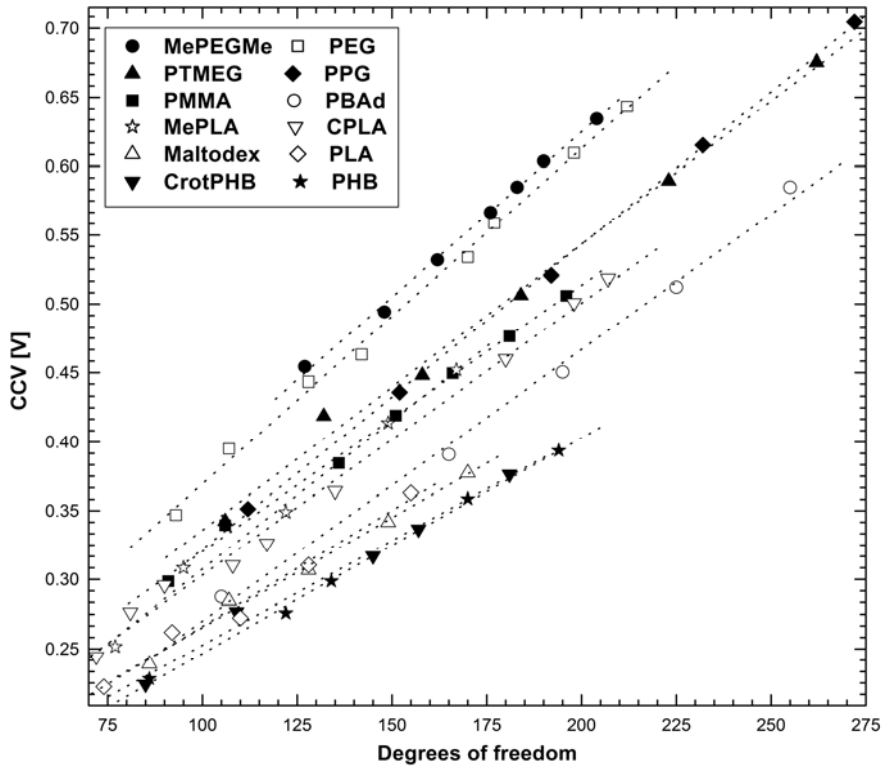


**Figure 5.3.** CCV vs the DoF of the studied lithium cationized polymers. The data points were linear fitted (Parameters shown in Table 5.2).

**Table 5.2. Parameters of the Fitted Linear Trend Lines (CCV vs the DoF)<sup>a</sup> Obtained for Various Polymers**

Polymer	Slope		Intercept		Linearity $R^2$
	Value	Error	Value	Error	
PEG	$2.43 \times 10^{-3}$	$\pm 0.06 \times 10^{-3}$	0.126	$\pm 0.009$	0.997
MePEGMe	$2.40 \times 10^{-3}$	$\pm 0.06 \times 10^{-3}$	0.145	$\pm 0.010$	0.997
PPG	$2.21 \times 10^{-3}$	$\pm 0.03 \times 10^{-3}$	0.101	$\pm 0.006$	0.999
PTMEG	$2.08 \times 10^{-3}$	$\pm 0.08 \times 10^{-3}$	0.128	$\pm 0.014$	0.994
MePLA	$2.15 \times 10^{-3}$	$\pm 0.14 \times 10^{-3}$	0.092	$\pm 0.014$	0.992
CPLA	$1.97 \times 10^{-3}$	$\pm 0.06 \times 10^{-3}$	0.106	$\pm 0.009$	0.993
PBAd	$1.97 \times 10^{-3}$	$\pm 0.08 \times 10^{-3}$	0.073	$\pm 0.016$	0.995
PMMA	$1.93 \times 10^{-3}$	$\pm 0.05 \times 10^{-3}$	0.127	$\pm 0.007$	0.997
PLA	$1.68 \times 10^{-3}$	$\pm 0.14 \times 10^{-3}$	0.098	$\pm 0.016$	0.980
Maltodextrin	$1.59 \times 10^{-3}$	$\pm 0.09 \times 10^{-3}$	0.106	$\pm 0.011$	0.991
PHB	$1.56 \times 10^{-3}$	$\pm 0.05 \times 10^{-3}$	0.090	$\pm 0.007$	0.997
CrotPHB	$1.51 \times 10^{-3}$	$\pm 0.10 \times 10^{-3}$	0.102	$\pm 0.014$	0.988

<sup>a</sup>The reported error values reflect the 95% confidence level.

There is an overall good ( $R^2 > 0.980$ ) linear relationship between the CCV values and the molecular size for all polymers studied. This indicates that all oligomers studied exhibit fast energy randomization in the range of  $m/z$  575 to 1,700. The coefficients of determination range between  $R^2_{PLA} = 0.980$  and  $R^2_{PPG} = 0.999$ . The variation in the coefficients of determination can be attributed to various causes. Firstly, there are statistical inaccuracies derived from the variations in the number of data points used for the linear fits, (*i.e.*, from 5 [PLA] to 9 [CPLA]) and the distribution over differing mass ranges (*i.e.*, from  $m/z$  484 [MePEGMe] to  $m/z$  1,080 [CPLA]). Previous results<sup>133</sup> using a QIT for the analysis of PEGs exhibited coefficient of determination of approximately 0.998 (on the data presented here the value for PEGs was 0.993). In addition to the statistical causes, other factors may contribute to the variation. Although based on drift tube experiments<sup>144,145</sup> the cross-section of the cationized PEG, PPG and PTMEG ions can be considered to increase with mass linearly (allowing the parallel linear increase of the number of collisions to compensate for the decrease of the center-of-mass collision energy), this assumption cannot be fully supported for other polymers (*e.g.*, PLA, PHB, CPLA, Maltodextrin, etc) without further study. The presence of different end-groups (CrotPHB, MePLA) at the two sides of the polymer chain can further affect the linear correlation between CCV and precursor ion mass, since their contribution to the polymer's DoF is gradually reducing with increasing polymer size. There may be a further effect due to a convolution of (1) cation affinity differences between monomer moieties in the polymer chain on the one hand and end-groups on the other and (2) the occurrence of cation-catalyzed fragmentation processes.

In Figure 5.2, evident differences are observed between the fitted linear trend lines. To confirm this observation, a statistical evaluation of the significance of the differences in intercepts and slopes was carried out (Table 5.3). The fitted linear trend lines of polyethers (*i.e.*, PEG, PPG, MePEGMe and PTMEG) have statistically similar slope values but significantly different (at the 99% confidence level) intercept values.

Table 5.3. Comparison of the Slope “a” and Intercept “b” of the Fitted Linear Trend Lines<sup>a</sup> of all Polymers Studied

Maltodex	CrotPHB		PHB		PLA		CPLA		MePLA		PBAd		PMMA		PEG		MePEGMc		PPG		
	a	b	a	b	a	b	a	b	a	b	a	b	a	b	a	b	a	b	a	b	
PTMEG	99	99	99	99	99	99	99	99	99	99	99	99	99	99	99	99	95	99	99	99	99
PPG	99	99	99	99	99	99	99	99	99	99	99	99	99	99	99	99	99	99	99	99	99
MePEGMc	99	99	99	99	99	99	99	99	99	99	99	99	99	99	99	99	99	99	99	99	99
PEG	99	99	99	99	99	99	99	99	99	99	99	99	99	99	99	99	99	99	99	99	99
PMMA	99	99	99	99	99	99	99	99	99	99	99	99	99	99	99	99	99	99	99	99	99
PBAd	99	99	99	99	99	99	99	99	99	99	99	99	99	99	99	99	99	99	99	99	99
MePLA	>95	99	>95	99	>95	99	>95	99	>90	99	>90	99	>90	99	>90	99	>90	99	>90	99	99
CPLA	>95	99	>90	99	>90	99	>90	99	>90	99	>90	99	>90	99	>90	99	>90	99	>90	99	99
PLA	>90	>90	>90	>90	>90	>90	>95	99	>90	99	>95	99	>90	99	>90	99	>90	99	>90	99	99
PHB	>90	>90	>90	>90	>90	>90	>90	>90	>90	>90	>90	>90	>90	>90	>90	>90	>90	>90	>90	>90	99
CrotPHB	>90	>90	>90	>90	>90	>90	>90	>90	>90	>90	>90	>90	>90	>90	>90	>90	>90	>90	>90	>90	99

<sup>a</sup>The fitted linear trend lines of the CCV as a function of precursor ion mass as presented in Figure 5.2 and with parameters as indicated in Table 5.1.

All values refer to the confidence level (in percentages) of statistical similarity or difference. Bold and underlined values refer to statistically similar values and with normal typeface the statistically different values.

Some polyesters (*i.e.*, PLA, PHB and croPHB) cannot be discriminated on the basis of the experimental results presented in Figure 5.2 since they are statistically similar, whereas others (*i.e.*, CPLA and PBAd) are well separated. PMMA is positioned between the polyethers and PBAd. Maltodextrin with its glycosidic bonds forms a distinct group. On the basis of both their position in the plot and their slopes, the fitted linear trend lines can be distributed in four major groups, in the following (reducing) order: polyethers > polymethacrylates > polyesters > polysaccharides. This order infers the notion that the slope value is closely related to the polymer type and the energy requirements for fragmenting a specific type of bond. An ether bond for instance needs more energy for fragmentation than an ester bond. A possible explanation for the position of PBAd (polyester group) and maltodextrin (polysaccharide group) will be given below.

In the case of the polyethers and also in the case of some polyesters, the slope values are similar. This confirms the hypothesis about the relation between slope and polymer type, since the activation energies within the same type of polymer could be supposed to remain the same (since the same type of backbone bonds are cleaved). Exceptions to this rule are CPLA, MePLA and PBAd and maltodextrin. The behavior of PBAd (in relation with the other polyesters) can be explained by an increased number of DoF. When the CCV values are plotted as a function of the number of monomer units in the polymer (Figure 5.4), the fitted line of the data points of PBAd have the highest slope of all polymers in this study (see also Table 5.4).

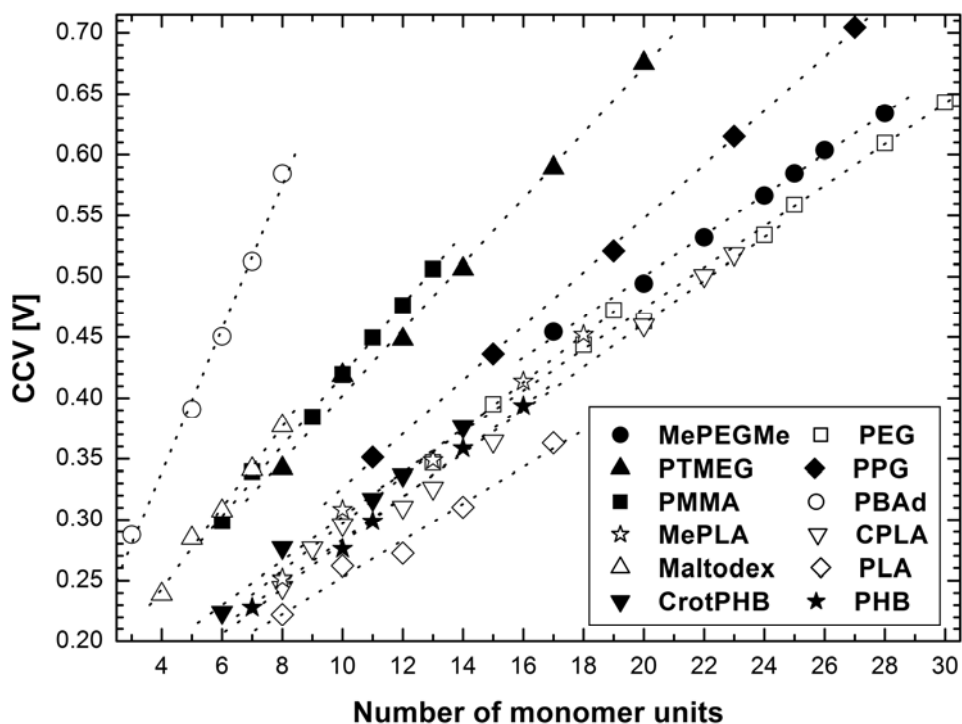


**Figure 5.4.** CCV vs the number of monomer units of the studied lithium cationized polymers. The data points were linear fitted (Parameters shown in Table 5.4).

**Table 5.4. Parameters of the Fitted Linear Trend Lines (CCV vs number of monomer units)<sup>a</sup> Obtained for Various Polymers**

Polymer	Slope		Intercept		Linearity $R^2$
	Value	Error	Value	Error	
PBAd	$5.904 \times 10^{-2}$	$\pm 0.243 \times 10^{-2}$	0.103	$\pm 0.015$	0.995
Maltodextrin	$3.329 \times 10^{-2}$	$\pm 0.175 \times 10^{-2}$	0.110	$\pm 0.011$	0.992
PMMA	$2.901 \times 10^{-2}$	$\pm 0.074 \times 10^{-2}$	0.129	$\pm 0.007$	0.997
PTMEG	$2.699 \times 10^{-2}$	$\pm 0.101 \times 10^{-2}$	0.132	$\pm 0.014$	0.994
PPG	$2.214 \times 10^{-2}$	$\pm 0.028 \times 10^{-2}$	0.105	$\pm 0.005$	0.999
MePLA	$1.939 \times 10^{-2}$	$\pm 0.102 \times 10^{-2}$	0.103	$\pm 0.014$	0.992
PHB	$1.877 \times 10^{-2}$	$\pm 0.055 \times 10^{-2}$	0.093	$\pm 0.007$	0.997
CrotPHB	$1.813 \times 10^{-2}$	$\pm 0.117 \times 10^{-2}$	0.121	$\pm 0.012$	0.988
CPLA	$1.777 \times 10^{-2}$	$\pm 0.056 \times 10^{-2}$	0.107	$\pm 0.009$	0.993
PEG	$1.687 \times 10^{-2}$	$\pm 0.053 \times 10^{-2}$	0.136	$\pm 0.011$	0.993
MePEGMe	$1.678 \times 10^{-2}$	$\pm 0.040 \times 10^{-2}$	0.165	$\pm 0.009$	0.997
PLA	$1.510 \times 10^{-2}$	$\pm 0.124 \times 10^{-2}$	0.102	$\pm 0.016$	0.980

<sup>a</sup>The reported error values reflect the 95% confidence level.

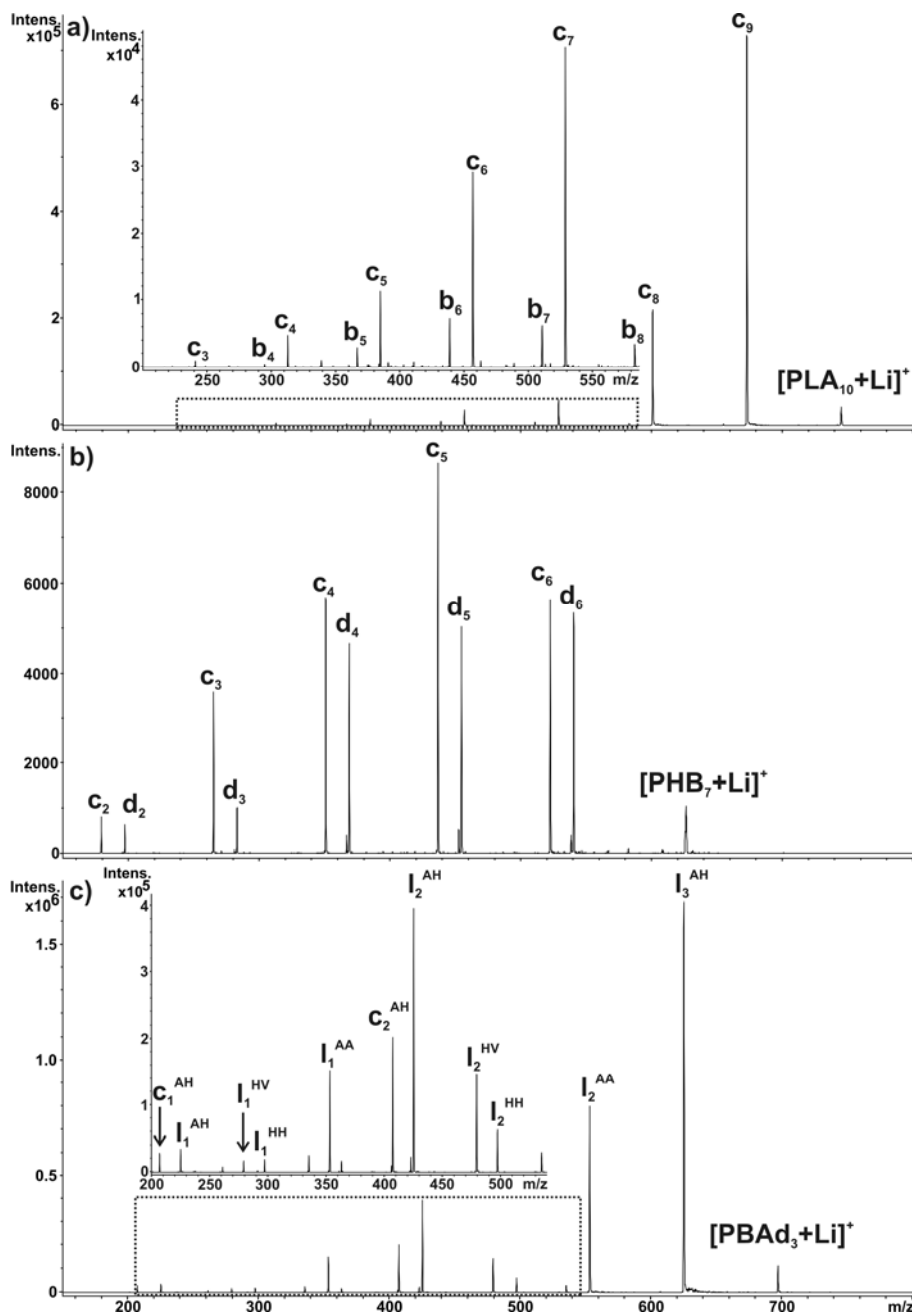


**Figure 5.5.** Collision induced dissociation of lithium cationized a) PLA, b) PHB and c) PBAd. Note: Inset figures are a magnification of the area of interest in the respective panels. Polymer fragmentation nomenclature is presented in Chart 5.2.

Based on the spectra showing the fragmentation patterns of PBA<sub>d</sub>, PHB and PLA (Figure 5.5 and Chart 5.2), the ratio of the number of bonds present in the repeating unit of PBA<sub>d</sub> (30) to the net number of bonds that is observed to break on fragmentation (four) equals 7.5. In the case of PLA and PHB, these ratios equal 4.5 (9:2) and 6 (12:2), respectively. This simple consideration of relative abundance of ‘weak’ bonds could explain why PBA<sub>d</sub> will require a surplus of collision energy for reaching the same degree of fragmentation as PLA and PHB.

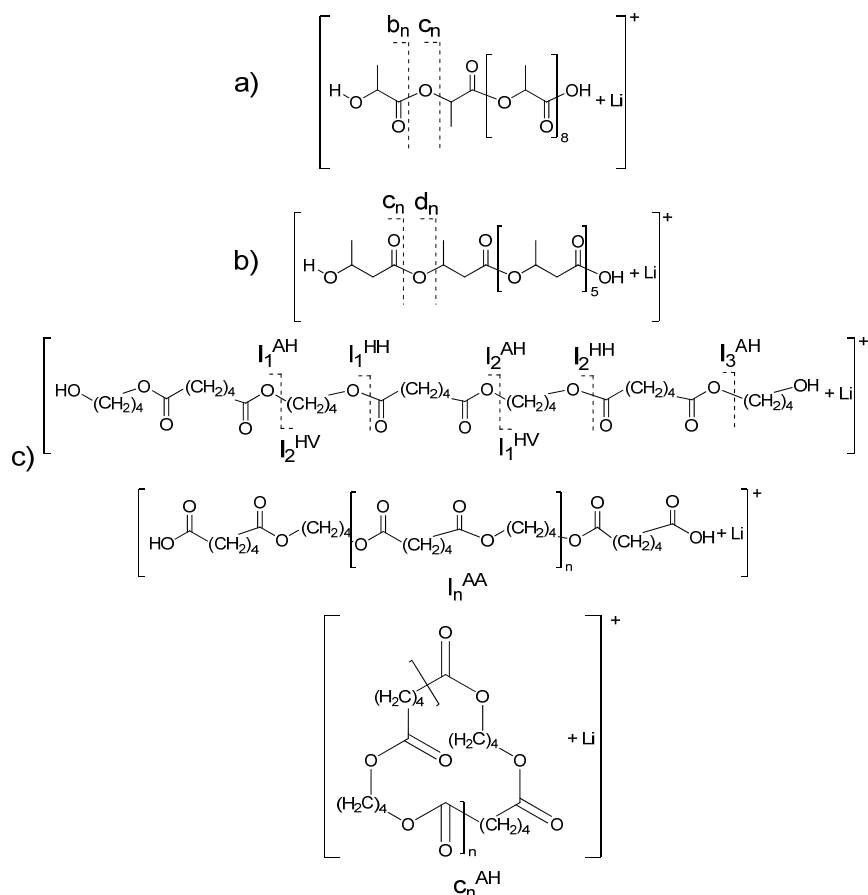


**Chart 5.2.** Fragmentation nomenclature of a) PLA, b) PHB, and c) PBA<sub>d</sub> based on Wesdemiotis *et al.*<sup>112</sup> **Note:** The product ion  $I_n^{\text{AA}}$  derives after consecutive fragmentation of product ion  $I_n^{\text{AH}}$  and neutral loss of 72 Da. Product ion  $c_n^{\text{AH}}$  is cyclic product ions after intramolecular transesterification.

Maltodextrin's low slope value (Table 5.1 and Figure 5.2) can be attributed to the weak strength of the glycosidic bond and/or an increased number of collisions due to its rigid and large structure, and thereby cross-section. The slope difference, between CPLA ( $2.468 \times 10^{-4}$ , Table 5.1) and linear PLA ( $2.098 \times 10^{-4}$ , Table 5.1) can be attributed to the additional energy needed to cleave the ring prior to the monomer loss. The behavior of MePLA is attributed to a prominent end-group effect that will be discussed later.

Figure 5.2 suggests that the fitted lines of polyethers and polyesters are suitable candidates to study the origin of the difference in intercepts, as the intercepts are ranked in the following (reducing) order PEG>PTMEG>PPG and PLA>PHB. At this stage, however, a direct correlation between the intercept values and the structural differences of the above polymer ions has not been identified. The attribution of observed differences in intercept values will need further experiments, specially designed for the investigation of various potential factors.

As mentioned before, three pairs of polymers with the same monomer but different end-groups were analyzed. In two (CrotPHB and MePEGMe) out of the three cases, the addition of a multi-atom end-group did not have a dramatic influence on the CCV values in comparison with the CCV values of the equivalent homopolymers with small, single atom end-groups. In the case of MePLA, the CCV values of the oligomers were dramatically increased and different from those of PLA oligomers. The small increase in the DoF due to the end-groups could explain the small difference in the CCV values between PEG and MePEGMe and between PHB and CrotPHB. To check this hypothesis, the CCV values as a function of the degrees of freedom were examined (*vide supra*, Figure 5.3 and Table 5.2). The results do not show a distinct difference between the lines of PEG and MePEGMe. The same is observed for PHB and CrotPHB. It is suggested that in order to observe a prominent end-group effect on the CCV, the insertion of a "strong bond" end-group (*e.g.*, long alkyl chain) in a "weak bond" polymer chain will be required. Additional experiments and theoretical calculations are necessary to investigate this. In the case of the PLA-MePLA pair, the structure of the end-group of PLA, featuring a labile proton, might contribute to the lower energy requirement for fragmentation. Further research, either by

comparison with other labile proton polymers or by quantum chemical calculations would be necessary to substantiate this.

### ***5.3.2 Energy-dependent analysis of block copolymers***

Since the monomer units of PLA and PTMEG differ by 36.41 mDa, any of their oligomers with the same number of monomer units (but with a degree of polymerization lower than 27) are nominally isobaric compounds. A copolymer of these two, in the same (<27) degree of polymerization range, may also be nominally isobaric to the respective homopolymers. In addition, the product ion spectra of both homopolymers and their copolymers are similar (Figure 5.6), showing differences in peak intensities of the product ions only, thus making the discrimination even more difficult, especially when these ions are in a mixture.

The resolving power of the QIT is not sufficient for resolving ions with such a small mass difference. Therefore, the analysis was performed on the LTQ-FTICR hybrid mass spectrometer performing isolation and excitation of the ions in the ion trap and mass analysis at high resolving power in the ICR cell.

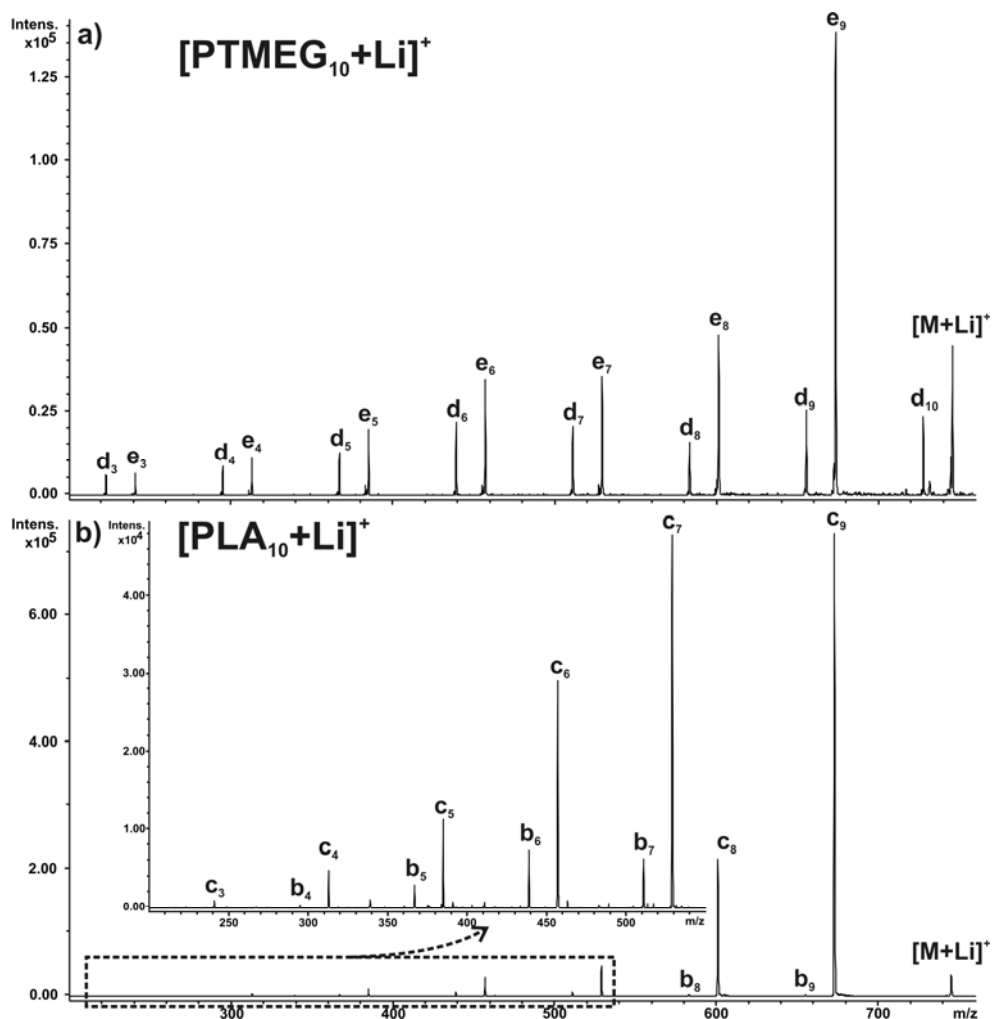


**Figure 5.6.** Collision induced dissociation of lithium cationized PLA and PTMEG in a QIT. a) Product ion spectra of  $[\text{PTMEG}_{10}+\text{Li}]^+$  and b)  $[\text{PLA}_{10}+\text{Li}]^+$ . Note: Inset figure is a magnification of the area of interest in panel b.

The high resolution MS spectrum of the synthesized PLA-*block*-PTMEG-*block*-PLA triblock copolymer (Figure 5.7) revealed that the sample consists of unreacted PTMEG oligomers and block copolymers of PLA with PTMEG. Since PTMEG has two hydroxyl groups, the anionic polymerization can take place in both sides of the chain. Thus the number of possible positional isomers increases with the size of the PLA blocks. To avoid this complexity, we focused on performing energy-dependent analysis of the precursor ion

at  $m/z$  457 where only four mass peaks are present. By accurate mass measurement, the observed peaks were assigned to the lithium cationized PTMEG (peak A) and PLA-*block*-PTMEG-*block*-PLA oligomers (peak B, C, D) (Table 5.5). Since PLA homopolymer was not present in the copolymer, the sample was spiked with an amount of PLA necessary to obtain a peak intensity in the same order of magnitude as the other peaks (except for the low intensity of peak D).

Figure 5.7 depicts the MS spectrum of the unspiked and spiked sample obtained in a LTQ-FTICR hybrid mass spectrometer. Although the presence of peak D cannot be neglected, we assumed that its very low intensity in comparison with the other four peaks will not affect the results. Due to the small mass difference among the four peaks, all four ions experienced the same activation during isolation and excitation in the ion trap.

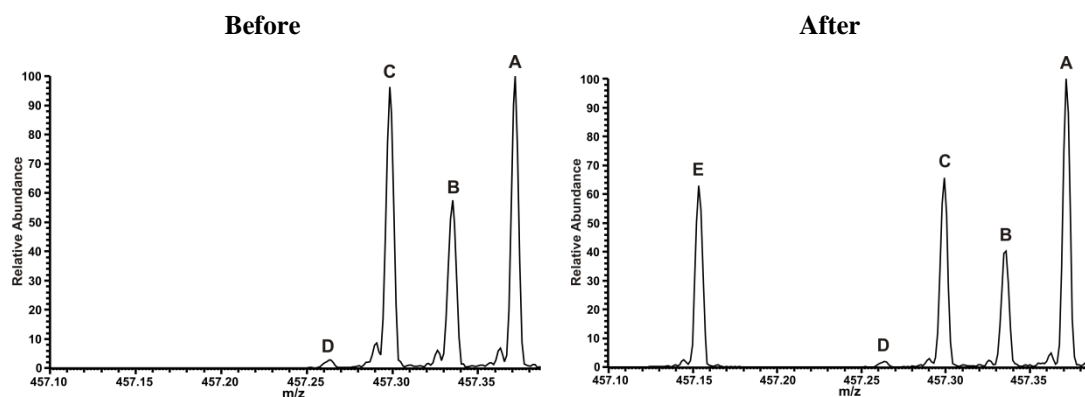


**Figure 5.7.** LTQ-FTICR mass spectra of PLA-*block*-PTMEG-*block*-PLA copolymer before and after being spiked with PLA. The peaks were assigned as follows: Peak A:  $[\text{PTMEG}_6+\text{Li}]^+$ ; Peak B:  $[\text{PTMEG}_5\text{-PLA}+\text{Li}]^+$ ; Peak C is  $[\text{PTMEG}_4\text{-PLA}_2+\text{Li}]^+$  or  $[\text{PLA-PTMEG}_4\text{-PLA}+\text{Li}]^+$ ; Peak D:  $[\text{PTMEG}_3\text{-PLA}_3+\text{Li}]^+$  or  $[\text{PLA}_2\text{-PTMEG}_3\text{-PLA}+\text{Li}]^+$ ; Peak E:  $[\text{PLA}_6+\text{Li}]^+$ .

**Table 5.5. Accurate Mass Measurement<sup>a</sup> of Peaks in Figure 5.7**

Peak code	Measured mass [Da]	Theoretical mass [Da]	Error [ppm]	Elemental composition	Assigned structure
A	457.3716	457.3711	1.03	$\text{C}_{24}\text{H}_{50}\text{O}_7\text{Li}$	$[\text{PTMEG}_6+\text{Li}]^+$
B	457.3353	457.3347	1.31	$\text{C}_{23}\text{H}_{46}\text{O}_8\text{Li}$	$[\text{PLA-PTMEG}_5+\text{Li}]^+$
C	457.2990	457.2983	1.47	$\text{C}_{22}\text{H}_{42}\text{O}_9\text{Li}$	$[\text{PLA}_2\text{-PTMEG}_4+\text{Li}]^+$
D	457.2638	457.2620	3.98	$\text{C}_{21}\text{H}_{38}\text{O}_{10}\text{Li}$	$[\text{PLA}_3\text{-PTMEG}_3+\text{Li}]^+$
E	457.1536	457.1528	1.71	$\text{C}_{18}\text{H}_{26}\text{O}_{13}\text{Li}$	$[\text{PLA}_6+\text{Li}]^+$

<sup>a</sup> Performed on LTQ FTICR hybrid mass spectrometer with external calibration.

Figure 5.8 presents the SY curves of the four nominally isobaric peaks as a function of the NCE; this is the way excitation energy is expressed in the instrument control software of the LTQ-FTICR hybrid mass spectrometer.

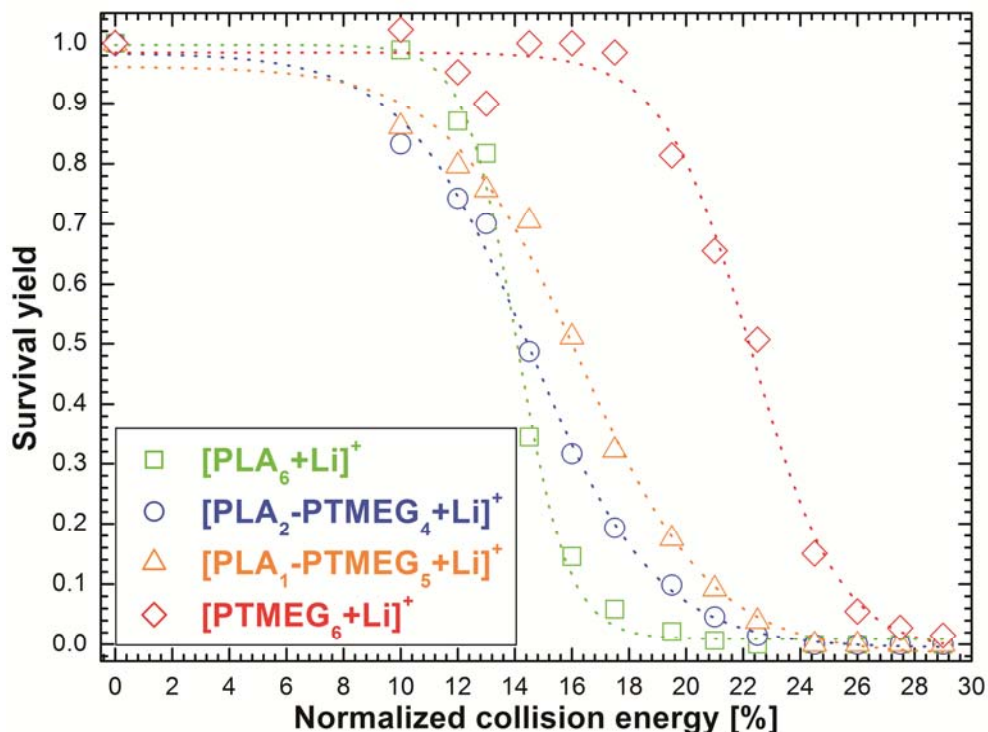


**Figure 5.8.** SY curves of  $[\text{PLA}_6+\text{Li}]^+$ ,  $[\text{PTMEG}_6+\text{Li}]^+$  and  $[\text{PLA}_n\text{-block-PTMEG}_m\text{-block-PLA}_n+\text{Li}]^+$  oligomers. The experimental data points are presented along with the corresponding sigmoidal fits. Note: SY is calculated from the following equation:  $\text{SY} = I_E/I_0$  where  $I_E$  is the intensity of the precursor ion peak after excitation with a specific percentage of NCE, and  $I_0$  the intensity of the precursor ion peak after excitation with zero % NCE.

It should be noted however that the calculation of the SY was not made in the same way as described above. Some product ions can derive from multiple precursor ions and therefore the contribution of each precursor ion to the peak intensity of specific product ions is not possible (Table 5.6). Therefore, the SY of each precursor ion was calculated as the ratio of its peak intensity at specific percentage of NCE to its intensity at zero % NCE. As expected, the SY curves of PLA and PTMEG follow the same behavior as described

previously; PLA needs less collision energy (14.1 % NCE) than PTMEG (22.3 % NCE) for fragmentation. It is striking, however, to observe that the curve from the copolymer structure that contains one LA monomer exhibits a CCV (*viz.* 16.3 % NCE) value that is significantly different from that of the PTMEG homopolymer (*viz.* 22.3 % NCE). This demonstrates that insertion of an easily fragmentable monomer (weak link) into a relatively strong chain significantly weakens the entire structure. The copolymer with two lactic acid (LA) monomer units has a lower CCV value (*viz.* 14.5 % NCE) than the copolymer with one LA monomer unit (*viz.* 16.3 % NCE). This discrimination of the two copolymers suggests that even small differences in the copolymer composition can be distinguished. Clearly, the CCV value of the copolymer with two LA monomer units may be the convolution of the CCV values of two possible isomeric forms: PLA-*block*-PTMEG-*block*-PLA triblock or PLA-*block*-PTMEG diblock copolymer. Since these isomers were not studied independently in the present experimental setup, their individual contributions were not determined. Ion mobility spectrometry MS and/or coupling of MS with a separation technique could provide the desired separation of isomers and allow the determination of the CCV of the two isomers.

**Table 5.6. Theoretical Mass Values of the Major<sup>a</sup> Product Ions of the Nominally Isobaric and/or Isomeric Compounds**

$[\text{PLA}_6+\text{Li}]^+$	$[\text{PLA}_2\text{-PTMEG}_3\text{-PLA}+\text{Li}]^+$	$[\text{PLA}_3\text{-PTMEG}_3+\text{Li}]^+$	$[\text{PLA-PTMEG}_4\text{-PLA}+\text{Li}]^+$	$[\text{PLA}_2\text{-PTMEG}_4+\text{Li}]^+$	$[\text{PLA-PTMEG}_5+\text{Li}]^+$	$[\text{PTMEG}_6+\text{Li}]^+$
457.1528	457.2620	457.2620	457.2983	457.2983	457.3347	457.3711
385.1322	385.2414	385.2414	385.2778	385.2778	385.3141	385.3141
367.1217	367.2308	367.2308	367.2672	367.2672	367.3036	367.3036
313.1116	313.2208	313.2208	313.2208	313.2572	313.2572	313.2572
295.1011	295.2102	295.1738	295.2102	295.2466	295.2466	295.2466
241.0911	241.1638	241.1274	241.1638	241.2002	241.2002	241.2002
223.0805	223.1533	223.1169	223.1533	223.1896	223.1896	223.1896
169.0705	169.1069	169.0705	169.1069	169.1432	169.1432	169.1432

<sup>a</sup>The complete table of the possible product ions is omitted. The presented product ions derive from consecutive neutral losses of  $\text{C}_3\text{H}_4\text{O}$  (PLA monomer unit),  $\text{C}_4\text{H}_6\text{O}$  (PTMEG monomer unit),  $\text{C}_3\text{H}_6\text{O}_3$  (PLA monomer units +  $\text{H}_2\text{O}$ ) and  $\text{C}_4\text{H}_{10}\text{O}_2$  (PTMEG monomer unit +  $\text{H}_2\text{O}$ ).

## 5.4 Conclusions

The size dependence study of various homopolymers revealed that there is a good linear relationship between the CCV and the precursor ion mass. Significant differences between homopolymers, which are related to the polymer structure, were found by plotting CCV values against the precursor ion masses. The linear correlation allows the use of the CCV vs precursor ion mass lines for the development of standardized fragmentation methods of polymers. The differences in the CCV vs precursor ion mass lines appear to be related to differences in the type of intermonomer bond, the difference between linear and cyclic structure of the polymer and end-groups of the polymer. Homopolymers with the same intermonomer bond generally have similar CCV per unit mass (although a few exceptions were also observed, which point at the influence of other factors). The order of fitted linear regression lines (CCV vs precursor ion mass) indicates the differences in energy requirements for dissociating different polymer types; polyesters and polysaccharides need less energy than polymethacrylates, which in turn need less energy than polyethers.

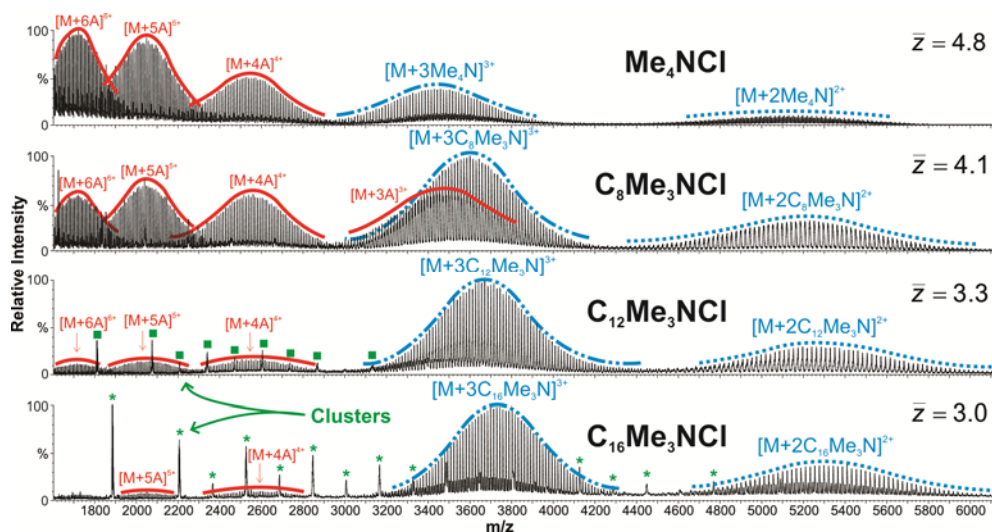
In addition, cyclic structures were distinguished from linear structures (*i.e.*, CPLA and PLA); cyclic structures have higher CCV values due to the additional energy needed for the ring opening. The influence of the end-group varies among the different cases studied; no clear trend was observed. Nevertheless the replacement of the acidic hydrogen atom with a methyl group was found to have a tremendous effect on the CCV value for MePLA. Further investigation is recommended so as to estimate the influence of various parameters (*e.g.*, DoF effect, conformation of ions, cation catalyzed fragmentation). These efforts could include study of the conformation of the polymers in the gas phase and quantum-chemical calculations of the predominant fragmentation paths.

The proof of principle of using the CCV as a tool for selective structural elucidation was demonstrated for a mixture of PLA, PTMEG and PLA-*block*-PTMEG-*block*-PLA copolymer. The CCV values of nominally isobaric ions were found to be different between the homopolymers (*i.e.*, PLA, PTMEG) and the copolymers, as well as between copolymers with different monomer composition. The observations fit the model of a chain with links of different strength; introducing a “weak link” in a “strong chain” has a significant effect on the required energy for fragmentation. Additional experiments studying the opposite

case (introduction of a “strong link” in a “weak chain”) are needed for confirmation of this model. Another prospect is to study the applicability and the value of this method in more complex polymers such as graft or random copolymers.

## 6

# Formation of Low Charge State Ions of Synthetic Polymers Using Quaternary Ammonium Compounds



Factors such as high polymer dispersity and variation in elemental composition (of copolymers) often complicate the electrospray ionization mass spectrometry (ESI-MS) analysis of high molar mass synthetic polymers. In the experiments described in this chapter various structurally different ammonium compounds were observed to facilitate the production of low charge state adduct ions when added to the spray solution for ESI-MS. This approach was then used for the ESI time-of-flight MS analysis of synthetic polymers.

Hexadecyltrimethylammonium chloride permitted the successful analysis of poly(ethylene glycol) of 2 kDa to 40 kDa, poly(propylene glycol) and poly(tetramethylene glycol) oligomers. Increasing the quaternary ammonium compounds' concentration, results in the production of low charge state adduct ions. A comparison of structurally different quaternary ammonium compounds showed that the best performance is expected from large molecules with specific charge localization, which leaves the charge available for interactions. The applicability of the method for the MS analysis of other polymeric systems was also studied. In the case of poly(tetramethylene glycol) the method not only shifted the distributions to higher mass-to-charge ratios but also allowed the detection of high molecular weight material that was not observed without addition of modifier to the spray solution.

**Nasioudis, A.; Joyce, W. F.; van Velde, J. W.; Heeren, R. M. A.; van den Brink, O. F. *Anal. Chem.* 2010, 82, 5735-5742.**

## 6.1 Introduction

MS has been proven to be a powerful complementary tool for the structural analysis of synthetic polymers along with nuclear magnetic resonance, size-exclusion chromatography (SEC) and vibrational spectroscopy. It can provide information about the monomer unit and end-group type,<sup>22,23,89,94</sup> the molar mass distribution<sup>95</sup> (MMD) and the sequence and composition of copolymers.<sup>87,96,97</sup> Soft ionization methods such as electrospray ionization (ESI)<sup>115</sup> and matrix-assisted laser desorption/ionization (MALDI)<sup>116</sup> have been the major techniques for the analysis of intact macromolecules for almost two decades. MALDI in combination with time-of-flight (TOF) MS is capable of analyzing synthetic polymers of any size (from oligomers till polymers in the MDa<sup>146</sup> mass range) and produce spectra that are easy to interpret since low charge state adducts ions are formed. Mass discrimination in disperse distributions and the difficulty of coupling MALDI with liquid chromatography (LC), SEC and capillary electrophoresis (CE) are the main weaknesses of this technique. Nevertheless, off-line and on-line coupling solutions were developed,<sup>16,17</sup> such as a direct-spray deposition on a rotating matrix-precoated substrate,<sup>18</sup> fraction collection/sample deposition,<sup>11</sup> continuous flow<sup>19</sup> and aerosol method.<sup>20</sup> On the other hand, ESI is easily coupled with LC,<sup>16,17,117</sup> SEC,<sup>21</sup> and CE,<sup>16</sup> but it has the tendency to form multiply-charged ions when the polymer's molecular mass is above some kilodaltons. This could be beneficial in the case of pure compounds with narrow distributions, but at the same time it is complicating for structurally complicated polymers with broad distributions, where the multiple charge state distributions are convoluted with the size distribution.

Several approaches have been proposed to overcome this challenge, such as charge reduction,<sup>44-55</sup> high resolution MS,<sup>95,147</sup> separation of ions with different charge state with ion mobility spectrometry (IMS) MS,<sup>148,149</sup> and combination of these.<sup>52,53</sup> Charge reduction has mainly been based on ion-ion,<sup>47-49</sup> ion-molecule<sup>45,46,49,50-53</sup>, and solution conditions alterations.<sup>54</sup> All of these strategies required hardware modification,<sup>44,51</sup> use of radioactive material<sup>50</sup> and/or expensive, state-of-the-art MS instrumentation.<sup>52,53,147-149</sup> Recently, the idea of adding post-column amines in the LC effluent<sup>150</sup> prior to the MS analysis was presented. With this method, the MS analysis of poly(ethylene glycols)

(PEGs) and PEGylated proteins up to 40 kDa were successfully performed. The main limitation of this method is that the amines modify the pH of the solution, which might induce hydrolysis of sensitive polymeric materials. Furthermore, the mechanism behind the production of low charge state adduct ions with amines is not fully understood.

Initial observations<sup>150</sup> revealed that adding quaternary ammonium compounds (Quats) with surface tension modification function such as hexadecyltrimethylammonium chloride ( $C_{16}Me_3NCl$ ), into a PEG solution had a great effect on the charge state reduction by forming low charge state PEG-Quat adducts ions. As an additional benefit, the ionic surfactants do not have any influence on the pH and can therefore be used with pH sensitive and/or easily hydrolyzable polymeric systems.

In this chapter, we investigate the capacity of producing low charge state ion populations with the addition of various Quats (with some having a surface tension modification function). PEGs from 2 kDa to 40 kDa and poly(propylene glycols) (PPGs) from 2 kDa to 4 kDa are tested by SEC-MS with post-column addition of Quats and direct-infusion MS (DI-MS) of solutions containing PEG or PPG and Quats. A comparison of different Quats and their efficiency to induce charge state reduction is made. Results showing the influences of the structure and concentration of the Quats on the charge state reduction are also presented. The applicability of the developed method is tested on other synthetic polymers such as polytetramethylene glycol (PTMEG), polylactic acid, polystyrene, polymethylmethacrylate and dextran.

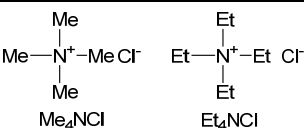
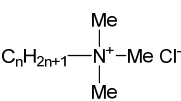
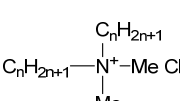
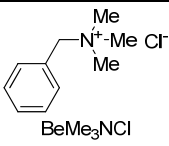
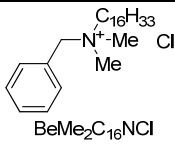
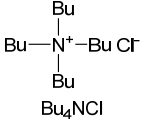
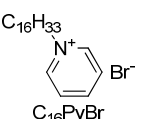
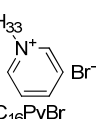
## 6.2 Experimental section

### 6.2.1 Chemicals

PEG 2 kDa, 5 kDa, 10 kDa and didecyldimethylammonium chloride ( $(C_{10})_2Me_2NCl$ ), were synthesized and characterized in house at AkzoNobel (Arnhem, Netherlands). PEG 23 kDa, PEG 40 kDa, PMMA 17 kDa, PS 3 kDa, 7 kDa and 13 kDa were from Polymer Standards Services (Mainz, Germany) and Dextran 10 kDa from Pharmacia Fine Chemicals (Uppsala, Sweden). PPG 2 kDa and 3.9 kDa were from Waters Associates (Framingham, MA). Tetramethylammonium chloride ( $Me_4NCl$ ), tetraethylammonium chloride ( $Et_4NCl$ ), tetrabutylammonium chloride ( $Bu_4NCl$ ), octyltrimethylammonium chloride ( $C_8Me_3NCl$ ),

dodecyltrimethylammonium chloride ( $C_{12}Me_3NCl$ ), and hexadecyltrimethylammonium chloride ( $C_{16}Me_3NCl$ ) were from Fluka (Steinheim, Germany). Terathane<sup>®</sup> 2,900 (PTMEG), cetylpyridinium bromide ( $C_{16}PyBr$ ), methanol (MeOH) and tetrahydrofuran (THF) both of HPLC grade were purchased from Sigma-Aldrich (St. Louis, MO). Benzyltrimethylammonium chloride ( $BeMe_3NCl$ ) was obtained from Merck-Schuchardt (Hohenbrunn bei München, Germany) and benzyl dimethylhexadecylammonium chloride ( $BeMe_2C_{16}NCl$ ) from Eastman Fine Chemicals (Rochester, NY). The structures of these Quats are provided in Table 6.1. Cation exchange resin AG MP-50 was purchased from Bio-Rad Laboratories (Hercules, CA). Ultra-pure water with a resistivity of 18.2 M $\Omega$ ·cm (at 25 °C) was obtained from a Millipore Direct-Q<sup>®</sup> 3 water purification system (Molsheim, France).

**Table 6.1. Structures of Quats With Specific Structural Characteristics.**

Chain length of all amine substituents	Chain length of one amine substituent	Chain length of two amine substituents	Amine substituent type	
 <p>Me<sub>4</sub>NCl      Et<sub>4</sub>NCl</p>	 <p><math>C_nH_{2n+1}-N^+-Me\ Cl^-</math></p> <p>n = 8 <math>C_8Me_3NCl</math> n = 12 <math>C_{12}Me_3NCl</math> n = 16 <math>C_{16}Me_3NCl</math></p>	 <p><math>C_nH_{2n+1}-N^+-Me\ Cl^-</math></p> <p>n = 8 <math>(C_8)_2Me_2NCl</math> n = 10 <math>(C_{10})_2Me_2NCl</math></p>	 <p>BeMe<sub>3</sub>NCl</p>	 <p>BeMe<sub>2</sub>C<sub>16</sub>NCl</p>
 <p>Bu<sub>4</sub>NCl</p>			 <p><math>C_{16}H_{33}-N^+-Me\ Cl^-</math></p>	 <p><math>C_{16}PyBr</math></p>

### 6.2.2 Sample preparation

For DI-MS, the samples were dissolved in a 50/50 (v/v) water/MeOH or water/THF solution (as such or after purification with the cation exchange resin, and depending on the polymer's solubility) at a concentration of 125–250  $\mu$ g/mL containing 1.2 mM of the Quats studied. In the case of SEC-MS analysis, samples were dissolved at a concentration of 20 mg/mL in pure water (for SEC with water) or THF (for SEC with THF) and the Quats at a concentration of 10 mM in 50/50 (v/v) water/MeOH or 90/10 (v/v) THF/water respectively.

### **6.2.3 Instrumentation**

#### **6.2.3.1 DI-MS**

DI-MS experiments were performed on Waters LCT and LCT Premier TOF mass spectrometers (Micromass, Manchester, UK). The transfer of ions from the source to the orthogonal accelerated TOF mass analyzer is made by two hexapole radio frequency lenses (LCT) and two ion guides and a hexapole (LCT premier). The settings of the LCT were the following: capillary voltage 3-4.25 kV, mass range 400–14,500 Da, desolvation temperature 150 °C and desolvation gas flow 395 L/hr. Since the cone voltage value has a great influence on the MS response (see results and discussion section), its value was optimized every time based on the experimental needs. The settings of the LCT premier were the following: capillary voltage 3 V, cone voltage 30 V, mass range 400–14,500 Da, desolvation temperature 300 °C and desolvation gas flow 700 L/hr. The sample was introduced via a Cole-Palmer syringe pump (Vernon Hills, IL) at a flow rate of 10  $\mu$ L/min.

#### **6.2.3.2 SEC-MS**

SEC-MS was carried out using an Agilent 1100 series HPLC system (Palo Alto, CA) equipped with a quaternary pump and a refractive index (RI) detector. Chromatographic separation was performed on 2 different columns: a TSKgel G3000PWXL (6  $\mu$ m, 300x7.8 mm) for aqueous eluents and a PLgel 100 Å (5  $\mu$ m, 600x7.5 mm) for THF eluent. The flow rate was 1 mL/min and the effluent was split in 2 flows, one for the RI detector and one for the MS at a ratio 9:1. Prior to delivery to the ESI source, the flow to the MS was mixed with the appropriate Quat solution (10mM) using a T-splitter connected to a Cole-Palmer syringe pump (Vernon Hills, IL) at a flow rate of 5  $\mu$ L/min.

## **6.3 Results and discussion**

### **6.3.1 DI-MS and SEC-MS analysis of PEGS with the use of Quats**

Preliminary experiments with DI-MS and SEC-MS of PEGs showed that the mass spectra obtained from both methods were similar for PEG 2 kDa to 10 kDa. For the analysis of PEG 23 kDa and 40 kDa, we focused mainly on DI-MS, because the signal intensity of the formed ions was too low to permit their analysis with SEC-MS, where the narrow

elution window does not allow the summation of the necessary mass spectra for a good signal-to-noise (S/N) ratio. Their analysis was mainly made by summing 300-600 spectra.

Figure 6.1 depicts the mass spectra of PEG 10 kDa without (Figure 6.1a) and with an optimized addition (Figure 6.1b) of  $C_{16}Me_3NCl$  at specific cone voltage values that permit the observation of the lowest charge state distribution possible in each case. Without the addition of any Quat (Figure 6.1a) PEG was heavily charged producing multiple charge state envelopes of protonated ions. In addition, some PEG fragment ions due to up-front fragmentation were observed.

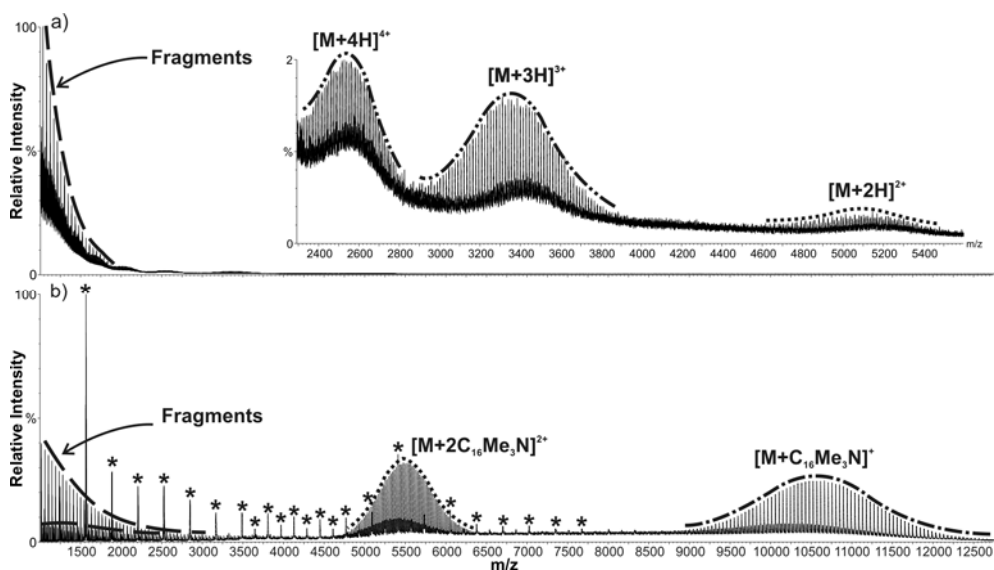


**Figure 6.1.** Mass spectra of 10 kDa PEG obtained by DI-MS: a) without addition of a Quat with 60 V cone voltage, and b) with addition of 1.2 mM  $C_{16}Me_3NCl$  with 180 V cone voltage. Note: Inset figure is a magnification of the area of interest in Figure 6.1a. Peaks indicated with an asterisk (\*) are Quat cluster ions. “M” refers to  $PEG_n$ .

It is generally known that modifying the cone voltage could reduce the multiply charged species in favor of ions with lower charge states. If the cone voltage is greatly increased, up-front fragmentation is observed. As expected (Figure 6.2), increasing the cone voltage led only to an increase in the intensity of the protonated fragment ions. With the addition of  $C_{16}Me_3NCl$  (Figure 6.1b and Figure 6.3a), the mass spectra were greatly simplified as  $[PEG_n+C_{16}Me_3N]^+$  and  $[PEG_n+2C_{16}Me_3N]^{2+}$  ions at high cone voltages were observed. Due

to the relatively high concentration of  $C_{16}Me_3NCl$ , the presence of  $[(C_{16}Me_3N)_{x+1}Cl_x]^+$  clusters is also apparent. PEG fragment ions are still present but their origin is attributed to the protonated PEG ions.

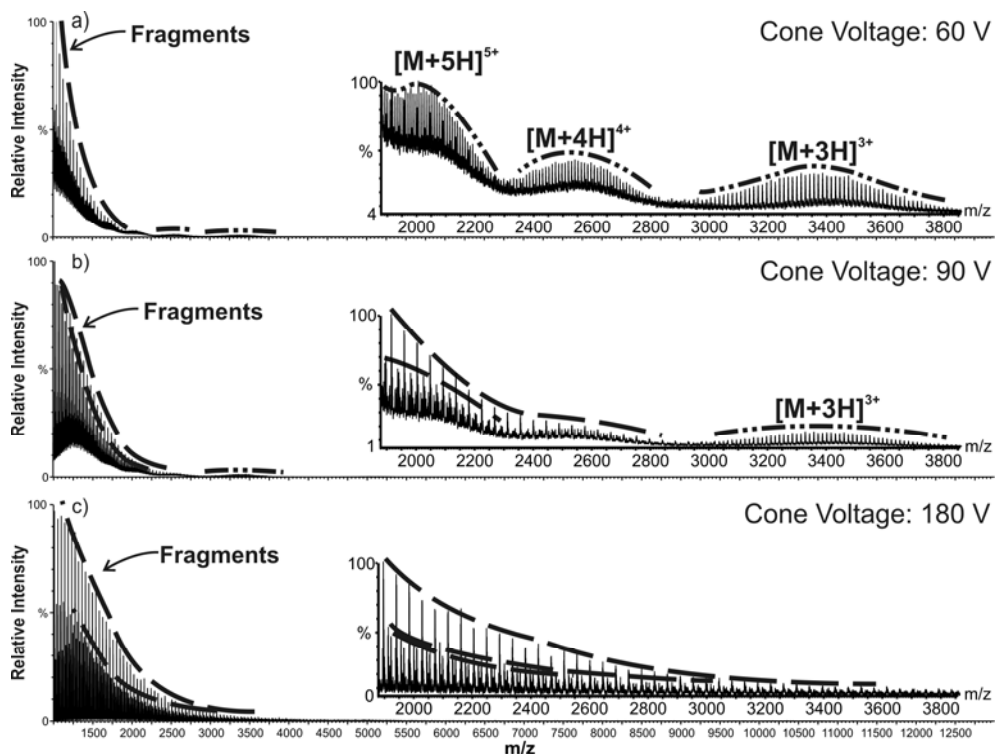


**Figure 6.2.** Mass spectra of 10 kDa PEG obtained by DI-MS without addition of a Quat at different cone voltage values: a) 60 V, b) 90 V and c) 180 V. Note: Inset figures are a magnification of the area of interest in Figures 6.2a, 6.2b and 6.2c. “M” refers to  $PEG_n$ .

Lowering the cone voltage had an effect on the mass spectra by shifting the distributions to higher charge states (Figure 6.3b and 6.3c). Nevertheless, the signal intensity and simplicity of the mass spectra is greatly improved compared with the mass spectra without the addition of  $C_{16}Me_3NCl$ .

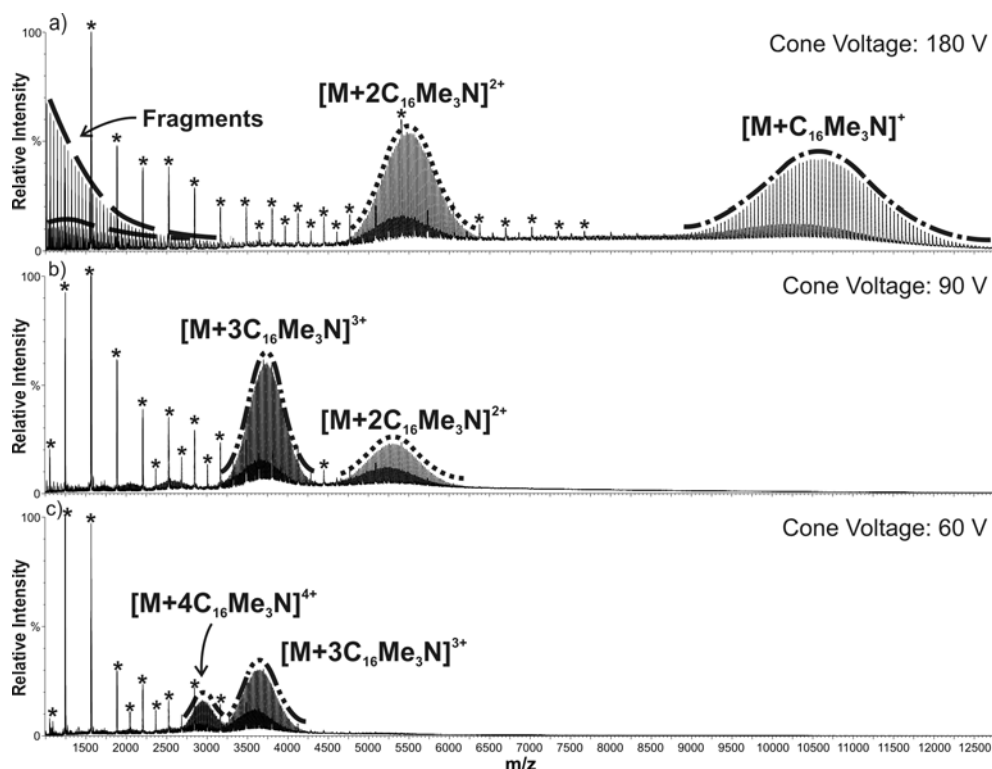


**Figure 6.3.** Mass spectra of 10 kDa PEG obtained by DI-MS with addition of 1.2 mM  $C_{16}Me_3NCl$  at different cone voltage values: a) 180 V, b) 90 V and c) 60 V. “M” refers to  $PEG_n$ .

The same behavior was observed in the analysis of larger PEG polymers such as PEG 23 kDa and 40 kDa (Figure 6.4). In the DI-MS of PEG 23 kDa with  $C_{16}Me_3NCl$  (Figure 6.4a), we observed distributions of  $[PEG_n+2C_{16}Me_3N]^{2+}$  and  $[PEG_n+3C_{16}Me_3N]^{3+}$  ions, whereas, in the case of PEG 40 kDa (Figure 6.4b), distributions of  $[PEG_n+3C_{16}Me_3N]^{3+}$  and  $[PEG_n+4C_{16}Me_3N]^{4+}$  ions. The detection of lower charge state ions of PEG 23 kDa and 40 kDa was not possible with the current MS instrumentation (maximum scan range 14,500 Da). In the case of PEG 23 kDa, additional multiply charged material between the doubly and triply charged distributions is observed. These peaks are attributed to the presence of PEGs of lower degrees of polymerization, which were also detected by SEC (Figure 6.5).

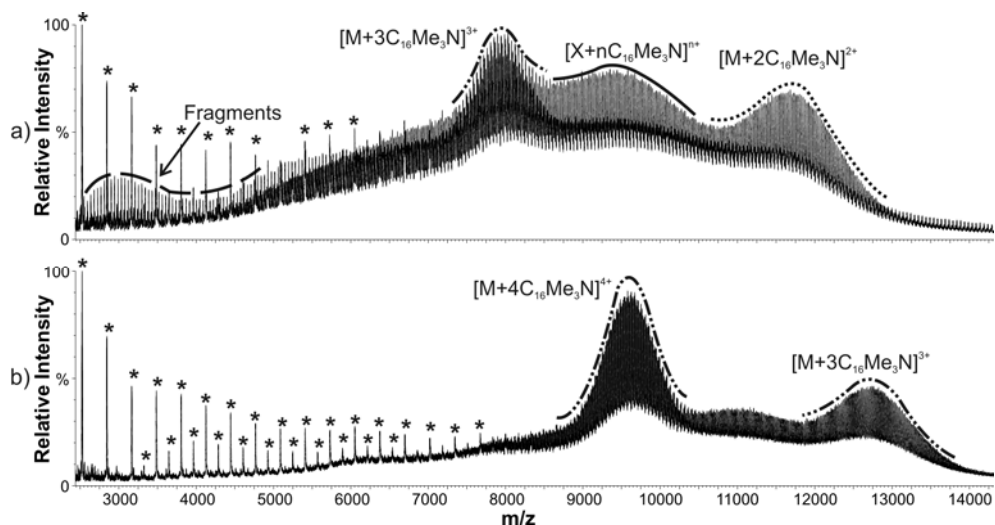


**Figure 6.4.** Mass spectra of a) 23 and b) 40 kDa PEG obtained by DI-MS with 1.2 mM  $C_{16}Me_3NCl$ . Note:  $[X+nC_{16}Me_3N]^{n+}$  is additional multiple charge state distributions, where X refers to the PEG polymer and n is 1 to 2. Peaks indicated with an asterisk (\*) are Quat cluster ions. “M” refers to  $PEG_n$ .

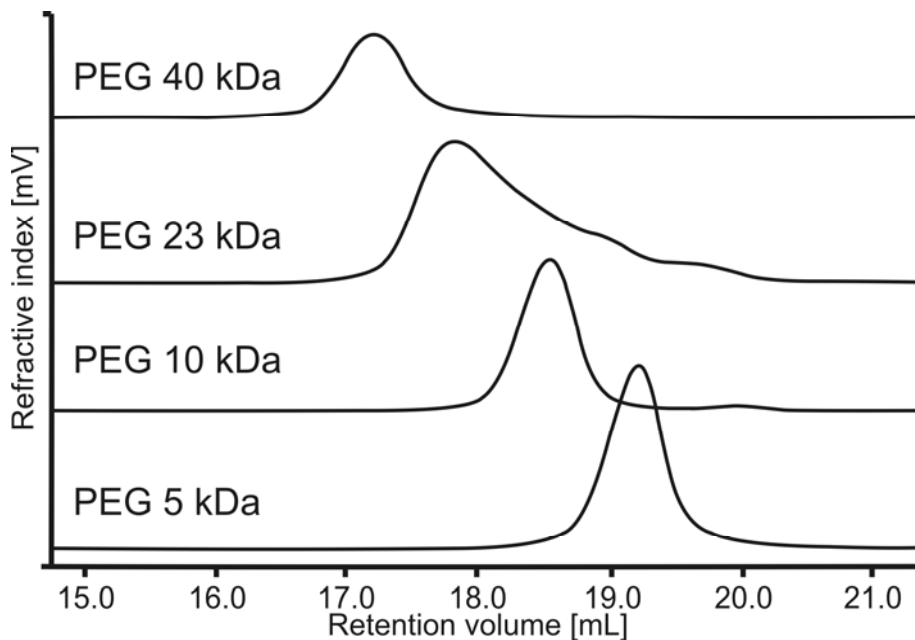


**Figure 6.5.** SEC analysis of various PEGs. Overlaid refractive index (RI) chromatograms of 5, 10, 23 and 40 kDa PEG. Note: Ordinate has an arbitrary scale.

### 6.3.2 Effect of Quat concentration on the production of low charge state adduct ions

Changing the concentration of the  $C_{16}Me_3NCl$  increases the intensity of the peaks in the mass spectra and favors the production of low charge state distributions for all PEGs in this study. To complement the visual comparison of the mass spectra, we introduced the calculation of the average charge state value as another expression of the charge state shift trend. The intensity weighted average charge state was calculated by the following equation:

$$\bar{z} = \frac{\sum_i z_i \cdot I_{i,z}}{\sum_i I_{i,z}} \quad \text{Equation 6.1}$$

where  $\bar{z}$  is the average charge state,  $z_i$  the charge state of each distribution  $i$  and  $I_{i,z}$  the absolute intensity of the highest peak in each charge state distribution  $i$ . It should be stressed, however, that this equation does not take in consideration other parameters that could influence this value, such as the width and the shape of the charge state distributions and the intensities of the Quat cluster ions. The multiple charge state distributions are convoluted (due to the low resolving power of the instrument used) making peak identification and intensity determination cumbersome. Since the MMD is not greatly influenced (see Table 6.2), we assumed that the most intense peak could represent the whole distribution.

**Table 6.2. Influence of the Quat Concentration on the MMD as Calculated From Figure 6.6**

Concentration <sup>a</sup> [uM]	$M_n - M_w^b$ [Da]	$M_n - M_w^c$ [Da]
0	4695 - 4735	ND
125	4863 - 4897	4852 - 4894
500	4922 - 4960	4833 - 4894
1000	ND	4943 - 4990
2000	ND	4974 - 5016

<sup>a</sup>Concentration of Quat in solution  
<sup>b</sup> $M_n, M_w$  calculated from  $[PEG_n+2H]^{2+}$  envelope  
<sup>c</sup> $M_n, M_w$  calculated from  $[PEG_n+2C_{16}Me_3N]^{2+}$  envelope.

Figure 6.6 depicts the mass spectra of PEG 5 kDa with increasing (from 0 to 2 mM)  $C_{16}Me_3NCl$  concentration. To allow direct comparison of the mass spectra in different  $C_{16}Me_3NCl$  concentrations, the same number of scans was acquired; the generated mass spectra were smoothed and zoomed so that the intensity of the polymer distributions is around the same order of magnitude. In the mass spectra (Figure 6.6a) without  $C_{16}Me_3NCl$ ,  $[PEG_n+H]^+$  fragment ions are the most intense peaks. In addition,  $[PEG_n+3H]^{3+}$  and  $[PEG_n+4H]^{4+}$  envelopes are observed. The addition of  $C_{16}Me_3NCl$  (125  $\mu M$ ) lowered the intensity of the protonated PEG fragment ions and improved the S/N ratio of the polymer distributions. In addition, as shown in the inset of Figure 6.6b, low intensity distributions of  $[PEG_n+2H]^{2+}$  and  $[PEG_n+2Quat]^{2+}$  ions are observed. On increasing the  $C_{16}Me_3NCl$  concentration from 125 to 500  $\mu M$  (see Figure 6.6c), the  $[PEG_n+H]^+$  fragment ions disappeared and the intensity of the  $[PEG_n+2C_{16}Me_3N]^{2+}$  distribution increased. In addition, the absence of fragment ions allows easier identification of the  $[PEG_n+5H]^{5+}$  distribution. The intensity increase of the  $[PEG_n+2C_{16}Me_3NCl]^{2+}$  ions on increasing the  $C_{16}Me_3NCl$  concentration was expected. The intensity increase of the  $[PEG_n+2H]^{2+}$  envelope and the reduction of up-front fragmentation, however, was not expected.

A possible explanation is that the amount of ionic surfactant added induced a modification of the ESI conditions, by increasing the surface tension of the droplets, thus, decelerating the solvent evaporation and/or stabilizing the solubility of the polymer inside the droplet. In addition, the modification of the ESI conditions seems to reduce the deposition of energy during the ionization and transfer processes, thus, stabilizing the ions and reducing up-front fragmentation. Further addition of  $C_{16}Me_3NCl$  (Figure 6.6d and 6.6e) resulted in the total ion count (TIC) increase, the formation of  $[(C_{16}Me_3N)_{x+1}Cl_x]^+$  clusters and the intensity increase of the  $[PEG_n+2 C_{16}Me_3N]^{2+}$  distribution.

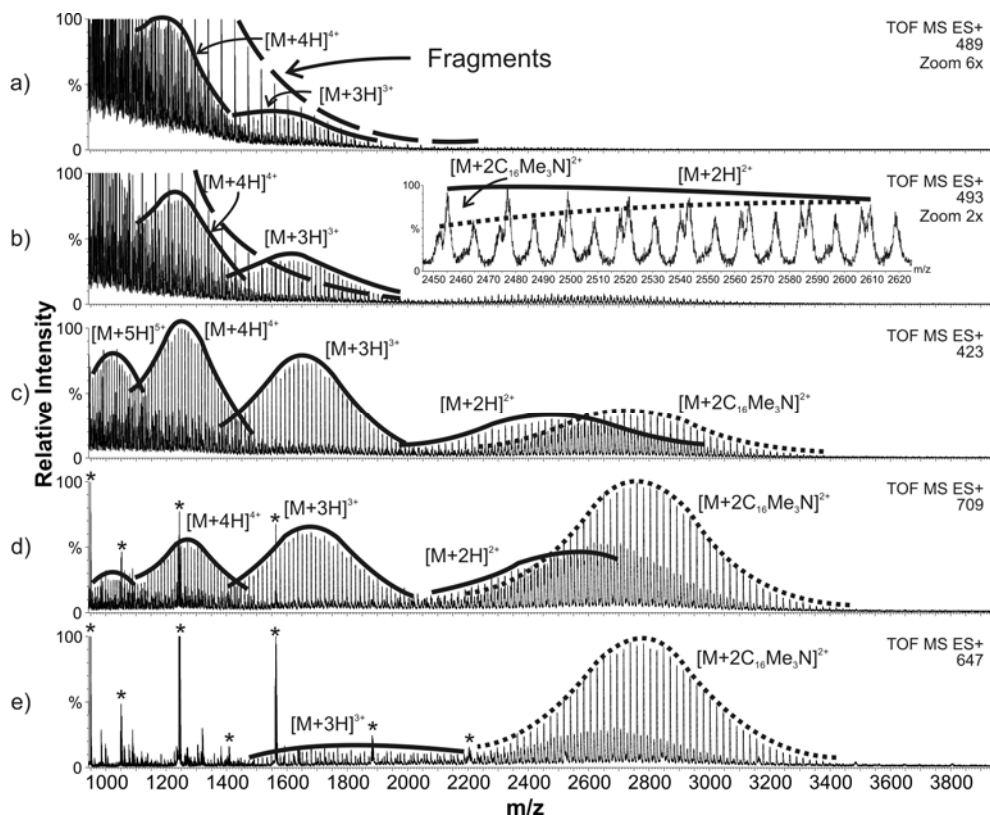


**Figure 6.6.** Zoomed mass spectra of 5 kDa PEG (25  $\mu\text{M}$ ) with addition of  $\text{C}_{16}\text{Me}_3\text{NCl}$  in various concentrations: a) without  $\text{C}_{16}\text{Me}_3\text{NCl}$ , b) 125  $\mu\text{M}$ , c) 500  $\mu\text{M}$ , d) 1mM, and e) 2mM of  $\text{C}_{16}\text{Me}_3\text{NCl}$ . **Note:** The mass spectra presented are the sum of the same number of scans after smoothing. Peaks indicated with an asterisk (\*) are Quat cluster ions. All mass spectra were obtained at 60 V cone voltage. “M” refers to  $\text{PEG}_n$ .

Besides the charge state shift, we investigated the influence of the  $\text{C}_{16}\text{Me}_3\text{NCl}$  concentration on the MMD as calculated from the  $[\text{PEG}_n + 2\text{C}_{16}\text{Me}_3\text{N}]^{2+}$  and  $[\text{PEG}_n + 2\text{H}]^{2+}$  envelopes. From the calculated values (Table 6.2), we could not identify a specific influence since the value fluctuations are within the margin of error. It is worth mentioning that the increase of the  $\text{C}_{16}\text{Me}_3\text{NCl}$  concentration has also an effect on the distributions of the multiply charged protonated PEG ions. By comparing Figures 6.6c and 6.6d, we observed that the intensity order of the multiply charged protonated PEG ions is shifted to lower charge state. A possible explanation is that the increased  $\text{C}_{16}\text{Me}_3\text{NCl}$  concentration provides an abundance of  $\text{C}_{16}\text{Me}_3\text{N}^+$  inside the droplets, shifting the ion equilibrium in their

favor. Subsequently, during the evaporation process, the amount of protons available for ionization is lower. As a result, lower charge state protonated PEG ions envelopes are favored. Verification of the validity of the abovementioned suggestions requires additional experiments focused on the ESI process and the stability of the ions in the gas phase, which are beyond the scope of this study.

### ***6.3.3 Effect of Quat structure on the production of low charge state adduct ions***

The structure of the Quats greatly affects the degree of formation of low charge state adduct ions and thereby the average charge state value. Specific molecules (Table 6.1) with different structural characteristics were studied. These characteristics are: a) chain length of all amine substituents, b) chain length of one of the amine substituent, c) chain length of two of the amine substituents, and d) amine substituent type.

We compared the mass spectra of 5 kDa PEG obtained with Quats with increasing chain length of all substituents (Figure 6.7). These mass spectra were obtained during SEC-MS experiments. Figure 6.7a depicts the RI signal and Figure 6.7b the TIC signal of the mass spectrometer. The horizontal line in Figure 6.7b depicts the summation region. Me<sub>4</sub>NCl (Figure 6.7d) was able to produce low charge state ions and formed [PEG<sub>n</sub>+3Me<sub>4</sub>N]<sup>3+</sup> and [PEG<sub>n</sub>+2Me<sub>4</sub>N]<sup>2+</sup> ions of PEG 5 kDa (but no singly charged ions as in the case of C<sub>16</sub>Me<sub>3</sub>NCl), whereas Et<sub>4</sub>NCl and Bu<sub>4</sub>NCl did not, since only the native protonated ions were observed (Figure 6.7e and 6.7f) as in the case of blank (Figure 6.7c). The lack of adduct formation of Et<sub>4</sub>NCl and Bu<sub>4</sub>NCl is attributed to a steric shielding effect, induced by the increasing amine substituent length. These large substituents increase the distance of polymer coordinating sites to the amine's positive charge, so that the non-covalent interactions are too weak to produce stable adduct ions (in the regime of the mass spectrometer).

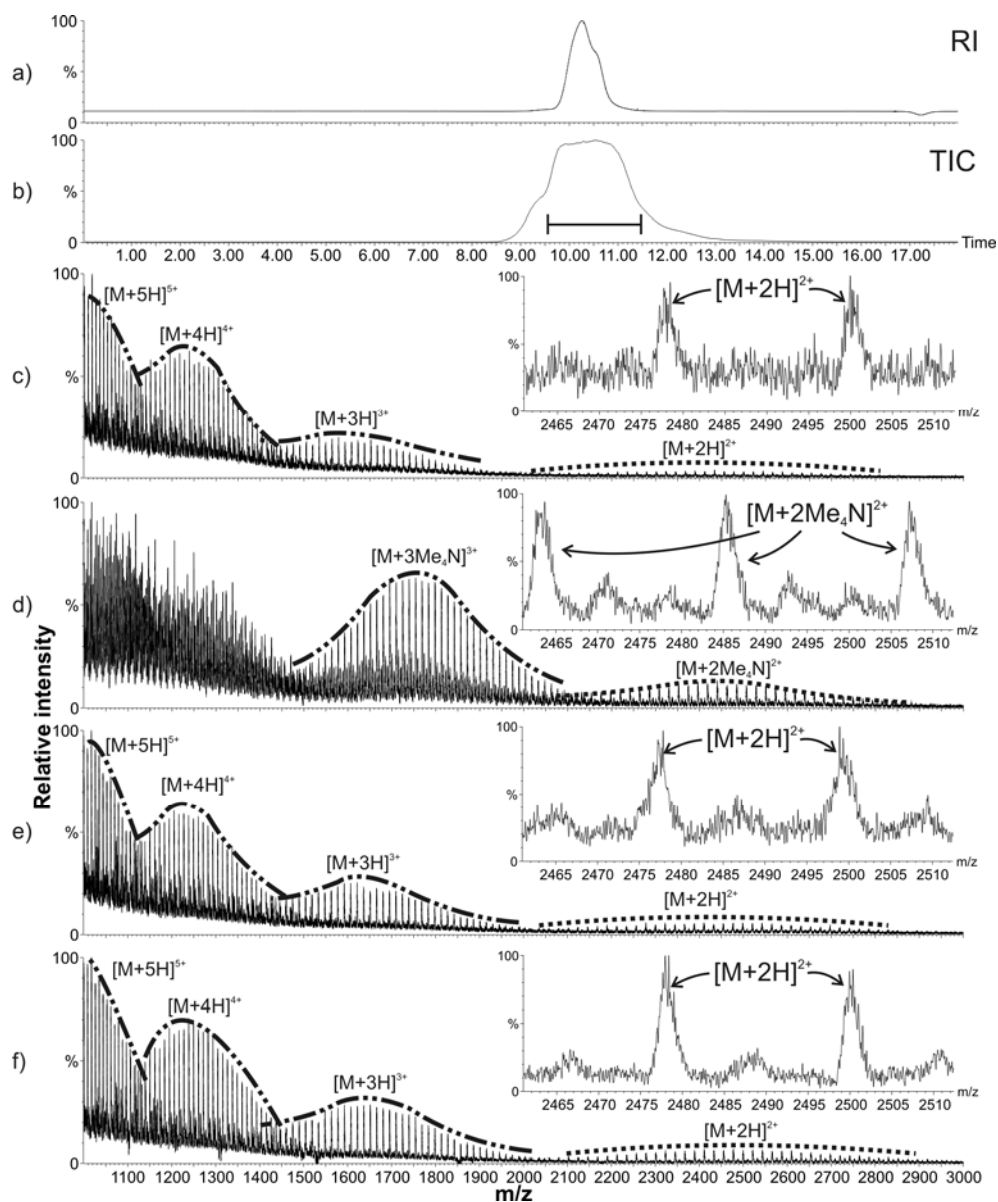


**Figure 6.7.** SEC-MS of 5 kDa PEG. Influence of the substituent size on the charge state reduction performance: a) RI signal, b) TIC signal and c), d), e) and f) are summed mass spectra of the main TIC peak of: c) no Quat (Blank), d) Me<sub>4</sub>NCl, e) Et<sub>4</sub>NCl and f) Bu<sub>4</sub>NCl. Note: All mass spectra are obtained in the same ESI conditions. Inset figures are a magnification of the area of interest in Figures 6.7c, 6.7d, 6.7e, and 6.7f. “M” refers to PEG<sub>n</sub>.

Based on these results, and in order to verify the above explanation the next logical step was to study the effect of the chain length of one substituent. This parameter was studied for the case of PEG 10 kDa (Figure 6.8) and not PEG 5 kDa because the performance improvement at the charge state reduction is more apparent in the case of the higher molecular weight material. In addition, the cone voltage values were optimized based on the lowest average charge state value obtained with  $\text{Me}_4\text{NCl}$  (This cone voltage value differs from the one in Figure 6.1b). With increasing substituent chain length, from one till 16 methylene groups, the  $\bar{z}$  value was reduced from 4.8 to 3.0. The  $M_n$ ,  $M_w$  values (Table 6.3) exhibit minor shifts. This indicates that the Quat structure does not influence the MMD.

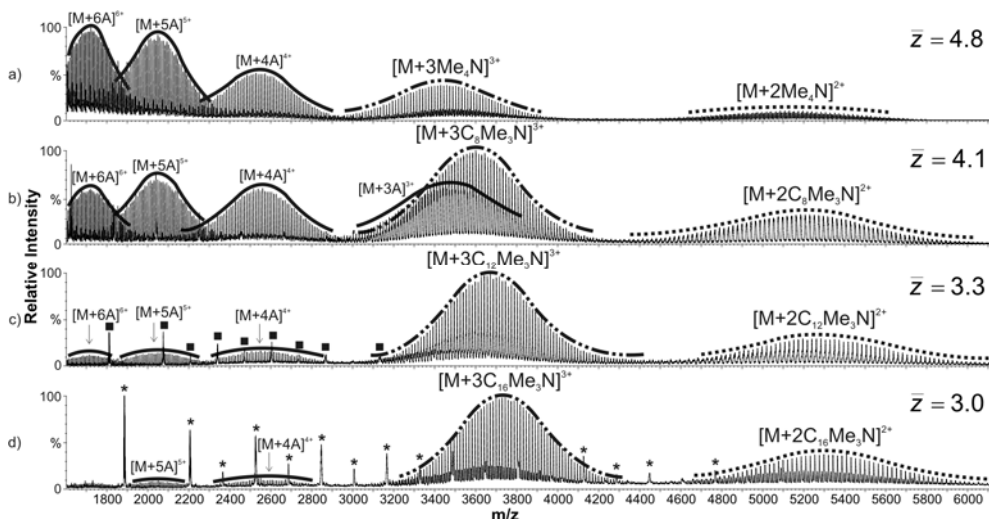


**Figure 6.8.** Influence of the substituent size on the charge state reduction performance: DI-MS mass spectra of 10 kDa PEG (250  $\mu\text{g}/\text{mL}$ ) with 1.2 mM solutions of: a)  $\text{Me}_4\text{NCl}$ , b)  $\text{C}_8\text{Me}_3\text{NCl}$ , c)  $\text{C}_{12}\text{Me}_3\text{NCl}$  and d)  $\text{C}_{16}\text{Me}_3\text{NCl}$ . Note: “A” refers to an unspecified adduct, because its nature cannot be determined accurately due to the low resolving power of the instrument. Peaks indicated with an asterisk (\*) and a solid square (■) are the respective Quat cluster ions. All mass spectra are obtained under the same ESI conditions. “M” refers to  $\text{PEG}_n$ .

**Table 6.3. Influence of the Alkyl Chain Length on the MMD as Calculated From Figure 6.8**

Quat	$M_n^a$	$M_w^a$
Me <sub>4</sub> NCl	10196	10234
C <sub>8</sub> Me <sub>3</sub> NCl	9984	10044
C <sub>12</sub> Me <sub>3</sub> NCl	10272	10323
C <sub>16</sub> Me <sub>3</sub> NCl	10078	10127

<sup>a</sup>The calculation of  $M_n$ ,  $M_w$  was made using the doubly charge distribution with each Quat.

A possible explanation of the observation that the length of the alkyl chain of the Quat greatly influences the degree of charge state reduction is that the long alkyl chain sterically hinders the approximation of another Quat in its vicinity. As a result the polymer can only retain a relatively limited number of charges. In addition, the alkyl chain might influence the folding of the polymer chain around the charge due to hydrophobic interactions.

The replacement of two methyl groups with two long alkyl chains was also tested. The DI-MS analysis of PEG 10 kDa, with the addition of (C<sub>10</sub>)<sub>2</sub>Me<sub>2</sub>NCl (Figure 6.9) showed that the signal intensity of the low charge state adduct ions is quite low in comparison with the observed [PEG<sub>n</sub>+H]<sup>+</sup> fragment ions, and therefore the average charge state value was not calculated.

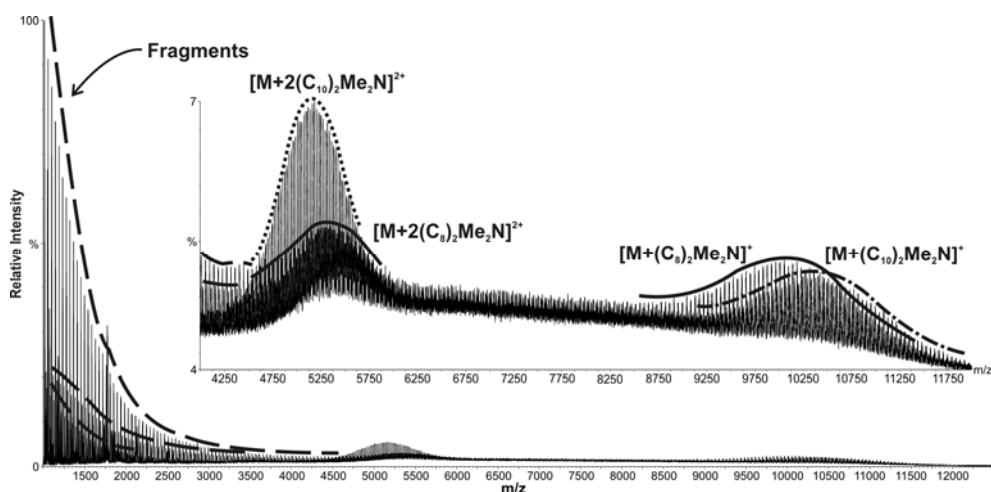


**Figure 6.9.** Mass spectra of 10 kDa PEG obtained by DI-MS with addition of 1.2 mM (C<sub>10</sub>)<sub>2</sub>Me<sub>2</sub>NCl. **Note:** The presence of [M+n(C<sub>8</sub>)<sub>2</sub>Me<sub>2</sub>N]<sup>n+</sup> ions are expected, because (C<sub>10</sub>)<sub>2</sub>Me<sub>2</sub>NCl sample is not pure and contains (C<sub>8</sub>)<sub>2</sub>Me<sub>2</sub>NCl. Inset figure is a magnification of the area of interest in Figure 6.9. “M” refers to PEG<sub>n</sub>.

This can be explained, in a similar way as in the case of  $\text{Et}_4\text{NCl}$  and  $\text{Bu}_4\text{NCl}$ , by the presence of two bulky chains increasing the distance of the positive charge from polymer coordinating sites. These observations indicate that the presence of at least three short substituents (three methyl groups) is necessary for strong non-covalent interactions and consequential effective adduct formation between the ammonium molecule and the PEG chain.

The replacement of the  $\text{C}_{16}$  alkyl chain with a benzyl group ( $\text{BeMe}_3\text{NCl}$ ) (Figure 6.10b) and a methyl group with a benzyl group ( $\text{BeMe}_2\text{C}_{16}\text{NCl}$ ) (Figure 6.10c) did not improve the performance and produced very low intensities of the low charge state distributions. The low performance of  $\text{BeMe}_2\text{C}_{16}\text{NCl}$  strengthens the hypothesis of the requirement of three methyl functionalities. In contrast to the replacement with benzyl, the replacement of the three methyl groups with a pyridine group ( $\text{C}_{16}\text{PyBr}$ ) (Figure 6.10d) had a positive influence exhibiting a comparable behavior with  $\text{C}_{16}\text{Me}_3\text{NCl}$  in both intensity and capability of forming low charge state adduct ions (both Quats had a  $\bar{z}$  value of 1.5). A possible explanation for the performance of  $\text{C}_{16}\text{PyBr}$  is that the planar structure of the pyridine ring does not sterically hinder the approximation of the PEG chain. It is not yet clearly understood what the correlation (if there is any) between the ion conformation and its ability to produce low charge state adduct ions is.

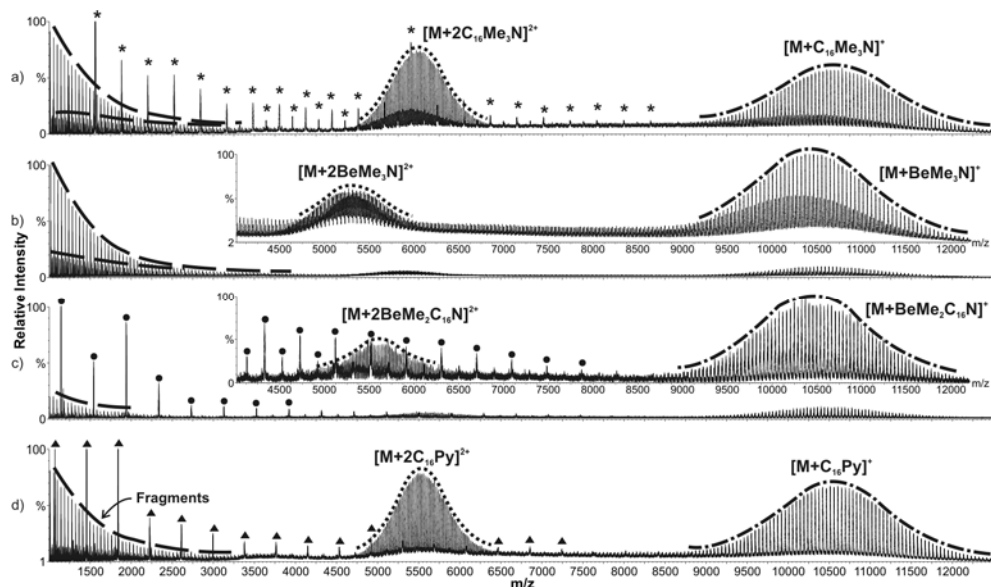
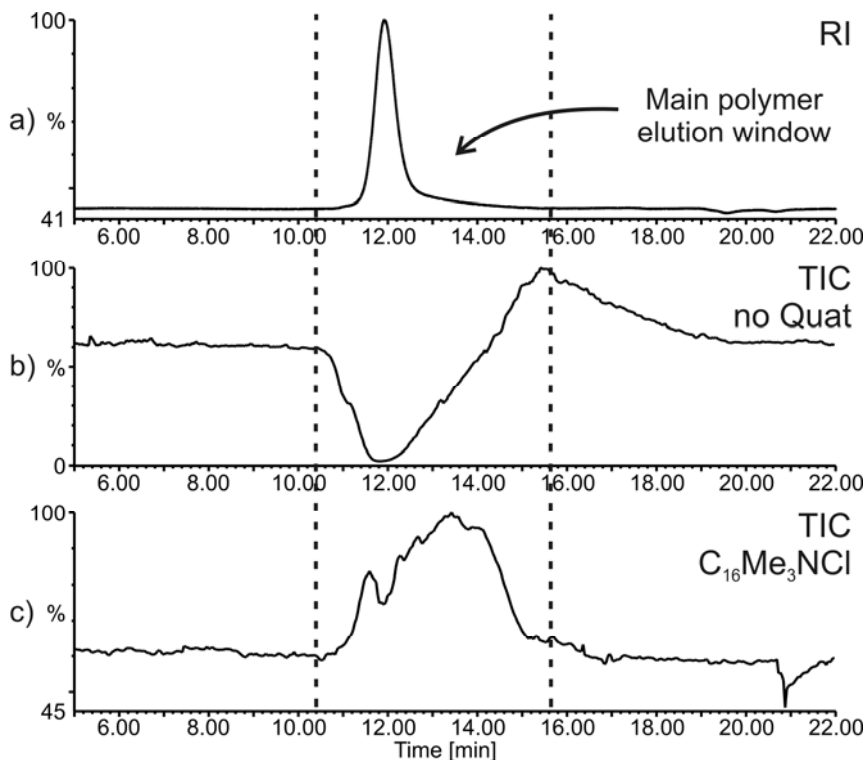


**Figure 6.10.** Mass spectra of 10 kDa PEG obtained by DI-MS with addition of 1.2 mM of: a)  $C_{16}Me_3NCl$ , b)  $BeMe_3NCl$ , c)  $BeMe_2C_{16}NCl$ , and d)  $C_{16}PyBr$ . Note: Peaks indicated with an asterisk (\*), solid circle (●) and solid triangle (▲) are the respective Quat cluster ions. Inset figures are a magnification of the area of interest in Figures 6.10b and 6.10c. “M” refers to  $PEG_n$ .

### 6.3.4 DI-MS and SEC-MS analysis of other synthetic polymers with addition of Quats

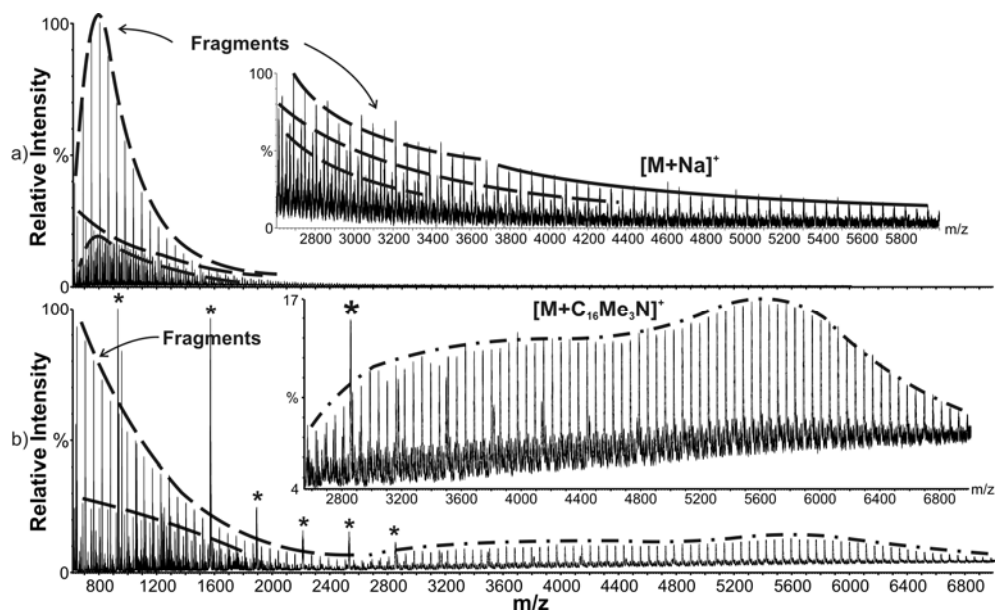
The applicability of the developed method was tested for other polymeric systems. The Quat of choice was  $C_{16}Me_3NCl$  since it gave the best results for PEGs. Figure 6.11 depicts the TIC signals resulting from SEC-MS analysis of PPG 2,000 with and without the post-column addition of  $C_{16}Me_3NCl$ . Without Quat (Figure 6.11b), the elution of the polymer analyte from the column results in a signal drop in the TIC (as indicated by the RI signal in Figure 6.11a). This signal loss could be attributed to ion suppression or the low ionization efficiency of high molar mass polymers. When  $C_{16}Me_3NCl$  is added (Figure 6.11c), no drop but an increase of signal is observed. Even in this case the TIC exhibits a small signal drop in the time period equivalent to the top of the RI peak, possibly due to oversaturation, and subsequently, ion suppression. The difference in peak width between the RI and the TIC signal (in both cases) is evident since the RI signal is mass and concentration dependent

whereas TIC is charge, concentration and ionization efficiency dependent and reflects the number of molecules eluting rather than the total mass eluting.



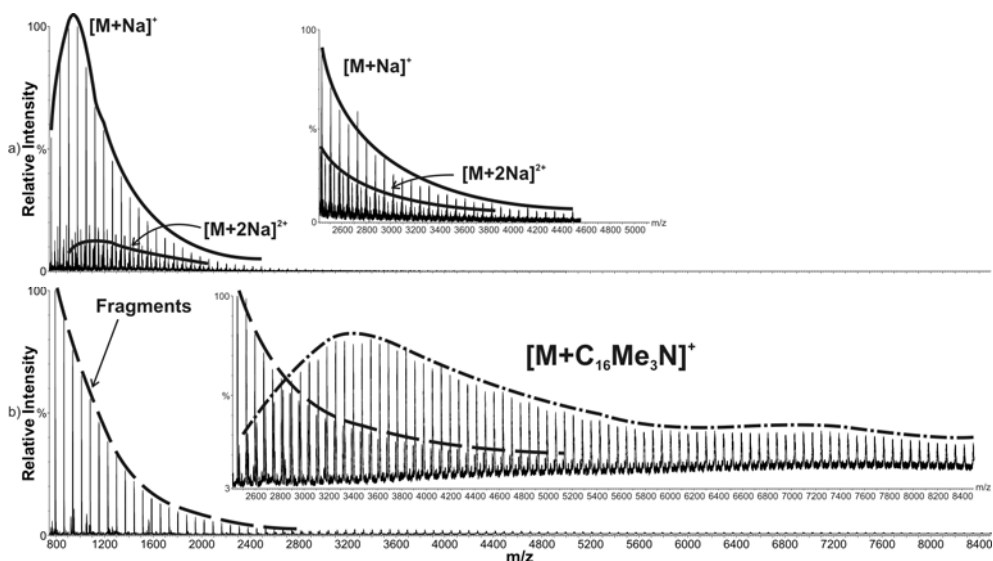
**Figure 6.11.** SEC-MS analysis of 2 kDa PPG. Proof that Quat improves TIC signal. a) RI chromatogram, b) TIC without Quat, and c) TIC with  $C_{16}Me_3NCl$ .

Figure 6.12 shows that  $C_{16}Me_3NCl$  has a clear effect on the mass spectra of PPG. Only  $[PPG_n + C_{16}Me_3N]^+$  ions of relatively low intensity were observed. Multiply charged ions were not observed. The broad distribution evident from Figure 6.12 was also confirmed by SEC-MS analysis. The lower intensity of singly charged ions and the absence of multiply-charged ions may be explained by the fact that PPG has a more rigid structure than PEG. This rigidity influences the polymer chain's folding capability, thus potentially lowering the degree of coordination of the nitrogen's positive charge by multiple ether oxygens.



**Figure 6.12.** Mass spectra of 3.9 kDa PPG obtained by DI-MS a) without Quat and b) with 1.2 mM  $C_{16}Me_3NCl$ . **Note:** Peaks indicated with an asterisk (\*) are Quat cluster ions. Inset figures are a magnification of the area of interest in Figures 6.12a and 6.12b. “M” refers to  $PPG_n$ .

Similar to the study of PPG, the applicability of this method was tested on PTMEG. In the DI-MS analysis of 2.9 kDa PTMEG (Figure 6.13a) without the addition of a Quat,  $[PTMEG_n+Na]^+$  and  $[PTMEG_n+2Na]^{2+}$  ions, which only represent the lower end of the PTMEG distribution are detected. This could lead to misinterpretation of the sample’s MMD. When  $C_{16}Me_3NCl$  was added, however, low intensity  $[PTMEG_n+C_{16}Me_3N]^+$  ions ranging from 2,400 to 8,500 Da were observed (Figure 6.13b). The top of the singly charged distribution (approx 3,200–3,600 Da) is closer to the value indicated by the manufacturer, in particular when corrected for the adduct mass (284 Da). In addition, the mass spectra of PTMEG with  $C_{16}Me_3NCl$  indicate that the method may be useful when samples of higher molar mass (~10 kDa) are analyzed. This was not further demonstrated in this study, because such material could not be obtained commercially. Also, the results indicate that the PTMEG-Quat interaction may be not as strong as that of PEG-Quat, but rather similar to that of PPG-Quat.



**Figure 6.13.** DI-MS analysis of PTMEG 2.9 kDa. Summed spectra a) without addition of a Quat, and b) with addition of 1.2 mM C<sub>16</sub>Me<sub>3</sub>NCl. Note: Inset figures are a magnification of the area of interest in Figures 6.13a and 6.13b. “M” refers to PTMEG<sub>n</sub>.

Quantum-chemical calculations and ion mobility experiments could provide additional information on the degree of coordination and the conformation of the PPG/PTMEG-Quat ions, and on the influence of the Quat structure.

Other common polymers (polylactic acid, polystyrene, polymethylmethacrylate and dextran) were also tested with C<sub>16</sub>Me<sub>3</sub>NCl but no charge state reduction or even adequate signal was observed. Although this might indicate that the applicability of our method is limited to polyethers, it also suggests that the polyether oxygens play a crucial role for the adduct formation with C<sub>16</sub>Me<sub>3</sub>NCl.

## 6.4 Conclusions

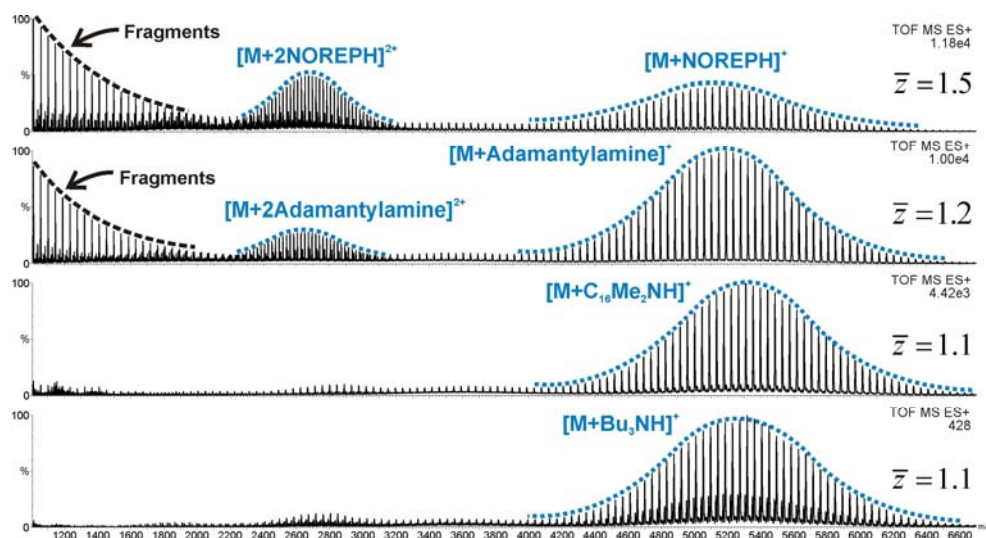
A new method for the ESI-MS analysis of high molecular weight synthetic polymers was developed. Addition of specific Quats greatly enhances the overall signal intensity, and facilitates the interpretation of the MS spectra. The production of low charge state adduct ions of PEGs from 2 kDa to 40 kDa and PPG from 2 kDa to 4 kDa was accomplished with the use of Quats such as C<sub>16</sub>Me<sub>3</sub>NCl as cationization agent. The performance of the method is dependent on molar concentration of the Quat in the spray solution. An increase of the

Quat concentration lowers the average charge state value. The structure of the Quat plays a crucial role in the performance and even the occurrence of the effect. A Quat with a structure that combines size with specific charge localization, and/or permits facile interactions with the polymer, like  $C_{16}Me_3NCl$  and  $C_{16}PyBr$ , produces the best results. The applicability of this method was studied for other polymeric systems. From these, only PTMEG was able to form low charge state PTMEG-Quat adduct ions, suggesting that the polyether oxygens are the determining element.



## 7

# Electrospray Ionization Mass Spectrometry of the Non-covalent Complexes of Ammonium Ions with High Molar Mass Polyethers



The formation of low charge state non-covalent complex ions of high molar mass polymers with primary and tertiary amines and quaternary ammonium salts (Quats) was studied by electrospray ionization (ESI) time-of-flight mass spectrometry (MS). The amines studied were of different degree of substitution and size, and were added to the acidic polymer solution prior to MS analysis. A comparison was made between the non-covalent complex ions of high molar mass polyethers with various amines and Quats, based on the ability to form low charge state adduct ions, overall MS response, and presence of fragment ions due to up-front fragmentation. Tertiary amines showed the best performance in forming low charge state adduct ions and produced mass spectra with the lowest degree of up-front fragmentation. In both primary and tertiary amines, more simplified mass spectra are produced, since no cluster ions are formed (as in the case of Quats). The comparison of the overall MS response did not reveal a specific trend. An amine and a Quat with an optimal performance for formation of low charge state adduct ions were applied to the mass spectrometric analysis of a poly(lactic acid)-*block*-poly(ethylene glycol)-*block*-poly(lactic acid) triblock copolymer, allowing the detection of low charge state adduct ions and revealing information about the molar mass distribution. The method demonstrated here shows that addition of primary/tertiary amines and quaternary ammonium salts to the spray solvent facilitates the analysis of high molar mass polyethers by ESI-MS.

**Nasioudis, A.; van Velde, J. W.; Heeren, R. M. A.; van den Brink, O. F. *Int. J. Mass Spectrom.* 2011, 303, 63-68.**

## 7.1 Introduction

Synthetic polymers, known for their variety of structural and functional properties, are nowadays of crucial importance in a large variety of industrial activities. Their success is partly attributed to the extensive application of analytical tools such as liquid chromatography (LC), nuclear magnetic resonance spectroscopy and mass spectrometry (MS) to characterize their structure. MS can provide structural information such as monomer unit and end-group type,<sup>22,23,89,94</sup> molar mass distribution (MMD),<sup>95</sup> monomer sequence and composition of copolymers.<sup>87,96,97</sup> This information is essential for polymer chemists, since knowledge of the microstructure of polymers enables the control of their synthesis and may provide the (cor)relation between structure and physicochemical and mechanical properties.<sup>151</sup>

As mentioned in Chapter 6, the major challenges in the analysis with MS remain the high molar mass, dispersity and structural complexity of polymers. In a period of approximately two decades soft-ionization methods such as ESI<sup>115</sup> and matrix-assisted laser desorption/ionization<sup>116</sup> have grown to become the major techniques for the analysis of intact macromolecules. In some cases they even allowed the detection of relatively high molar mass synthetic polymers. The challenge of structural complexity has been dealt with so far by coupling the MS to separation techniques such as LC,<sup>16,17,117</sup> size-exclusion chromatography<sup>21</sup> and capillary electrophoresis.<sup>16</sup> On the other hand, the challenge of dispersity, when combined with one or both of the above challenges, requires more advanced MS methods (see also Introduction, Chapter 6) that require hardware modification,<sup>44,50</sup> use of radioactive material<sup>51</sup> and/or expensive, state-of-the-art MS instrumentation.<sup>52,53,147-149</sup>

Another strategy that may overcome the obstacles of dispersity and high molar mass is to employ additives into the sample solution prior to the ESI-MS analysis, which can induce charge reduction. This has been demonstrated in Chapter 6. Amines and Quats form low charge state adduct ions in the ESI source. In this way, poly(ethylene glycols) (PEGs) and PEGylated proteins till 40 kDa can be analyzed. In addition, Quats are also applicable to other polyether systems (*e.g.*, poly(propyleneglycol) and poly(tetramethylene glycol)) and have the additional benefit that they do not modify the pH of the solution which

prevents hydrolysis of sensitive polymeric materials. The drawback of the use of Quats is that the mass spectra are dominated by Quat cluster ions. The high abundance of these cluster ions reduces the overall sensitivity of the method, especially in instruments with narrow dynamic ranges.

In this chapter, the potential of other amines that provide the same benefits as in previous reports<sup>55,150,152</sup> but without the drawbacks of previously used Quats will be investigated. The research focus is on amines with different degree of substitution (*i.e.*, primary and tertiary) and size. A comparison is made on the degree of low charge state adduct ion formation, the overall MS response, and the level of up-front fragmentation between various amines and the best performing Quats from our previous Chapter (Chapter 6). In addition, the potential of the method for the MS analysis of high molar mass copolymers is investigated for the case of a poly(lactic acid)-*block*-PEG-*block*-poly(lactic acid) (PLA-*block*-PEG-*block*-PLA) triblock copolymer.

## 7.2 Experimental section

### 7.2.1 Chemicals

PEG 10 kDa, 2-[(2-aminoethyl)amino]-ethanol (AEEA) , N-(2-aminoethyl)-1,2-ethanediamine (DETA) and 1-Piperazineethanamine (AEP) were synthesized and characterized in house at AkzoNobel (Arnhem, Netherlands). 1-N,N-dibutyl-butanamine (TBA) and cyclohexanamine (CHA) were from Fluka (Steinheim, Germany), N,N-diethyl-ethanamine (TEA) was from J. T. Baker (Deventer, The Netherlands). Adamantan-1-amine (ADAMA), N,N,N-trimethyl-1-hexadecanaminium chloride ( $C_{16}Me_3NCl$ ), 1-hexadecyl-dimethylamine ( $C_{16}Me_2N$ ), 1-hexadecyl-pyridinium bromide ( $C_{16}PyBr$ ), (*IR,2S*)-2-amino-1-phenyl-propan-1-ol (NOREPH) and methanol (MeOH) of HPLC grade were purchased from Sigma-Aldrich (St. Louis, MO). The structures of the Quats and amines used in this work are provided in Chart 7.1. (PLA-*block*-PEG-*block*-PLA) triblock copolymer was synthesized<sup>143</sup> and characterized in the Centre of Polymer and Carbon Materials of the Polish Academy of Sciences (Zabrze, Poland). Cation exchange resin AG MP-50 was purchased from Bio-Rad Laboratories (Hercules, CA). Ultra-pure water with a resistivity of

18.2 M $\Omega$ -cm (at 25 °C) was obtained from a Millipore Direct-Q<sup>®</sup> 3 water purification system (Molsheim, France).

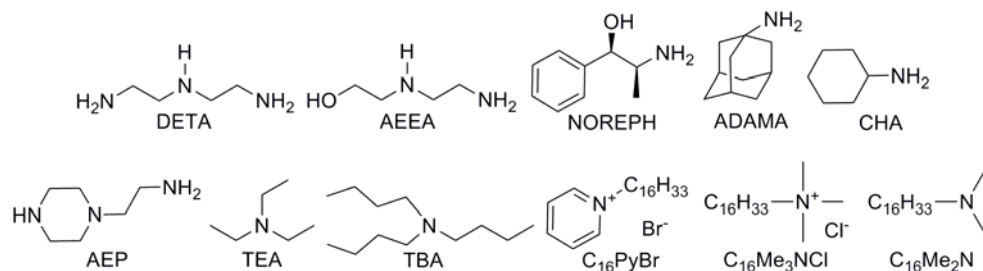


**Chart 7.1.** Structures of amines and Quats used in this chapter.

### 7.2.2 Sample preparation and methods

The samples were dissolved in a 50/50 (v/v) water/MeOH mixture or in pure MeOH (after purification with the cation exchange resin) at a concentration of 125–250  $\mu\text{g/mL}$ . For the comparison of the mass spectra obtained with the addition of different Quats and amines, the calculation of the average charge state value  $\bar{z}$  (see equation 6.1, Chapter 6) was used as another expression of the charge state shift trend. It should be stressed, though one more time that this equation is applied only for semi-quantitative purposes. It does not take into consideration parameters, such as width of the each charge state distribution and abundance of the product ions due to up-front fragmentation that could influence its value (see also Chapter 6).<sup>150</sup> An additional complicating factor is that identical values of amine molarities do not necessarily result in the same concentration of ammonium ions, because structurally different amines have different basicities. To avoid this complication, the amount of amine added was optimized so that the pH of the solutions was slightly basic (pH 7.5–8). The optimal concentration for all amines was 1.2 mM (50–100 times higher than the analyte concentration).

### 7.2.3 Instrumentation

MS experiments were performed on a Waters LCT TOF mass spectrometer (Micromass, Manchester, UK) equipped with an ESI source. The transfer of ions from the source to the orthogonal accelerated TOF mass analyzer is made by two hexapole radio

frequency lenses. The settings of the LCT were the following: capillary voltage 3–4.25 kV, desolvation temperature 150 °C, desolvation gas flow 395 L/hr, and mass range 400–14,500 Da. The cone voltage has a great influence on the MS response.<sup>150</sup> Therefore, its value was optimized every time for maximum MS response. The sample was introduced via a Cole-Palmer syringe pump (Vernon Hills, IL) at a flow rate of 10  $\mu$ L/min.

## 7.3 Results and discussion

### 7.3.1 MS analysis of PEG with addition of Quats and amines: A comparison

Previous results<sup>150</sup> demonstrated that the addition of Quats or amines to a high molar mass polyether solution has a double benefit: reduction of product ions due to up-front fragmentation and increase of the signal intensity of the low charge state ions. Figure 7.1 depicts this effect showing the mass spectra of PEG 10 kDa without amine or Quat (Figure 7.1a), with an optimized addition of  $C_{16}Me_3NCl$  (Figure 7.1b) and with an optimized addition of  $C_{16}Me_2N$  (Figure 7.1c). Without the addition of any Quat or amine (Figure 7.1a) the mass spectrum is dominated by protonated PEG product ions due to up-front fragmentation at high cone voltages. It was demonstrated in Chapter 6 that lowering the cone voltage reduces the intensity of the protonated PEG product ions and allows the detection of multiply charged protonated PEG adduct ions, albeit at very low abundance. The addition of  $C_{16}Me_2N$  (Figure 7.1c) resulted in an overall improvement of the mass spectra.  $[PEG_n + C_{16}Me_2NH]^+$  and  $[PEG_n + 2C_{16}Me_2NH]^{2+}$  adduct ions, that provide information about the MMD of the polymer sample, are observed. Although protonated PEG product ions are still observed, their abundance is lower than that of the observed singly and doubly-charged adduct ion distributions. The  $C_{16}Me_2N$  tertiary amine maintains the structural requirement (combination of large size with specific charge localization and/or facile interactions with the polymer) that was mentioned previously (see Conclusions, Chapter 6) and has a similar structure as  $C_{16}Me_3NCl$ .

A comparison between the mass spectra obtained after the addition of  $C_{16}Me_2N$  and  $C_{16}Me_3NCl$  clearly shows the three additional benefits of the use of this tertiary amine. Firstly, the addition of  $C_{16}Me_2N$  results in mass spectra with lower average charge state values ( $\bar{z} = 1.2$ ) than with the addition of  $C_{16}Me_3NCl$  ( $\bar{z} = 1.6$ ). Secondly, the abundance of

the protonated PEG product ions compared with the singly and doubly charged adduct ion distributions is lower than in the case with  $C_{16}Me_3NCl$ . Thirdly, the cluster ion peaks present in the mass spectra obtained with addition of  $C_{16}Me_3NCl$  are not present when  $C_{16}Me_2N$  is used, which simplifies the mass spectra. These improvements are attributed to the physicochemical nature of  $C_{16}Me_2N$ . This tertiary amine functions as a base and reacts with the protons in the solution (these protons are present after the treatment of the solution with the cation exchange resin), producing the  $C_{16}Me_2NH^+$  tertiary ammonium ion. The amount of protons in the solution is lowered and, consequently, the peak intensity of the protonated PEG product ions is lowered. A possible explanation for the absence of cluster ions is that there is no counter ion in the solution capable of forming a strong complex ion with  $C_{16}Me_2NH^+$  in the gas phase.

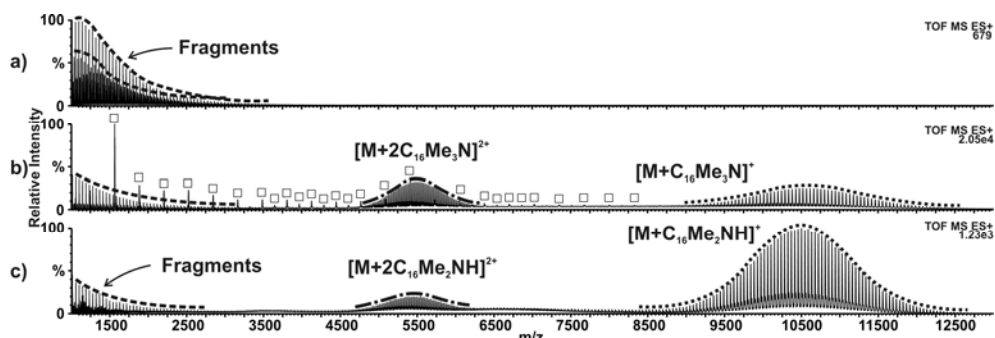


**Figure 7.1.** Mass spectra of 10 kDa PEG obtained by direct-infusion (DI) MS a) without addition of a Quat or amine, b) with addition of 1.2 mM  $C_{16}Me_3NCl$ , and c) with addition of 1.2 mM  $C_{16}Me_2N$ . **Note:** Peaks indicated with a square ( $\square$ ) are  $[(C_{16}Me_3N)_{x+1}Cl_x]^+$  cluster ions and “Fragments” are protonated PEG fragment ions. All mass spectra were obtained at 180 V cone voltage. “M” refers to  $PEG_n$ .

The potential of other amines for their capability to form low charge state adduct ions was investigated. To allow as much as possible a direct comparison between the performance of the different amines, the concentration of the ammonium ions needs to be the same. As demonstrated (Chapter 6), an increase in the Quat concentration influences the mass spectra by favoring the lower charge states. The addition of 1.2 mM of amine was sufficient to react with the protons of the solution (pH measurements showed a shift in pH values from  $\sim 6$  to  $\sim 8$ ) and provide an excess of ammonium ions in all cases. Figure 7.2

shows a selection of the mass spectra of PEG 10 kDa after the addition of structurally different amines. The remaining mass spectra of PEG 10 kDa with the other amines of this study are presented in Figure 7.3. In each case the same number of scans was summed. The calculated average charge state values for all cases are presented in Table 7.1.

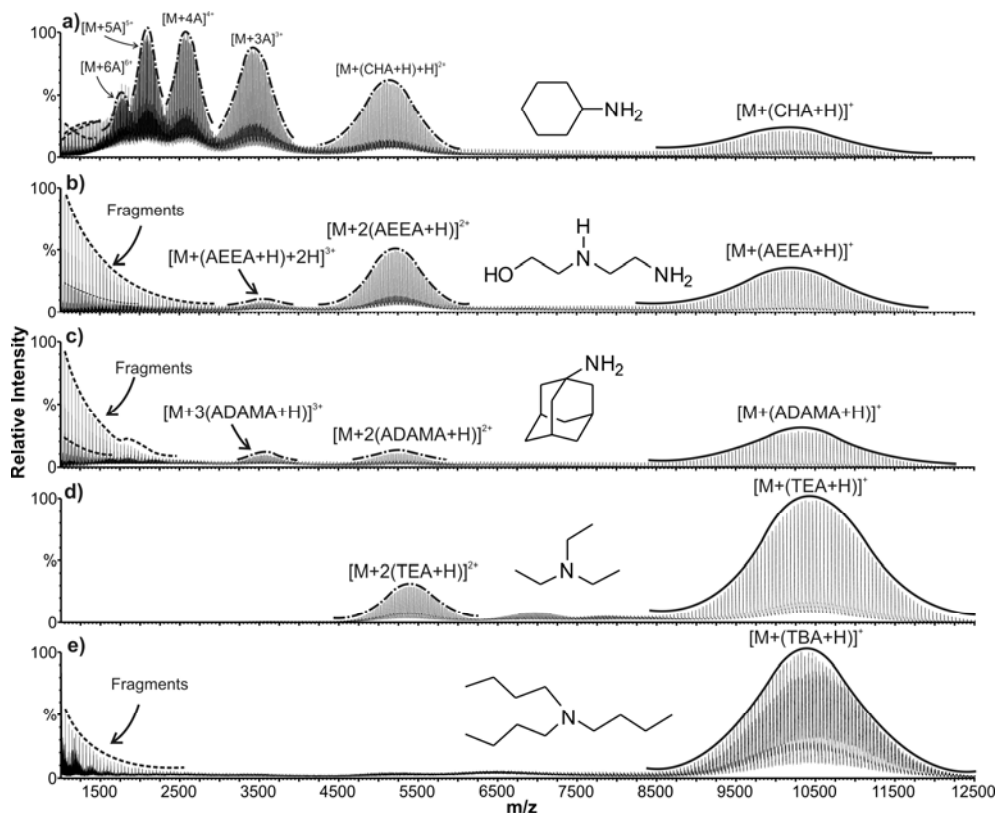


**Figure 7.2.** Mass spectra of 10 kDa PEG obtained by DI-MS with addition of 1.2 mM of: a) CHA, b) AEEA, c) ADAMA, d) TEA, and e) TBA. Note: “A” refers to an unspecified cation or mixture of adducts (*e.g.*, (CHA+H) or H), because the exact nature of the adduct ion cannot be determined accurately due to the low resolving power of the instrument. “Fragments” were protonated PEG product ions. All mass spectra were obtained under the same ESI conditions. “M” refers to PEG<sub>n</sub>.

Figure 7.2a shows the mass spectrum of PEG 10 kDa with the addition of CHA. The singly and doubly charged distributions were assigned to the  $[\text{PEG}_n+(\text{CHA}+\text{H})]^+$  and  $[\text{PEG}_n+(\text{CHA}+\text{H})+\text{H}]^{2+}$  adduct ions, respectively. The other multiply charged distributions

detected could not be assigned due to the insufficient resolving power of the TOF instrument, but it is suggested that a mixture of one  $(\text{CHA}+\text{H})^+$  primary ammonium ion with multiple protons is present. Figure 7.2b shows the mass spectrum of PEG 10 kDa after addition of AEEA. AEEA produces adduct ions of lower average charge state ( $\bar{z}=1.7$ ) than CHA ( $\bar{z}=3.4$ ). Envelopes assigned to  $[\text{PEG}_n+(\text{AEEA}+\text{H})]^+$ ,  $[\text{PEG}_n+2(\text{AEEA}+\text{H})]^{2+}$  and  $[\text{PEG}_n+(\text{AEEA}+\text{H})+2\text{H}]^{3+}$  adduct ions were detected. The detection of  $[\text{PEG}_n+(\text{AEEA}+\text{H})+2\text{H}]^{3+}$  adduct ions and the absence of the expected  $[\text{PEG}_n+3(\text{AEEA}+\text{H})]^{3+}$  and/or  $[\text{PEG}_n+2(\text{AEEA}+\text{H})+\text{H}]^{3+}$  adduct ions indicate that steric hindrance plays a role in higher charge state non-covalent complex ions. This is also shown with other primary amines (e.g., AEP and NOREPH), where cations in the multiply-charged adduct ions were a mixture of one primary ammonium ion with multiple protons (Figure 7.3a and 7.3b). The addition of ADAMA (Figure 7.2c), a primary amine with a large and rigid substituent gave an average charge state value ( $\bar{z}=1.6$ ) comparable to AEEA and the best performing Quats of the previous chapter,  $\text{C}_{16}\text{Me}_3\text{NCl}$  ( $\bar{z}=1.6$ ) and  $\text{C}_{16}\text{PyBr}$  ( $\bar{z}=1.5$ ).

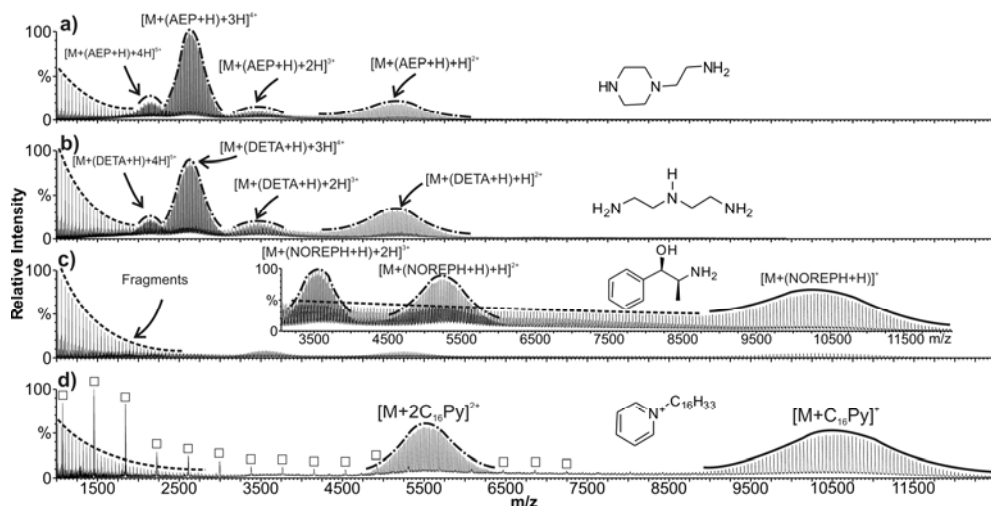


**Figure 7.3.** Mass spectra of 10 kDa PEG obtained by DI-MS with addition of 1.2 mM of: a) AEP, b) DETA, c) NOREPH, and d)  $\text{C}_{16}\text{PyBr}$ . Note: Peaks indicated with a square ( $\square$ ) are  $[(\text{C}_{16}\text{Py})_{x+1}\text{Br}_x]^+$  cluster ions. “Fragments” are protonated PEG product ions. All mass spectra were obtained under the same ESI conditions. “M” refers to  $\text{PEG}_n$ .

**Table 7.1. Average Charge State Values and Peak Intensities of Various 10 kDa PEG-Quat/Amine Adduct Ions.**

Quat/Amine	Average Charge State Value $\bar{z}$	Absolute Intensity of Highest Singly Charged Peak <sup>a</sup>
AEP	3.8	0 (946)
DETA	3.6	0 (915)
CHA	3.4	357
NOREPH	2.1	453
AEEA	1.7	676
ADAMA	1.6	1050
C <sub>16</sub> Me <sub>3</sub> NCl	1.6	1840
C <sub>16</sub> PyBr	1.5	186
TEA	1.2	6410
C <sub>16</sub> Me <sub>2</sub> N	1.2	425
TBA	1.1	224

<sup>a</sup>For the cases where singly charged ions were not detected, the intensity of the doubly charged distribution is shown in parenthesis.

The average charge state value is directly related to the ability to form low charge state adduct ions, and can, therefore, be used as a parameter for assessing the suitability of amines or Quats to deal with the dispersity challenge. However, other parameters such as absolute peak intensity of these ions and the presence of fragment ions due to up-front fragmentation should also be taken into consideration. These factors are important since they are closely related with the sensitivity of the method. An MS method with high sensitivity may allow the analysis of low analyte concentrations and polymer impurities. In addition, mass spectra with good signal-to-noise (S/N) ratio can be produced even with a limited number of scans. This can be of great help when hyphenated techniques are used, such as LC or SEC coupled to MS. Table 7.1 shows the highest peak intensity of the singly charged PEG-Amine/Quat non-covalent complex ions. It should be noted that the absolute intensity measurement was made after summing the same number of mass spectra. The highest intensity is observed in the case of TEA (6410 ion counts) followed by C<sub>16</sub>Me<sub>3</sub>NCl (1840 ion counts), which is almost 3.5 times lower than TEA. ADAMA (1040 ion counts) is third in rank, with the rest being below 1000 ion counts.

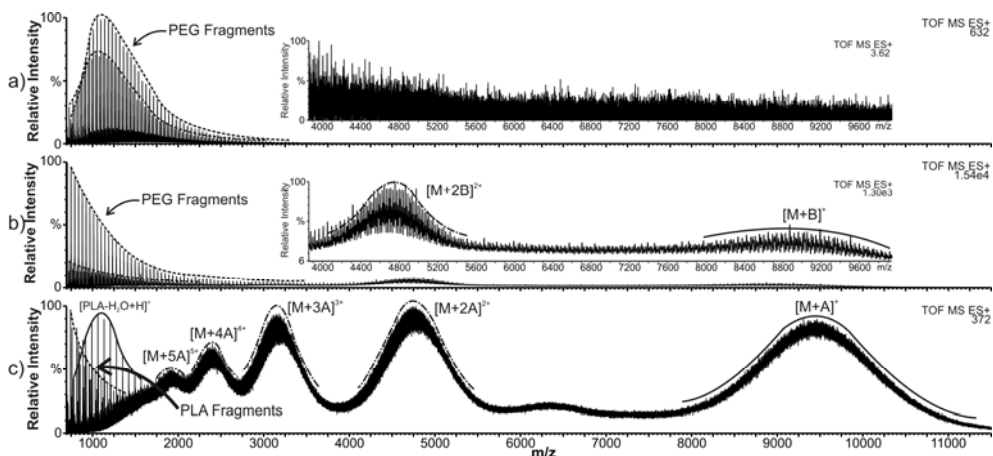
A relation between the structure of the amines and the presence of protonated PEG product ions has so far not been established. The source of these ions is still under investigation and will be addressed in later work on the fragmentation behavior of the low charge state non-covalent complex ions of high molar mass polymers with amines or Quats.

The efficiency of the various amines and Quats is determined by the analytical needs. As a general rule, when the simultaneous analysis of low and high molar mass polymers is needed, the presence of cluster ions and fragments is not wanted, and therefore a tertiary amine should be preferred. When additional information about the structure of the polymer is required, then a primary amine should be preferred so that fragments can still be observed. Quats should be used for more easily hydrolyzable or pH sensitive polymeric materials.

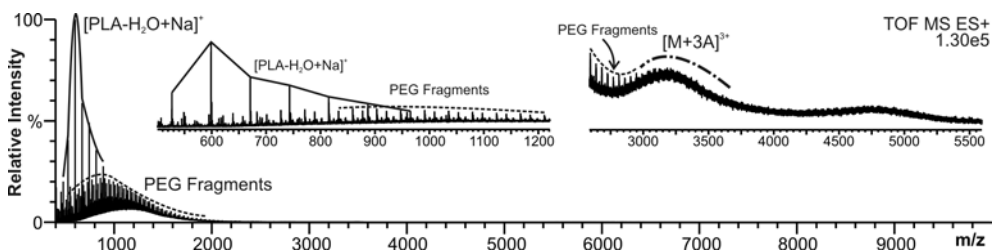
### 7.3.2 MS analysis of block copolymers with addition of Quats and amines

Figure 7.4 shows the mass spectra of a PLA-*block*-PEG-*block*-PLA triblock copolymer without and with the addition of TEA or C<sub>16</sub>Me<sub>3</sub>NCl. These two compounds were selected based on a good balance between their performance in the formation of low charge state ions (low  $\bar{z}$  value) and the intensity of their singly charged ions. They produced average charge state values of 1.2 and 1.6 respectively and the highest absolute intensities of singly charged ions (see Table 7.1). In addition, this pair allows a comparison between the use of a Quat and a tertiary amine.

Figure 7.4a depicts the mass spectrum of the block copolymer without the addition of any Quat or tertiary amine. The mass spectrum is dominated by protonated PEG fragment ions produced due to up-front fragmentation. The addition of sodium iodide (Figure 7.5) did not result to a substantial improvement. The addition of C<sub>16</sub>Me<sub>3</sub>NCl (Figure 7.4b), however, leads to an overall signal intensity increase (from 632 ion counts to 15,400 ion counts) and features the presence of low intensity peaks of singly and doubly charged adduct ion distributions of the copolymer. The addition of TEA results in the detection of singly to quintuply charged adduct ions (Figure 7.4c).



**Figure 7.4.** Mass spectra of 10 kDa PLA-*block*-PEG-*block*-PLA copolymer obtained by DI-MS: a) without addition of any Quat or amine, b) with addition of 1.2 mM  $C_{16}Me_3NCl$ , and c) with addition of 1.2 mM of TEA. **Note:** “M” refers to the block copolymer. “A” and “B” refer to the  $(TEA+H)^+$  and  $C_{16}Me_3N^+$  cations, respectively. All mass spectra were obtained under the same ESI conditions.



**Figure 7.5.** Mass spectrum of 10 kDa PLA-*block*-PEG-*block*-PLA copolymer obtained by DI-MS of a sample solution to which 0.25 mM of sodium iodide had been added. **Note:** “M” refers to the block copolymer. “A” refers to the cation adduct ion. Inset figures are magnified areas of the mass spectrum.

In addition, PLA fragment ions and PLA oligomers are detected. These PLA ions were not detected in the case of  $C_{16}Me_3NCl$ , possibly due to the oversaturation of the low mass region with protonated PEG fragment ions. The low S/N ratio and the limited resolving power of the TOF do not allow the confirmation of the various copolymer structures in both cases by DI-MS analysis (A resolving power higher than 170,000 at  $m/z$  10,000 would be required). The sample is a complex mixture of various copolymer distributions, since the initiating block was a polydisperse 8 kDa PEG sample. Lee *et al.*<sup>153</sup> demonstrated the successful separation of the copolymer distributions of a PLA-*block*-PEG-*block*-PLA

triblock copolymer (of approximately the same molar mass) by LC at critical conditions. The application of such a separation in this MS method could provide the necessary deconvolution and allow the generation of more detailed information on the copolymer structures.

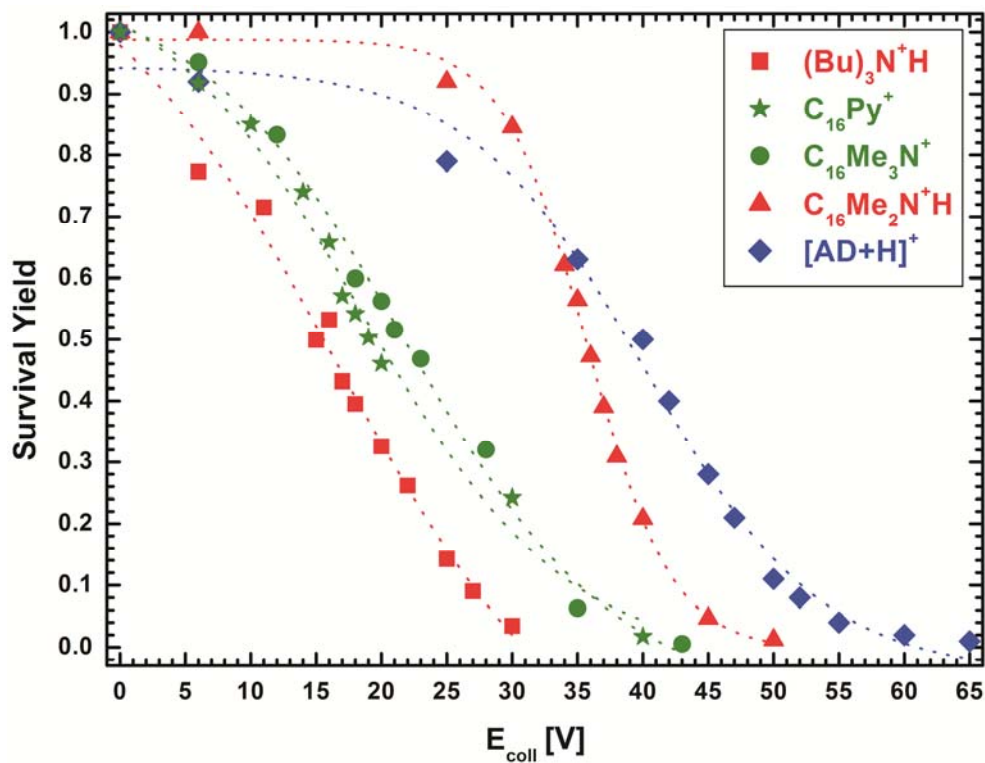
## 7.4 Conclusions

Addition of various amines and Quats to a PEG 10 kDa and PLA-*block*-PEG-*block*-PLA triblock copolymer 10 kDa solution facilitates the formation of low charge state adduct ions. A comparison between the various amines and Quats has been performed based on: a) the ability to form low charge state adduct ions, b) the signal intensity of the low charge state adduct ions, and c) the degree of up-front fragmentation. The performance of the amines and Quats as additives in ESI depends on their structure. Primary amines tend to produce adducts ions with higher average charge state values than tertiary amines and Quats. They also produce mass spectra with fragment ions, due to up-front fragmentation, but they do not produce cluster ions (as in the case with Quats). The use of the tertiary amine  $C_{16}Me_2N$ , instead of its quaternary equivalent,  $C_{16}Me_3NCl$ , results in a lower average charge state value, reduction of up-front fragmentation and absence of the high intensity peaks from the Quat clusters ions. This example shows the benefit of using tertiary amines instead of primary amines and Quats. These results show that the MS analysis of high molar mass polyethers (homopolymers or copolymers containing large polyether blocks) is facilitated by the use of various amines and Quats. The selection of amines and Quats in an application depends on the research question; the system can be optimized so as to get molecular weight information (and good sensitivity) or additional structure information through up-front activation.



## 8

# Electrospray Ionization Tandem Mass Spectrometry of ammonium cationized polyethers



Quaternary ammonium salts (Quats) and amines are known to facilitate the MS analysis of high molar mass polyethers, by forming low charge state adduct ions. The formation, stability and behavior upon collision-induced dissociation (CID) of adduct ions of polyethers with a variety of Quats and amines were studied by electrospray ionization quadrupole time-of-flight, quadrupole ion trap and linear ion trap (LIT) tandem mass spectrometry (MS/MS). The LIT was part of an Orbitrap hybrid mass spectrometer that allowed accurate mass MS/MS measurements. The Quats and amines studied were of different degree of substitution, structure and size. The stability of the adduct ions was related to the structure of the cation, especially the amine's degree of substitution. CID of singly/doubly charged primary and tertiary ammonium cationized polymers resulted in the neutral loss of the amine followed by fragmentation of the protonated product ions. The latter reveals information about the monomer unit, polymer sequence and endgroup structure. In addition the detection of product ions retaining the ammonium ion was observed. The predominant process in the CID of singly charged quaternary ammonium cationized polymers was cation detachment, whereas their doubly charged adduct ions provided the same information as the primary and tertiary ammonium cationized adduct ions. This study shows the potential of specific amines as tools for the structural elucidation of high molar mass polyethers.

**Nasioudis, A.; Heeren, R. M. A; van Doormalen, I.; de Wijs-Rot, N.; van den Brink, O. F. J. *Am. Soc. Mass Spectrom.* 2011, 22, 837-844.**

## 8.1 Introduction

The formation of non-covalent complexes between ammonium ions (*e.g.*, Quats or primary or tertiary ammonium ions) and polymers has been shown to be a versatile tool that can address various analytical challenges in MS. This versatility derives from the fact that these non-covalent complex ions can be used to study either the neutral polymer or the cation itself.

It has been demonstrated that polyethers and crown ethers can be used as shift reagents for ion mobility spectrometry (IMS) MS and separate isobaric and/or isomeric ammonium ions (*e.g.*, protonated peptides, small ammonium molecules).<sup>154-157</sup> This is accomplished by the formation of non-covalent complexes between the ether and the ammonium ions. The non-covalent complex ions exhibit a different mobility behavior than their naked peptide ions or ammonium ions (in the case of small amine molecules). As a result, they extend the ability to separate components. In addition, the intensity of the non-covalent complex ions is significantly increased in relation to the intensity of other polymer adduct ions present, indicating a possible stabilization effect.

The use of this technique for the analysis of polymers is still in an early stage. Obtaining information, such as monomer composition, end-group type and molar mass distribution<sup>22,23,25,89</sup> by MS is well established for relatively pure and narrow dispersed polymers of relatively low molecular weight and it is sufficient for a number of applications. The current challenge in polymer analysis is to get the same type of information for structurally complicated polymers with broad distributions and high molar mass. To some extent liquid chromatography and size-exclusion chromatography coupled to electrospray ionization (ESI) MS can face this challenge of structural complexity.<sup>16,17,21,117</sup> When disperse and high molar mass polymers are analyzed, convolution of the multiple charge state distributions with the size distribution is a common phenomenon. Various attempts to deal with this challenge have been reported (see also Introduction, Chapter 6). All of these strategies require advanced and/or custom made MS instruments. Another approach, that requires only relatively simple MS instrumentation, is to facilitate the formation of polymer adduct ions with ammonium containing molecules as shown in Chapters 6 and 7.

Although the use of various ammonium ions for the formation of low charge state adduct ions has been demonstrated, the behaviour of these ions upon excitation has not been thoroughly studied. To the best of our knowledge, only Howdle *et al.*<sup>158</sup> presented a tandem MS (MS/MS) spectrum of a PEG-amine adduct ion. The amine used was an active pharmaceutical ingredient, lamivudine (a primary amine). Activation of the adduct ion resulted in dissociation of the non-covalent complex ion to its constituents. Fragment ions that could provide structural information (*e.g.*, sequence, monomer unit, end-group) about the polyether were not reported.

This chapter will focus on the identification of the type of polyether-amine non-covalent complex ions that can best be used as a source of structural information of the polyether by MS/MS. A comparative study is made for non-covalent complex ions of polyethers with ammonium ions with different degree of substitution, structure and size. These ions are investigated with the most readily available MS instruments that cover both low and relatively high collision energy regimes. In addition, breakdown diagrams are constructed from the energy-dependent MS/MS measurements of selected non-covalent complex ions. These diagrams provide insight in the non-covalent complex ions' stability and potential use for structural elucidation of high molar mass polyethers.

## 8.2 Experimental section

### 8.2.1 Chemicals and sample preparation

PEG 2 kDa was synthesized and characterized in house at AkzoNobel (Arnhem, Netherlands). Poly(propylene glycol) (PPG) 2 kDa from Waters Associates (Framingham, MA) and 1-N,N-dibutyl-butanamine (TBA) was from Fluka (Steinheim, Germany). Poly(tetramethylene glycol) (PTMEG) 2 kDa, Adamantan-1-amine (AD), hexadecyltrimethylammonium chloride ( $C_{16}Me_3NCl$ ), 1-hexadecyl-pyridinium bromide ( $C_{16}PyBr$ ), hexadecyldimethylamine ( $C_{16}Me_2N$ ) and methanol (MeOH) of HPLC grade were purchased from Sigma-Aldrich (St. Louis, MO). Cation exchange resin AG MP-50 was purchased from Bio-Rad Laboratories (Hercules, CA). Ultra-pure water with a resistivity of 18.2  $M\Omega \cdot cm$  (at 25 °C) was obtained from a Millipore Direct-Q<sup>®</sup> 3 water purification system (Molsheim, France). The samples were dissolved in a 50/50 (v/v)

water/MeOH or pure MeOH (after purification with the cation exchange resin) at a concentration of 25–50  $\mu\text{g/mL}$  containing 0.25–0.75 mM of the amines and Quats studied. The concentration of the samples for the experiments in the LTQ Orbitrap hybrid mass spectrometer was 2–5  $\mu\text{g/mL}$ . The concentration of the amines remained the same as previously.

### 8.2.2 Instrumentation and methods

MS and MS/MS experiments were performed in a Waters Synapt G1 IMS time-of-flight (TOF) mass spectrometer (Waters, Manchester, UK), a Bruker Esquire 3000<sup>plus</sup> quadrupole ion trap (QIT) mass spectrometer (Bruker Daltonics, Bremen, Germany), and a LTQ Orbitrap hybrid Fourier transform mass spectrometer (FTMS) (Thermo Scientific, San Jose, CA). The settings of the IMS-TOF mass spectrometer were the following: capillary voltage 3 kV; desolvation temperature 150 °C; desolvation gas flow 600 L/hr; collision gas was Ar and the average pressure in the trap cell was  $9.33 \times 10^{-3}$  mbar. The potential of the sampling cone was adjusted in each case to prevent upfront fragmentation and never exceeded 45 V. The isolation settings in the quadrupole (LM and HM resolution) were optimized to maximize the intensity of the precursor ion (indicative values were 20 and 10 arbitrary units for LM and HM, respectively). Isolation and fragmentation of the precursor ions was performed in the trap cell. The mobility cell was inactive during these measurements. Hence, the IMS-TOF mass spectrometer was used as a regular quadrupole TOF (*q*-TOF) mass spectrometer. The settings of the QIT mass spectrometer were the following: capillary voltage 3 kV; nebulizer pressure 76 kPa; dry gas flow 4 L/min; dry gas temperature 250 °C; the collision gas was He and the average pressure in the ion trap was  $8.82 \times 10^{-6}$  mbar (uncorrected gauge reading, although the real pressure in the trap is known to be 2–3 orders of magnitude higher<sup>138</sup>). The number of trapped ions was approximately 5,000 and was kept constant by using the ion charge control (ICC) option throughout all measurements. It was observed that when the abundance of the precursor ions was low, the necessary accumulation time to obtain an ICC of 5,000 was too long, and resulted in space charge effects. Therefore, the maximum accumulation time was set between 3 and 5 ms, depending on the precursor ion's abundance. The isolation parameters (*e.g.*, isolation width and

isolation mass) were optimized to increase the abundance of the isolated precursor ion. A cooling period of 50 ms was inserted between the isolation and excitation steps. The excitation time was set to 60 ms and the level of excitation was varied by changing the setting of the fragmentation amplitude. The “Smart Frag” feature was disabled. The settings of the LTQ Orbitrap FTMS were the following: source voltage 4 kV; capillary temperature 300 °C; Tube lens voltage 70 – 200 V; Capillary voltage 50 V. The MS/MS experiments were performed in the linear ion trap (LIT). The isolation parameters (*e.g.*, isolation width and isolation mass) were optimized to increase the abundance of the isolated precursor ion. The excitation time was set to 30 ms and the Q value at 25 %. The level of excitation was varied by changing the setting of the normalized collision energy (NCE). The “wide band activation” feature was disabled. The sample was introduced via a Cole-Palmer syringe pump (Vernon Hills, IL) at a flow rate of 10  $\mu\text{L}/\text{min}$  in the case of QIT. For the other instruments, the onboard syringe pump was used at the same flow rate as for the QIT.

## 8.3 Results and discussion

### 8.3.1 *q*-TOF MS/MS of singly and doubly charged non-covalent complex ions

Figure 8.1a depicts the product ion mass spectrum of the  $[\text{PEG}_{41} + \text{C}_{16}\text{Me}_3\text{N}]^+$  generated in a *q*-TOF mass spectrometer. Three peaks are observed assigned to the precursor ion,  $\text{C}_{16}\text{Me}_3\text{N}^+$  and the dimer  $[(\text{C}_{16}\text{Me}_3\text{N})_2\text{Cl}]^+$ . The  $[(\text{C}_{16}\text{Me}_3\text{N})_2\text{Cl}]^+$  dimer is not a product of the activation of the precursor ion, because it is also present in the isolation step. This phenomenon may result from the relatively high Quat concentration used in this experiment. It should be noted that this was only observed in the *q*-TOF MS/MS experiment; it was not seen in QIT and LIT MS/MS experiments (*vide infra*). The absence of product ions relating to the polymer chain shows that the predominant fragmentation process is loss of the cation. The same behavior was observed in the product ion mass spectrum of  $[\text{PEG}_{41} + \text{C}_{16}\text{Py}]^+$  and  $[\text{PEG}_{41} + (\text{Bu})_3\text{NH}]^+$  (Figure 8.2). In both cases the only product ion observed was the respective cation due to cation detachment.

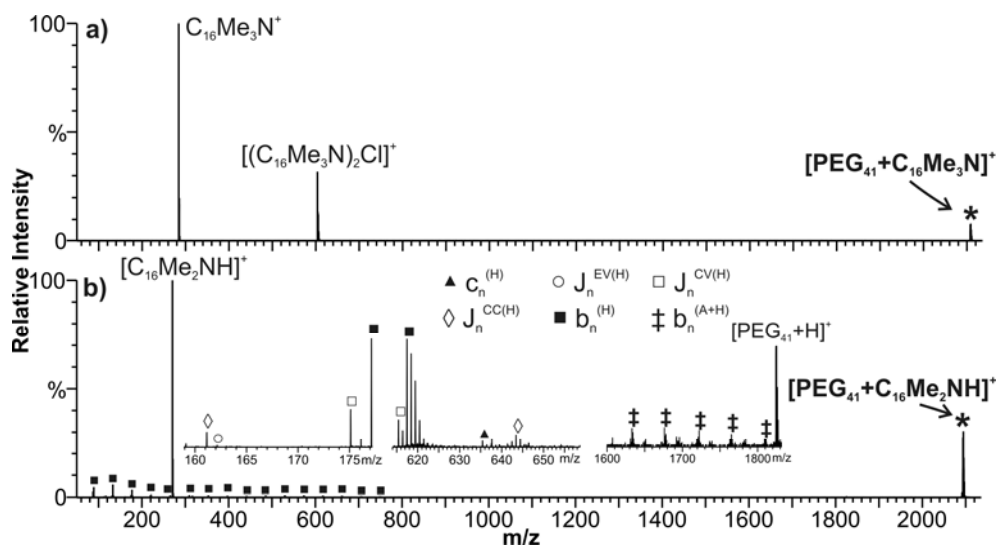


**Figure 8.1.** Product ion mass spectrum of: a)  $[\text{PEG}_{41}+\text{C}_{16}\text{Me}_3\text{N}]^+$  and b)  $[\text{PEG}_{41}+\text{C}_{16}\text{Me}_2\text{NH}]^+$  in a  $q$ -TOF mass spectrometer. Note: Asterisks (\*) indicate the respective precursor ions. Inset figures are magnification of areas of the product ion spectrum of  $[\text{PEG}_{41}+\text{C}_{16}\text{Me}_2\text{NH}]^+$ . Product ion notation based on Wesdemiotis *et al.*<sup>112</sup> (see below Table 8.1).

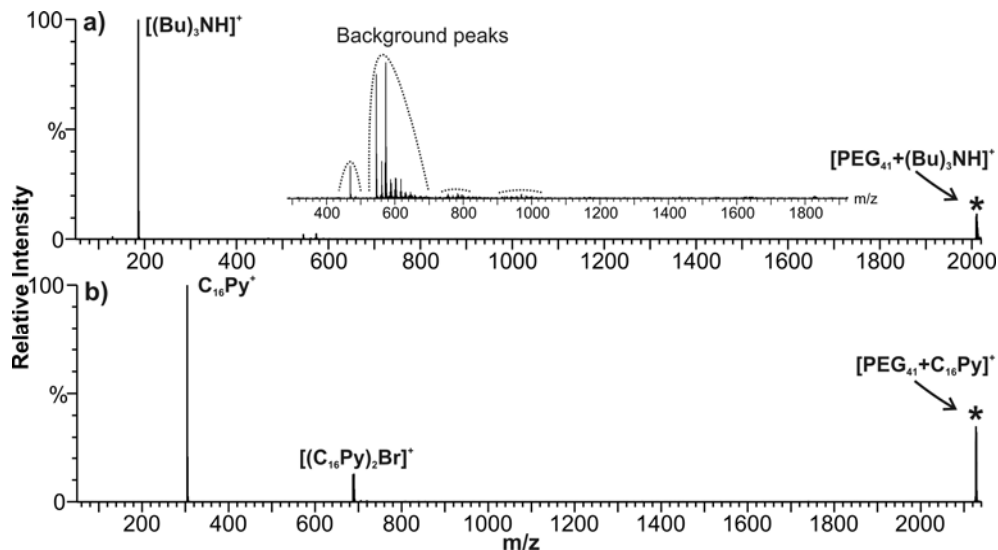


**Figure 8.2.** Product ion mass spectrum of: a)  $[\text{PEG}_{41}+(\text{Bu})_3\text{NH}]^+$  and b)  $[\text{PEG}_{41}+\text{C}_{16}\text{Py}]^+$  obtained in a  $q$ -TOF mass spectrometer. Note: Asterisks (\*) indicate the respective precursor ions. Inset figure is a magnification of a part of the product ion spectrum of  $[\text{PEG}_{41}+(\text{Bu})_3\text{NH}]^+$ . The presence of  $[(\text{C}_{16}\text{Py})_2,\text{Br}]^+$  dimer is the result of imperfect isolation, as these ions are also observed in the isolation spectra.

The  $C_{16}Py^+$  cation retains the charge, as in the case of  $[PEG_{41}+C_{16}Me_3N]^+$ , hence no other product ions are observed. However, in the case of  $[PEG_{41}+(Bu)_3NH]^+$  the proton charge can migrate to the polymer and induce fragmentation. The fact that also in this case only cation detachment is observed suggests that the proton affinity (PA) of the amine as well as the strength of interactions between the polymer and the cation do play a crucial role.  $(Bu)_3N$  has a high PA and will not allow the proton to easily migrate to the polymer. In addition, the bulky alkyl chains of  $(Bu)_3N$  hinder the formation of strong interactions between the cation and the polymer, as indicated by the observation of low intensity adduct ions of this type in previous work.<sup>150</sup>

Figure 8.1b shows the product ion mass spectrum of  $[PEG_{41}+C_{16}Me_2NH]^+$ , where the most dominant peak is the tertiary ammonium ion  $C_{16}Me_2NH^+$  as a result of cation detachment. The  $[PEG_{41}+H]^+$  formed after the neutral loss of the amine  $C_{16}Me_2N$  was also detected (see respective panel in Figure 8.1b), but its abundance was very low in relation to the abundance of the precursor ion and the dominant product ion  $C_{16}Me_2NH^+$ . In addition, six series of ions spaced by 44u were identified as product ions. Their identification was based on the fragmentation nomenclature as proposed by Wesdemiotis *et al.*<sup>112</sup> The notation for polyethers is presented in Chart 8.1.

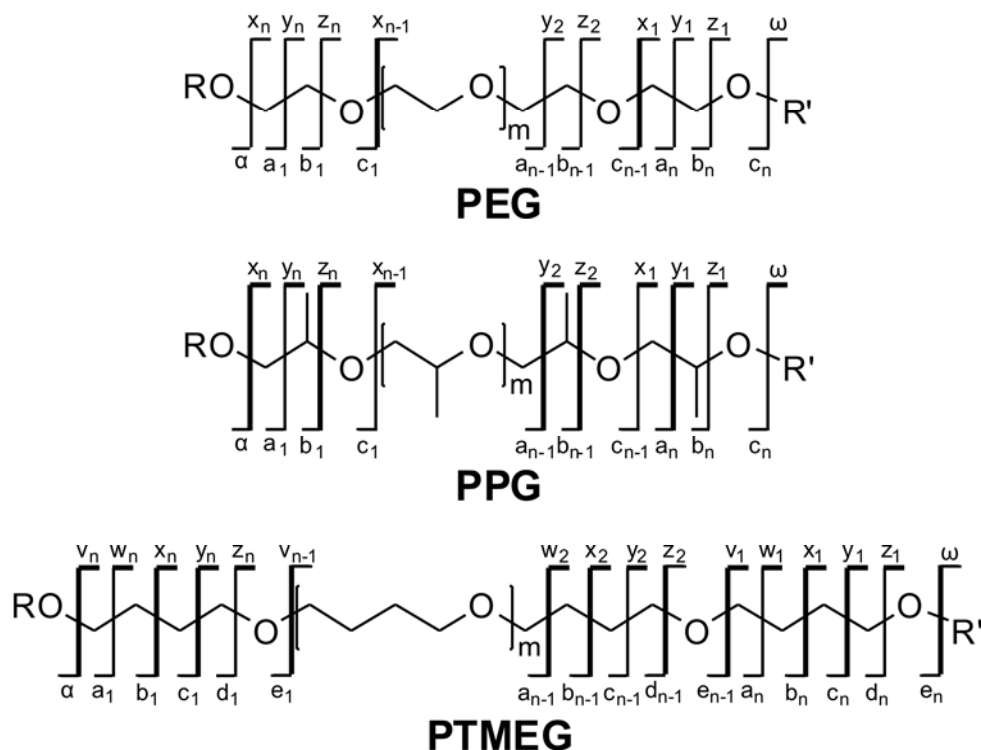


**Chart 8.1.** Nomenclature scheme of polyethers with different initiating ( $\alpha$ ) and terminating ( $\omega$ ) end-groups. Note:  $n=m+3$ . Product ions with a double prime (not presented in the Chart) such as  $c_n''$  have two more H atoms than the product ion with no double prime (in this specific case,  $c_n$ ). An elaborate explanation of the nomenclature is presented in Reference 112.

Wesdemiotis' nomenclature although is comprehensive, it does not cover the few cases where a precursor ion can result in a product ion with a different kind of adduct ion. Two of the six series identified in Figure 8.1b are of the same type ( $b$  ions) but with different cations. To avoid confusion in the annotation of these ions, the addition of a new notation rule in the nomenclature proposed by Wesdemiotis<sup>112</sup> is suggested. The addition of superscripted (<sup>X</sup>) (where X is the cation) to the product ions, indicates the type of cation present in each ion. Based on this amendment, five series were identified as product ions of fragmentation of  $[\text{PEG}_{41}+\text{H}]^+$ . These ions were identified as the  $c_n^{(H)}$ ,  $b_n^{(H)}$ ,  $J_n^{CC(H)}$ ,  $J_n^{CV(H)}$  and  $J_n^{EV(H)}$  product ions as proposed previously by Wesdemiotis *et al.*<sup>112</sup> Table 8.1 lists these product ions along with their structures.

**Table 8.1. List of Identified Product Ions for the Respective Polymer**

Polymer Type	Structure of product ion	Notation of product ion <sup>a</sup>
PEG		$c_n^{(X)}$
		$c_n^{(X)}$
		$b_n^{(X)}$
		$J_n^{EV(X)}$
		$J_n^{CE(X)}$
		$J_n^{CC(X)}$
		$J_n^{CV(X)}$
PPG		$c_n^{(X)}$
		$c_n^{(X)}$
		$b_n^{(X)}$
PTMEG		$e_n^{(X)}$
		$d_n^{(X)}$

<sup>a</sup>The notation of the product ions was based on the fragmentation nomenclature proposed by Wesdemiotis *et al.*<sup>112</sup> Note: Superscripted “(X)” indicates the type of cation adduct

The sixth series of peaks with the same spacing (44u) was identified as product ions after the direct dissociation of the precursor ion. These were  $b_n^{(A+H)}$  type of ions and hence tertiary ammonium  $C_{16}Me_2NH^+$  adducts (for simplification indicated as “A+H” in the ion notation; “A” stands for amine, and subsequently “A+H” is the ammonium ion). The presence of  $x_n^{(A+H)}$  (where x is b, c, e, etc) type of ion with  $C_{16}Me_2N$  but not with  $(Bu)_3N$  (also a tertiary amine) is attributed to differences in the binding energies of the cation with the oxygens’ lone pairs in the polymer chain and in the PAs. The shorter substituents of  $C_{16}Me_2N$  (two methyl groups) may cause higher binding energies than the large butyl groups of  $(Bu)_3N$  and allow the detection of  $x_n^{(A+H)}$  type of product ions. In addition,

differences in the PAs of  $C_{16}Me_2N$  and  $(Bu)_3N$  could explain why protonated PEG product ions are detected in the former case.

Figure 8.3 presents the product ion mass spectrum of the same PEG oligomer cationized with a primary ammonium ion,  $(AD+H)^+$  in a  $q$ -TOF. Figure 8.3a presents the product ion spectrum of the singly charged  $[PEG_{41}+(AD+H)]^+$  and Figure 8.3b of the doubly charged equivalent  $[PEG_{41}+2(AD+H)]^{2+}$ .

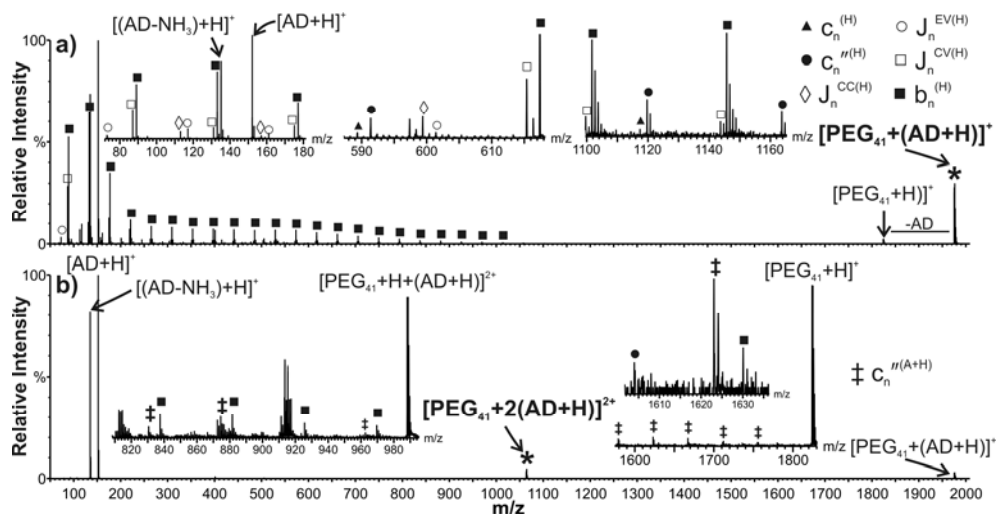


**Figure 8.3.** Product ion mass spectra of  $[PEG_{41}+n(AD+H)]^{n+}$  non-covalent complex ions obtained in a  $q$ -TOF mass spectrometer: a) Singly charged ( $n=1$ ) and b) doubly charged ( $n=2$ ). Note: Asterisks (\*) indicate the respective precursor ions. Inset figures are magnifications of areas of the respective product ion spectra. Product ion notation based on Wesdemiotis *et al.*<sup>112</sup> (see also Table 8.1).

The fragmentation behavior of the singly charged adduct ion partly resembles the one of  $[PEG_{41}+C_{16}Me_2NH]^+$ . Protonated AD,  $[AD+H]^+$  and  $[PEG_{41}+H]^+$  were the main product ions. The carbocation  $[(AD-NH_3)+H]^+$  is possibly formed on consecutive fragmentation of  $[AD+H]^+$  by loss of ammonia. In addition, low intensity peaks of six different series of PEG product ions were detected. These were the  $c_n^{n(H)}$ ,  $c_n^{(H)}$ ,  $b_n^{(H)}$ ,  $J_n^{CC(H)}$ ,  $J_n^{CV(H)}$  and  $J_n^{EV(H)}$  series (see insets in Figure 8.3a). Product ions that maintain the ammonium adduct, like in the case of  $C_{16}Me_2NH^+$ , were not detected. These were observed only when the doubly charged PEG oligomer  $[PEG_{41}+2(AD+H)]^{2+}$  was activated (see Figure 8.3b). The product

ion mass spectrum of the doubly charged adduct ion shows intense peaks of  $[\text{AD}+\text{H}]^+$  and  $[(\text{AD}-\text{NH}_3)+\text{H}]^+$ . The singly charged adduct ion  $[\text{PEG}_{41}+(\text{AD}+\text{H})]^+$  results from loss of one ammonium ion from the precursor ion.  $[\text{PEG}_{41}+\text{H}]^+$  is also observed (possibly from consecutive fragmentation of  $[\text{PEG}_{41}+(\text{AD}+\text{H})]^+$ ). Low intensity  $[\text{PEG}_{41}+(\text{AD}+\text{H})+\text{H}]^{2+}$  and  $[\text{PEG}_{41}+2\text{H}]^{2+}$  product ions as a result of direct amine loss from the precursor ion and low intensity peaks of  $c_n^{(H)}$  and  $b_n^{(H)}$  product ion series were also detected. Product ions with the ammonium ion were also present. Their type was  $c_n^{(A+H)}$ .

It is not clear why  $x_n^{(A+H)}$  type product ions are not observed on activation of the singly charged ion but only in the doubly charged. The suggestion that PA plays a crucial role in the detection of  $x_n^{(A+H)}$  type product ions cannot fully explain this phenomenon. Additional experiments are necessary with various primary, secondary and tertiary amines with known PAs.

### 8.3.2 LIT and QIT MS/MS of singly and doubly charged non-covalent complex ions

For comparison, the fragmentation behavior of  $[\text{PEG}_{41}+(\text{AD}+\text{H})]^+$  and  $[\text{PEG}_{41}+2(\text{AD}+\text{H})]^{2+}$  was also investigated in a LIT and a QIT mass spectrometer. QITs and LITs are known for fragmentation under low collision energy regimes. This is reflected also in the product ion mass spectra of  $[\text{PEG}_{41}+(\text{AD}+\text{H})]^+$  generated in the LIT and QIT instruments. In the case of LIT (Figure 8.4), the major product ions observed were the “charge-catalyzed”  $c_n^{(H)}$  and  $b_n^{(H)}$  and the  $J_n^{CV(H)}$  type of product ions. The high mass accuracy of the LIT instrument (LTQ Orbitrap) confirmed the above attribution. In addition two other (unconfirmed) series of product ions were detected. These could be product ions retaining the ammonium ions such as  $c_n^{(A+H)}$  and  $J_n^{HE(A+H)}$  but the accurate mass measurement could not confirm this attribution.

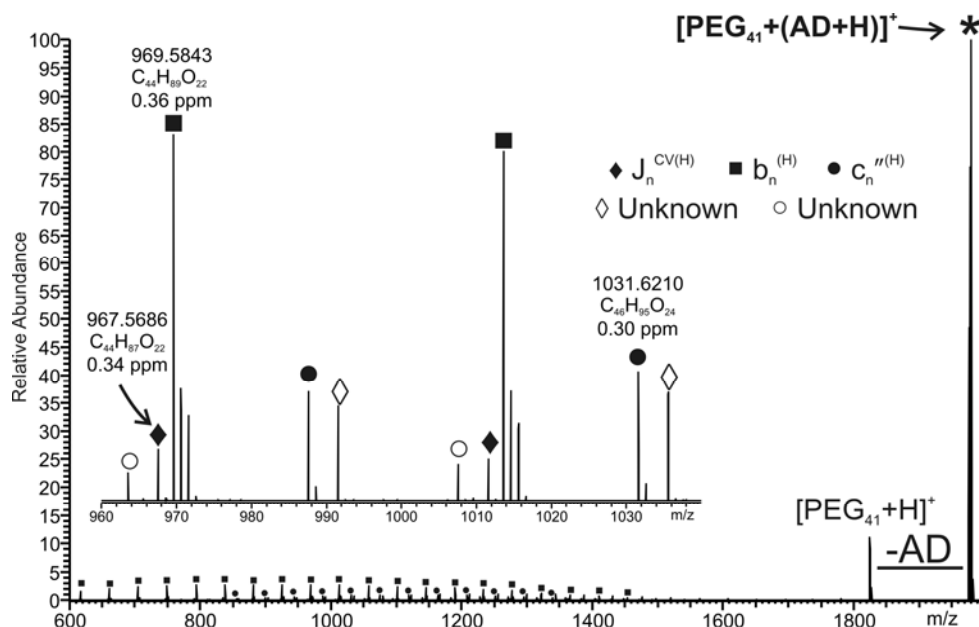


**Figure 8.4.** Product ion mass spectrum of  $[\text{PEG}_{41}+(\text{AD}+\text{H})]^+$  obtained in a LTQ Orbitrap. Note: The asterisk (\*) indicates the precursor ion. Inset figure is a magnified area of the product ion spectrum. Product ion notation based on Wesdemiotis *et al.*<sup>112</sup> (see also Table 8.1).

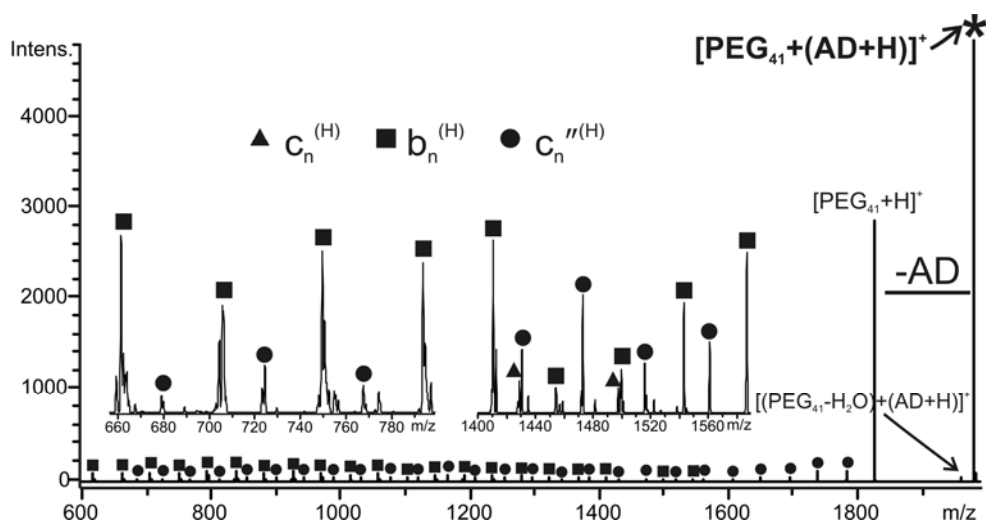


**Figure 8.5.** Product ion mass spectrum of  $[\text{PEG}_{41}+(\text{AD}+\text{H})]^+$  obtained in a QIT mass spectrometer. Note: The asterisk (\*) indicates the precursor ion. Inset figures are magnified areas of the product ion spectrum. Product ion notation based on Wesdemiotis *et al.*<sup>112</sup> (see also Table 8.1).

The spectrum produced in the QIT (Figure 8.5) shows a similar pattern to the one produced in a LIT. The major product ions observed were the “charge-catalyzed”  $c_n^{(H)}$  and  $b_n^{(H)}$ . Low intensity “charge-independent”  $c_n^{(H)}$  type of product ions were also detected, while  $J_n^{CC(H)}$ ,  $J_n^{CV(H)}$  and  $J_n^{EV(H)}$  type are absent. These “internal” product ions are usually observed under relatively high collision energy regimes (*e.g.*, *q*-TOF).

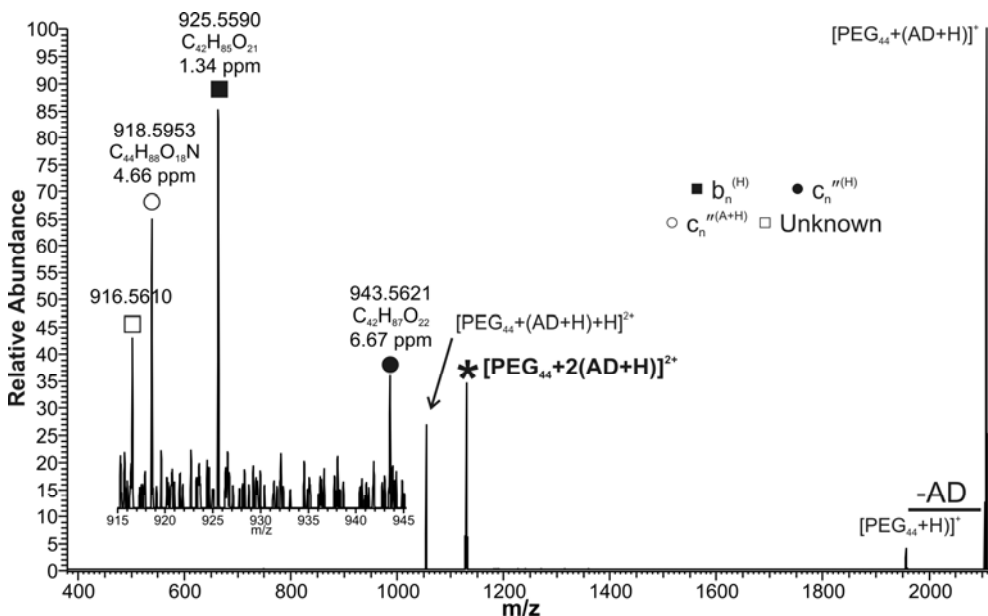


**Figure 8.6.** Product ion mass spectrum of  $[\text{PEG}_{44}+2(\text{AD}+\text{H})]^{2+}$  obtained in a LTQ Orbitrap. **Note:** The asterisk (\*) indicates the precursor ion. Inset figure is a magnified area of the product ion spectrum. The  $m/z$  value is the measured value along with the proposed elemental composition and mass error. Product ion notation based on Wesdemiotis *et al.*<sup>112</sup> (see also Table 8.1).

On the other hand, the product ion mass spectrum of  $[\text{PEG}_{44}+2(\text{AD}+\text{H})]^{2+}$  (Figure 8.6) resembles the one generated in a *q*-TOF (Figure 8.3). The major product ions detected derived from fragmentation processes dealing with loss of the ammonium ion or amine. The detection of  $[\text{PEG}_{44}+(\text{AD}+\text{H})]^+$  and  $[\text{PEG}_{44}+\text{H}]^+$  is explained as previously. The higher abundance of  $[\text{PEG}_{44}+(\text{AD}+\text{H})+\text{H}]^{2+}$  product ion, in comparison with its abundance in the product ion mass spectrum from the *q*-TOF, suggests that it is favorably formed in low collision energy regimes. In addition,  $c_n^{(H)}$ ,  $b_n^{(H)}$  and  $c_n^{(A+H)}$  product ion series were

detected and confirmed by accurate mass measurement. A fourth ion with  $m/z$  919.5610 could be a  $c_n^{(A+H)}$  type of product ion, but the accurate mass measurement does not confirm this attribution. It should be noted that the cut-off selection in LIT does not allow the detection in the low mass region (actually ions with  $m/z$  lower than 25 % of the precursor ion's  $m/z$ ).

A comparable fragmentation pattern with similar type of product ions was also observed in the product ion mass spectrum of  $[\text{PEG}_{41}+2(\text{AD}+\text{H})]^{2+}$  produced in the QIT (Figure 8.7). A distinct difference is that in the QIT product ion mass spectrum the product ion,  $[\text{PEG}_{41}+2\text{H}]^{2+}$ , was detected. This ion derives by neutral loss of two amines from the precursor ion and is explained as previously. In addition,  $c_n^{(H)}$  and  $b_n^{(A+H)}$  type of product ions were detected.

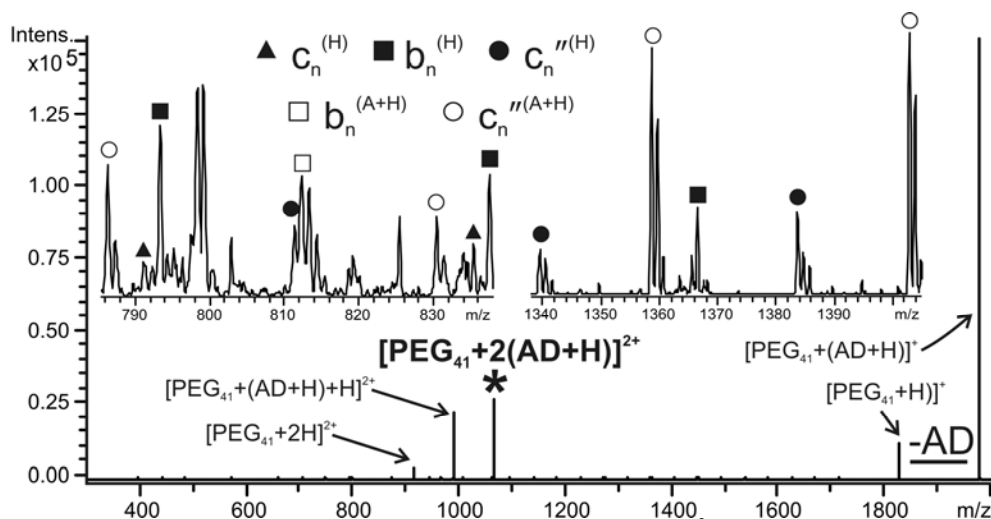


**Figure 8.7.** Product ion mass spectrum of  $[\text{PEG}_{41}+2(\text{AD}+\text{H})]^{2+}$  obtained in a QIT mass spectrometer. **Note:** The asterisk (\*) indicates the precursor ion. Inset figures are magnified areas of the product ion spectrum. Product ion notation based on Wesdemiotis *et al.*<sup>112</sup> (see also Table 8.1).

To establish if the observation of the  $x_n^{(A+H)}$  type of product ions is related to the cation's and/or the polymer's structure, the CID of ammonium adduct ions of PPG and PTMEG was explored in both instruments (*i.e.*, QIT and LIT). The activation of

$[\text{PPG}_{39}+(\text{AD}+\text{H})]^+$  in the QIT did not result in the detection of any product ions. In the LIT one product ion resulting from the neutral loss of the amine was detected (Figure 8.8).

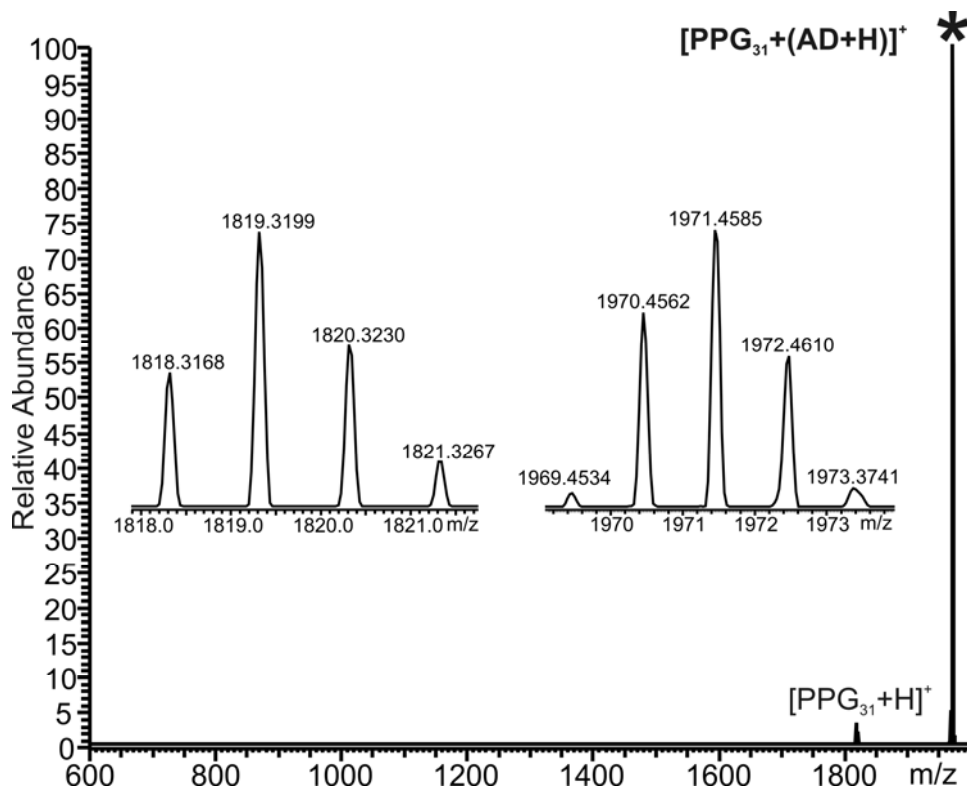


**Figure 8.8.** Product ion mass spectrum of  $[\text{PPG}_{31}+(\text{AD}+\text{H})]^+$  obtained in a LTQ Orbitrap. Note: The asterisk (\*) indicates the precursor ion. Inset figures are magnified areas of the product ion spectrum showing the isotopic distribution of the precursor ion and the detected product ions.

The activation of  $[\text{PPG}_{38}+2(\text{AD}+\text{H})]^{2+}$  in the LIT, however, resulted in a product ion mass spectrum (Figure 8.9) with five series of product ions. These were  $c_n^{(H)}$ ,  $c_n^{(H)}$ ,  $b_n^{(H)}$ ,  $c_n^{(A+H)}$  and  $b_n^{(A+H)}$  type. Their structures are presented in Table 8.1. The product ion mass spectrum of a same type of ion produced in a QIT was similar to the one in Figure 8.9 (Figure 8.10). Six series of product ions were observed. These were  $c_n^{(H)}$ ,  $c_n^{(H)}$ ,  $b_n^{(H)}$ ,  $c_n^{(A+H)}$ ,  $c_n^{(A+H)}$  and  $b_n^{(A+H)}$  type of product ions.

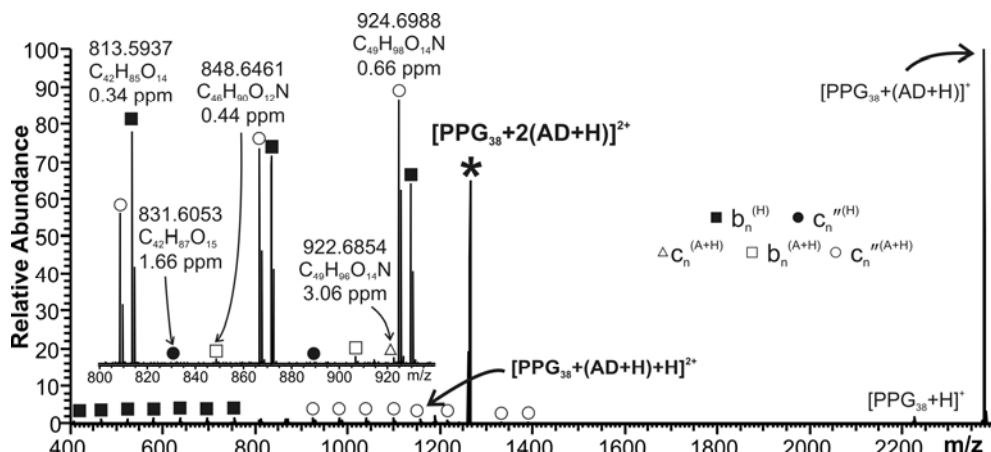


**Figure 8.9.** Product ion mass spectrum of  $[\text{PPG}_{38}+2(\text{AD}+\text{H})]^{2+}$  obtained in a LTQ Orbitrap. Note: The asterisk (\*) indicates the precursor ion. Inset figure is a magnified area of the product ion spectrum. Product ion notation based on Wesdemiotis *et al.*<sup>112</sup> (see also Table 8.1).

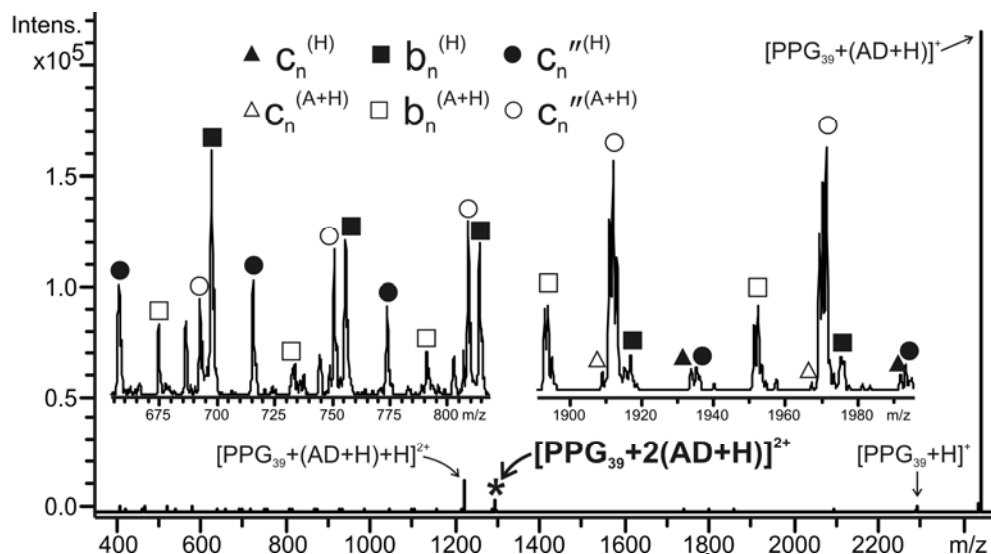


**Figure 8.10.** Product ion mass spectrum of  $[\text{PPG}_{39}+2(\text{AD}+\text{H})]^{2+}$  obtained in a QIT mass spectrometer. Note: The asterisk (\*) indicates the precursor ion. Inset figures are magnified areas of the product ion spectrum. Product ion notation based on Wesdemiotis *et al.*<sup>112</sup> (see also Table 8.1).

The activation of  $[\text{PTMEG}_{25}+(\text{AD}+\text{H})]^{+}$  in the LIT (Figure 8.11) resulted in a product ion spectrum with main ions generated by combined neutral loss of the amine and

fragmentation, forming  $d_n^{(H)}$  and  $e_n^{r(H)}$  type product ions (see also Table 8.1 for structures of the product ions). The same fragmentation behavior was observed in the QIT (Figure 8.12).

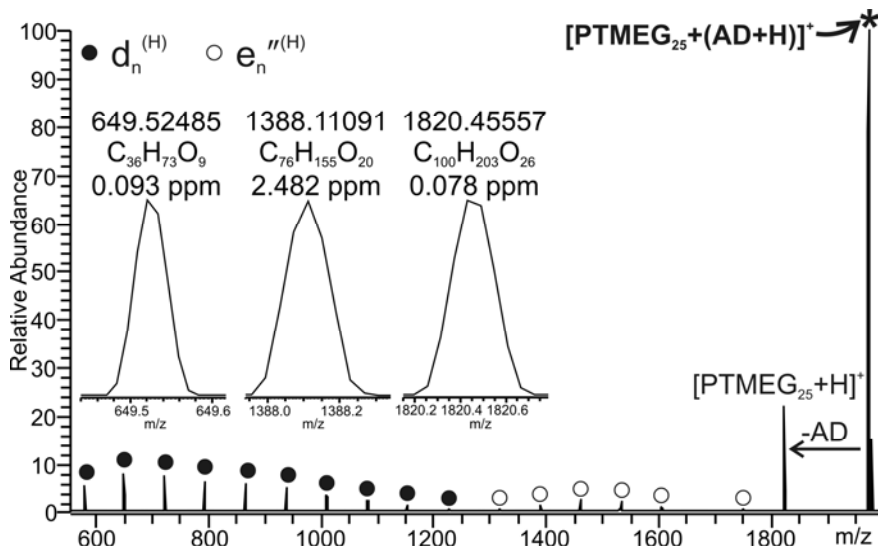


**Figure 8.11.** Product ion mass spectrum of  $[PTMEG_{25}+(AD+H)]^+$  obtained in a LTQ Orbitrap mass spectrometer. Note: The asterisk (\*) indicates the precursor ion. Product ion notation based on Wesdemiotis *et al.*<sup>112</sup> (see also Table 8.1). Inset figures are magnified profile spectra of representative product ions ( $d_n^{(H)}$ ,  $e_n^{r(H)}$ , and of  $[PTMEG_{25}+H]^+$  product ions) with information about their measured  $m/z$ , proposed elemental composition and mass error.

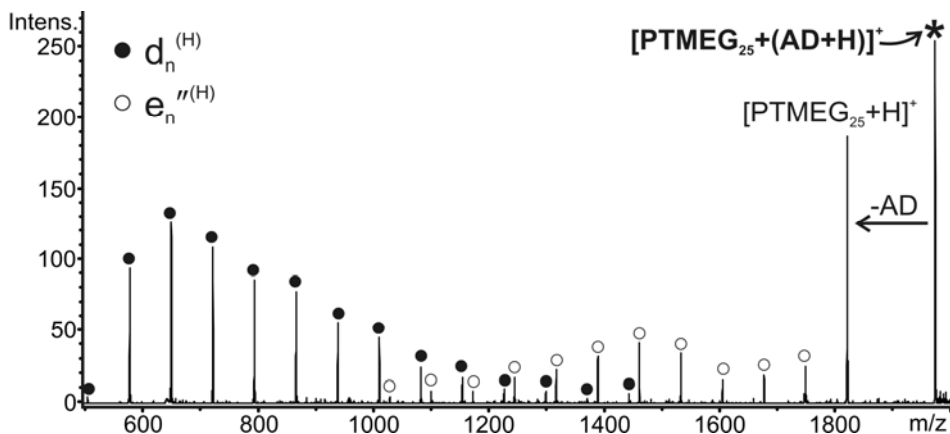


**Figure 8.12.** Product ion mass spectrum of  $[PTMEG_{25}+(AD+H)]^+$  obtained in a QIT mass spectrometer. Note: The asterisk (\*) indicates the precursor ion. Product ion notation based on Wesdemiotis *et al.*<sup>112</sup> (see also Table 8.1).

CID of  $[\text{PTMEG}_{29}+2(\text{ADAMA}+\text{H})]^{2+}$  (Figures 8.13 [QIT] and 8.14 [LIT]) resulted in a product ion mass spectrum comparable to the singly charged PTMEG-ammonium non-covalent complex ion with only difference the presence of product ions retaining the ammonium ion (*i.e.*,  $e_n^{(A+H)}$ ). These experiments show that the presence of  $x_n^{(A+H)}$  type of product ions is related to the cation's structure and its binding energy and not to the polyether structure.

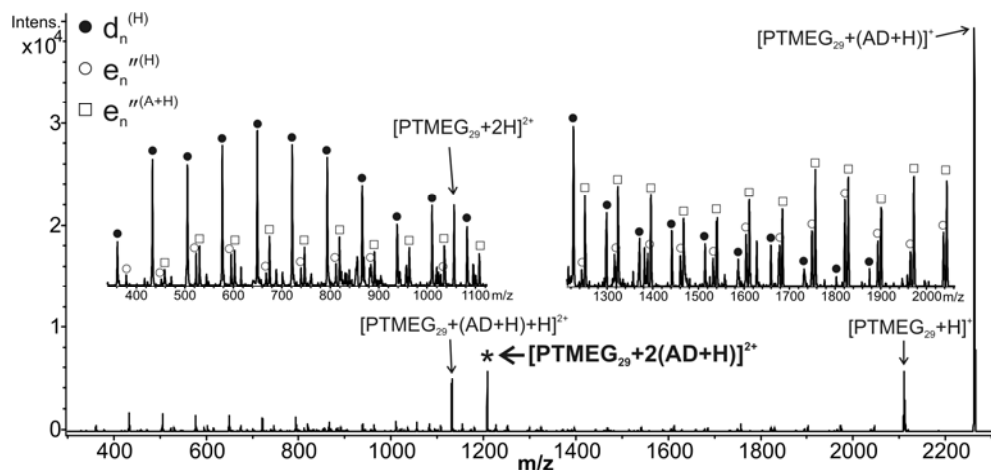


**Figure 8.13.** Product ion mass spectrum of  $[\text{PTMEG}_{29}+2(\text{AD}+\text{H})]^{2+}$  obtained in a QIT mass spectrometer. Note: The asterisk (\*) indicates the precursor ion. Product ion notation based on Wesdemiotis *et al.*<sup>112</sup> (see also Table 8.1).

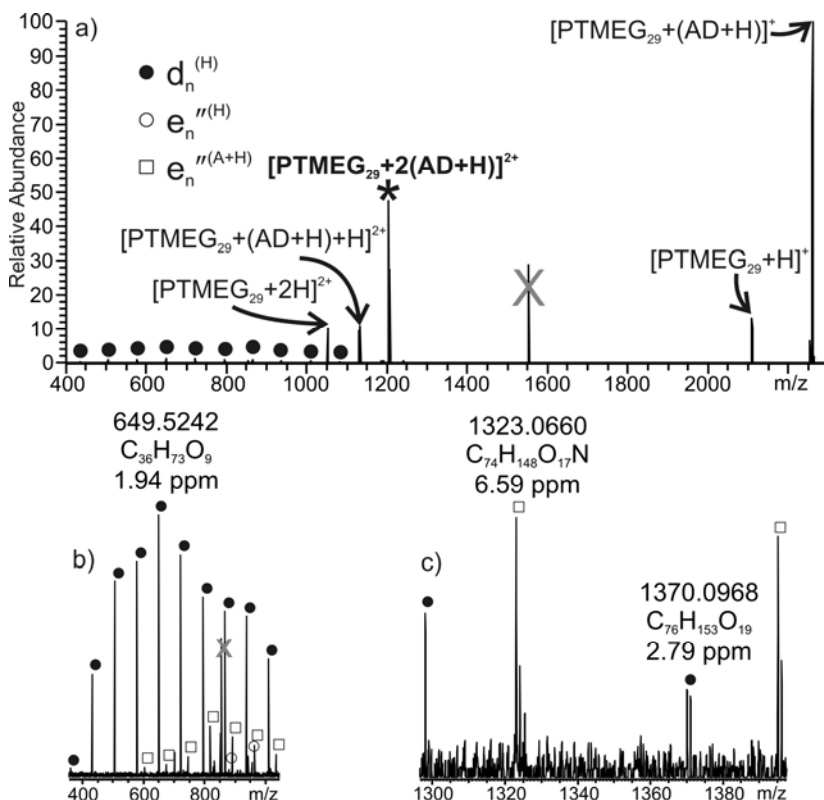


**Figure 8.14.** a) Product ion mass spectrum of  $[\text{PTMEG}_{29}+2(\text{AD}+\text{H})]^{2+}$  obtained in a LTQ Orbitrap, b) and c) magnified areas of the product ion mass spectrum of  $[\text{PTMEG}_{29}+2(\text{AD}+\text{H})]^{2+}$ . Note: The asterisk (\*) indicates the precursor ion. Product ion notation based on Wesdemiotis *et al.*<sup>112</sup> (see also Table 8.1). Peaks indicated with a grey “X” are electronic noise.

### 8.3.3 Energy-dependent analysis of singly charged non-covalent complex ions

To test the hypothesis that the structure of the cation influences the binding energy, and consequently the detection of product ions retaining the cation, the stability of the non-covalent complex ions in CID was investigated. Figure 8.15 depicts the survival yield (SY) of the precursor adduct ions as a function of the collision energy (expressed as collision voltage, instrument setting). The SY is the ratio of the intensity of the precursor ion to the sum of the intensities of the precursor and product ions at a given collision energy (Equation 4.1, Chapter 4). Comparison of the curves is done using the characteristic point of 50% survival yield. The rationale for use of this reference point is described in previous

work<sup>34</sup> and in Chapter 4. The ranking based on this point is:  $(AD+H)^+$  (40.1 V) >  $C_{16}Me_2NH^+$  (35.7 V) >  $C_{16}Me_3N^+$  (21.8 V) >  $C_{16}Py^+$  (18.5 V) >  $Bu_3NH^+$  (16.4 V). The curves show that the non-covalent complex ions of PEG with Quats and tertiary amines with bulky substituents need less energy to fragment than the non-covalent complex ion with primary amines and short-substituent tertiary amines. This ranking indicates a trend that confirms with the above-mentioned hypothesis.

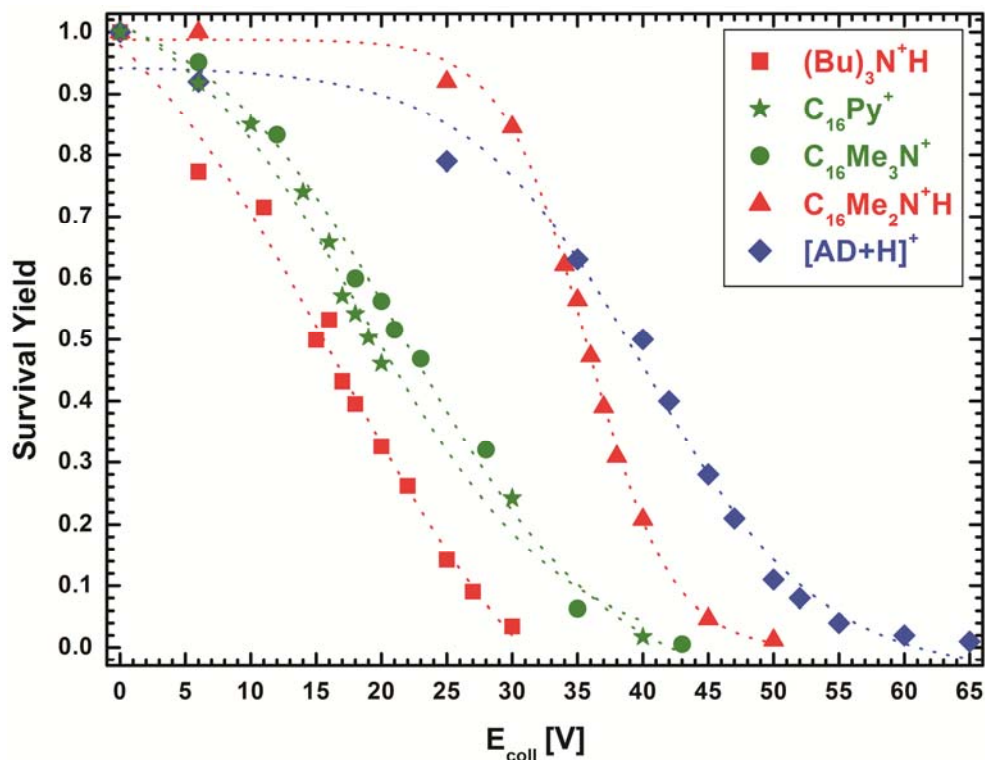


**Figure 8.15.** SY vs collision energy ( $E_{coll}$ ) (expressed as collision voltage, instrument setting) of non-covalent complexes of PEG<sub>41</sub> with different ammonium ions. Note: SY was calculated as the ratio of the precursor ion peak intensity to the sum of peak intensities of the precursor and all product ions (see equation 4.1, Chapter 4).

It is noteworthy that the SY curve of the PEG-[AD+H]<sup>+</sup> non-covalent complex ion has a different shape compared to the rest of the SY curves. Two major (almost contradictory) characteristics can be observed: 1) the curve shows a drop in SY already at minimal

collision energies, and 2) the width of the sigmoidal curve is the largest among the SY curves generated. The first observation hints that the stability of the non-covalent complex ion is low since product ions are generated even at low collision energies. On the other hand, the second observation contradicts the first one, since at increasing collision energies the SY drops slower than that of the other ions. This behavior suggests that the PEG-[AD+H]<sup>+</sup> non-covalent complex ion has multiple fragmentation pathways activated in different collision energies. When a new fragmentation channel opens, the additional collision energy will dissipate into multiple channels instead of one. This results in deviation of the normal sigmoidal function. To provide a confirmation of this hypothesis additional experiments with other primary amines are necessary as well as theoretical calculations.

## 8.4 Conclusions

Non-covalent complex ions of PEGs with structurally different ammonium ions can be formed by ESI and activated at both low energy (*e.g.*, QIT and LIT) and relatively high energy (*e.g.*, *q*-TOF) collision regimes. The amount and quality of the information obtained from the product ion mass spectra is strongly influenced by the structure of the ammonium ion. Quaternary and tertiary ammonium ions with bulky substituents do not have enough binding energy to prevent their expulsion during excitation. Hence, in those cases only cation detachment is observed. With tertiary and primary ammonium ions that contain only one long chain substituent, however, product ions from charge-catalyzed reactions and homolytic bond cleavages are observed. These include product ions that retain the tertiary and primary ammonium and protonated product ions. This behavior is not limited to PEG, as similar results were obtained on PPG and PTMEG. The results show that these non-covalent complex ions can be used as a source of structural information of synthetic polymers. The fragmentation of these relatively low mass non-covalent complex ions allowed the assignment of the major product ions. The creation of such a “product ion library”, in combination with the ability of the ammonium ions to form low charge state adduct ions, could facilitate the structural elucidation of high molar mass polyethers by ESI-MS/MS.

# References

1. Staudinger, H. *Ber. Deut. Chem. Ges.* **1920**, *53*, 1073-1085.
2. Yamashita, M.; Fenn, J. B. *J. Phys. Chem.* **1984**, *88*, 4451-4459.
3. Yamashita, M.; Fenn, J. B. *J. Phys. Chem.* **1984**, *88*, 4671-4675.
4. Whitehouse, C. M.; Robert, R. N.; Yamashita, M.; Fenn, J. B. *Anal. Chem.* **1985**, *57*, 675-679.
5. Fenn, J. B.; Mann, M.; Meng, C. K.; Wong, S. F.; Whitehouse, C. M. *Science* **1989**, *246*, 64-71.
6. Tanaka, K.; Waki, H.; Ido, Y.; Akita, S.; Yoshida, Y.; Yoshida, T.; Matsuo, T. *Rapid Commun. Mass Spectrom.* **1988**, *2*, 151-153.
7. Karas, M.; Hillenkamp, F. *Anal. Chem.* **1988**, *60*, 2299-2301.
8. Karas, M.; Bahr, U.; Ingendoh, A.; Hillenkamp, F. *Angew. Chem.* **1989**, *101*, 805-806.
9. Bahr, U.; Deppe, A. Karas, M.; Hillenkamp, F.; Giessmann, U. *Anal. Chem.* **1992**, *64*, 2866-2869.
10. Montaudou, G.; Montaudou, M. S.; Puglisi, C.; Samperi, F. *Rapid Commun. Mass Spectrom.* **1995**, *9*, 453-460.
11. Montaudou, G.; Montaudou, M. S.; Puglisi, C.; Samperi, F. *Rapid Commun. Mass Spectrom.* **1995**, *9*, 1158-1163.
12. Nielen, M. W. F.; Malucha, S. *Rapid Commun. Mass Spectrom.* **1997**, *11*, 1194-1204.
13. Wong, S. F.; Meng, C. K.; Fenn, J. B. *J. Phys. Chem.* **1988**, *92*, 546-550.
14. Nohmi, T.; Fenn, J. B. *J. Am. Chem. Soc.* **1992**, *114*, 3241-3246.
15. Flory, P. J. *Principles of polymer chemistry*; 1<sup>st</sup> ed; Cornell University Press: Ithaca, 1953.
16. Tomer, K. B. *Chem. Rev.* **2001**, *101*, 297-328.
17. Murgasova, R.; Hercules, D. M. *Anal. Bioanal. Chem.* **2002**, *373*, 481-489.
18. Kassis, C. E.; DeSimone, J. M.; Linton, R. W.; Remsen, E. E.; Lange, G. W.; Friedman, R. M. *Rapid Commun. Mass Spectrom.* **1997**, *11*, 1134-1138.
19. Li, L.; Wang, A. P. L.; Coulson, L. D. *Anal. Chem.* **1993**, *65*, 493-495.
20. Murray, K. K.; Russell, D. H. *Anal. Chem.* **1993**, *65*, 2534-2537.
21. Prokai, L.; Simonsick, W. J. *Rapid Commun. Mass Spectrom.* **1993**, *7*, 853-856.

22. de Koster, C. G.; Duursma, M. C.; van Rooij, G. J.; Heeren, R. M. A.; Boon, J. J. *Rapid Commun. Mass Spectrom.* **1995**, *9*, 957-962.
23. van Rooij, G. J.; Duursma, M. C.; Heeren, R. M. A.; Boon, J. J.; de Koster, C. G. *J. Am. Soc. Mass Spectrom.* **1996**, *7*, 449-457.
24. Selby, T. L.; Wesdemiotis, C.; Lattimer, R. P. *J. Am. Soc. Mass Spectrom.* **1994**, *5*, 1081-1092.
25. Jackson, A. T.; Yates, H. T.; Scrivens, J. H.; Critchley, G.; Brown, J.; Green, M. R.; Bateman, R. H. *Rapid Commun. Mass Spectrom.* **1996**, *10*, 1668-1674.
26. Jackson, A. T.; Yates, H. T.; Scrivens, J. H.; Green, M. R.; Bateman, R. H. *J. Am. Soc. Mass Spectrom.* **1998**, *9*, 269-274.
27. Montaudo, M. S.; Montaudo, G. *Macromolecules* **1992**, *25*, 4264-4280.
28. Montaudo, M. S.; Puglisi, C.; Samperi, F.; Montaudo, G. *Macromolecules* **1998**, *31*, 8666-8676.
29. Jiang, X.; van der Horst, A.; Lima, V.; Schoenmakers, P. J. *J. Chrom. A* **2005**, *1076*, 51-61.
30. Herbert, C. G.; Johnstone, R. A. W. *Mass Spectrometry Basics*; CRC Press: Boca Raton, FL, 2003.
31. De Hoffmann, E.; Stroobant, V. *Mass Spectrometry: Principles and Applications*; John Wiley & Sons: West Sussex, England, 2007.
32. Gross, J. H. *Mass Spectrometry: A Textbook*; Springer-Verlag: Berlin, Germany, 2004.
33. Nielen, M. W. F. *Mass Spectrom. Rev.* **1999**, *18*, 309-344.
34. Karas, M.; Bahr, U.; Fournier, I.; Glückmann, M.; Pfenninger, A. *Int. J. Mass Spectrom.* **2003**, *226*, 239-248.
35. Cotter, R. J. *Anal. Chim. Acta* **1987**, *195*, 45-59.
36. Zeleny, J. *Phys. Rev.* **1917**, *10*, 1-7.
37. Dole, M.; Mack, L.L.; Hines, R. L.; Mobley, R. C.; Ferguson, L. D.; Alice, M. B. *J. Chem. Phys.* **1968**, *49*, 2240-2249.
38. Dole, M.; Hines, R. L.; Mack, L.L.; Mobley, R. C.; Ferguson, L. D.; Alice, M. B. *Macromolecules* **1968**, *1*, 96-97.

39. Taylor, G.I. *Proc. Royal Soc. London A* **1964**, *280*, 383-397.
40. Iribarne, J. V.; Thomson, B. A. *J. Chem. Phys.* **1976**, *64*, 2287-2294.
41. Thomson, B. A.; Iribarne, J. V. *J. Chem. Phys.* **1979**, *71*, 4451-4463.
42. Rayleigh, L. *Philos Mag.* **1882**, *5*, 184-186.
43. McLuckey, S. A.; Huang, T. Y. *Anal. Chem.* **2009**, *81*, 8669-8676.
44. Stephenson, J. L. J.; McLuckey, S. A. *J. Am. Soc. Mass Spectrom.* **1998**, *9*, 957-965.
45. McLuckey, S. A.; Goeringer, D. E. *Anal. Chem.* **1995**, *67*, 2493-2497.
46. Stephenson, J. L. J.; McLuckey, S. A. *J. Am. Chem. Soc.* **1996**, *118*, 7390-7397.
47. Cheng, X.; Gale, D. C.; Udseth, H. R.; Smith, R. D. *Anal. Chem.* **1995**, *67*, 586-593.
48. Ebeling, D. D.; Westphall, M. S.; Scalf, M.; Smith, L. M. *Anal. Chem.* **2000**, *72*, 5158-5161.
49. Mirza, U. A.; Chalt, B. T. *Anal. Chem.* **1994**, *66*, 2898-2904.
50. Scalf, M.; Westphall, M. S.; Smith, L. M. *Anal. Chem.* **2000**, *72*, 52-60.
51. Lennon, J. D. I.; Cole, S. P.; Glish, G. L. *Anal. Chem.* **2006**, *78*, 8472-8476.
52. Bagal, D.; Zhang, H.; Schnier, P. D. *Anal. Chem.* **2008**, *80*, 2408-2418.
53. Chakraborty, A. B.; Chen, W.; Gebler, J. C. *Pharmaceutical Technology* [Online] **2008**, 80-87.
54. Muddiman, D. C.; Cheng, X.; Udseth, H. R.; Smith, R. D. *J. Am. Soc. Mass Spectrom.* **1996**, *7*, 697-706.
55. Huang, L.; Gough, P. C.; DeFelippis, M. R. *Anal. Chem.* **2009**, *81*, 567-577.
56. Iavarone, A. T.; Williams, E. R. *Int. J. Mass Spectrom.* **2002**, *219*, 63-72.
57. Iavarone, A. T.; Williams, E. R. *J. Am. Chem. Soc.* **2003**, *125*, 2319-2327.
58. Kebarle, P.; Verkerk, U. H. *Mass Spectrom. Rev.* **2009**, *28*, 898-917.
59. Covey, T. R.; Thomson, B. A.; Schneider, B. B. *Mass Spectrom. Rev.* **2009**, *28*, 870-897.
60. Hayen, H.; Karst, U. *J. Chromatogr. A* **2003**, *1000*, 549-565.
61. Robb, D. B.; Covey, T. R.; Bruins, A. P. *Anal. Chem.* **2000**, *72*, 3653-3659.
62. Raffaeli, A.; Saba, A. *Mass Spectrom. Rev.* **2003**, *22*, 318-331.
63. Stephens, W. E. *Phys. Rev.* **1946**, *69*, 691.
64. Mamyrin, B. A. *Int. J. Mass Spectrom. Ion Proc.* **1994**, *131*, 1-19.

65. Cotter, R. J. *Anal. Chem.* **1992**, *64*, 1027A-1039A.
66. *UHR-TOF: A revolution in Time-of-Flight Technology*; Technical Note TN-29: Bremen, Germany, 2008.
67. Waters Corporation *LCT Premier: Enhanced MS Resolution*; Technical Note APNT1545286: Milford, MA, 2004.
68. March, R. E. *Mass Spectrom. Rev.* **2009**, *28*, 961-989.
69. Paul, W. *Angew. Chem.* **1990**, *102*, 780-789.
70. Paul, W.; Steinwedel, H. *Naturforsch.* **1953**, *8A*, 448-450.
71. Douglas, D. J.; Frank, A. J.; Mao, D. *Mass Spectrom. Rev.* **2005**, *24*, 1-29.
72. Glish, G. L.; McLuckey, S. A.; Ridley, T. Y.; Cooks, R. G. *Int. J. Mass Spectrom. Ion Phys.* **1981**, *39*, 219-230.
73. Bradley, C. D.; Curtis, J. M.; Derrick, P. J.; Wright, B. *Anal. Chem.* **1992**, *64*, 2628-2635.
74. Schoen, A. E.; Amy, J. W.; Ciupek, J. D.; Cooks, R. G.; Dobberstein, P.; Jung, G. *Int. J. Mass Spectrom. Ion Proc.* **1985**, *65*, 125-140.
75. Aicher, K. P.; Müller, M.; Wilhelm, U.; Grottemeyer, J. *Eur. Mass Spectrom.* **1995**, *1*, 331-340.
76. Makarov, A. *Anal. Chem.* **2000**, *72*, 1156-1162.
77. Kingdon, K. H. *Phys. Rev.* **1923**, *21*, 408-418.
78. Perry, R. H.; Cooks, R. G.; Noll, R. J. *Mass Spectrom. Rev.* **2008**, *27*, 661-699.
79. Lawrence, E. O.; Livingston, M. S. *Phys. Rev.* **1932**, *40*, 19-35.
80. Sommer, H. Thomas, H. A.; Hipple, J. A. *Phys. Rev.* **1951**, *82*, 697-702.
81. Comisarow, M. B.; Marshall, A. G. *Chem. Phys. Lett.* **1974**, *25*, 282-283.
82. Comisarow, M. B.; Marshall, A. G. *Chem. Phys. Lett.* **1974**, *26*, 489-490.
83. Comisarow, M. B.; Marshall, A. G. *J. Mass Spectrom.* **1996**, *31*, 581-585.
84. He, F.; Hendrickson, C. L.; Marshall, A. G. *Anal. Chem.* **2001**, *73*, 647-650.
85. Hughey, C. A.; Rodgers, R. P.; Marshall, A. G. *Anal. Chem.* **2002**, *74*, 4145-4149.
86. Shi, S. D. H.; Drader, J. J.; Hendrickson, C. L.; Marshall, A. G. *J. Am. Soc. Mass Spectrom.* **1999**, *10*, 265-268.

87. Van Rooij G. J.; Duursma M. C.; de Koster C. G.; Heeren, R. M. A.; Boon J. J.; Wijnand-Schuyl, P. J.; van der Hage, E. R. E. *Anal. Chem.* **1998**, *70*, 843-850.
88. Bottrill, A.R., Giannakopoulos, A. E.; Waterson, C.; Haddleton, D. M.; Lee, K. S.; Derrick, P. J. *Anal. Chem.* **1999**, *71*, 3637-3641.
89. Jackson, A. T.; Green, M. R.; Bateman, R. H. *Rapid Commun. Mass Spectrom.* **2006**, *20*, 3542-3550.
90. Jandera, P.; Holčapek, M.; Theodoridis, G. *J. Chromatogr. A* **1998**, *813*, 299-311.
91. Keil, C.; Esser, E.; Pasch, H. *Mater. Eng.* **2001**, *286*, 161-167.
92. Levine, L. H.; Garland, J. L.; Johnson, J. V. *Anal. Chem.* **2002**, *74*, 2064-2071.
93. Nasioudis, A.; van Velde, J. W.; Heeren, R. M. A.; van den Brink, O. F. *LC-MS<sup>n</sup> determination of non-ionic surfactants. Structure analysis of poly (oxyethylene-co oxypropylene) fatty ethers and poly(oxyethylene) fatty esters*. Proceedings of the 56th ASMS Conference on Mass Spectrometry and Allied Topics, Denver, CO, June 1 – June 5, 2008.
94. Jackson, A. T.; Yates, H. T.; Scrivens, J. H.; Critchley, G.; Brown, J.; Green, M. R.; Bateman, R. H. *Rapid Commun. Mass Spectrom.* 1996, *11*, 1668-1674.
95. O' Connor. P. B.; McLafferty, F. W. *J. Am. Chem. Soc.* **1995**, *117*, 12826-12831.
96. Cerda, B. A.; Horn, D. M.; Breuker, K.; McLafferty, F. W. *J. Am. Chem. Soc.* **2002**, *124*, 9287-9291.
97. Terrier, P.; Buchmann, W.; Cheguillaume, G.; Desmazieres, B.; Tortajada, J. *Anal. Chem.* **2005**, *77*, 3292-3300.
98. Lattimer, R.P. *J. Am. Soc. Mass Spectrom.* **1992**, *3*, 225-234.
99. Selby, T.L.; Wesdemiotis, C.; Lattimer, R. P. *J. Am. Soc. Mass Spectrom.* **1994**, *5*, 1081-1092.
100. Ayorinde, F. O.; Gelain, S. V.; Johnson, J. H. Jr.; Wan, L. W. *Rapid Commun. Mass Spectrom.* **2000**, *14*, 2116-2124.
101. Chen, R.; Li, L. *J. Am. Soc. Mass Spectrom.* **2001**, *12*, 832-839.
102. Chen, R.; Yu, X.; Li, L. *J. Am. Soc. Mass Spectrom.* **2002**, *13*, 888-897.
103. Raith, K.; Schmelzer, C. E. H.; Neubert, R. H. H. *Int. J. Pharm.* **2006**, *319*, 1-12.

104. Hilton, G. R.; Jackson, A. T.; Thalassinou, K.; Scrivens, J. H. *Anal. Chem.* **2008**, *80*, 9720-9725.
105. Borisov, R. S.; Polovkov, N. Yu.; Zaikin, V. G. *Rapid Commun. Mass Spectrom.* **2009**, *23*, 3309-3312.
106. Zu, C.; Praay, H. N.; Bell, B. M.; Redwine, O. D. *Rapid Commun. Mass Spectrom.* **2010**, *24*, 120-128.
107. Meyer, T.; Kunkel, M.; Frahm, A. W.; Waidelich, D. *J. Am. Soc. Mass Spectrom.* **2001**, *12*, 911-925.
108. Meyer, T.; Waidelich, D.; Frahm, A. W. *Electrophoresis* **2002**, *23*, 1053-1062.
109. Meyer, T.; Waidelich, D.; Frahm, A. W. *J. Pharm. Biomed. Anal.* **2002**, *30*, 263-271.
110. Kunkel, M.; Böhler, J.; Keller, E.; Frahm, A. W. *Pharmazie* **1997**, *52*, 109-121.
111. Müller, K. *Tenside* **1966**, *2*, 37-45.
112. Wesdemiotis, C.; Solak, N.; Polce, M. J.; Dabney, D. E.; Chaicharoen, K.; Katzenmeyer, B. C. *Mass Spectrom. Rev.* **2010**; in press.
113. Cheng, C.; Gross, M. L.; Pittenauer, E. *Anal. Chem.* **1998**, *70*, 4417-4426.
114. O' Lenick, A. J. Jr; Parkinson, J. K. *J. Soc. Cosmet. Chem.* **1993**, *44*, 319-328.
115. Fenn, J. B.; Mann, M.; Weng, C. K.; Wong, S. F.; Whitehouse C. M. *Mass Spectrom. Rev.* **1990**, *9*, 37-70.
116. Hillenkamp, F.; Karas, M.; Beavis, R. C.; Chait, B. T. *Anal. Chem.* **1991**, *63*, 1193A-1203A.
117. Nielen, M. W. F.; Buijtenhuijs, F. A. *Anal. Chem.* **1999**, *71*, 1809-1814.
118. Polce, M. J.; Wesdemiotis, C. Tandem Mass Spectrometry and Polymer Ion Dissociation. In *MALDI Mass Spectrometry for Synthetic Polymer Analysis*; Li, L.. Ed.; Chemical Analysis, Vol 175; Wiley: Hoboken, NJ, 2010; pp 85-127.
119. Jedliński, Z.; Adamus, G.; Kowalczyk, M.; Schubert, R.; Szewczyk, Z.; Stefanowicz, P. *Rapid Commun. Mass Spectrom.* **1998**, *12*, 357-360.
120. Arslan, H.; Adamus, G.; Hazer, B.; Kowalczyk, M. *Rapid Commun. Mass Spectrom.* **1999**, *13*, 2433-2438.
121. Osaka, I.; Watanabe, M.; Takama, M.; Murakami, M.; Arakawa, R. *J. Mass Spectrom.* **2006**, *41*, 1369-1377.

122. Rizzarelli, P.; Puglisi, C.; Montaudo, G. *Rapid Commun. Mass Spectrom.* **2006**, *20*, 1683-1694.
123. Domon, B.; Costello, C. E. *Glycoconjugate J.*, **1988**, *5*, 397-409.
124. Thibault, P.; Alexander, A. J.; Boyd, R. K.; Tomer, K. B. *J. Am. Soc. Mass Spectrom.* **1993**, *4*, 845-854.
125. Vékey, K.; Somogyi, Á.; Wysocki, V. H. *Rapid Commun. Mass Spectrom.* **1996**, *10*, 911-918.
126. Heeren, R. M. A.; Vékey, K. *Rapid Commun. Mass Spectrom.* **1998**, *12*, 1175-1181.
127. Goeringer, D. E.; Asano, K. G.; McLuckey, S. A. *Int. J. Mass Spectrom.* **1999**, *183*, 275-288.
128. Gabelica, V.; Karas, M.; de Pauw, E. *Anal Chem.* **2003**, *75*, 5152-5159.
129. Louris, J. N.; Cooks, R. G.; Syka, J. E. P.; Kelley, P. E.; Stafford, G. C. Jr; Todd, J. F. *J. Anal Chem.* **1987**, *59*, 1677-1685.
130. McLuckey, S. A.; Goeringer, D. E.; Glish, G. L. *Anal. Chem.* **1992**, *64*, 1455-1460.
131. Lopez, L. L.; Tiller, P. R.; Senko, M. W.; Schwartz, J. C. *Rapid Commun. Mass Spectrom.* **1999**, *13*, 663-668.
132. Herrmann, K. A.; Somogyi, Á.; Wysocki, V. H.; Drahos, L.; Vekey, K. *Anal. Chem.* **2005**, *77*, 7626-7638.
133. Memboeuf, A.; Nasioudis, A.; Indelicato, S.; Pollreis, F.; Kuki, A.; Kéki, S.; van den Brink, O. F.; Vékey, K.; Drahos, L. *Anal Chem.* **2010**, *82*, 2294-2302.
134. Winkler, F. J.; Golacar, F. O.; Mermoud, F.; Stahl, D.; Gäumann, T.; Buchs, A. *Int. J. Mass Spectrom. Ion Phys.* **1983**, *46*, 321-324.
135. Dongre, A. R.; Jones, J. L.; Somogyi, A.; Wysocki, V. H. *J. Am. Chem. Soc.* **1996**, *118*, 8365-8374.
136. Gabelica, V.; de Pauw, E. *Mass Spectrom. Rev.* **2005**, *24*, 566-587.
137. Heeren, R. M. A.; Vékey, K. *Rapid Commun. Mass Spectrom.* **1998**, *12*, 1175-1181.
138. Danell, R. M.; Danell, A. S.; Glish, G. L.; Vachet, R. W. *J. Am. Soc. Mass Spectrom.* **2003**, *14*, 1099-1109.
139. Williams, J. D.; Cox, K. A.; Cooks, R. G.; McLuckey, S. A.; Hart, K. J.; Goeringer, D. E. *Anal. Chem.* **1994**, *66*, 725-729.

140. Ude, S.; de la Mora, F.; Thomson, B. A.; *J. Am. Soc. Mass Spectrom.* **2004**, *126*, 12184-12190.
141. Kuki, Á.; Nagy, L.; Memboeuf, A.; Drahos, L.; Vékey, K.; Zsuga, M.; Kéki, S. *J. Am. Soc. Mass Spectrom.* **2010**, *21*, 1753-1761.
142. Kertesz, T. M.; Hall, L. H.; Hill, D. W.; Grant, D. F. *J. Am. Soc. Mass Spectrom.* **2009**, *20*, 1759-1767.
143. Dechy-Cabaret, O.; Martin-Vaca, B.; Bourissou, D. *Chem. Rev.* **2004**, *104*, 6147-6176.
144. Wyttenbach, T.; von Helden, G.; Bowers, M. T. *Int. J. Mass Spectrom. Ion Process.* **1997**, *165-166*, 377-390.
145. Gidden, J.; Wyttenbach, T.; Jackson, A. T.; Scrivens, J. H.; Bowers, M. T. *J. Am. Chem. Soc.* **2000**, *122*, 4692-4699.
146. Schriemer, D. C.; Li, L. *Anal. Chem.* **1996**, *68*, 2721-2725.
147. Maziarz, P. E. I.; Baker, G. A.; Wood, T. D. *Macromolecules* **1999**, *32*, 4411-4418.
148. Trimpin, S.; Plasencia, M.; Isailovic, D.; Clemmer, D. E. *Anal. Chem.* **2007**, *79*, 7965-7974.
149. Trimpin, S.; Clemmer, D. E. *Anal. Chem.* **2008**, *80*, 9073-9083.
150. Nasioudis, A.; Joyce, W. F.; van Velde, J. W.; van den Brink O. F. Charge-state reduction of synthetic polymers by SEC-ESI-MS with postcolumn addition of ionic surfactants. *Proceedings of the 57th ASMS Conference on Mass Spectrometry and Allied Topics*, Philadelphia, PA, May 31 – June 4, 2009.
151. Koenig, J. L. *Physical Properties of Polymers*, 3rd ed.; Cambridge University Press: New York, 2004.
152. Lu, X.; Gough, P. C.; DeFelippis, M. R.; Huang, L. *J. Am. Soc. Mass Spectrom.* **2010**, *21*, 810-818.
153. Lee, H.; Chang, T.; Lee, D.; Shim, M. S.; Ji, H.; Nonidez, W. K.; Mays, J. W. *Anal. Chem.* **2001**, *73*, 1726-1732.
154. Creaser, C. S.; Griffiths, J. R.; Stockton, B. M. *Eur. J. Mass Spectrom.* **2000**, *6*, 213-218.
155. Creaser, C. S.; Griffiths, J. R. *Anal. Chim. Acta* **2001**, *436*, 273-279.

156. Colgrave, M. L.; Bramwell, C. J.; Creaser, C. S. *Int. J. Mass Spectrom.* **2003**, *229*, 209-216.
157. Hilderbrand, A. E.; Myung, S.; Clemmer, D. E. *Anal. Chem.* **2006**, *78*, 6792-6800.
158. Howdle, M. D.; Eckers, C.; Laures, A. M. -F.; Creaser, C. S. *J. Am. Soc. Mass Spectrom.* **2009**, *20*, 1-9.

# **Glossary of Symbols and Abbreviations**

## Abbreviations

ACN	Acetonitrile
APCI	Atmospheric-pressure chemical ionization
API	Atmospheric-pressure ionization
APPI	Atmospheric-pressure photoionization
BPC	Base peak chromatogram
CAD	Collision-activated dissociation
CASEO	Castor oil ethoxylates
CCV	Characteristic collision voltage
CE	Capillary electrophoresis
CID	Collision-induced dissociation
CRM	Charge residue model
Da	Dalton
DC	Direct current
DE	Delayed extraction
DHSTE	Didehydrostearic acid
DI	Direct infusion
DoF	Degrees of freedom
EIC	Extracted ion chromatogram
ESI	Electrospray Ionization
FA	Formic acid
FAE	Fatty acid ethoxylate
FT-ICR MS	Fourier-transform ion cyclotron resonance mass spectrometry
GPC	Gel permeation chromatography
HM	High mass (supplier specific abbreviation)
HPLC	High performance liquid chromatography
ICC	Ion charge control (supplier specific abbreviation)
IEM	Ion evaporation model
IMS-MS	Ion mobility spectrometry mass spectrometry
LC	Liquid chromatography
LA	Lactic acid
Lin	Linoleic acid
LIT	Linear ion trap
LM	Low mass (supplier specific abbreviation)
MALDI	Matrix-assisted laser desorption/ionization
Maltodex	Maltodextrin
MeOH	Methanol
MMD	Molar mass distribution
MS	Mass spectrometry
MS/MS	Tandem mass spectrometry
MS <sup>n</sup>	Multistage mass spectrometry
NCE	Normalized collision energy (supplier specific abbreviation)

NMR	Nuclear magnetic resonance
<i>oaq</i> -TOF	Orthogonal accelerated quadrupole time-of-flight
Ole	Oleic acid
PA	Proton affinity
PBA <sub>d</sub>	Poly(butylene adipate) diol
PEG	Poly(ethylene glycol)
PHB	Poly(3-hydroxybutyric acid)
PLA	Poly(lactic acid)
PMMA	Poly(methyl methacrylate)
ppm	Parts per million
PTMEG	Poly(tetramethylene glycol)
QIT	Quadrupole ion trap
<i>QqQ</i>	Triple quadrupole
<i>q</i> -TOF	Quadrupole time-of-flight
Quat	Quaternary ammonium ion
RF	Radio frequency
RI	Refractive index
Ric	Ricinoleic acid
RPLC	Reverse-phase liquid chromatography
RSD	Relative standard deviation
SD	Standard deviation
SEC	Size exclusion chromatography
Ste	Stearic acid
SY	Survival yield
Th	Thomson
TIC	Total ion count
THF	Tetrahydrofuran
TOF	Time-of-flight

### **Symbols**

$\alpha_z$	Parameter of the Mathieu equation
$\beta_z$	Parameter of the Mathieu equation
$\Delta$	mass error
$\omega$	Angular velocity
$D$	Dispersity
$e$	Elementary charge
$E_{el}$	Potential energy
$E_{kin}$	Kinetic energy
$I_F$	Intensity of product ion
$I_{i,z}$	Intensity of distribution $I$ with charge state $z$
$I_M$	Intensity of precursor ion
$m/z$	Mass-to-charge ratio
$m/z_{exc}$	Excitation mass

$m/z_{isol}$	Isolation mass
$m_{cat/an}$	Mass of the cation/anion
$m_e$	Mass of the electron
$m_{end}$	Mass of the endgroup
$m_{meas}$	Accurate measured mass
$m_{mon}$	Mass of the monomer unit
$m_{Th}$	Theoretical (exact) mass
$\bar{M}_n$	Number average molecular weight
$\bar{M}_w$	Weight average molecular weight
$\bar{M}_v$	Viscosity average molecular weight
$\bar{M}_z$	z-average molecular weight
$n$	Degree of polymerization
$q_z$	Parameter of the Mathieu equation
$R^2$	Coefficient of determination
$r_0$	r-stable
$S$	Distance
$t_f$	Flight time
$U$	Direct potential
$V$	“zero-to-peak” voltage
$\bar{z}$	Average charge state
$z_0$	z-stable

# Summary

Synthetic polymers are the products of humans' attempts to imitate nature's gigantic molecular chain architectures. The extended variety of building blocks and reaction mechanisms resulted in a plethora of different polymeric architectures and products that can satisfy most of the human (*e.g.*, industrial, consumer, pharmaceutical, etc) needs. The biggest challenge for polymer chemists is to develop the next generation of polymer systems that can outperform the current state-of-the-art products, and at the same time, address the environmental concerns and raw material depletion. A prerequisite of success with this challenge is to develop an understanding of the relation between the chemical structure of the polymer and its physicochemical and mechanical properties. This can be achieved by using a combination of various analytical techniques, because most of them can only provide part of the information on the size and micro/macrostructure of the synthetic polymer. Among these, mass spectrometry (MS) maintains a special position because it provides information on individual molecules instead of averages of the whole polymer distribution. MS is a very sensitive technique that can provide detailed information about the elemental composition, monomer unit and end-group structure of polymeric systems. However, MS also has its limitations. The analysis of high molar mass and/or disperse and/or structurally complicated synthetic polymers remains a big challenge. Some solutions have been presented such as hyphenation with separation techniques (*e.g.*, liquid chromatography, capillary electrophoresis, etc) and tandem mass spectrometry (MS/MS) that address (to some extent) some of the abovementioned challenges. To provide new solutions that complement the existing ones and can meet more effectively this big challenge, answers to some specific questions need to be given. These are:

- 1) Can the electrospray ionization (ESI) process be modified so that the mass limits in the analysis of high molar mass synthetic polymers can be extended?
- 2) Can MS/MS be used as a selective tool in the analysis of synthetic polymers?
- 3) What is the level of information that can be obtained by combining separation techniques with multistage mass spectrometry (MS<sup>n</sup>)?

**Chapter 2** gives a general introduction to polymer analysis and MS. The analysis of synthetic polymers is not an easy task because these are mixtures of molecules of different sizes as a result of the polymerization process. To fully characterize a synthetic polymer

means to determine the size, structure, functionality, sequence, and architecture of each of the components of the whole distribution. MS can provide detailed information about many of these parameters when soft ionization techniques, such as ESI and matrix-assisted laser desorption/ionization are used. These techniques transfer adduct ions of intact large molecules into the gas phase. Since both techniques favor the ionization of polar compounds, other ionization techniques have been developed for the analysis of less polar and apolar molecules, such as atmospheric-pressure chemical ionization (APCI) and atmospheric-pressure photoionization (APPI). Besides the contribution of the ionization step in the successful analysis of synthetic polymers, mass analyzers remain the key contributors. Various concepts have been developed based on different principles of ion physics. In this chapter, the description of various mass spectrometers, such as quadrupole/linear ion traps (QIT/LIT), orthogonal accelerated quadrupole TOF, Fourier-transform ion cyclotron resonance, and Orbitrap is presented.

Besides the introduction, **Chapter 2** presents some examples of current practical state-of-the-art MS, and liquid chromatography (LC) coupled to MS, methods for the analysis of synthetic polymers. Comparing the amount of information obtained by MS and LC-MS, it is shown that for complicated mixtures of polymers and copolymers the use of hyphenated techniques becomes a necessity. The chromatographic separation allows the distinction between nominally isobaric compounds, reduces ion suppression effects, and thus provides a more accurate representation of the sample's composition.

**Chapter 3** provides an example of the current performance of LC coupled to MS<sup>n</sup> in the analysis of more structurally complicated polymeric systems, such as vegetable oil ethoxylates. After optimization of the LC conditions, a high separation selectivity of closely related polymer structures (33 different polymer distributions, with some being nominally isobaric and/or isomeric structures) is achieved. Complementary information is obtained when the ESI-MS analysis is performed in positive and negative ion mode as well as with different ionization techniques such as APCI and APPI. The MS<sup>n</sup> analysis with different adducts ions (*i.e.*, sodium, lithium, ammonium and potassium) shows that lithium and ammonium cationized analytes provide the most detailed structural information. High

accuracy MS/MS is used to confirm the structure of characteristic fragment ions that reveal information about the ethoxylation site in the biomolecule.

**Chapter 4** presents the method development to achieve an accurate and reproducible control of the applied excitation energy in a QIT. Various instrumental parameters are investigated and optimized, such as the accumulation time, isolation mass, isolation width, delay period between isolation and excitation, excitation width, excitation mass and excitation time. The method is further checked by studying the required excitation energy for fragmentation of poly(ethylene glycol)s as a function of their size. This dependence is shown to be linear and in agreement with other MS instruments where the applied excitation energy can be controlled in a more accurate way.

In **Chapter 5**, the methodology for accurate and reproducible control of the applied excitation energy is used to discriminate between different polymer classes. It is shown that discrimination is achieved by determining a “characteristic” parameter (*i.e.*, the characteristic collision voltage (CCV)), which is related to the polymer’s structure and expresses the stability of the respective polymer ion upon excitation. This parameter is determined for polymer ions of different sizes and plotted against the respective ion masses. The generated lines follow a linear trend and are different from each other. The differences appear to be related to the type of intermonomer bond, and within one polymer class, the difference between linear and cyclic structure of the polymer and end-group structures of the polymer. The order of these lines indicates the differences in energy requirements for dissociating different polymer classes; Polyethers need more energy than methacrylates, which in turn need more energy than polyesters and polysaccharides. This method is then applied in the analysis of a mixture of a structurally complicated copolymer system (*i.e.*, poly(lactic acid)-*block*-poly(tetramethylene glycol)-*block*-poly(lactic acid)) and its nominally isobaric homopolymers poly(tetramethylene glycol) (PTMEG) and poly(lactic acid) (PLA). When these compounds are in a mixture, they cannot be discriminated by conventional MS and MS<sup>n</sup> methods. The CCV values of the nominally isobaric ions were found to be different between the homopolymers (*i.e.*, PLA, PTMEG) and the copolymers, as well as between copolymers with different monomer composition.

**Chapters 6, 7 and 8** present the study of non-covalent complex ions of high molar mass synthetic polymers and molecules containing ammonium functionalities. These complex ions appear to have a preference for low charge states. **Chapter 6 and 7** present the investigations of the parameters that influence the formation of these low charge state adduct ions. The concentration of the ammonium-containing molecule/ion in the spray solution has a direct impact on the formation of these ions. In addition the structure of the ammonium containing molecule/ion plays a crucial role in the performance of the method in forming low charge state adduct ions, and even the occurrence of the effect. The major structural characteristics are the degree of substitution and the size of the substituents. Ammonium ions that combine high binding energies and steric hindrance to the polymer molecule can coordinate with the higher molar mass synthetic polymers and form low charge state adduct ions. Quaternary ammonium compounds, such as hexadecyl-trimethylammonium chloride and hexadecyl-pyridinium bromide, and tertiary amines, such as triethylamine and tributylamine, have such a kind of structure (*i.e.*, size, specific charge localization, and facile interactions with the polymer) and have the best performance in forming low charge state adduct ions. **Chapter 8** presents the behavior of these non-covalent complex ions upon activation at both low and relatively high collision regimes. The amount and type of fragments ions is strongly influenced by the structure of the ammonium ion. The dissociation of the non-covalent complex ions of synthetic polymers with quaternary and tertiary ammonium ions (with multiple bulky substituents) result in cation detachment of the ammonium ion. On the other hand, tertiary and primary ammonium ions, that contain only one long chain substituent, form non-covalent complex ions that on dissociation display charge-catalyzed reactions and homolytic bond cleavages. The results show that MS/MS of these non-covalent complex ions can be used as a source of polymer structural information.



# Samenvatting

Synthetische polymeren kunnen gezien worden als het product van menselijke pogingen om de indrukwekkende moleculaire structuren die in de natuur voorkomen na te maken. De uitgebreide variëteit aan bouwstenen en reactiemechanismen zorgde ervoor dat een veelheid van verschillende polymere structuren en producten ontwikkeld is die in de meeste van de menselijke behoeften (industriële, van consumenten, farmaceutisch, enz.) kan voorzien. De grootste uitdaging voor polymeerchemici is de volgende generatie van polymeren te ontwikkelen die beter is dan de huidige meest geavanceerde producten en tegelijkertijd rekening te houden met milieuproblematiek en toenemende schaarste van grondstoffen. Een vereiste voor succes bij deze uitdaging is de ontwikkeling van begrip van de relatie tussen de chemische structuur van een polymeer en zijn fysisch-chemische en mechanische eigenschappen. Omdat de meeste analytische technieken slechts een deel van de informatie over grootte en micro-/macrostructuur van de synthetische polymeren verschaffen, moet hiervoor een combinatie van verschillende analytische technieken gebruikt worden. Massaspectrometrie (MS) bevindt zich in dat gezelschap op een bijzondere positie omdat ze informatie verschaft over individuele moleculen in plaats van gemiddelde waarden over de gehele polymeerdistributie. MS is een zeer gevoelige techniek die gedetailleerde informatie over de elementaire samenstelling, monomeereenheden en eindgroepstructuren van polymere systemen kan verschaffen. MS heeft echter ook haar beperkingen. De analyse van synthetische polymeren met een hoge moleculaire massa en/of een hoge dispersiteit en/of een gecompliceerde structuur blijft een grote uitdaging. Er zijn enkele oplossingen aangedragen om deze uitdagingen (gedeeltelijk) aan te pakken, zoals koppeling met scheidingsmethoden (bijvoorbeeld vloeistofchromatografie en capillaire elektroforese) en tandem-massaspectrometrie (MS/MS). Om nieuwe oplossingen te bieden die de bestaande methoden aanvullen en de eerdergenoemde grote uitdaging effectiever aangaan, moet een aantal specifieke vragen beantwoord worden:

- 1) Kan het electrospray-ionisatieproces aangepast worden zodat de massalimiet in de analyse van synthetische polymeren met hoge moleculaire massa verhoogd wordt?
- 2) Kan MS/MS gebruikt worden om selectiviteit in de analyse van synthetische polymeren te bewerkstelligen?

3) Hoeveel informatie kan verkregen worden door scheidingsmethoden te combineren met meervoudige massaspectrometrie ( $MS^n$ )?

**Hoofdstuk 2** is een algemene inleiding tot de polymeeranalyse en MS. De analyse van synthetische polymeren is niet eenvoudig omdat deze, als gevolg van het polymerisatieproces, mengsels zijn van moleculen van verschillende grootte. Volledige karakterisering van een synthetisch polymeer betekent vaststelling van de grootte, structuur, functionaliteit, volgorde en architectuur van elk van de componenten van de gehele verdeling. MS kan gedetailleerde informatie over veel van deze parameters verschaffen wanneer zachte ionisatietechnieken zoals electrospray-ionisatie (ESI) en matrixgeassisteerde laserdesorptie/-ionisatie worden gebruikt. Deze technieken brengen die adducten van intacte grote moleculen in de gasfase. Omdat beide technieken preferent werken voor de ionisatie van polaire stoffen zijn voor de analyse van minder polaire en apolair moleculen andere ionisatietechnieken ontwikkeld, zoals chemische ionisatie bij atmosferische druk (APCI) en atmosferische druk foto-ionisatie (APPI). Naast ionisatietechnieken blijven ook de massa-analysatoren van essentieel belang voor de analyse van synthetische polymeren. Er zijn verschillende concepten ontwikkeld die gebaseerd zijn op verschillende principes in de ionenfysica. In dit hoofdstuk worden verschillende massaspectrometers beschreven, zoals quadrupool/lineaire ionenval massaspectrometers (QIT/LIT-MS), orthogonaal versnelde quadrupool vluchtijd massaspectrometers, Fourier transformatie ionen cyclotron resonantie massaspectrometers en Orbitrap massaspectrometers.

Naast de inleiding laat **Hoofdstuk 2** enkele voorbeelden zien van de huidige stand van de techniek in de methoden voor analyse van synthetische polymeren met behulp van zowel MS als vloeistofchromatografie (LC) gekoppeld met MS. Vergelijking van de hoeveelheid informatie die wordt verkregen met MS met de informatie die wordt verkregen met LC-MS laat zien dat gebruik van gekoppelde technieken een noodzaak is voor de analyse van complexe mengsels van polymeren. De chromatografische scheiding zorgt voor het onderscheid tussen nominaal isobare stoffen, reduceert de effecten van ionsuppressie en zorgt zo voor een meer accurate presentatie van de samenstelling van het monster.

**Hoofdstuk 3** geeft een voorbeeld van de huidige prestaties van LC gekoppeld aan MS<sup>n</sup> in de analyse van polymere systemen met complexe structuren zoals ethoxylaten van plantaardige oliën. Door optimalisatie van de LCcondities wordt een hoge selectiviteit verkregen bij de scheiding van gelijksoortige polymere structuren (33 verschillende polymeerdistributies, waarvan sommige nominaal isobaar of zelfs isomeer zijn). Complementaire informatie wordt verkregen wanneer de ESI-MS analyse zowel in de positieve als in de negatieve polariteit wordt uitgevoerd en wanneer verschillende ionisatietechnieken worden gebruikt, zoals APCI en APPI. MS<sup>n</sup> analyse met verschillende adductionen (in dit geval natrium, lithium, ammonium en kalium) laat zien dat analyten die met behulp van lithium of ammonium gekationiseerd zijn de meest gedetailleerde informatie verschaffen. Hoog-accurate MS/MS is toegepast om de structuur van karakteristieke fragmentionen te bevestigen die informatie geven over de ethoxyleringspositie van het biomolecuul.

**Hoofdstuk 4** presenteert de ontwikkeling van een methode om de toegepaste excitatie-energie in een QIT accuraat en reproduceerbaar in te stellen. Verschillende instrumentparameters, zoals de ionenaccumulatielijd, de isolatiemassa, het isolatiebereik, de vertragingperiode tussen isolatie en excitatie, het excitatiebereik en de excitatietijd, worden onderzocht en geoptimaliseerd. De methode wordt verder geverifieerd door een studie van de relatie tussen de grootte van poly(ethyleenglycol)en en de vereiste energie voor fragmentatie. Dit verband blijkt lineair en in overeenstemming met andere MS instrumenten waarin de toegepaste excitatie-energie op meer accurate wijze gedoseerd kan worden.

In hoofdstuk 5 wordt de methode voor accurate en reproduceerbare instelling van de toegepaste excitatie-energie gebruikt om onderscheid te maken tussen verschillende polymeerklassen. Er wordt aangetoond dat discriminatie bewerkstelligd kan worden door een 'karakteristieke' parameter (d.w.z. het karakteristieke botsingsvoltage (CCV)), die gerelateerd is aan de structuur van het polymeer en die een representatie is van de stabiliteit van het betreffende polymeerion bij excitatie. Deze parameter wordt bepaald voor polymeerionen van verschillende afmetingen en uitgezet tegen de betreffende ionmassa's. De resulterende lijnen laten alle een lineaire trend zien, maar zijn wel onderling

verschillend. De verschillen blijken gerelateerd te zijn aan het type binding tussen de monomeereenheden en, binnen een polymeerklasse, het verschil tussen lineaire en cyclische structuren van het polymeer en de structuur van de eindgroepen. De volgorde van de lijnen een indicatie voor de benodigde energie voor de dissociatie van verschillende polymeerklassen; voor polyethers is meer energie nodig dan voor methacrylaten, die op hun beurt weer meer energie nodig hebben dan polyester en polysacchariden. Deze methode wordt vervolgens toegepast in de analyse van een mengsel van een copolymeer met complexe structuur (in dit geval poly(melkzuur)-*block*-poly(tetramethyleenglycol)-*block*-poly(melkzuur)), en de daarmee nominaal isobare homopolymeren poly(tetramethyleenglycol) (PTMEG) en poly(melkzuur) (PLA). Als deze stoffen zich in een mengsel bevinden, kunnen ze niet onderscheiden worden met conventionele MS- en MS<sup>n</sup>-methoden. De CCV waarden van de nominaal isobare ionen bleken zowel te verschillen tussen de homopolymeren (PLA en PTMEG) en het copolymeer als tussen de copolymeren met onderling verschillende monomeerverhoudingen.

**Hoofdstukken 6, 7 en 8** beschrijven de studie van noncovalent-gebonden complexen van synthetische polymeren met hoge molaire massa enerzijds en moleculen die ammonium functionaliteiten bevatten anderzijds. Dit type ioncomplexen blijkt een voorkeur te hebben voor lage ladingstoestanden. **Hoofdstukken 6 en 7** presenteren het onderzoek naar de parameters die de vorming van deze adducten met lage ladingstoestanden beïnvloeden. De concentratie van het ammonium bevattende molecuul/ion in de sprayoplossing heeft een direct effect op de vorming van de adducten. Daarnaast speelt de structuur van het ammonium bevattende molecuul/ion een cruciale rol in de prestatie van de methode met betrekking tot de vorming van adducten met een lage ladingstoestand en zelfs in het zich überhaupt voordoen van dit effect. De belangrijkste structuurkarakteristieken zijn de substitutiegraad en de grootte van de substituenten. Ammoniumionen die een hoge bindingsenergie combineren met sterische hindering aan het polymeermolecuul kunnen coördineren met synthetische polymeren met hoge molaire massa en vormen daarbij adducten met een lage ladingstoestand. Quaternaire ammoniumverbindingen zoals hexadecyltrimethylammoniumchloride en hexadecylpyridiniumbromide en tertiaire amines zoals triethylamine en tributylamine hebben zulke structuren (d.w.z. grootte, specifieke

ladingslocatie en eenvoudige interactie met het polymeer) en presteren het best als het aankomt op de vorming van adducten met een lage ladingstoestand. **Hoofdstuk 8** laat het gedrag van deze noncovalent-gebonden ioncomplexen bij activering in zowel laag-energetische als relatief hoog-energetische botsingsregimes zien. De hoeveelheid en kwaliteit van de fragmenten wordt sterk beïnvloed door de structuur van het ammoniumion. De dissociatie van noncovalent-gebonden ioncomplexen van synthetische polymeren met quaternaire en tertiaire ammoniumionen (met meerdere grote substituenten) resulteert in afsplitsing van de ammoniumionen. Tertiaire en primaire ammoniumionen die slechts één substituent met een lange keten bevatten, daarentegen, vormen noncovalent-gebonden complexen die gedurende dissociatie ladingsgekatalyseerde reacties en homolytische splitsing laten zien. De resultaten tonen aan dat MS/MS van deze noncovalent-gebonden ioncomplexen gebruikt kan worden als bron voor structuurinformatie van polymeren.

# Acknowledgements

I consider acknowledgements as a very unique part of any scientific publication. It is the only piece of text where scientists can express emotions and speak from their heart. Therefore, I deliberately planned to write this piece of text just before sending the whole manuscript to the printing agency. There is no better moment than this...filled with emotions of accomplishment, happiness, and also sadness, because a four-year journey comes to an end. Nevertheless, a voice in my brain tries to break through this loud waterfall of emotions and scream: “Do not forget to acknowledge all the people you want to!!!”. I hope I will do a good job...

Turning back in the first pages of this book, you can find some lines of ancient Greek. In these lines, I recognize the true incentive of this work; my pursuit in becoming a better man, who is proud to lay his own small brick in Babel. Socrates calls upon the “divine essence” and prays so that he can become a better man. A weird prayer from a man who believed that the pursue of knowledge starts from within and not by divine intervention. I do not need to pray to the Gods. I have found support among the people I have met throughout my journey.

First of all, I want to thank my two fellow travellers: my promoter Ron Heeren and my co-promoter Oscar van den Brink. Without their support, guidance and coaching, I would not have been able to finalize this work. Ron is in my eyes an example of the modern scientist. He is a person full with energy, enthusiasm and curiosity. He did not stop to amaze and challenge me every time we had a discussion. He is a true innovative spirit that found ways to connect the dots in a, sometimes, unbelievable manner. Oscar was my mentor in science and the corporate world, my coach and role model. I learned from him how to become a critical scientist and communicate effectively my results. He was always available to support me and discuss with me scientific problems and ideas, even when he was in the middle of the African jungle or on his bike during one of his trainings. He helped me to understand what it means to be a scientist in the industry, and how to deal with conflicts, problems and people.

I did most of the “travelling” on the “AkzoNobel boat”. AkzoNobel’s R&D labs in Arnhem and Deventer were my basis for the last four years thanks to Oscar, Cees Groenenboom and Tony Jackson. My colleagues at AkzoNobel created a stimulating

environment where I was able to develop my ideas. I want to thank a colleague from the spectroscopy group, Jan van Velde, for teaching me how to operate the instrumentation and for his everyday technical support. I still do not understand how he was able to tune the instruments and recover the signal everytime I was in trouble. He surely saved me from a lot of lost hours and restless nights. Jindra, Bram, Jose and Ab from the chromatography group help me with the chromatographic separations and the determination of the molar mass distributions. All of them and especially Ab helped me to improve my knowledge on liquid chromatography. Joke Speelman and Bill Joyce from AkzoNobel Surface chemistry had a big contribution to my work on the formation of low charge state adduct ions of synthetic polymers with ammonium compounds. Bill made the initial trials that initiated this work and Joke was my source of polymer samples and ammonium compounds. Another colleague from the spectroscopy group, Henk-Jan van Manen, helped me refine my articles. His sharp eye and thoroughness helped me extract positive comments about the quality of the articles from the reviewers. I want to thank my office-mates (Aart, Judit and Marcel) and the rest of the AkzoNobel colleagues for creating a nice working environment and helping me learn Dutch. Without them, I wouldn't have been able to get so many compliments about my knowledge of Dutch!

Most of the funding of this work was from the Marie Curie Actions and one of its projects, the POLY-MS project. The additional financial support from AkzoNobel allowed me to finalize this work. For this I want to thank my R&D manager at AkzoNobel Tony Jackson.

Being part of a Marie Curie Action means that you have the chance to cooperate with different research institutes. I had the opportunity to work with some great scientists and PhD students. I want to thank the POLY-MS "Hungarian team" of Károly, László and Antony. The result of our numerous discussions, frequent email communication and joint experimental work is presented in Chapters 4 and 5. My interaction with the POLY-MS "Polish team" of Marek, Witold, Alena and Cristi was really important. During my secondment in Poland I was able to learn the basics of polymer synthesis and successfully synthesize specific synthetic polymers that I used in this thesis. With Cristian I had a lot of enjoyable moments, discussing about science, life and the world...of course with the

companion of polish beer and homemade honey vodka. Although not part of the POLY-MS project, the “three Michals” in Marek’s lab played a major role to the quality of the polymerized material. The third partner in this project was AMOLF. I spend quite some time at AMOLF (especially before the demolition of the “villa”) using their state-of-the-art instrumentation. Don, Marc, Camila and Luc helped me with a lot of my experiments; Lennaert, Andras, Erika, and Andriy had fruitfull discussions with me. As last, I would like to acknowledge my teammate in the POLY-MS “AkzoNobel” team, Junkan Song (a.k.a. Charlie). Charlie was my physical connection to the Chinese culture. Through him I was able to revive one of my unfinished dreams; to learn more about China. We travelled together to conferences, followed courses and discussed various times about our scientific problems. What else does someone need from a teammate?

Some of the work presented in this thesis was supported by some colleagues at the R&D labs of MSD in Oss. Maarten and Nicollete allowed me to use their instruments and successfully finalize Chapter 8. Their willingless to help me in short notice is something that I will never forget.

For last I would like to thank all of my friends and the people who stood by my side. My Your AkzoNobel “Boardies” (Frank, Qiyue, Dhaneshwar and Boudewijn) with whom I had some of the most unforgettable moments inside AkzoNobel. We were a great team and we achieved a lot for our young professional network. My friends Benoit and Christos for their support and friendship throughout these four years. I want to thank also Eliane for her support and love. Without you I might not have become the person I am now and I would not have finished this book.

Finally, I want to write something to my parents, my brothers and sister (apologies for writing it in Greek): Ελπίζω να σας κάνω περήφανους με αυτό το βιβλίο και να σας ευχαριστήσω για όλες τις θυσίες που κάνατε για εμένα, τη βοήθεια και την αγάπη σας. Σας αγαπώ όλους!



# Curriculum Vitae

Andreas Nasioudis was born on the 27<sup>th</sup> of January 1978 in Thessaloniki, Hellas.

He graduated from Aristotle University of Thessaloniki in 2006. His major studies were in the fields of analytical chemistry, chemical technology and industrial chemistry. He did his graduation thesis (Analysis of: a) Phenolic Compounds and Resveratrol in Wines, b) Sulfides in Onions and Garlic with Capillary Electrophoresis), while participating in the European Student Exchange Program “Socrates – Erasmus”. This work was performed at the University of Reunion Island, France.

During his studies, he participated in the I.A.E.S.T.E. program (International Association for the Exchange of Students for Technical Experience) and joined a research team in the Hong Kong Polytechnic University. His main task was the development of a method for the determination of fatty acid derivatives with HPLC. He also did various internships (State Lab of Hellas, Procter & Gamble, “Souroti”-Water Bottling Company) and worked in companies in the pharmaceuticals and water-wastewater treatment sector as a chemist.

In 2007, he received the Marie Curie Early Stage Training Fellowship and started his PhD research, as a member of the “POLY-MS” project, on the structural characterization of synthetic polymers and synthetically modified biopolymers with multistage mass spectrometry. This thesis presents the major results of this research.

# List of Publications

## Publications

1. **Nasioudis, A.**; van Velde, J. W.; Heeren, R. M. A.; van den Brink, O. F. Detailed Molecular Characterization of Castor Oil Ethoxylates by Liquid Chromatography Multistage Mass Spectrometry. submitted (**Chapter 3**)
2. **Nasioudis, A.**; van Velde, J. W.; Heeren, R. M. A.; van den Brink, O. F. Electrospray Ionization Mass Spectrometry of The Non-covalent Complexes of Ammonium Ions With High Molar Mass Polyethers. *Int. J. Mass Spectrom.* 2011, *303*, 63-68. (**Chapter 7**)
3. **Nasioudis, A.**; Heeren, R. M. A; van Doormalen, I.; de Wijs-Rot, N.; van den Brink, O. F. Electrospray Ionization Tandem Mass Spectrometry of Ammonium Cationized Polyethers. *J. Am. Soc. Mass Spectrom.* **2011**, *22*, 837-844. (**Chapter 8**)
4. **Nasioudis, A.**; Memboeuf, A.; Heeren R. M. A.; Smith, D. F.; Vékey, K.; Drahos, L.; van den Brink, O. F. Discrimination of Polymers by Using Their Characteristic Collision Energy in Tandem Mass Spectrometry. *Anal. Chem.* **2010**, *82*, 9350-9356. (**Chapter 4 & 5**)
5. **Nasioudis, A.**; Joyce, W. F.; van Velde, J. W.; Heeren, R. M. A.; van den Brink, O. F. Formation of Low Charge State Ions of Synthetic Polymers Using Quaternary Ammonium Compounds. *Anal. Chem.* **2010**, *82*, 5735-5742. (**Chapter 6**)
6. Memboeuf, A.; **Nasioudis, A.**; Indelicato, S.; Pollreisz, F.; Kuki, A.; Kéki, S.; van den Brink, O. F.; Vékey, K.; Drahos, L. Size Effect on Fragmentation in Tandem Mass Spectrometry. *Anal. Chem.* **2010**, *82*, 2294-2302. (**Chapter 4 & 5**)

## Oral and Poster Presentations at Conferences & Meetings

1. *ESI-MS and MS/MS of Low Charge State Adduct Ions of High Molar Mass Synthetic (Co)Polymers With Ammonium Compounds*, 59<sup>th</sup> ASMS Conference on Mass Spectrometry and Allied Topics, Denver, Colorado, USA, June 5-9, 2011 (**Oral presentation**)
2. *Structural Analysis of Ethoxylated Products by MS & LC-MS<sup>n</sup>*, AkzoNobel Surface Chemistry Webinar, Deventer, The Netherlands, November 5, 2010 (**Webinar**)

3. *Discrimination of Polymers by Using Their Characteristic Collision Voltage in Tandem Mass Spectrometry*, The Analytical Challenge, Lunteren, The Netherlands, November 1-2, 2010 (**Oral presentation**)
4. *A MS Study of Quaternary Ammonium Ions of Synthetic polymers*, 28<sup>th</sup> Informal Meeting on Mass Spectrometry, Kőszeg, Hungary, May 2-6, 2010 (**Oral presentation**)
5. *Structural Analysis of Polyethers with MS: Solutions for the High Complexity and High Molar Mass Challenges*, AkzoNobel Meeting, Sassenheim, The Netherlands, April 19, 2010 (**Internal Oral presentation**)
6. *Charge State Reduction of Synthetic Polymers by SEC-ESI-MS With Post-column Addition of Ionic Surfactants*, The Analytical Challenge, Utrecht, The Netherlands, December 2, 2009 (**Oral presentation**)
7. *Extending the Detection Boundaries of Synthetic Polymers With ESI-MS by the Formation of Polymer-Ionic Surfactant Adducts*, NWO-CW & NVMS Meeting, Lunteren, The Netherlands, November 2-3, 2009 (**Oral presentation**)
8. *Charge State Reduction of Synthetic Polymers by SEC-ESI-MS With Post-column Addition of Ionic Surfactants*, 57<sup>th</sup> ASMS Conference on Mass Spectrometry and Allied Topics, Philadelphia, Pennsylvania, USA, May 31-June 4, 2009 (**Oral presentation**)
9. *Advanced Mass Spectrometric Methods for the Structure Analysis of Synthetic Polymers*, Polish Academy of Sciences Seminar, Zabrze, Poland, May 20, 2009 (**Seminar**)
10. *Structure Analysis of Castor Oil Ethoxylates by LC-MS<sup>n</sup>*, NVMS-BSMS 2009, Kerkrade, The Netherlands, March 26-27, 2009 (**Oral presentation**)
11. *LC-MS<sup>n</sup> Determination of Non-ionic Surfactants: Structure Analysis of Castor Oil Ethoxylates*, 4<sup>th</sup> International Symposium on the Separation and Characterization of Natural and Synthetic Macromolecules, Amsterdam, The Netherlands, January 28-30, 2009 (**Poster presentation**)
12. *LC-MS<sup>n</sup> Determination of Non-ionic Surfactants: Structure Analysis of Castor Oil Ethoxylates*, NWO-CW Annual Meeting, Lunteren, The Netherlands, November 3-4, 2008 (**Poster presentation**)

13. *LC-MS<sup>n</sup> Determination of Non-ionic Surfactants: Structure Analysis of Poly(oxyethylene-co-oxypropylene) Fatty Ethers and Poly(oxyethylene) Fatty Esters*, 56<sup>th</sup> ASMS Conference on Mass Spectrometry and Allied Topics, Denver, Colorado, USA, June 1-5, 2008 (**Poster presentation**)
14. *MS<sup>n</sup> & LC-MS<sup>n</sup> Studies of Modified Biomolecules*, 26<sup>th</sup> Informal Meeting on Mass Spectrometry, Fiera di Primiero, Italy, May 4-8, 2008 (**Oral presentation at fireplace discussion groups**)
15. *Structure Analysis of Ethoxylated & Propoxylated Fatty Alcohols by LC-MS<sup>n</sup>*, NVMS Meeting, Haarlem, The Netherlands, November 15, 2007 (**Flash presentation**)